NUREG/CR-0577
UCRL-52632

A PROBABILISTIC SAFETY ANALYSIS FOR SOLIDIFIED HIGH-LEVEL NUCLEAR WASTE MANAGEMENT SYSTEMS: A STATUS REPORT

Richard A. Heckman
Thomas Holdsworth

Prepared for
U. S. Nuclear Regulatory Commission
by
Lawrence Livermore Laboratory

Available from
National Technical Information Service
Springfield, Virginia 22161

NUREG/CR 0577
UCRL-52632

A PROBABILISTIC SAFETY ANALYSIS FOR SOLIDIFIED HIGH-LEVEL NUCLEAR WASTE MANAGEMENT SYSTEMS: A STATUS REPORT

Richard A. Heckman
Thomas Holdsworth

Manuscript Submitted: February 1979
Date Published: July 1979

Prepared for
Office of Nuclear Material
Safety and Safeguards
U.S. Nuclear Regulatory Commission
Washington, D. C. 20555
Under Interagency Agreement DOE 40-550-75
NRC FIN No. A 0277

by
Lawrence Livermore Laboratory
Livermore, CA 94550

operated by University of California

for the U.S. Department of Energy

NOTICE

This report describes the status of a preliminary investigation of the characteristics of solid waste which influence radiological risks. This work was completed during fiscal year 1977 (through September 30, 1977). Since the time that this investigation was conducted, the Nuclear Regulatory Commission Staff has recognized the large uncertainties inherent in long-term analysis of geologic systems, and has changed its position to emphasize reliance on multiple barriers to waste migration (similar to the "defense-in-depth" philosophy followed in reactor licensing) rather than placing primary emphasis on probabilistic analysis of potential radiological impacts. Ongoing studies will be used to help identify sensitive aspects of postulated waste disposal systems. More recently reported studies on risk methodology that were conducted by Sandia Laboratory are:

R. L. Iman, J. C. Helton, J. E. Campbell, Risk Methodology for Geologic Disposal of Radioactive Waste: Sensitivity Analysis Techniques; Sandia Laboratories, Albuquerque, New Mexico; NUREG/CR-0394, SAND78-0912; October 1978.

R. T. Dillon, R. B. Lantz, S. B. Pahwa, Risk Methodology for Geologic Disposal of Radioactive Waste: The Sandia Waste Isolation Flow and Transport (SWIFT) Model; Sandia Laboratories, Albuquerque, New Mexico; NUREG/CR-0424, SAND78-1267; October 1978.

J. E. Campbell, et. al., Risk Methodology for Geologic Disposal of Radioactive Waste: Interim Report; Sandia Laboratories, Albuquerque, New Mexico; NUREG/CR-0458, SAND78-0029; October 1978.

FOREWORD

The Nuclear Regulatory Commission (NRC) is responsible for regulating the management and disposal of nuclear wastes from licensed facilities. The NRC also has licensing responsibility for long-term storage and disposal of high-level radioactive wastes from Department of Energy (DOE) and commercial operations. Furthermore, under the National Environmental Policy Act, the NRC must assess the environmental impact of waste management activities at licensed facilities.

In keeping with its responsibilities, the Commission has established a nuclear waste management program designed to (1) provide objective performance goals, (2) provide a framework of regulations, standards, and guides, (3) develop a methodology and establish an information base to implement these goals and regulations, and (4) perform licensing reviews.

The Lawrence Livermore Laboratory (LLL) is providing technical support to the NRC to help develop standards for the management and disposal of high-level and transuranic wastes in deep geologic repositories. The major objectives of the LLL support program are to provide an information base and to provide a methodology for developing standards for (1) waste-form performance, (2) repository site suitability, (3) repository design performance, and (4) radiological performance objectives.

Safe management of nuclear waste is clearly one of the pivotal issues in the debate over light water reactor systems. These systems generate nuclear waste in the "back end" of the fuel cycle, hence regulations must cover all phases of handling solidified high-level waste (SHLW) from processing to permanent storage. Critical performance criteria must be available for each phase.

Establishing these criteria for a nuclear waste system is, however, more difficult than licensing new power reactor facilities. Many regulatory issues that surround reactors can be addressed by carefully analyzing an existing

data base for the current generation of light water reactors. Unfortunately, no data base exists for a commercial nuclear waste system. Therefore, we have approached these licensing questions by using mathematical models of the chemical and physical processes that govern the generation, movement, and ultimate disposition of nuclear wastes. We have used both deterministic and probabilistic techniques in our analyses. Using a systems-analysis approach we are able to produce evaluations of societal risk, at stated confidence levels, so that the NRC can develop regulations for the broadest conditions possible.

The problem under study can be split logically into two parts. The first covers the preemplacement portion of the waste management system and the second the repository postsealing period. This report covers work completed during fiscal year 1977 (through September 30, 1977) on those characteristics of solid waste which influence radiological risks during both parts of the waste management system. It is intended as a status report with emphasis on reducing the uncertainties associated with the probabilistic and deterministic analyses.

The report consists of six major sections and a number of appendixes. Section 1 serves as an introduction. It provides background information for the entire study, describes the nature and scope of the work, and discusses the basic principles behind our methodology. Sections 2 and 3 deal with the preemplacement portion of the waste management system--interim storage and transportion. Sections 4 and 5 cover the handling of the nuclear waste at the repository and the repository postsealing period. Section 6 summarizes our findings and presents the results of our sensitivity analyses for the preemplacement and postemplacement portions of the system. Appendixes A through E contain details of the analysis methods and calculations used in the study. Appendix F presents the radionuclide source terms used in our models.

Delays in the publication of this report have been the result of the document review process in an evolutionary regulatory environment and changes in programmatic priorities.

Follow-up work on SHLW carried out in FY 78 was suspended as a result of the decision of the President to defer the reprocessing of spent reactor fuel. Emphasis was shifted from SHLW disposal to the study of spent fuel disposal and retrieval in the environment of a deep geologic repository.

A companion report, "High-Level Waste Repository Site Suitability" (NUREG/CR 0578, UCRL 52633) gives a more detailed analysis of the problem of site suitability for SHLW repositories. A summary report, "Investigations of the Performance of Solidified High-Level Nuclear Waste Forms" (NUREG/CR-0612, UCRL 52700), covering the status of work done during FY 76, FY 77, and FY 78, is in press.

TABLE OF CONTENTS

LIST OF ILLUSTRATIONS

526 012

526 013

526 01

LIST OF TABLES

ABSTRACT

The Lawrence Livermore Laboratory is providing technical support to the Nuclear Regulatory Commission to help develop standards for the management and disposal of nuclear wastes in deep geologic repositories. This report covers work completed during FY 77 on those characteristics of solidified high-level waste which influence radiological risk during both the preemplacement portion of the waste management system and the repository postsealing period. It is intended as a status report with emphasis on reducing the uncertainties associated with the analyses of the chemical and physical processes involved in the waste management system.

EXECUTIVE SUMMARY

SECTION 1: INTRODUCTION AND METHODOLOGY

Regulatory decisions regarding proposed systems for the management of solidified high-level waste (SHLW) must be based on a broad analysis that posits such unexpected events as accidents and natural disasters. Such an analysis is best handled by a computer simulation model, which can rapidly compute the expected risk for a variety of waste-form parameters, as well as estimate the consequences of a range of unexpected events.

The systems-analysis model we developed considers four SHLW forms: spray calcine, fluidized-bed calcine, borosilicate glass, and supercalcine multibarrier (pelletized supercalcine coated with aluminum oxide and suspended in a lead matrix). The model considers accidental releases during all phases of SHLW management: interim storage, transportation, handling, emplacement in a deep geologic medium, and after sealing of the repository. However, it deals only with the technical questions and does not address the environmental or societal issues associated with the risks.

Event trees were constructed for each waste management operation to identify potential release mechanisms (failure modes). Published data for failure probabilities were used whenever available.

Release fractions were then developed to evaluate quantitatively the consequences of these failure modes. Release fractions were determined for each combination of the following characteristics:

- Accident type
- Release mechanism (airborne particulate dispersion, volatilization, or dissolution)
- Reference waste form
- Radionuclide released.

The output of an event tree is the product of accident probability and release fraction, that is, the expected fraction of waste released to the biosphere. Releases were normalized to Ci/MWe-y. Expected values were then computed for individual and population exposures, again normalized to Ci/MWe-y. These expected-value calculations provide information on "integrated risks," which may help regulators to identify critical parameters in establishing SHLW performance criteria.

SECTION 2: INTERIM STORAGE

Accidents that might release radioactive materials from canisters at an interim storage facility fall into two general categories: handling events and storage-pool events.

Two key handling events are (1) a handling crane might stall and (2) a canister might be dropped outside the storage pool. The expected release from handling accidents at the interim storage site is insignificant compared to expected releases from other portions of the waste management sequence, even if unrealistically high release fractions from the canister are used.

Two storage-pool accident scenarios were considered: loss of coolant circulation and catastrophic loss of coolant due, for example, to a basin rupture following an earthquake. The second event would contribute a major risk, whereas the first would not. (Even if cooling circulation were lost--owing, say, to pump failure--coolant lost by boiloff would continue to be replaced by makeup water. The canisters would thus never be exposed to air and would never fail.) In both cases absolute values of expected risk are sensitive to modeling assumptions.

A thermal analysis was performed to (1) set up a computer model to determine the thermal behavior of SHLW canisters as a function of time in an interim storage loss-of-coolant accident (LOCA) and (2) apply this model to representative solid waste forms.

SECTION 3: TRANSPORTATION

REFERENCE SHIPPING CASKS

Shipping casks designed specifically for SHLW have never been built. We established conceptual designs for a railroad shipping cask and a truck shipping cask and verified that they would meet current regulations, i.e., type-B packaging specifications 10 CFR 71 and 49 CFR 173.398. The GE IF-300 spent-fuel cask was the basis of the reference rail shipping cask. The truck reference cask was based on the Nuclear Fuel Services NFS-4 (NAC-1) cask.

We then analyzed the responses of the casks to a series of impact and fire accidents considerably more severe than those specified in the regulations. Although these accidents are highly unlikely, we included them to determine the expected risk and releases from all possible transportation events and to establish the thresholds for the release functions.

CASK FAILURE MECHANISMS

Fire

The high heat capacity of the SHLW transport casks makes it unlikely that a fire of relatively low heat output could supply enough energy to cause gross melting of the cask material. A more likely serious consequence of a fire is that certain key components, which might be more sensitive to temperature, would fail. To determine the threshold for cask breaching due to fire, we identified these components for the cask design in question, estimated the conditions (temperature and length of exposure) under which they would fail, and performed heat transfer calculations to see if and wher these conditions might occur in various fire scenarios.

In using heat transfer calculations to simulate fires, the simplest approach

is to assume that the fire completely surrounds the cask, presenting it with a uniform ambient temperature and conditions for effective emissivity. This situation is more severe than likely in an actual fire accident.

Impact

We made several conservative approximations. First, corner-impact calculations were used to derive the release functions. As a result, our approximation is conservative, since we chose the angle for which maximum damage is expected. Next, we partially accounted for the rigidity of real objects by using only the accident probabilities for "extremely rigid" objects. Even objects such as trains and bridges are not completely rigid. Finally, we assumed that a constant amount of cask kinetic energy is used in deforming the vehicle structure, independently of impact velocity. The value was derived from a fit made to data points from recent truck impact tests.

Other

The following scenarios were also considered and found to present no significant risk:

- Puncture accidents
- Rupture by thermal shock
- Internal pressure buildup
- Defective sealing.

This study does not consider either explosive attack or combinations of breaching mechanisms.

CANISTER FAILURE MECHANISMS

The canister failure mechanisms and the rates at which they take place depend on the materials involved. The following discussion pertains to the calcine and glass waste forms in canisters made of 304L stainless steel.

Overheating

Canisters could be overheated by (1) internally generated radioactive decay heat, (2) externally applied heat during a fire, or (3) adjacent canisters, as in an interim storage loss-of-coolant accident. Several temperature-dependent mechanisms come into play at high temperatures: corrosion by heated waste, external oxidation in air, creep, and melting. Canister failure could result from a single mechanism or a combination of them.

Impact

The probability that a full canister will breach on impact, as well as the character and size of the breach, depends on the velocity at impact, the rigidity of the impact surface, the design of the canister, the canister material and waste material (including their thermal and mechanical histories), the temperature of the canister, and the geometry of impact. Fractures in 304L stainless steel are expected to be ductile at plausible temperatures and strain rates. Thus, we expect that the breach will normally be only a small crack--say, 10^{-3} times the canister area --for impact velocities below 45 mph.

Other

The following scenarios were not considered in detail in the study:

- Puncture
- Defective sealing
- Corrosion by water
- Rupture by thermal shock
- Internal pressure buildup

- Pullout of lifting device
- External pressurization.

Combined effects were not considered, except for the case of pressurization resulting from overheating.

RADIONUCLIDE RELEASE MECHANISMS

We considered three radionuclide release mechanisms--dissolution, volatilization, and airborne particulate dispersion. Dissolution includes both leaching, which involves selective diffusion of radionuclides from inside the waste matrix, and corrosion or etching of the solid waste by a solvent, in this case water. Volatilization is simply the evaporation of chemical species from the waste at elevated temperatures. Radionuclides can also disperse as part of particulate matter spread by air currents. The respirable fraction of these particulates (less than 10 μm in diameter) is particularly important. As in the other processes, canister breaching is a prerequisite for particulate dispersion.

RAILROAD EVENTS

In evaluating the risk associated with railroad transport, we considered accidents involving impact and fires in detail. Both air and water pathways were modeled to calculate expected values of risk.

The corner-drop impact analysis showed that the lid closure bolts are likely to fail at an impact velocity only about 12% above that at which the 10 CFR 71 regulations are met. An impact that causes cask failure would almost certainly rupture the canisters, subsequently releasing radioactivity. Using this observation as the basis of computed radioactivity release functions, and using available accident statistics, the expected value of risk was calculated. The water path contribution was computed using a conditional probability of 10^{-2} that the waste enters a waterway.

In fire-induced releases, the canister is the critical component; breaching of the cask occurs because of early seal failure in a fire. Canister failures then occur because of corrosion of the wall by the melted glass or, in the case

of calcine, by oxidation and creep of the wall. Since these mechanisms are Arrhenian processes, we established discrete canister failure temperatures. We then treated heat transfer through the cask as a time-dependent process and thus defined a failure locus on a plot of fire temperature vs failure time. This failure locus describes the combinations of fire temperature and duration that will cause canister failure.

The failure temperature, T_{fail}, is the fire temperature above which the waste canister will eventually fail. For spray and fluidized-bed calcines, canister failure by oxidation, creep, and corrosion mechanisms occurs at fire temperatures above $1570^{o} \pm 50^{o}K$ ($2370^{o} \pm 90^{o}F$). For glass waste, corrosion failure takes place at fire temperatures above $1470^{o} \pm 50^{o}K$ ($2190^{o} \pm 90^{o}F$). The supercalcine multibarrier waste form fails because of internal corrosion and cracking of the Al_2O_3 coatings when exposed to fire temperatures above $1570^{o} \pm 100^{o}K$ ($2370^{o} \pm 180^{o}F$).

TRUCK EVENTS

We considered only truck accidents involving fire. Both air and water pathways were modeled, and volatilization releases were modeled using experimental laboratory data.

For the calcine wastes, canister failure by oxidation, creep, and corrosion occurs with fire temperatures above $1570^{o} \pm 50^{o}K$ ($2370^{o} \pm 90^{o}F$). Corrosion failure of the canister can take place with glass waste at fire temperatures over $1470^{o} \pm 50^{o}K$ ($2190^{o} \pm 90^{o}F$). The multibarrier waste form will fail from internal corrosion and from cracking of the Al_2O_3 coatings when exposed to fire temperatures above $1570^{o} \pm 100^{o}K$ ($2370^{o} \pm 180^{o}F$).

The reference truck cask design is adequate for normal steady-state operation, with no mechanical cooling needed, because:

- The calcine centerline temperature does not exceed the calcine bakeout temperature.
- The maximum canister temperature is well below that required for rapid corrosion.

- The lead shielding remains in the solid state.
- The temperatures of the stainless-steel outer wall are moderate, about $405^{o}K$ ($270^{o}F$).

SECTION 4: HANDLING AT THE REPOSITORY

We analyzed the possible risks of accidents during handling operations at the repository and found the most significant dangers to be (1) handling accidents in which the canister is accidentally dropped and (2) airplane crashes into the surface facility. As was the case in the interim-storage analysis, we found that the conditional probability of canister rupture after a crane drop is zero. Nonetheless, we conservatively assumed that each crane drop released 100% of the volatiles in the canister. The maximum expected release (in Ci/MWe-y) due to drops caused by crane failures was then found to be 10^{-16} times the activity of volatiles in 1 MWe-y of waste. The maximum expected release due to aircraft impact was 7.09×10^{-17} times the activity in 1 MWe-y of waste. The total risk from these two scenarios is relatively unimportant compared to that from interim storage and transportation.

SECTION 5: REPOSITORY POSTPLACEMENT PERIOD

Bedded rock formations that might be satisfactory nuclear waste repository sites include argillaceous formations and bedded rock salt deposits. Generally, it is expected that suitable sites will be in regions of low earthquake activity, that the formation will contain few joints, fractures, and faults, and that the host rock will have low porosity and permeability.

REPOSITORY SITE MODEL

We described the reference repository as located in a rock formation of six layers, with variable properties for each layer. The repository layer lies between adjoining barriers, or aquitard layers, which in turn are adjoined by aquifers. The lower aquifer provides the upward driving force for water intrusion into the repository; the upper aquifer allows transport of radioactivity away from the repository into a surface water system. This type of groundwater intrusion is the greatest threat to containment since it provides a mechanism to transport radioactivity into the biosphere.

The variable dimensions and variable hydrological parameters that define the repository site are as follows:

Hydraulic factors

- Porosities
- Permeabilities
- Cross section of pathway
- Length of pathway
- Artesian head
- Pressure head
- Pressure gradient (horizontal)
- Dispersion coefficient.

Chemical factors

- Retardation factor (K_f) of I and Tc
- Retardation factor (K_f) of other fission products
- Retardation factor (K_f) of actinides
- Rate of waste dissolution.

Geometric factors

- Layer thickness
- Distance to surface water
- Tunnel length.

These parameters and dimensions can be varied to simulate different media and different geometries. Taken together they determine flow-path configurations, path lengths, and the properties that influence flow rates and waste-product concentrations. In our studies so far, we have selected parameter values that simulate layered sedimentary environments, with the repository in either shale or salt, and with water flow through interstices or fractures.

We calculated radiological releases and doses for a range of these parameters and for various release mechanisms. Additional variations in the reference model were made by specifying additional flow paths by their location, dimensions, and hydraulic properties (e.g., porosity, permeability, and pressures). These added flow paths allowed us to simulate faults and breccia pipes, as well as such features as failed seals and backfill in the tunnels and shafts at the repository.

EXTENT OF THE HAZARD

The potential hazard of high-level waste from the reprocessing of light water reactor fuel was calculated as a function of time for three groups of nuclides using the biosphere transport and dose model. These nuclides, which dominate the potential hazard after 1,000 y, are the actinides and daughters (^{243}Am, ^{241}Am, ^{240}Pu, ^{239}Pu, ^{229}Th, and ^{226}Ra) fission products without retardation (^{129}I* and ^{99}Tc) and fission products with retardation (^{126}Sn and ^{93m}Nb).

The model accounts for radionuclide transport in the ecosystem and bioaccumulation in the food chain. Plots were made of potential hazard in terms of the whole-body population dose (per MWe-y of waste), which is defined as the total dose to the population that would be incurred if 1 MWe-y of soluble waste were to be dumped directly into the river. Curves for critical organs and for individual doses have a similar form.

The shapes of these curves do not depend on the half-life of ^{239}Pu. There are, rather, two time periods during which the total potential hazard from the waste declines significantly:

- The period from 30 to 400 y, during which ^{90}Sr and ^{137}Cs decay.
- The period from 5×10^5 to 2×10^6 or 3×10^6 y, during which ^{226}Ra (produced by the decay of ^{234}U, which arises from ^{242}Cm and ^{238}Pu) decays. The time constant governing this process is the quarter-million year half-life of ^{234}U. After 3×10^6 y, the remaining ^{226}Ra in the waste is that produced by decay of the original inventory of ^{238}U.

Given these time dependences, we can divide the future of the repository after decommissioning into three distinct periods. This division comes directly from the categorization of nuclides and the time dependence of their hazard and does not depend on the description of the repository site. The three periods are:

- An initial period lasting not more than 400 y. During this interval the consequences of a direct release of radioactivity to the biosphere could be quite severe. For example, whole-body population dose could be as high as 10^5 man-rem/MWe-y

526 033

- An intermediate period lasting at least 5×10^5 y, but not more than 3×10^6 y. The consequences of release during this period would be considerably smaller than during the earlier interval (less than 10^2 man-rem/MWe-y whole-body population dose).
- A final period beginning not more than 3×10^6 y after reactor shutdown. During this period the hazard of the waste will be primarily a result of natural ^{238}U and its decay products. The repository will contain little more than the equivalent of ore mined near the surface and buried in a deep, stable formation.

Individual Dose

The potential hazard of high-level waste released to the biosphere is determined by accounting for all pathways that might lead to man. This hazard is reflected in the calculation of the dose to an individual. Doses were calculated for releases into a river system at some distance from the waste repository. In all of the cases we studied, the maximum dose was far below background.

The peak individual dose to the critical organs varied over three orders of magnitude for the salt repository and two orders of magnitude for the shale repository, depending on the values assigned to model parameters. For example, in the unflawed shale repository with interstitial flow, variation of the following parameters caused increases of at least 200% above reference levels (doses calculated for the reference model):

- Actinide and fission product retardation factors
- Shale permeability of shaft/tunnel
- Fracture zone permeability of shaft/tunnel
- Thickness of repository layer
- Thickness of barrier layer
- Dissolution rate of waste.

With the exception of the dissolution rate of the waste, all of these parameters are related to the travel time between the repository and the biosphere, either affecting flow velocities for the waste or changing the path length.

In the salt repository the situation is similar except that the salt permeability replaces the fracture zone permeability in the list above.

Population Dose

One can expect the dose to an individual to be far below background for any repository that isolates ^{90}Sr and ^{137}Cs for at least 400 y and allows wastes to reach the biosphere only through a sizable surface water system. For such a repository, integrated population dose rather than individual dose may be a more appropriate measure of risk.

To measure the total effect, the population dose is integrated over the lifetime of the repository, and doses are assumed to be of equal concern, regardless of when they occur. The total integrated dose is thus limited by the repository inventory, radionuclide decay, existence of paths to the biosphere, the fraction of water from liquid pathways used for irrigation and drinking water, and the quantity of aquatic food harvested from the liquid pathways.

Integrated population dose is relatively insensitive to changes in the reference repository parameters. In nearly all cases studied, the critical organ dose was between 0.16 and 0.51 man-rem/MWe-y to the gastrointestinal tract and lower large intestine (GI-LLI). The few cases where the dose exceeded these values by significant amounts involved actinides reaching the river within about 3×10^6 y. For the actinides to affect the dose in this way, the permeability of the rock and the head gradient all along the flow pathway must be high enough or the effective porosity low enough to overcome ion exchange processes that retard actinide migration.

The following conclusions can be drawn regarding population dose:

- Population dose showed the least variation of the three measures of risk (individual dose and concentration are the other two) in the sensitivity studies.
- Population dose varied according to whether actinides were released, which in turn depended most strongly on sorption retardation factors.

- Once waste reaches the river, the population dose depends on the yearly usage rates of the water system and is independent of the river flow rate for a fixed fractional usage rate.

Concentration

Concentrations were calculated for radionuclides in the aquifer water just above the repository cavity. We assumed a line source in the aquifer with a length equal to the width of the repository. Studies so far indicate that peak concentrations in the aquifer at this location often approach or exceed the maximum permissible concentrations in water. This would be important if the water in the aquifer is potable and if wells are drilled in the vicinity of the repository.

As with individual doses, concentrations are sensitive to parameters having a major effect on travel time from the repository to the aquifer. This is because concentrations are primarily a function of the time over which radioactive decay and dispersion can occur.

The concentrations in the aquifer fall off at large distances from the repository because of dispersion. For a steady flux of waste into the aquifer, the peak concentration in the direction of water flow far from the repository is inversely proportional to the square root of the distance from the repository, even if radioactive decay is not significant. The peak concentrations at large distances perpendicular to the direction of flow fall off exponentially. Therefore, the hazard due to possible high concentrations of waste in the aquifer depends on where the water becomes accessible to man.

Because of the greater retardation of the actinides, only the fission products are released into the aquifer from the unflawed shale repository within the first 3×10^6 y (as long as flow is assumed to be through pores and the fracture-zone of the tunnel/shaft and not through fractures in undisturbed rock). However, relatively high concentrations of both the actinides and the long-lived fission products were calculated in the aquifer for the unflawed salt repository. The difference in concentrations between the two

repositories was largely a result of the assumption that no geochemical retardation occurs in the repository and barrier layers of the salt repository.

From concentration studies so far, we have concluded the following:

- Aquifer concentrations are most sensitive to changes in the model parameters.
- Any decrease in concentrations caused by increasing aquifer flow rates will generally increase individual and population doses from a nearby surface water body.
- Peak aquifer concentrations are very sensitive to barrier failures such as faults, boreholes, fracture zones, and breccia pipes.

Fracture Flow Vs Interstitial Flow

The foregoing discussion covered cases in which we assumed interstitial flow in undisturbed rock. In cases with fracture flow rather than interstitial flow in the shale layers, reference levels were consistently higher and occurred much earlier, mainly because of the higher flow velocities in the fractured rock. For example, concentrations of ^{126}Sn increase by three orders of magnitude. Also, the actinides reach the aquifer in less than 3×10^6 y.

SECTION 6 OVERVIEW AND SENSITIVITY ANALYSIS

OVERVIEW

To minimize radiological risk from the operation of a waste management system, performance objectives must be established for volatilization, particulate dispersion, and dissolution characteristics of solidified high-level waste. Our studies indicate that transportation and interim storage are the most critical operations in the management system, hence they are likely to require the greatest scrutiny as objectives are established.

Section 6 summarizes the expected values of risk for both preemplacement and postemplacement activities, normalized to man-rem/MWe-y. We calculated the risk associated with each waste management operation as a function of waste type, then integrated the risk values over 10^6 y. After 10^6 y the risk is relatively insignificant in all cases studied. We considered radiation doses due to external irradiation as well as internal uptake of radionuclides through food, water, and air pathways.

Although the preemplacement risks are much greater than the postemplacement risks, the absolute values are very sensitive to modeling assumptions, and variations of several orders of magnitude are possible.

For preemplacement risk, we assumed initial repository waste-canister criteria of a maximum thermal output of 3.5 kW per waste canister and 12-in. o.d. canisters. We also assumed that the waste is stored for 10 y before being placed in the repository. To meet these requirements, the calcine waste forms could not be solidified until 5 y after reactor shutdown, even with dilution. The glass waste form could be solidified after 1 y. No risk assessment was made of storage before solidification. As a reference design, we chose a spacing based on a previous study, and a sequence of operations that grouped together waste canisters of a similar age to minimize handling. These last assumptions yielded high estimates of risk when we studied the scenario of a

pool drainage, but a change in spacing and a different handling mode would reduce the expected risk.

The post emplacement calculated risk values are based on the conservative assumption that water enters the repository immediately after it is sealed.

The most critical segment in the waste management system appears to be the transportation system. The fine particle size associated with calcine leads to risks from particulate dispersion, and the solubility of calcine leads to higher risks from dissolution than expected for glass. On the other hand, a fire severe enough to melt the glass can cause rapid corrosion of the canister wall, which in turn produces risks from volatile radionuclides that are higher in the glass form than in calcine.

SENSITIVITY ANALYSIS FOR PREEMPLACEMENT ACCIDENTS

Previous calculations of expected dose for preemplacement accidents have depended on nominal data for accident probabilities, release functions, and thermal-failure temperature and age thresholds. Uncertainties exist in these nominal data, and they can be affected by engineering choices. The effect of these uncertainties on expected dose must be explored. Accordingly, we have concentrated on the two types of accidents shown in previous analyses to be major contributors to total expected preemplacement dose to man. These are (1) interim-storage-pool drainage accidents caused by severe earthquakes, and (2) impact and fire accidents involving truck and train shipment of SHLW. We looked at four forms of SHLW (spray calcine, fluidized-bed calcine, borosilicate glass, and multibarrier) and considered only those parameters that have a nonlinear effect on dose.

Interim-Storage-Pool Drainage Accidents

From this sensitivity study and from values of the time to failure derived from thermal analyses, the following conclusions may be drawn:

- The worst-case population dose (1.5 man-rem/MWe-y for multibarrier form and 2.5 man-rem/MWe-y for glass) is a major component of the total expected preemplacement dose.

- Through a judicious choice of age aggregation and canister spacing, the expected dose from glass and multibarrier SHLw in pool drainage accidents can probably be reduced to insignificantly small values. This conclusion must be advanced tentatively because of factors neglected in the simple thermal analysis of the waste and because of uncertainties in the failure temperatures.

Transportation Accidents

Our approach was to compute best-case, nominal-case, and worst-case expected doses for each of two fire temperature distributions by simultaneously setting the remaining variable factors to their best-case, nominal-case, and worst-case values. Results are tabulated in Section 6.

SENSITIVITY ANALYSIS FOR POSTEMPLACEMENT PERIOD

Methods are summarized and results given for the sensitivity analysis of our SHLW repository model. By changing parameter values in the model, we simulated the results of release through a number of pathways and the breaching of barriers in four repository types:

- Sandstone-shale sedimentary sequence; repository in the shale layer with interstitial flow in the shales.
- Same as type 1 with fracture flow in the shales.
- Sandstone-shale-salt sequence; repository in the salt layer, with interstitial flow in the shales.
- Sandstone-shale-salt sequence; repository in the salt layer, with fracture flow in the shales.

The results from 85 separate computer runs and the parameter values used in the calculations are tabulated.

SECTION 1

INTRODUCTION

THE NUCLEAR FUEL CYCLE

The development of a waste management strategy to safely manage and dispose of nuclear wastes from the commercial light water nuclear power industry is one of the pivotal issues in the debate over nuclear power. These high-level wastes are generated in the fuel-reprocessing plants at the "back end" of the nuclear fuel cycle. As Fig. 1 shows, the back end includes all activities following removal of spent fuel rods from the reactor. The front end thus includes all activities that precede the use of the fuel in the reactor.

Public misgivings about the management of nuclear wastes arise in part from misconceptions and in part from the failure of the Government and the nuclear power industry to produce and demonstrate effective waste management strategies. A substantial amount of dangerous nuclear waste, mostly of military origin, does exist. Table 1 shows the quantities of high level wastes existing in the United States and the rates at which they are generated. However, an effective waste management system should be able to deal with these wastes.

To understand how radioactive wastes are generated in nuclear power production, we need to take a closer look at the nuclear fuel cycle. This cycle comprises the operations and facilities that prepare, use, and reconstitute nuclear fuel. Uranium, the basic fuel for commercial power reactors, must first be mined, milled, processed, and enriched, then made into reactor fuel rods. After the reactor extracts energy from the rods, they to interim storage. They may later be sent to a reprocessing plant that recovers and recycles the unused uranium and the plutonium produced in the reactor. The residual high-level radioactive waste must then be solidified, stored to allow decay of radioactive heat, and sent to a repository site for final disposition.

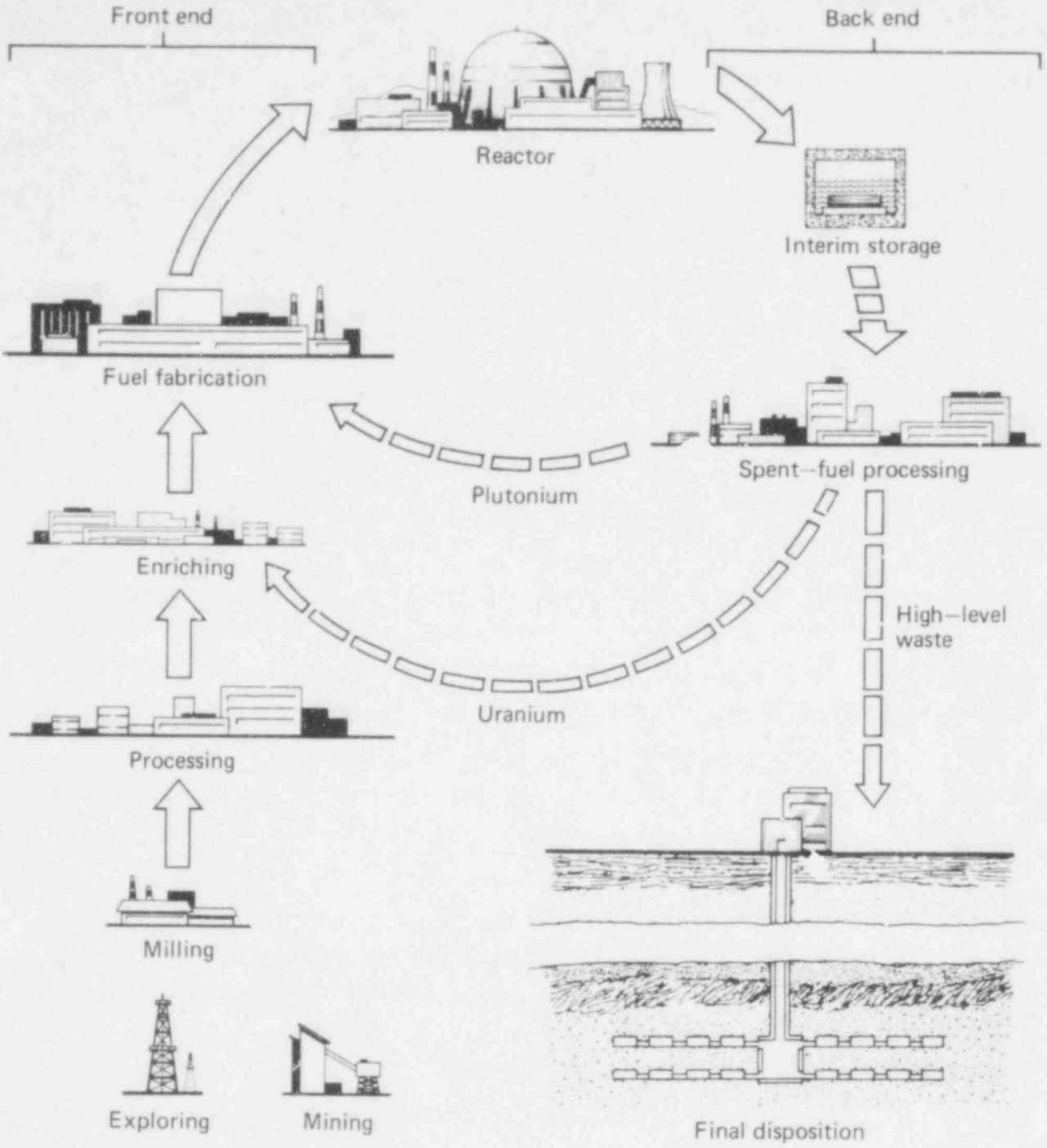

FIG. 1. Nuclear fuel cycle.

526 042

TABLE 1. Quantities of existing high-level waste (HLW) and rates of generation.

Existing: January 1977	
Military (150 RRY[a])	280,000 m^3 (mixed)
Commercial (100 RRY)	2,300 m^3 (liquid) HLW 3,500 m^3 Spent fuel
Generation rates	
1 RRY	35 m^3 Spent fuel or 8 m^3 HLW (solid)
Present industry, 1 y (64 RRY)	2,200 m^3 Spent fuel or 512 m^3 HLW (solid)
1 reactor for life (32 RRY)	1,050 m^3 Spent fuel or 256 m^3 HLW (solid)

[a]RRY = Reference reactor years as used in Bishop and Miraglia (1976).

Only the reprocessing portion of the nuclear fuel cycle produces high-level waste (HLW), as defined by the U.S. Code of Federal Regulations. Appendix F in 10 CFR Part 50 (1976) defines high-level liquid radioactive wastes as "those aqueous wastes resulting from the operation of the first cycle solvent extraction system, or equivalent, and the concentrated wastes from subsequent extraction cycles, or equivalent, in a facility for reprocessing irradiated reactor fuels." For the purposes of this study, solidified high-level waste (SHLW) is defined as waste resulting from the conversion of these high-level liquid wastes to a solid form, plus any undissolved solids removed by centrifugation in the steps that follow the dissolving of the spent fuel elements. Appendix F also requires that all high-level wastes be solidified within 5 y of their generation and transferred to a Federal repository within 10 y.

526 043

Closing the back end of the fuel cycle would require the following steps, none of which is being taken currently:

- Operating the spent-fuel processing plants.
- Recycling uranium and plutonium and subsequently fabricating new reactor fuel rods.
- Solidifying and storing HLW.
- Moving the wastes to the repository site.
- Permanently disposing of the SHLW in deep geologic rock formations.

Developing regulations specifying the performance criteria for an acceptable solidified form of the HLW is, therefore, one of the first steps toward closing the fuel cycle.

GENERAL CHARACTERISTICS OF SHLW

All SHLW forms contain radioactive fission products and actinides, and all emit ionizing radiation, much of which is converted to heat energy in the body of the waste. As an example, consider the SHLW resulting from the generation of 1 MWe-y of energy. The volume of this waste, depending on the form selected, lies in the range of about 10^{-3} to 3×10^{-3} m^3; that is a cube between 10 and 15 cm on a side. The external gamma dose rate and heat output of this cube are shown in Table 2 for three ages of waste. Figure 2 shows the heat output from this cube of SHLW as a function of time for 100 y.

TABLE 2. External gamma dose rate and heat output of SHLW in a 10- to 15-cm cube of SHLW.

Age	Gamma radiation, rads/h at distance of 0.1 m	Heat, W
150 d	25,000	600
1 y	12,000	300
10 y	1,700	30

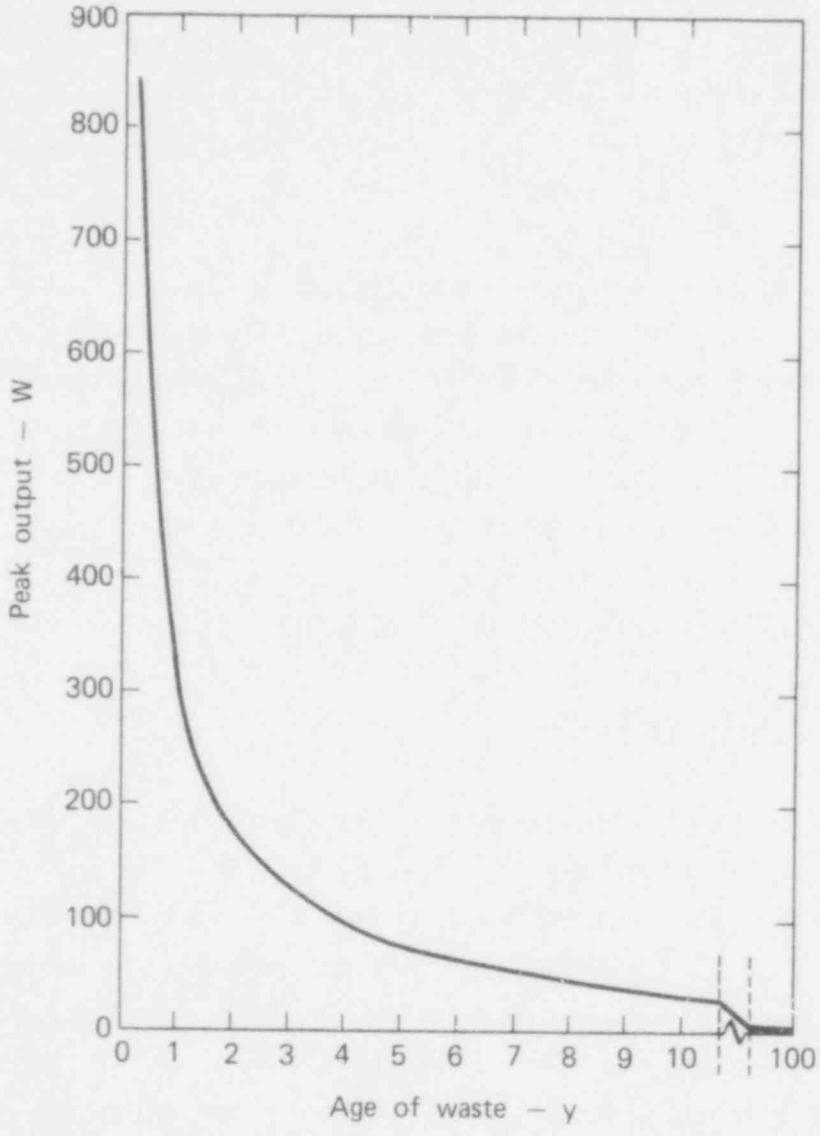

FIG. 2. Heat generation rate of a 10- to 15-cm cube of SHLW.

Radionuclide Content

The amount and the identity of the radionuclides present in SHLW can be predicted from the history of the spent reactor fuel being processed and the partitioning that occurs in the reprocessing plant and in the waste solidification facility. Calculations of this type have been made by Blomeke et al. (1974) at Oak Ridge National Laboratory (ORNL), using the ORIGEN computer code (Bell, 1973). Because of radioactive decay and the wide spread in the half-lives of the various nuclides, the amounts and identities of the species present depend greatly on the age of the wastes. The current study considers only the nuclides that are potential major hazards. Tellurium is included because of its high volatility.

The activities of these potentially hazardous nuclides are as shown in Table 3, expressed curies per MWe-y of waste. The calculations assume a power level of 30 MW/Mg of uranium, a burnup of 3.3×10^4 MW-d/Mg of uranium, a flux of 2.92×10^{13} neutrons per cm^2-s, and a thermal-to-electrical conversion efficiency of 35.4%. The fuel is assumed to be UO_2. If it were mixed oxide (PuO_2 as well as UO_2), the numbers would be similar for the fission products (within a factor of two) but larger for the actinides (about a factor of ten larger depending on the species).

Waste Forms and Their Properties

A major effort has been made during the last few years both in this country and elsewhere, to develop SHLW forms. A recent ERDA document on technical alternatives for waste management (U.S. Energy Research and Development Administration, 1976) and the proceedings of two conferences held in Europe (Organization for Economic Cooperation and Development, 1972; International Atomic Energy Agency, 1976) describe much of this work. In addition, numerous papers in the technical journals have described various treatment processes and waste forms.

TABLE 3. Activities (expressed in Ci/MWe-y) of potentially hazardous nuclides.[a]

Nuclide	Time after removal from reactor									
	150 d	1 y	2	5	10	10^2	10^3	10^4	10^5	10^6
^{89}Sr	3.0E3	1.7E2	1.4E0	8.7E-7	0.0	0.0	0.0	0.0	0.0	0.0
^{90}Sr	2.4E3	2.4E3	2.3E3	2.1E3	1.9E3	2.0E2	4.7E-8	0.0	0.0	0.0
^{90}Y	2.4E3	2.4E3	2.3E3	2.1E3	1.9E3	2.0E2	4.7E-8	0.0	0.0	0.0
^{91}Y	5.0E3	3.9E2	5.4E0	1.4E-5	0.0	0.0	0.0	0.0	0.0	0.0
^{93}Zr	5.9E-2	5.9E-2	5.9E-2	5.9E-2	5.9E-2	5.9E-2	5.9E-2	5.9E-2	5.7E-2	3.9E-2
^{93m}Nb	1.2E-3	2.9E-3	5.7E-3	1.3E-2	2.4E-2	5.9E-2	5.9E-2	5.9E-2	5.7E-2	3.9E-2
^{95}Zr	8.6E3	8.7E2	1.9E1	1.7E-4	0.0	0.0	0.0	0.0	0.0	0.0
^{95}Nb	1.6E4	1.9E3	4.1E1	3.6E-4	0.0	0.0	0.0	0.0	0.0	0.0
^{99}Tc	4.4E-1	4.4E-1	4.4E-1	4.4E-1	4.4E-1	4.4E-1	4.4E-1	4.4E-1	3.3E-1	1.7E-2
^{103}Ru	2.8E3	6.5E1	1.1E-1	0.0	0.0	0.0	0.0	0.0	0.0	0.0
^{106}Ru	1.3E4	8.5E3	4.2E3	5.3E2	1.7E1	0.0	0.0	0.0	0.0	0.0
^{106}Rh	1.3E4	9.5E3	4.2E3	5.3E2	1.7E-1	0.0	0.0	0.0	0.0	0.0
^{125}Sb	2.5E2	2.2E2	1.7E2	7.9E1	2.2E1	0.0	0.0	0.0	0.0	0.0
^{126}Sn	1.7E-2	1.7E-2	1.7E-2	1.7E-2	1.7E-2	1.7E-2	1.7E-2	1.7E-2	9.1E-3	1.8E-5
^{127m}Te	1.9E2	4.9E1	4.8E0	4.5E-3	4.1E-8	0.0	0.0	0.0	0.0	0.0
^{127}Te	1.9E2	4.9E1	4.8E0	4.5E-3	4.1E-8	0.0	0.0	0.0	0.0	0.0
^{129m}Te	2.1E2	2.6E0	1.6E-3	0.0	0.0	0.0	0.0	0.0	0.0	0.0
^{129}Te	1.3E2	1.7E0	1.0E-3	0.0	0.0	0.0	0.0	0.0	0.0	0.0
^{129}I	2.4E-6	2.4E-6	2.4E-6	2.4E-6	2.4E-6	2.4E-6	2.4E-6	2.4E-6	2.4E-6	2.4E-6
^{134}Cs	6.7E3	5.5E3	3.9E3	1.4E3	2.6E2	0.0	0.0	0.0	0.0	0.0
^{137}Cs	3.3E3	3.3E3	3.2E3	3.0E3	2.7E3	3.3E2	3.1E-7	0.0	0.0	0.0

[a]These values are based on studies by Blomeke (1974) and Gera (1975) and at Oak Ridge National Laboratory (1970).

TABLE 3 (continued).

Nuclide	Time after removal from reactor									
	150 d	1 y	2	5	10	10^2	10^3	10^4	10^5	10^6
^{144}Ce	2.4E4	1.4E4	5.7E3	3.5E2	4.7E0	0.0	0.0	0.0	0.0	0.0
^{147}Pm	3.1E3	2.7E3	2.1E3	9.3E2	2.5E2	1.1E-8	0.0	0.0	0.0	0.0
^{154}Eu	2.1E2	2.1E2	2.0E2	1.8E2	1.4E2	2.9E0	0.0	0.0	0.0	0.0
^{210}Pb	0.0	0.0	0.0	0.0	0.0	2.3E-8	2.2E-6	8.8E-5	7.0E-4	1.7E-4
^{210}Po	0.0	0.0	0.0	0.0	0.0	2.3E-8	2.2E-6	8.8E-5	7.0E-4	1.7E-4
^{226}Ra	0.0	0.0	0.0	1.7E-9	3.4E-9	3.5E-8	2.2E-6	8.8E-5	7.0E-4	1.7E-4
^{229}Th	0.0	0.0	0.0	0.0	1.3E-9	2.3E-8	2.2E-6	1.7E-4	3.7E-3	9.1E-3
^{230}Th	6.6E-7	6.6E-7	6.6E-7	6.6E-7	6.6E-7	1.0E-6	1.2E-5	1.1E-4	6.9E-4	1.7E-4
^{231}Pa	7.7E-7	7.7E-7	7.7E-7	7.7E-7	7.7E-7	7.7E-7	8.1E-7	1.2E-6	7.5E-6	1.0E-5
^{233}U	4.6E-7	4.6E-7	4.6E-7	4.6E-7	4.6E-7	4.6E-6	4.8E-5	4.9E-4	4.0E-3	9.0E-3
^{237}Np	1.1E-2	1.1E-2	1.1E-2	1.1E-2	1.1E-2	1.1E-2	1.2E-2	1.2E-2	1.1E-2	8.5E-3
^{238}Pu	1.1E0	2.5E0	5.2E0	1.5E1	3.2E0	1.6E0	3.8E-3	0.0	0.0	0.0
^{239}Pu	5.2E-2	5.2E-2	5.2E-2	5.2E-2	5.2E-2	5.2E-2	6.4E-2	1.3E-1	1.8E-2	7.6E-9
^{240}Pu	7.6E-2	8.1E-2	9.2E-2	1.2E-1	1.4E-1	2.7E-1	2.5E-1	9.9E-2	9.7E-6	0.0
^{241}Pu	1.8E1	1.7E1	1.6E1	1.4E1	1.0E1	1.5E-1	9.8E-3	4.6E-3	2.4E-6	0.0
^{241}Am	5.4E0	5.4E0	5.4E0	5.4E0	5.5E0	5.1E0	1.1E0	4.6E-3	0.0	0.0
^{243}Am	5.4E-1	5.4E-1	5.4E-1	5.4E-1	5.4E-1	5.4E-1	5.0E-1	2.3E-1	6.6E-5	5.2E-9
^{242}Cm	4.7E2	1.9E2	4.5E1	4.2E-1	2.2E-1	1.5E-1	2.4E-3	0.0	0.0	0.0
^{244}Cm	7.8E1	7.6E1	7.3E1	6.5E1	5.4E1	1.7E0	0.0	0.0	0.0	0.0

Although the detailed performance requirements for disposable forms of HLW have not been evaluated before now, the development of waste forms appears to have had these general objectivies: (1) to reduce the volume of the liquid waste; (2) to convert the waste into a form having greater chemical, thermal, radiolytic, and mechanical stability; and (3) to develop a treatment process that is simple, reliable, and economical.

Solidification of the wastes is generally regarded as the best way to satisfy these objectives. Consequently, this approach has become the policy of the U.S. Government, as stated in 10 CFR 50, Appendix F (1976), as well as several European countries. Accordingly, several forms of solid waste have been put forward to meet the objectives above. Those most often proposed include salt cake, calcines, glasses, supercalcine, coated particles, sintered products, glass ceramics, nepheline syenite, metal matrix composites, ion exchange products, and rock melt. In general, the more complex SHLW forms or those demanding higher technology are more expensive, but they offer greater insurance against radionuclide release.

We have dealt with four SHLW forms in this study: spray calcine, fluidized-bed calcine, borosilicate glass, and supercalcine multibarrier. We chose them because they span a wide range of important physical and chemical properties, and because they have seen much development in the United States and elsewhere. Each of these four forms is described in the following paragraphs and their pertinent properties summarized in Table 4.

Spray Calcine. The reference spray calcine is patterned after that developed at Battelle Pacific Northwest Laboratories (BNWL) (Bonner et al., 1976). Its composition is designated by Mendel as PW-7 (Mendel, 1974). This calcine is a fine powder assumed to have been heated to 1100^{o}K to drive off the residual water and to convert the residual nitrates to oxides.

Fluidized-Bed Calcine. The reference fluidized-bed calcine is similar to the material produced at Idaho National Engineering Laboratory (Dickey et al., 1974; Freeby, 1975; Rindfleisch, 1976; and Berreth et al., 1977), but is assumed to be solidified by an electrically heated, steam-fluidized bed (TERA, 1977) rather than a kerosene-heated, air-fluidized bed.

526 049

TABLE 4. Waste form properties.

Property	Temperature, °C	Spray calcine	Fluidized-bed calcine	Borosilicate glass	Supercalcine multibarrier
Specific mass (kg waste/t uranium		66 (undiluted) 78 (diluted)	66 (undiluted) 78 (diluted)	207	
Density (kg/m^3)		1240	2200	3300	5700
Thermal conductivity (W/m-°K)	25	0.094	0.094	0.85	
	200	0.12	0.12	1.0	
	400	0.14	0.14	1.2	
	800	0.20	0.20	3.7	10
Heat capacity (J/kg-°K)	25	600	600	630	
	400	660	660	780	
	800	710	710	780	430
Melting or softening temperature (°C)		1400	1400	900 (easy flow)	1400
Size distribution		Powder, 50% (by wt) below 10 μm		Large block with some cracks	
Solubility		All cesium and strontium immediately soluble; slow leaching of other nuclides		Very slow leaching of all radionuclides	
Volatility		All cesium, tellurium, and ruthenium lost above about 1200°C		All cesium lost above about 1200°C	

Borosilicate Glass. The reference glass is a zinc borosilicate glass patterned after the reference glass developed at Battelle Pacific Northwest Laboratories and described by Mendel (1977), except that it is assumed to be formed of waste having PW-7 composition.

Supercalcine Multibarrier. The reference multibarrier waste form is made up of supercalcine pellets (McCarthy, 1977) coated with aluminum oxide and interspersed in a lead alloy matrix (van Geel et al., 1976). J. Rusin and co-workers at Battelle Pacific Northwest Laboratories are developing multibarrier waste forms.

ANALYSIS METHODS

The high-level waste management system, as defined by Bishop and Miraglia (1976), comprises four stages: interim storage, transportation to the repository site, handling at the repository, and finally the course of events after sealing the repository. This system is shown in Fig. 3.

Given this sequence of operations, the regulator must decide on critical performance characteristics at each stage to minimize human exposure and environmental impact. Systems analysis is an efficient way to approach these decisions.

Proposed systems for SHLW management, under normal operating conditions, appear to pose little danger of human exposure. However, regulatory decisions must be based on a broader analysis that accounts for the possibility of unexpected events, such as accidents and natural disasters. Such an analysis is best handled by a computer simulation model, which can rapidly compute the expected risk for a variety of waste-form parameters, as well as estimate the consequences of a range of unexpected events. This computer analysis thus provides a data base of expected risks for the entire reasonable range of parameters and events. The inherent risk of each waste form, computed by this simulation model, appears as "Waste forms A...N" in Fig. 3.

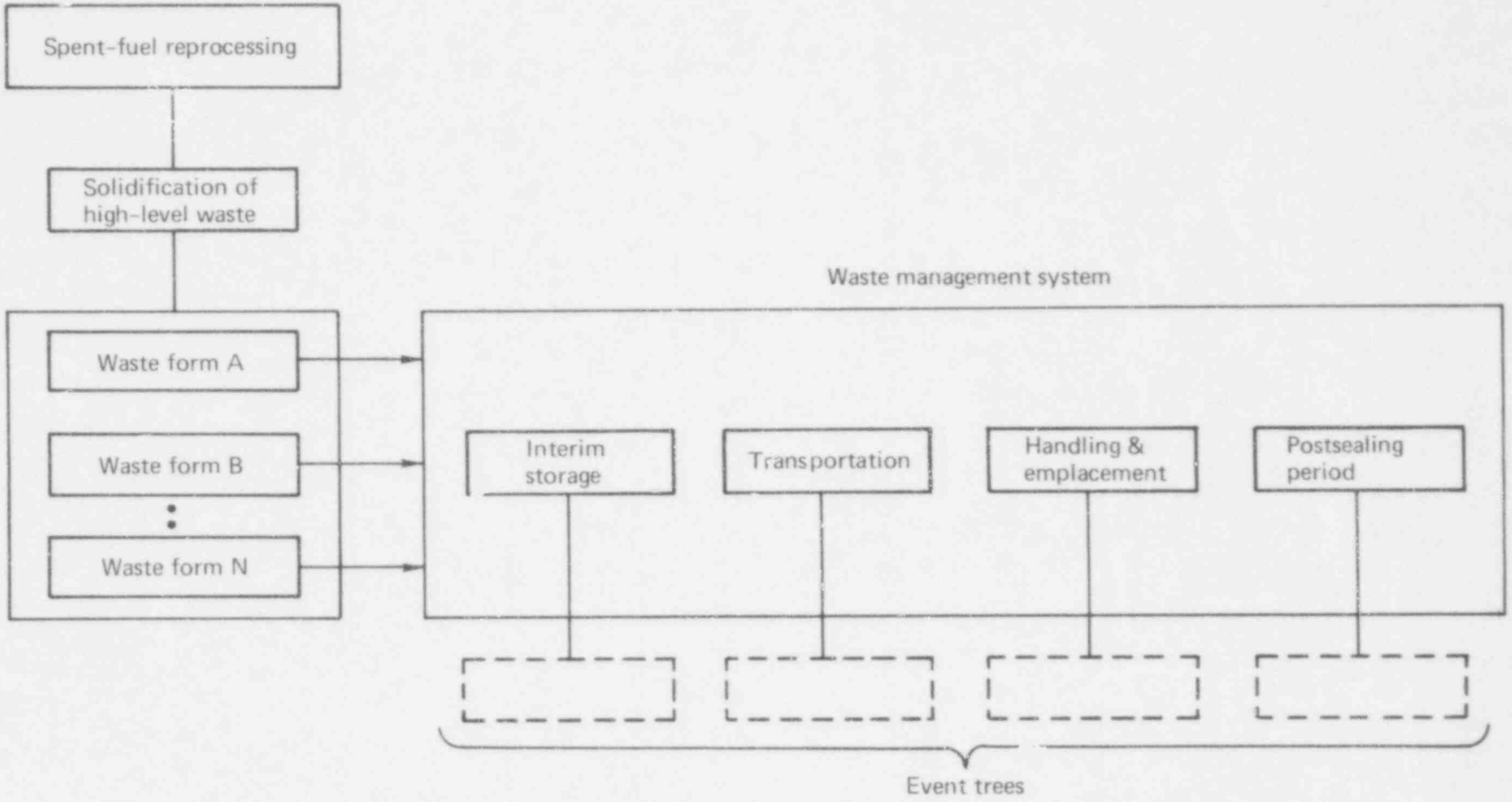

FIG. 3. High-level nuclear waste management system: a systems-oriented view.

Interim Storage Scenarios

Spent fuel is highly radioactive when first discharged from a reactor. It is generally stored under water for 90 to 150 d to allow decay of the shorter-lived nuclides. This period reduces the decay-heat output and the shielding requirement enough to make shipment to the reprocessing plant practicable. On arrival at the reprocessing plant, the spent fuel may be stored even longer, depending on the ultimate form of the solid waste. This preprocessing storage period is important since it determines the length of interim storage (Fig. 4). The length of interim storage, in turn, is important since it is the first stage of the waste management system.

For spray or fluidized-bed calcine we assumed that the spent fuel is held for 5 y or, if reprocessed sooner, that HLW is held in liquid form for 5 y. After 5 y the waste is diluted with enough inert material to ensure that after 10 y, when it is solidified and sealed in internally finned canisters, its heat output will be no greater than 3.5 kW per canister.

For the borosilicate glass, the canisters are filled after 1 y and do not have fins. Supercalcine multibarrier canisters are filled after 150 d and likewise require no fins.

All of the waste forms are sealed in 12-in. (0.305-m) diameter canisters, which are held in interim storage until 10 y have elapsed since the waste was first recovered from the reactor. The canisters are then shipped to a Federal repository.

Event Trees

Figure 5 illustrates the sequence of operations within the waste management system (Bishop and Miraglia, 1976). This list of routine operations then forms the basis for a more extensive list of possible events and pathways.

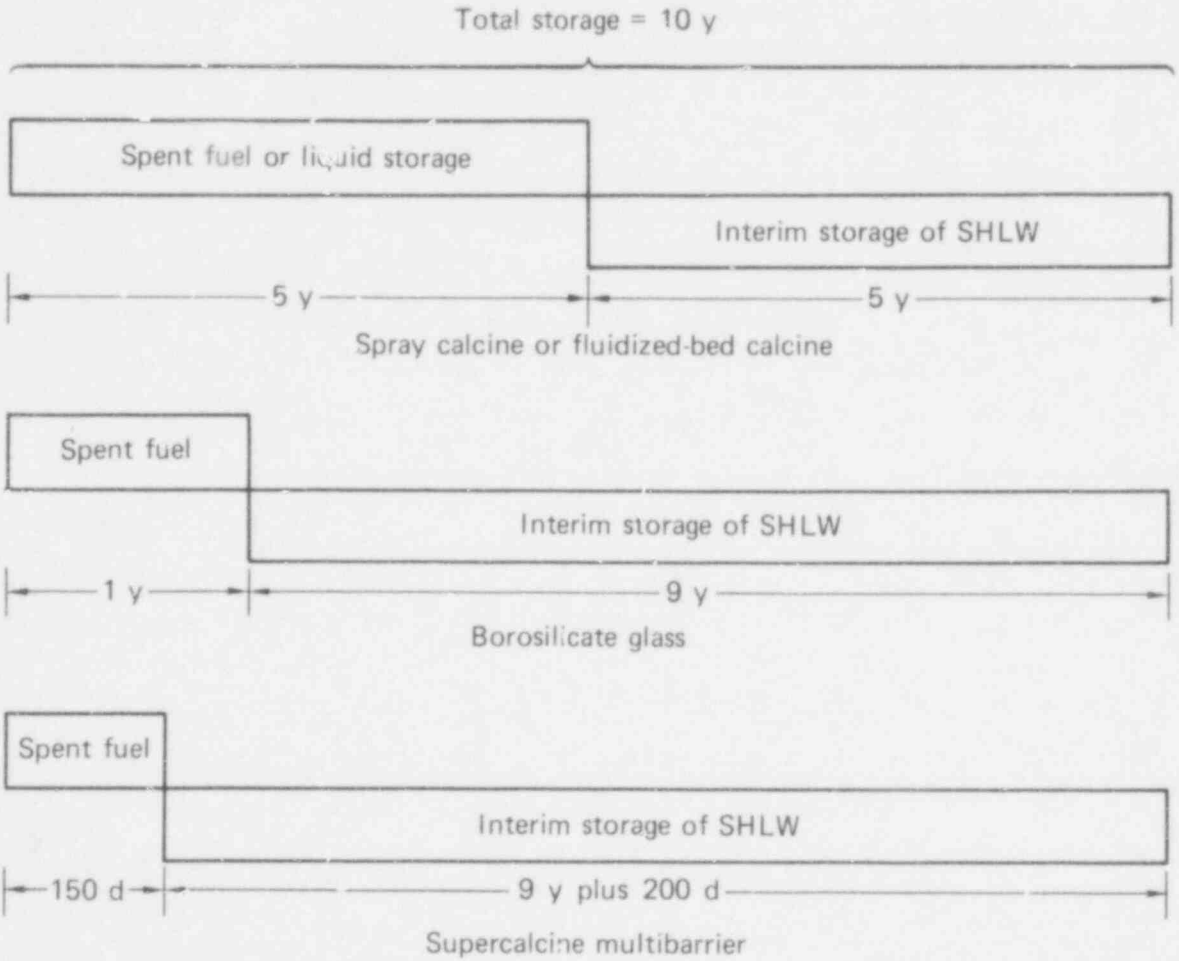

FIG. 4. Spent fuel and SHLW storage schedules.

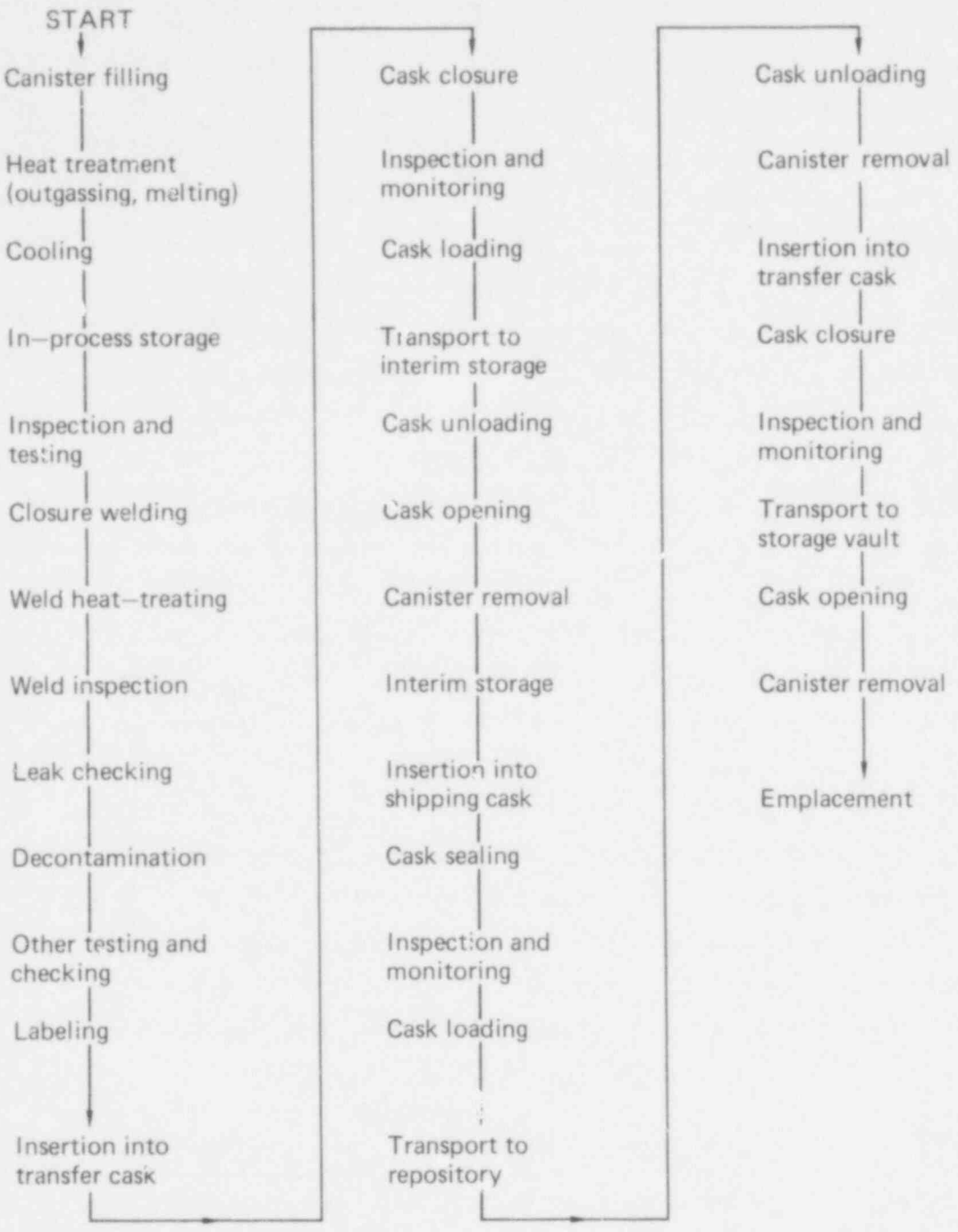

FIG. 5. SHLW management sequence.

526 055

These event trees are useful for analyzing the importance of accidents that can take place during the nuclear fuel cycle. However, this detailed list of accidents, accident sequences, and pathways to the biosphere is so large that a method is needed to ensure that we focus our energies on the most critical elements of the list. The steps we have taken to assemble these event trees, as well as to simplify them (Fig. 6) is the subject of the paragraphs below.

Listing Accidents. The event tree methodology in this study begins with an extensive list of accidents and pathways that might release radionuclides to the biosphere and expose the general public to radiation. This list was compiled by referring to previous work in this field and by conferring with experts. Although large, the list can never be considered complete, and the effort of compiling it has been limited by time and resources. We must always be prepared to scrutinize other accident scenarios when they are put forward.

Computing Consequences. The goal of this analysis is to determine the risks to the general public associated with all or parts of the fuel cycle. Consequently, in light of limited resources, emphasis must be placed on those accidents with the largest risks. Accident scenarios and associated pathways that can be shown to provide very low risks must be eliminated, at least temporarily. Some of these elements can be eliminated even as the event tree is being formed, since they are clearly of little consequence. For most, however, a more precise mathematical justification is necessary. Since most of our analysis is statistical, this justification must be based on the expected values of risk, called the expected risks. In many cases we also compute the worst-case consequences of an accident scenario.

Eliminating Events and Pathways. If the worst case risk of an accident scenario is orders of magnitude less than the expected risks of other scenarios, that scenario need not be analyzed further, nor must we consider any of its possible consequences. This results in the truncation of the event tree. (It must be emphasized that the reverse comparison is not valid: accidents and pathways whose expected risks are well below the worst-case risks computed for others cannot be eliminated on that basis alone.) This

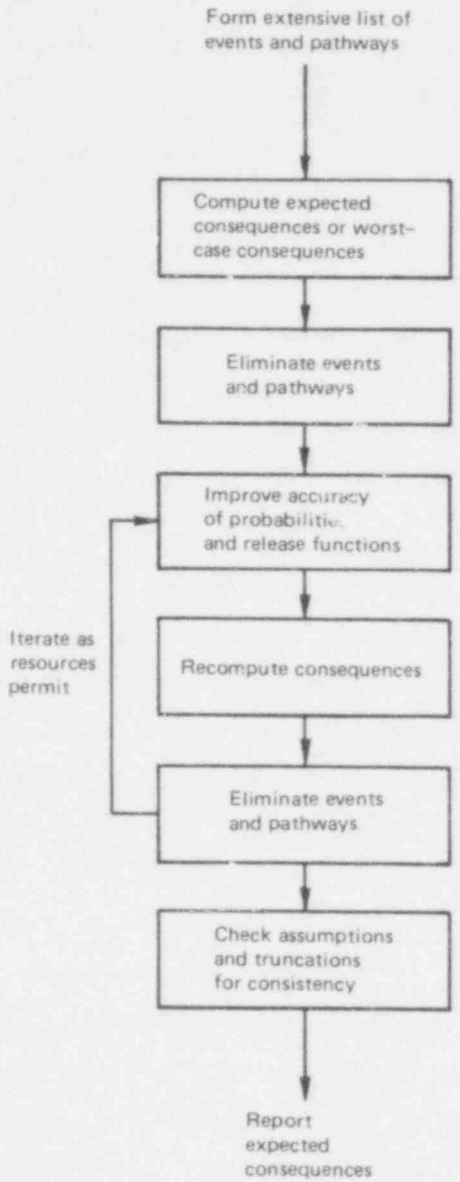

FIG. 6. Truncation methodology.

type of comparison often permits events for which complete statistics are unavailable to be eliminated on the basis of worst-case risks alone. Fortunately, statistics are usually available for accidents presenting the greatest risk.

Attention must also be paid to the uncertainties in the expected risk calculations since these may affect the legitimacy of event-tree truncations. At the end of the analysis, the assumptions on which truncations have been based must be rechecked and confirmed.

Improving Analysis of Events. Eliminating events and pathways from the event tree makes the risk analysis more efficient by allowing us to focus attention on critical events. We can then seek more precise descriptions of accident statistics and of the physical processes associated with the release and migration of radionuclides. During the course of this work, for example, we have considerably enhanced our understanding of radionuclide release during transportation accidents.

Recomputing Consequences. At this point in the analysis, expected risks for all events and pathways remaining on the truncated tree are computed. The results provide a significant means by which various parts of the fuel cycle can be compared, and they provide the only basis on which future truncation can be made. Furthermore, these increasingly accurate statistical results must be periodically checked to ensure that they do not invalidate earlier truncations of the event tree.

Eliminating Additional Events and Pathways. After recomputing the consequences associated with the accidents and pathways remaining on the event tree, it is sometimes possible to eliminate additional elements. An element can be eliminated only if its expected risk is orders of magnitude below those computed for other elements. Again, the uncertainties associated with the risk calculations must be borne in mind lest too many events or pathways be eliminated.

As Fig. 6 shows, the process of improving the accuracy of the data underlying the risk calculations, recomputing the risks, and truncating the event tree can be iterated several times as more and better information about the critical accidents and pathways becomes available.

Checking Assumptions. Simplifying the event tree is a necessary operation. However, since it is based largely on statistical comparisons, we must discard elements with care. To ensure that truncated events do not prove to be critical elements in the light of subsequent information, it is necessary to check the assumptions and data on which truncations were based. This can be a continuous process but it must be performed at least once before reporting the results of the risk analysis. Any elements of the event tree that have been eliminated on the basis of invalid assumptions or inaccurate data must be restored to the tree and subjected to the same level of analysis as those elements that were retained. It may turn out that an element restored to the tree can still be eliminated on the basis of the final assumptions and current data.

Reporting Expected Consequences. The output of the risk analysis can be reported after the final consistency check is completed. In addition to risk values associated with the various events and pathways on the truncated tree, this report will include the assumptions and data used in the calculations, a list of elements that were considered but eliminated, and where possible, uncertainties in the computed risks.

Accidental Release Evaluations

To analyze the effects of potential accidental releases of nuclear materials into the environment, the entire range of possible accidents must be considered. This means that even when interest is focused on a particular kind of accident, we must consider a range of potential severities. The example we will use here is a collision of a truck with a stationary object.

In this case the severity of the accident would have a direct bearing on whether nuclear materials are released and, if so, how much escapes. While there may be some value in speculating about the most severe accident possible, another approach is to turn to what is already known about similar accidents. This is the approach that will be illustrated in the following paragraphs.

Probability Distributions and Density Functions. Information about accidents comes in the form of probability distributions or probability density functions. Just as a distribution of discrete probabilities can be drawn for the throw of a pair of dice, as shown in Fig. 7, truck accident data can be used to generate the probabilities of an accident taking place within specific ranges of speeds--which in turn determine the severities of the accident. Such information may look like that shown in Table 5.

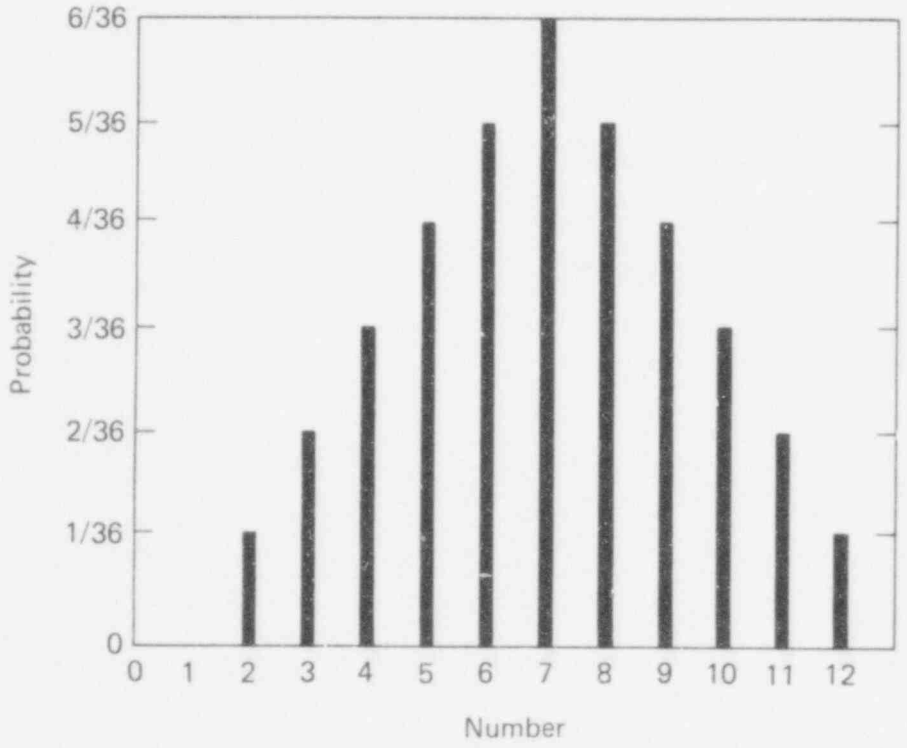

FIG. 7. Probability distribution for a single throw of a pair of dice.

TABLE 5. Hypothetical data on the probability of truck accidents for several speed ranges.

Speed range, mph	Probability of accident
0-10	0.10
10-20	0.12
20-30	0.18
30-40	0.25
40-50	0.16
50-60	0.12
60-70	0.07
Total	1.00

Figure 8 is a plot of the information shown in Table 5. The vertical scale is not probability but probability per mph, which means that the probabilities have been expressed for each speed, say 21 mph, rather than a range of speeds, such as 20 to 30 mph. The incompleteness of the data in Table 5 has produced a discontinuous, stairstepped probability density function (PDF), where the probabilities at both 21 mph and 29 mph must be taken as 0.18/10 mph = 0.018/mph. The total probability that an accident will take place in the range 20 to 30 mph is 0.018/mph × 10 mph = 0.18, as demanded by Table 5.

If more complete information were available, it might be possible to construct a continuous PDF, generally expressed as $p(x)$, where x in this case is the accident severity. The probability of an accident occurring in a given range of severities, x_1 to x_2, would then be given by the integral

$$\int_{x_1}^{x_2} p(x)\, dx \quad .$$

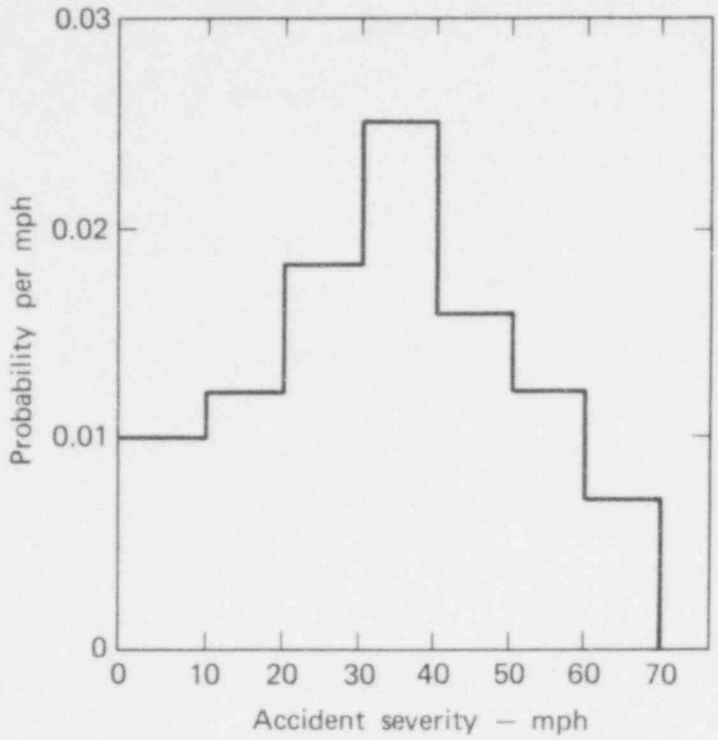

FIG. 8. Probability density function calculated from Table 5.

For example we can use this equation to check our simpler calculation above of the probability of an accident occurring in the range 20 to 30 mph, for which p(x) is 0.018/mph. Thus,

$$\int_{20\ \text{mph}}^{30\ \text{mph}} p(x)\,dx = 0.018/\text{mph} \times \int_{20\ \text{mph}}^{30\ \text{mph}} dx$$

$$= 0.018/\text{mph} \times 10\ \text{mph}$$

$$= 0.18, \text{ as before.}$$

Release Functions. The risk associated with accidental release of nuclear material depends not only on the accident probabilities but also on the expected release associated with each accident. To complement Table 5 (and Fig. 8), therefore, we must determine the amount of material released as a function of truck speed. Table 6 summarizes this information.

TABLE 6. Hypothetical nuclide release fractions for various speed ranges.

Speed range, mph	Release fraction
0-10	0.0
10-20	0.0
20-30	0.0
30-40	0.05
40-50	0.10
50-60	0.20
60-70	0.30

In its more general form, the release information is a continuous function of accident severity, such as that illustrated in Fig. 9. This release function indicates that there is no release below a threshold of about 35 mph. Above 35 mph the fraction released grows rapidly, but not necessarily linearly. Though not shown in Fig. 9, there may be a separate release function for each radionuclide under consideration and some release functions can be zero over the entire practical range of accident severities. In some cases the release function may be specified analytically from first principles. In others it may be approximated by an analytic function fitted to empirical data.

Determining Expected Release. In the example illustrated by Tables 5 and 6, there is no material released at speeds below 30 mph. That means (see Table 5) that 40% of all truck accidents release no nuclides. The 25% of accidents taking place in the range 30 to 40 mph will release 0.05 of the material carried, the 16% of accidents that occur in the range 40 to 50 mph will release 0.10 of the material, and so on. Thus the expected fraction released is the sum of the accident probabilities (Table 5) multiplied by the corresponding release fractions (Table 6):

$$(0.25)(0.05) + (0.16)(0.10) + (0.12)(0.20) + (0.07)(0.30) = 0.0735.$$

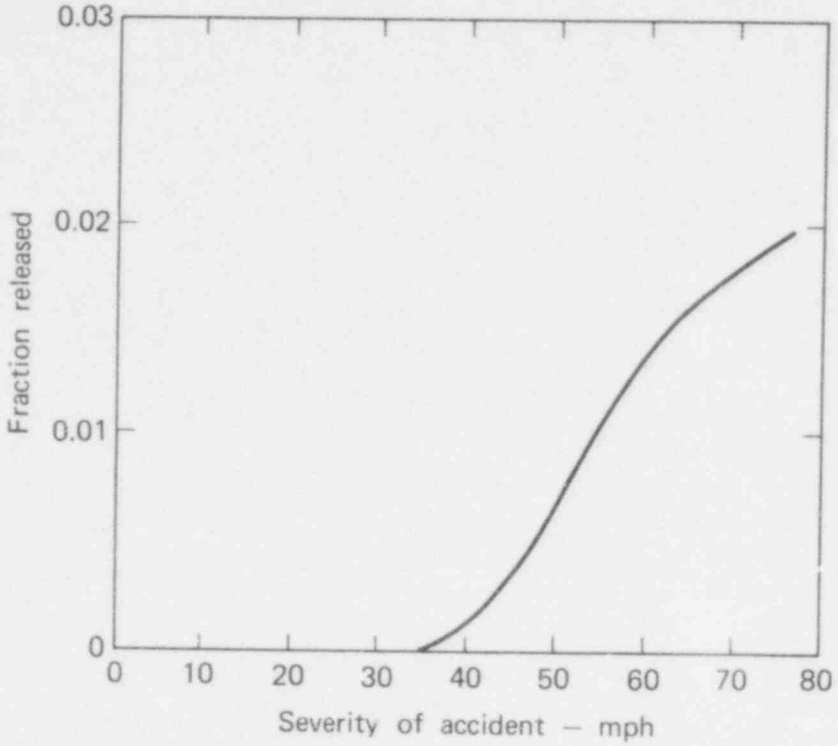

FIG. 9. Hypothetial continuous release function.

That is, the average fraction (over all truck accidents) of the nuclides carried that will be released is 0.0735. If this number is then multiplied by the total probability of a truck accident, the result is the expected fraction of total nuclides transported by truck that will be released in accidents.

More generally, when accident probabilities and release fractions are expressed as analytic functions--p(x) and r(x), respectively--of the accident severity, x, the expected release fraction in an accident is expressed by

$$\int_0 r(x)\, p(x)\, dx \quad .$$

Probabilistic Risk Assessment

Evaluating accident probabilities, release functions, and release fractions for each event in the event tree allows us to calculate the total risks from the various operations in the waste management system. The systems-analysis model we have developed considers mechanisms for accidental release during all phases of the SHLW management system: interim storage, transportation, handling, emplacement in a deep geologic medium, and after sealing of the repository. However, it deals only with the technical questions and does not address the environmental or societal issues associated with the risks.

Figure 10 provides a summary of how the systems-analysis approach has been applied to the waste management system. Event trees were constructed for each waste management operation to identify potential release mechanisms (failure modes). Published data for failure probabilities were used whenever available. Release functions, expressed as expected values of risk, were then developed to evaluate quantitatively the consequences of these failure modes. Releases were normalized to Ci/MWe-y. Expected values were then computed for individual and population exposures, again normalized to Ci/MWe-y. These expected-value calculations provide information on "integrated risks," but they do not indicate the consequences of individual contributing events. In establishing SHLW performance criteria both the integrated risks and single-event risks to the public must be considered.

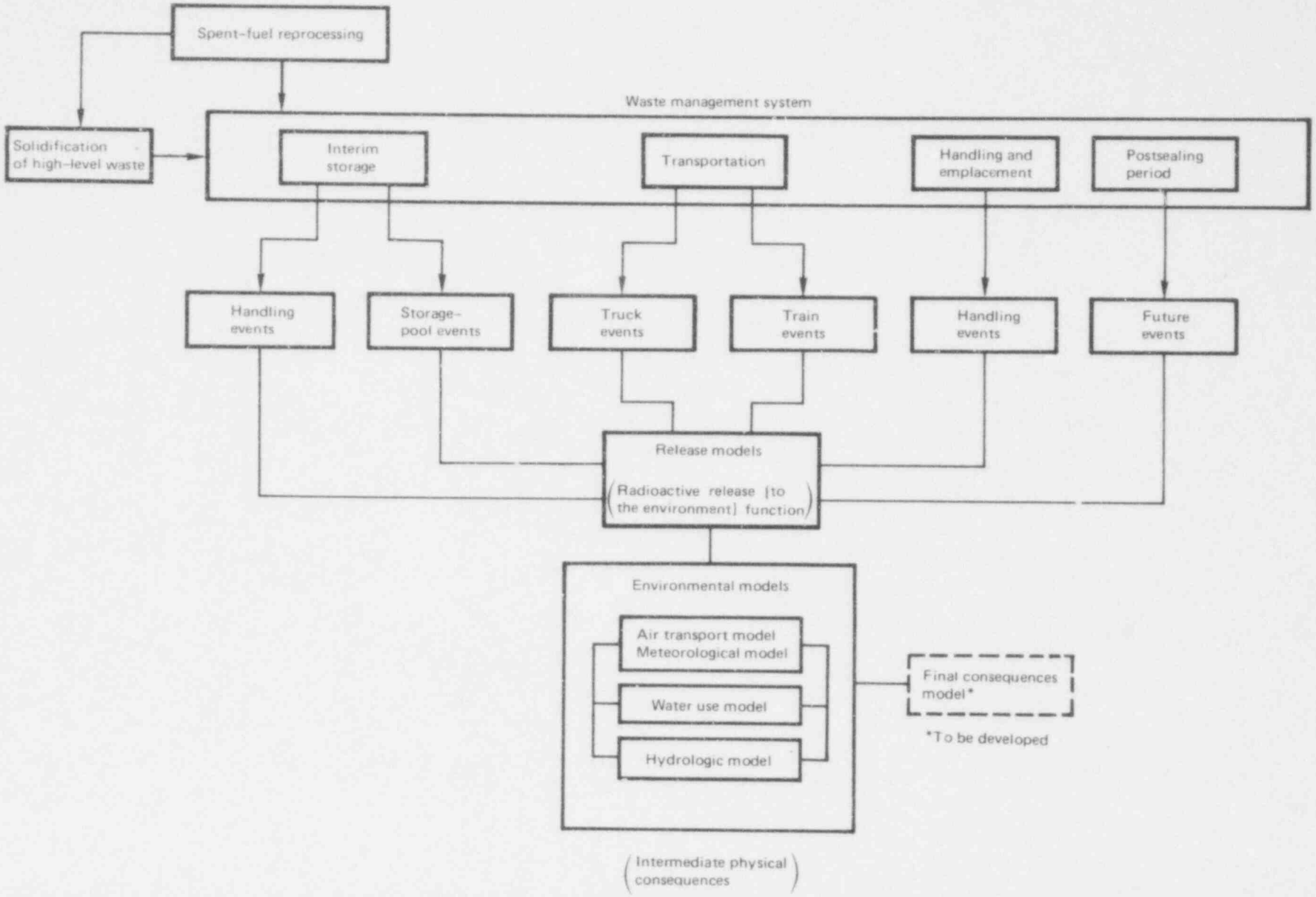

FIG. 10. Overview of systems-analysis models.

SECTION 2

INTERIM STORAGE

Accidents that might release radioactive materials from canisters at an interim storage facility fall into two general categories: handling events and storage-pool events. These are discussed below, following an introductory discussion of some underlying assumptions.

BASIC ASSUMPTIONS

Figure 11 shows the design and some of the characteristics of the reference canister considered in our analysis.

We have arbitrarily assumed that the heat generated in each canister must not exceed 3.5 kW after 10 y, when it is placed in the Federal repository. Some dilution of the calcine waste form is necessary to meet this requirement. The calcine waste form also requires a canister with internal fins to control the waste centerline temperature. During normal operating conditions, the waste temperature should remain below the highest temperature reached during reprocessing--the bake-out temperature. Although this may be a conservative requirement, it is good engineering practice.

We have also assumed that the filled and sealed stainless-steel canisters at the interim storage facility are stored in a concrete basin filled with water, and that the canisters depend on the building structure and a mechanical cooling system for shielding, physical protection, and cooling. Other general assumptions about interim storage of the solidified waste are as follows:

- Large numbers of canisters are grouped in regular arrays in multiple storage cells, each cell having a nominal capacity equal to about one year's inventory from the reprocessing plant.
- The basins are filled with demineralized water, which cools the waste and provides radiation shielding.

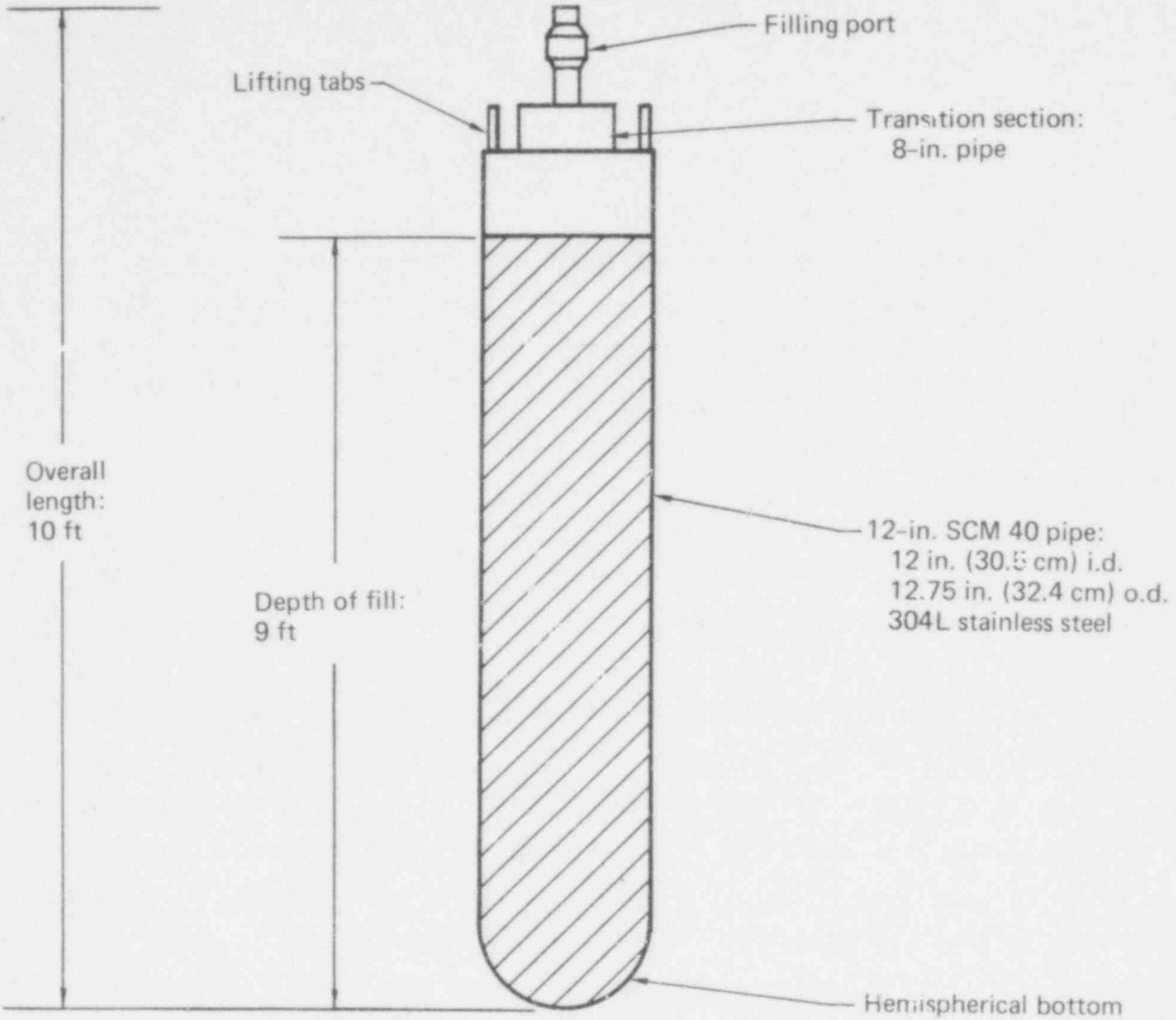

Filled Canister Characteristics		
	Glass	Calcine
Approximate weight of waste (kg)	660.0	248.0
Fuel equivalent (t uranium/can)	2.5	3.1
Energy equivalent (MWe-y/can)	81.0	100.0
Volume (m^3)	0.2	0.2

FIG. 11. Reference waste canister.

- Heat is removed by the constant circulation of the pool water in direct contact with the canisters and is transferred to the atmosphere through open cooling towers.
- The chloride ion concentration in the water is maintained at less than 10 ppm.
- All operations during interim storage take place within a building that remains sealed under normal operating conditions.
- When out of the water the canister is usually protected by a transfer cask capable of protecting the canister from damage if it is dropped. The only time the canister is not protected by the transfer cask is during insertion into and removal from the pool.
- Equipment within the area of the interim storage water basin is arranged so that the transfer cask cannot be moved over the basins; thus, the cask cannot drop into the basins.
- The air filtration system comprising stacked high-efficiency particulate-aerosol (HEPA) filters passes 10^{-11} of all volatiles released from canister accidents within the plant.
- The probability of filtration-system failure, 10^{-6} per y, is identical to the HEPA failure rate given in the WASH study of reactor safety (U.S. Nuclear Regulatory Commission, 1976b). The probability that filter failure will allow release of volatile materials from an accident within the sealed building is equal to the probability that the filter will fail within one week after the accident ($1/52 \times 10^{-6}$). One week is required to clean up failed canisters.
- If the filter fails within one week of an accident, 1% of the volatiles released within the building will escape into the atmosphere. The rest will condense inside the building.
- The probability of a canister being dropped by a crane is 3×10^{-6} per h of operation (U.S. Nuclear Regulatory Commission, 1976b).
- The probability of a crane stall is 1.5×10^{-6} per h of operation (Smith and Ross, 1975).
- The time spent handling each canister in air outside the cask is 20 min, including time for insertion into the pool, retrieval, and insertion into a transportation cask.

HANDLING EVENTS

There are two significant events during which radionuclides might be released from SHLW at a fuel-reprocessing plant (FRP): a handling crane might stall and a canister might be dropped outside the storage pool. An event tree that summarizes these possible accidents and their important consequences appears in Fig. 12.

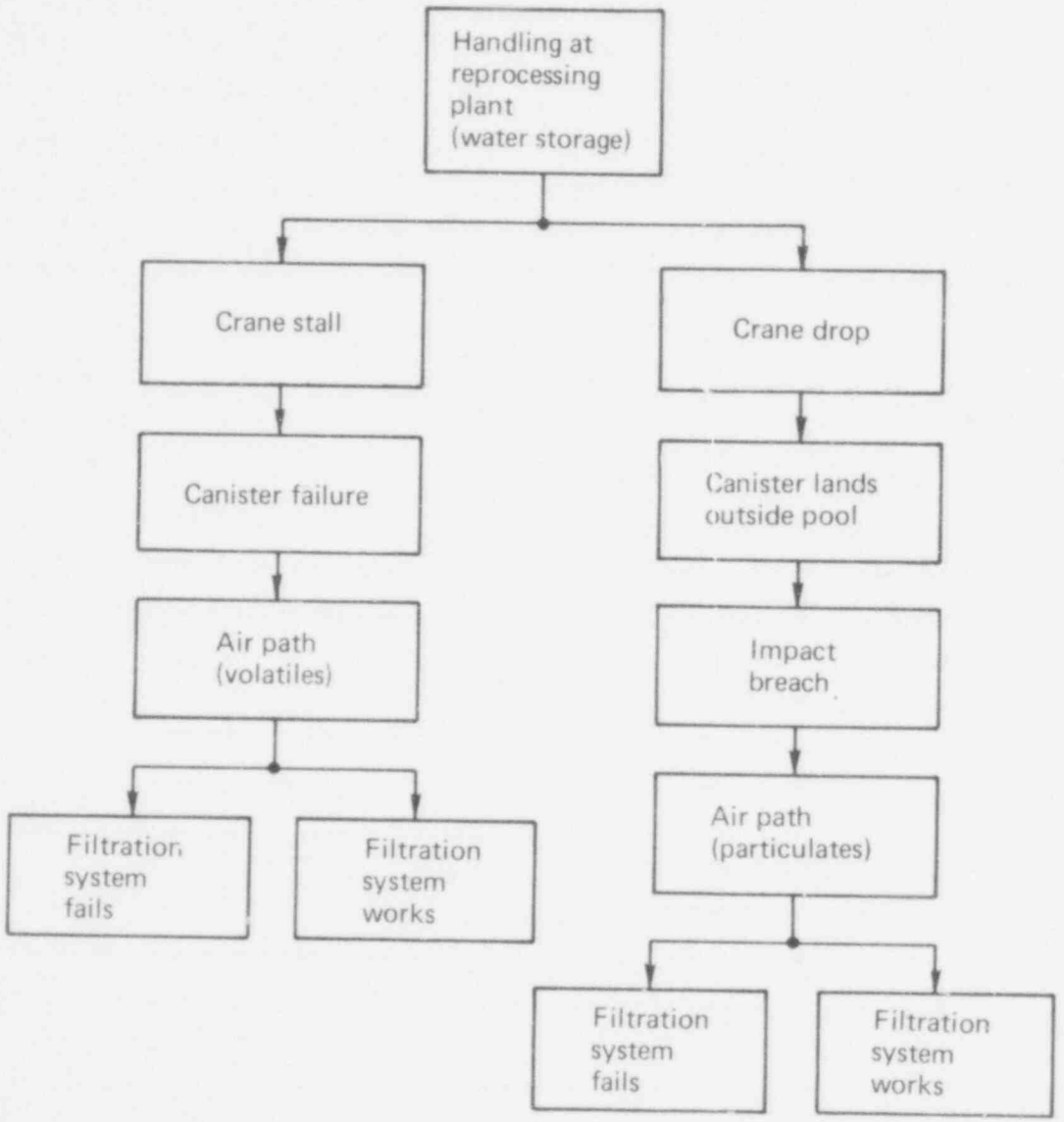

FIG. 12. Interim storage event tree.

During a crane stall the only significant danger is that the canister will melt from decay heat; however, we found that the probability of canister melt is zero. Heat transfer calculations show that enough heat is dissipated by convection to keep the canister wall below the critical temperature. Considering the right-hand branch of the tree, we found the probability of canister breach to be zero as well.

Probable Release Fractions

Given the assumptions outlined in the introductory discussion above, we need consider only one consequence of a crane stall: canister melt.

Crane Stall. Heat transfer calculations for a canister containing a 1-y-old glass, suspended in air, give a steady-state wall temperature of about $750^{o}K$ ($900^{o}F$). For a canister containing 5-y-old diluted calcine, the temperature is $490^{o}K$ ($428^{o}F$).

For a canister filled with glass waste, corrosion by the waste is predicted to be the critical process. Failure by this mechanism would require a temperature of $1470^{o} \pm 50^{o}K$ ($2190^{o} \pm 90^{o}F$) for several hours. For a canister filled with calcine waste, the corresponding failure temperature is estimated at $1570^{o} \pm 50^{o}K$ ($2370^{o} \pm 90^{o}F$) since creep or corrosion would likely cause failure somewhat below the melting point.

Since the steady-state canister temperatures are well below the estimated failure temperatures, we estimate the release fraction to be zero for the crane stall.

Crane Drop. With a crane drop, the maximum height from which a canister might fall is not likely to be greater than 4 m since we do not expect the canisters to be handled at heights that exceed its length by more than 1 m. Although the water basin is deeper than 4 m, no release would occur if a canister fell into the pool because the water would substantially reduce the impact velocity of the canister.

526 0/1

Smith and Ross (1975) dropped flat-bottomed canisters on their corners--a more severe test than dropping canisters with hemispherical bottoms (like the reference canister). The tests showed no canisters breached when dropped from a height of 9.15 m (30 ft) and about half of them breached when dropped from more than 20.7 m (68 ft). We conclude, therefore, that the release fraction would be zero for all canister-drop accidents at the interim storage facility.

Maximum Expected Releases

To calculate the maximum expected values for released waste, we ignore our estimates that the release fractions are zero during handling accidents and assume that 100% of the available volatiles (Cs, Ru, and Te) are released into the building that houses the pool. This conservative assumption is made to demonstrate that the expected release from handling accidents at the interim storage site is insignificant compared to expected releases from other portions of the waste management sequence, even if unrealistically high release fractions from the canister are used.

Crane Stall. The probability of a crane-stall accident per canister of solidified waste is

$$1.5 \times 10^{-6} \frac{\text{stalls}}{\text{h of operation}} \frac{1 \text{ h operation}}{3 \text{ can.}} = 5 \times 10^{-7} \frac{\text{stalls}}{\text{can.}} .$$

Since we have made the conservative assumption that each stall releases all of the volatiles in the canister into the sealed storage building, 5×10^{-7} of all volatiles handled will be released as a result of crane stalls. The amount that then enters the atmosphere depends on whether the filtration system fails or not.

If we approximate the probability that the system continues to work as 1, then the maximum expected fraction of the volatiles that reach the atmosphere with the filter operating is

$$(1)(10^{-11})(5 \times 10^{-7}) = 5 \times 10^{-18} .$$

Since the probability of filter failure is

$$(10^{-6} \text{ per y})(1 \text{ y}/52 \text{ wk}) = 1.92 \times 10^{-8} \text{ per wk} \quad ,$$

the maximum expected fraction of the volatiles that reach the atmosphere following a failure is

$$(1.92 \times 10^{-8})(10^{-2})(5 \times 10^{-7}) = 9.6 \times 10^{-17} \quad .$$

Since this value is about 20 times as large as the maximum expected release during normal filter operation, the maximum expected release (in Ci/MWe-y) from all crane-stall accidents is 10^{-16} times the activity of volatiles in one MWe-y of waste. We will show that this figure is small relative to releases expected during interim storage and transportation accidents. Population distribution differences used in dose calculations do not alter this conclusion.

Crane Drop. Similar calculations yield the maximum expected release for a crane-drop accident. The probability of a crane drop is twice that of a stall. Also, more radioactivity (in Ci) is available for release since particulates as well as volatiles will be released. All other numbers in the calculation are the same. Consequently, the maximum expected value of radioactivity (in Ci/MWe-y) released to the atmosphere from all crane-drop accidents is about 2×10^{-16} times the activity of all radionuclides in one MWe-y of waste. This figure will also be shown to be small relative to releases during interim storage and transportation accidents.

Storage-Pool Events

As shown in the event tree in Fig. 13, two accident scenarios were considered: loss of coolant circulation and catastrophic loss of coolant due, for example, to a basin rupture following an earthquake. For these two possibilities, we found that the second would contribute a major risk, whereas the first would not. (We found that even if cooling circulation were lost--owing, say, to pump failure--coolant lost by boiloff would continue to

be replaced by makeup water. The canisters would thus never be exposed to air and would never fail.) In both cases absolute values of expected risk are sensitive to modeling assumptions.

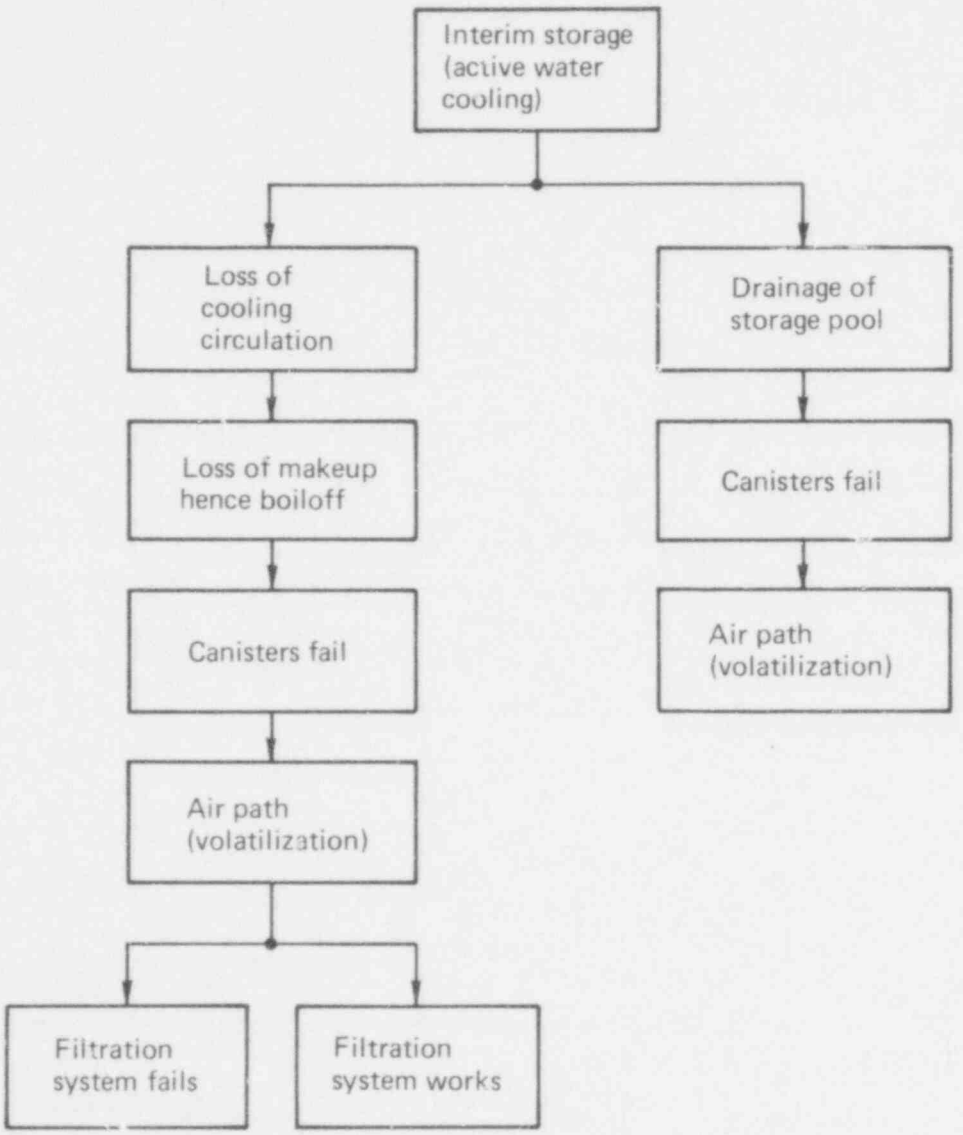

FIG. 13. Interim storage LOCA event tree.

A thermal analysis was performed to (1) set up a computer model to determine the thermal behavior of SHLW canisters as a function of time in an interim storage loss-of-coolant accident (LOCA) and (2) apply this model to representative solid waste forms.

Thermal Analysis

During interim storage at a surface storage facility, high-level wastes are contained in stainless-steel canisters, which in turn are grouped in regular arrays and located in a concrete basin filled with water to remove heat generated by the waste. A seismic event or other catastrophic accident could cause rupture of the basin and loss of the coolant water. As a consequence, canister failures could occur because of corrosion or melting of the canister wall. The speed of failure depends on the heating rate of the wastes and on the geometry of the canister array.

Modeling of the thermal response of single canisters and of multiple canister arrays was done by Janson et al. (1974). Of particular interest were their analyses of transient temperatures following an instantaneous loss of cooling water from a surface storage facility. This facility was assumed to consist of 506 waste canisters, each producing 5 kW of heat, set into a rectangular concrete basin. Janson's approach was to use a model that represented the system by a small number of nodes interconnected by a network of thermal transmittances. The Analytic Sciences Corporation (TASC) has developed a similar, but expanded, method that differs from Janson's in the following ways:

- The HEATING5 code (Turner et al., 1972) was used to solve the finite difference heat-flow equations. Although a one-dimensional parameter approach was used by TASC for initial results, a full two-dimensional treatment of heat transfer through the waste-canister array is possible for more accurate computations in the future.
- Results were obtained for a variety of waste forms and ages, hence for a variety of heat-generation rates.

- Heat transfer between the waste canisters and naturally circulating air was modeled by TASC to reflect more accurately the actual air-flow rates and convective transfer coefficients.

The configuration used by TASC was nearly the same as that treated by Janson:

- An open 36-ft-wide basin measuring 36-1/2 × 18-1/2 ft.
- Canisters 1 ft in diameter and 10 ft long, spaced 18 in. center-to-center.
- A total of 506 upright canisters in two layers, one directly above the other, with a 1-ft spacing between layers.
- Instantaneous loss of cooling water to initiate the temperature excursion.
- Cooling of the canisters by the mechanisms of natural convection, radiation to space, radiation to the concrete basin walls, and conduction through the concrete walls.

Waste Forms. The waste forms included in our analysis were spray calcine and borosilicate glass, with ages ranging from 1 to 10 y after reprocessing. The wastes were assumed to be diluted so that 10-y-old wastes would produce 3.5 kW of heat per canister. With this dilution, the heat-generation rates per canister for the other ages studied were: 7.4 kW for 5 y, 18.1 kW for 2 y, and 32.8 kW for 1 y.

Model Geometry. As shown in Fig. 14, the waste canister array was modeled as a single block of homogeneous material (waste and canister) having a volume of 12,680 ft^3 (359 m^3). To simplify computations this rectangular solid was represented by a cylinder of equivalent volume and height. This approximation gave the advantage of a two-dimensional geometry with axial symmetry. The cylinder dimensions were: radius, 13.9 ft (4.24 m); height, 21 ft (6.4 m).

A concrete ring 4 ft (1.2 m) thick was assumed to surround the waste block with an air gap between the waste and the ring. The thermal conductivity of the concrete was chosen low enough that the thermal resistance of the wall was essentially infinite. The height of the concrete ring was 36 ft (11 m). A mass of air was located on top of the waste block. The boundary condition between the air and the waste block simulated natural convective heat flow

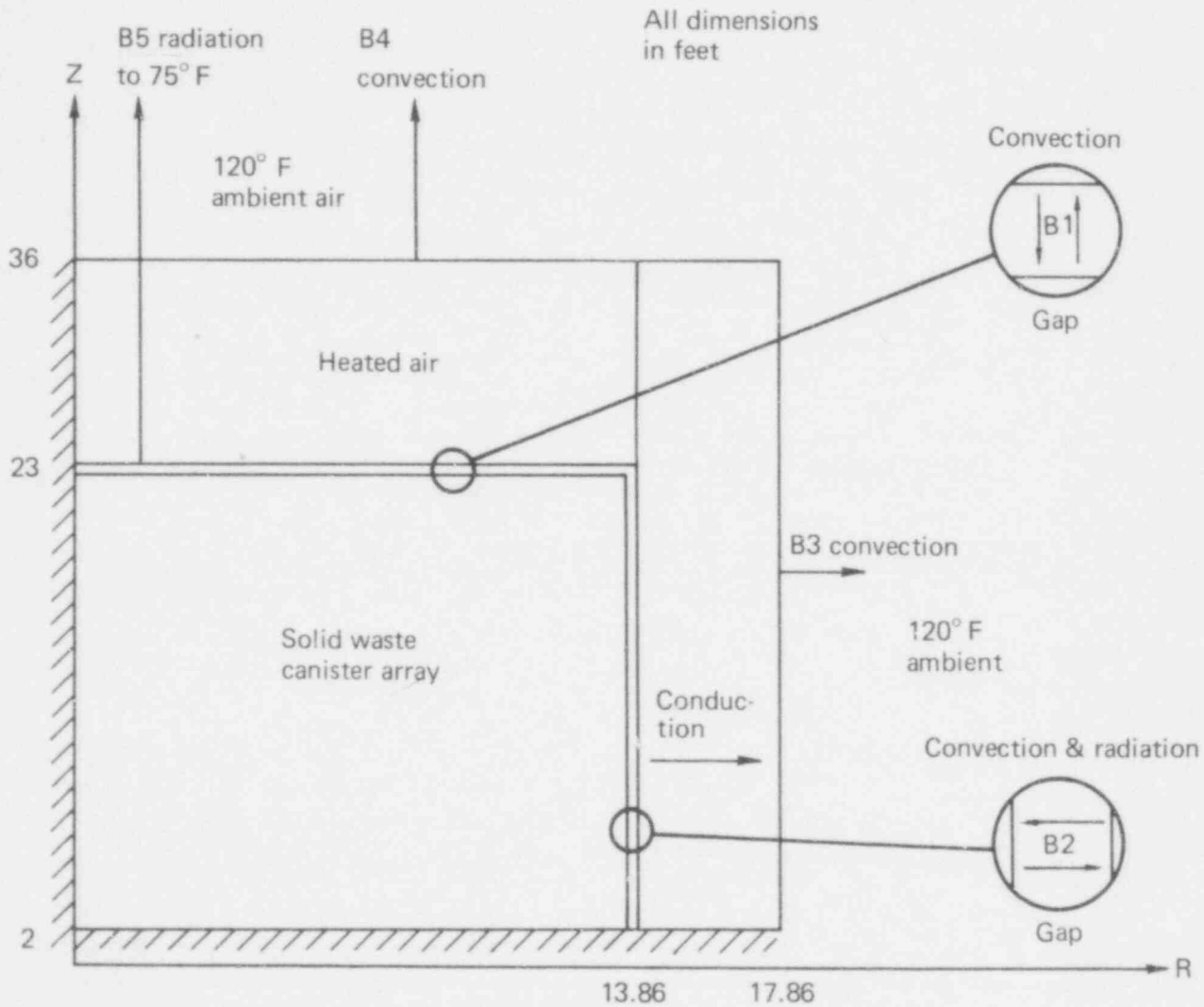

FIG. 14. Geometry for interim storage thermal model.

526 077

between canister surfaces and air. The simulation of the heat transfer process is described in more detail in Appendix A.

Material Properties. Table 7 lists the material properties used in the thermal calculations. All values were taken to be independent of temperature. In addition, we made the following adjustments:

- Thermal conductivity values for air and waste were made very high (greater than 10^3 Btu/h-ft-^{o}F) to give essentially uniform spatial temperatures. Hence derived temperatures are spatial averages, and radial and axial gradients are neglected.
- Density values for glass and calcine were averaged over the waste block and were reduced from their normal values because of the large air volume.
- Heat capacity values for glass and calcine were adjusted to include a contribution from the stainless-steel canisters.

TABLE 7. Material properties.

Material	Conductivity, Btu/h-ft-^{o}F	Density, lb/ft^3	Specific heat, Btu/lb-^{o}F
Glass	$>10^3$	83.8	0.1700
Calcine	$>10^3$	43.5	0.156
Air	$>10^3$	0.06	0.237
Concrete	0.792	131.0	0.210

Results. Loss-of coolant accidents were simulated by HEATING5 for times up to 40 h following coolant loss. In addition, a steady-state run was performed for each simulated accident to determine the temperature distributions a very long time after the accident. Runs were made for the following: 1-y-old glass, 2-y-old glass, 5-y-old calcine, and 10-y-old glass. Figures 15 through 18 show the 40-h temperature profiles, plus the steady-state temperatures, for these four wastes.

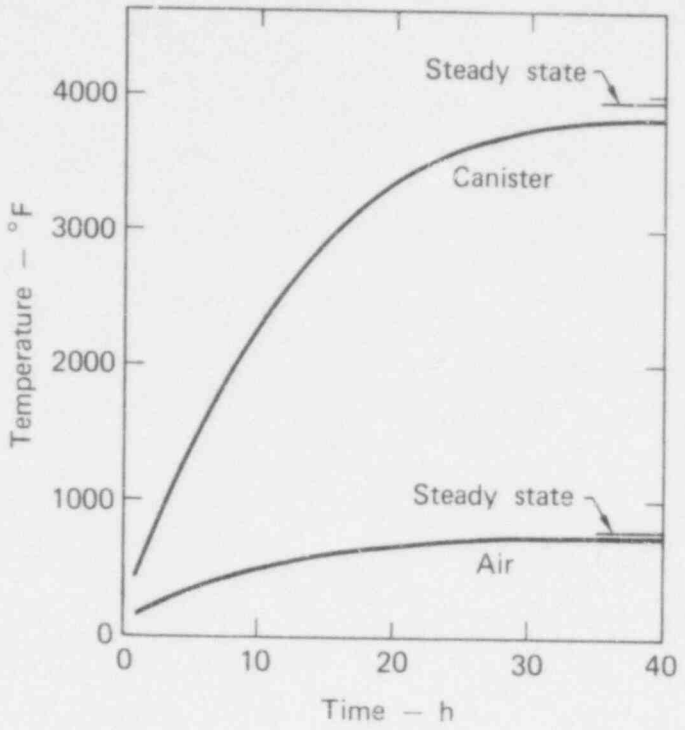

FIG. 15. Loss-of-coolant temperature profiles: 1-y-old glass.

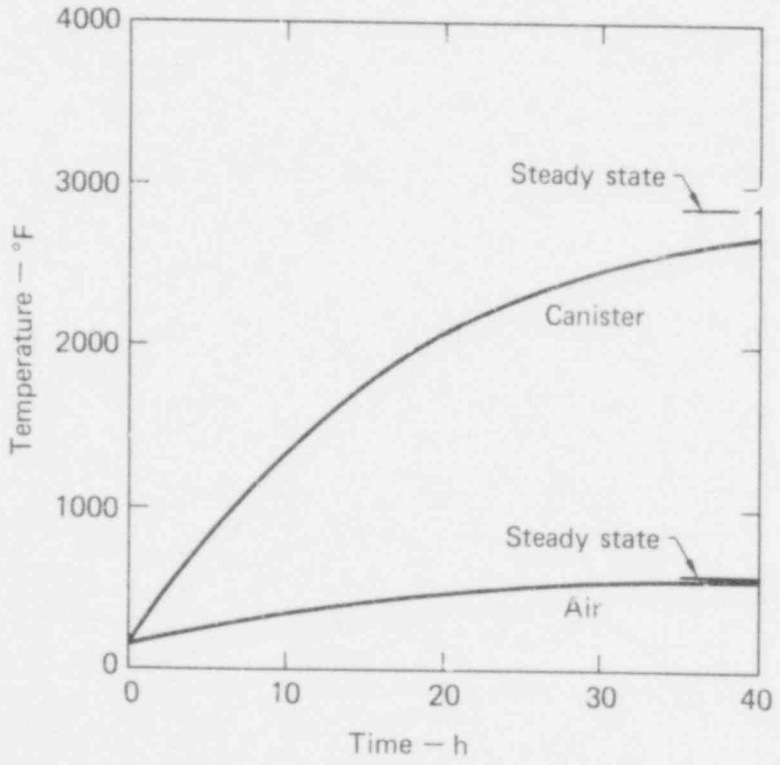

FIG. 16. Loss-of-coolant temperature profiles: 2-y-old glass.

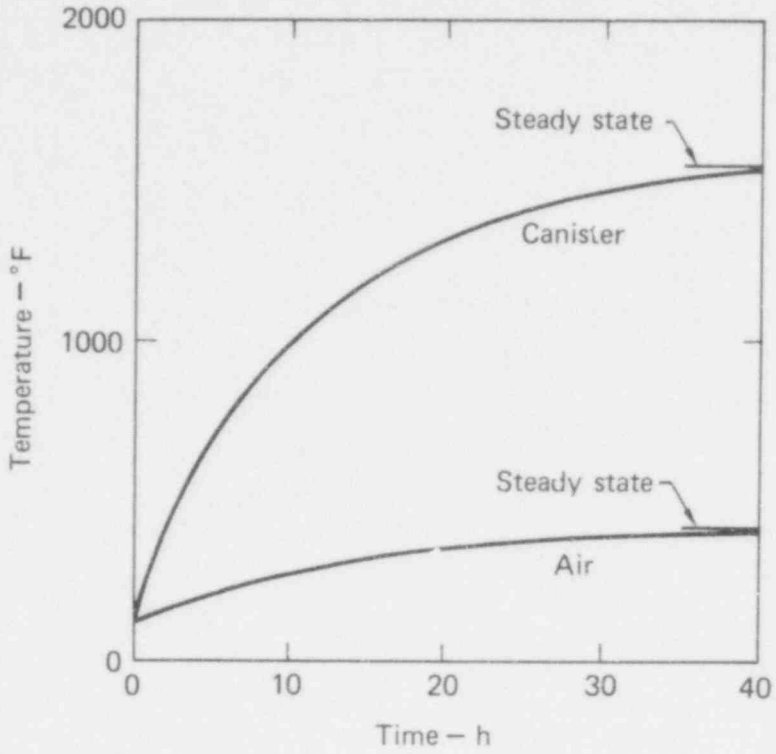

FIG. 17. Loss-of-coolant temperature profiles: 5-y-old calcine.

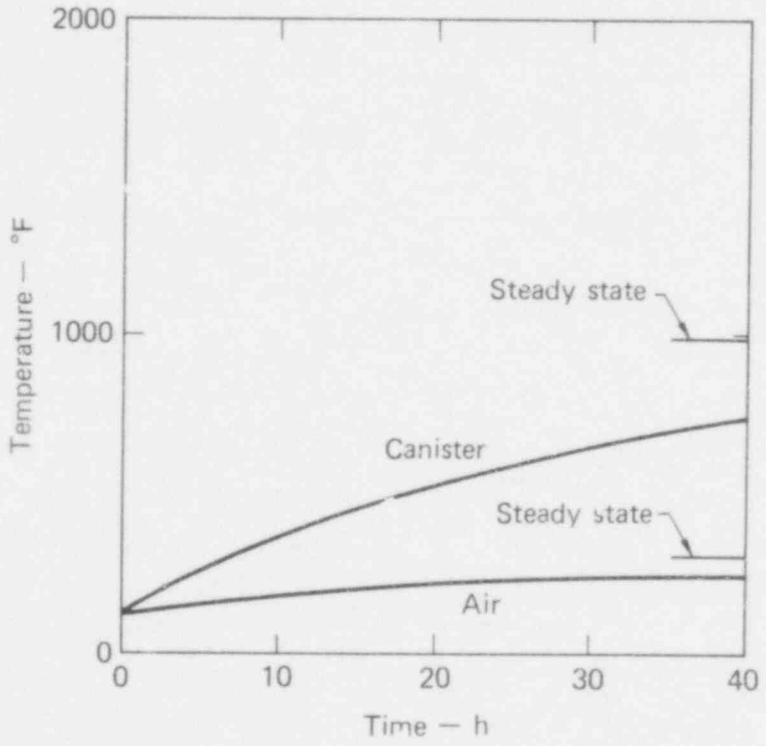

FIG. 18. Loss-of-coolant temperature profiles: 10-y-old glass.

The figures illustrate both the average canister temperatures and the average air temperatures. For glass and calcine of the same age, the steady-state temperatures are the same. The temperature profiles are different, however. Because of its lower heat capacity, the calcine approaches the steady-state more rapidly.

To evaluate the probability of canister failure, it is desirable to have an estimate of the peak canister temperature rather than the average. An exact computation of this kind, which requires calculation of the radiation transfer from canister to canister in a large array, is difficult. However, a rough determination of the difference, ΔT, between the peak central-canister temperature and the average canister temperature was carried out by approximating the canister array as a series of concentric rings, each with an emissivity equal to that of the canister surface. The results are shown in Table 8. The temperature differences are relatively small.

TABLE 8. Differences between peak and average canister temperatures.

Age of waste, y	ΔT, ^{o}F
1	11
2	17
5	36
10	72

Canister failure due to rapid corrosion of the stainless steel requires temperatures above $1470^{o}K$ ($2190^{o}F$) for glass and $1570^{o}K$ ($2370^{o}F$) for calcine. Using these criteria we can predict whether canisters containing glass or calcine wastes would fail in an interim storage loss-of-coolant accident (Table 9). Failure or survival depends on the rate at which heat is generated by the waste, thus for a given dilution, on the waste age.

TABLE 9. Results of study of interim storage loss-of-coolant accidents.

Waste age, y	Heat rate, kW	Result	
		Glass	Calcine
1	32.8	Failure	Failure
2	18.1	Failure	Failure
5	7.4	No Failure	No Failure
10	3.5	No Failure	No Failure

SECTION 3

TRANSPORTATION

REFERENCE SHIPPING CASKS

The first step in evaluating transportation risks was to establish conceptual designs for a railroad shipping cask and a truck shipping cask. With the designs established, we had to verify that they would meet current regulations, i.e., type-B packaging specifications 10 CFR 71 and 49 CFR 173.398. Computer calculations confirmed that our reference casks would survive the accident conditions spelled out in the specifications. Both impact and thermal calculations were done.

Shipping casks designed specifically for shipping SHLW have never been built. In fact, a recent survey of the literature showed that only two conceptual cask studies (Perona et al., 1970; and Perona and Blomeke, 1972) have been published. Several scale models for SHLW shipment have recently been built and exhibited under an ERDA-funded research contract, but information on full-scale designs has not been made public. However, since SHLW containers are expected to resemble the casks currently available for spent fuel, we decided to use modifications of currently licensed spent-fuel shipping casks as our reference designs.

A recent ERDA study (U.S. Energy Research and Development Administration, 1976) states that most shipments of SHLW are expected to be made by rail. Truck shipments are technically feasible but less efficient, and probably less economical. Since the current study does not include economic considerations, however, we have analyzed reference designs for both a truck cask and a rail cask.

Licensed spent-fuel casks that had been fabricated when the reference designs were needed included the following:

For rail shipment	IF-300
	NLI-24/10
For truck shipment	NFS-4 (NAC-1)
	TN8/9
	NLI-1/2

For rail shipment of 10-y-old SHLW, either cask could easily satisfy the thermal requirements of the waste. However, we had initially planned to investigate shipment of more active wastes (approximately 1 y old) and on that basis selected the uranium-shielded IF-300 cask. We also felt that the cavity size and thermal characteristics of the IF-300, in general, could better accommodate the transport of 12-in.-diameter waste cans. We plan to examine alternative cask configurations but do not expect them to change the risk assessment much.

Selection of the truck cask, was more arbitrary, since all three casks are similar in design. We selected the NFS-4 cask because its 34.3-cm (13.5-in.) diameter opening was considered a good match for transporting one 30.5-cm (12-in.) diameter canister.

Rail Shipping Cask

The GE IF-300 spent-fuel cask, which is the basis of the reference rail shipping cask, has been described by General Electric (1973). The salient features of the modified cask, depicted in Fig. 19, are the following:

- A cavity 95 cm (37.5 in.) in diameter and 3 m (10 ft) long cortaining four SHLW canisters 30.5 cm (12 in.) in diameter.
- A dry stainless-steel insert surrounding the canisters and acting as a heat transfer medium.
- A depleted-uranium gamma-ray shield 10 cm (4 in.) thick.
- A water neutron shield 12.7 cm (5 in.) thick on the outside of the cask, enclosed by a corrugated stainless-steel outer sleeve.

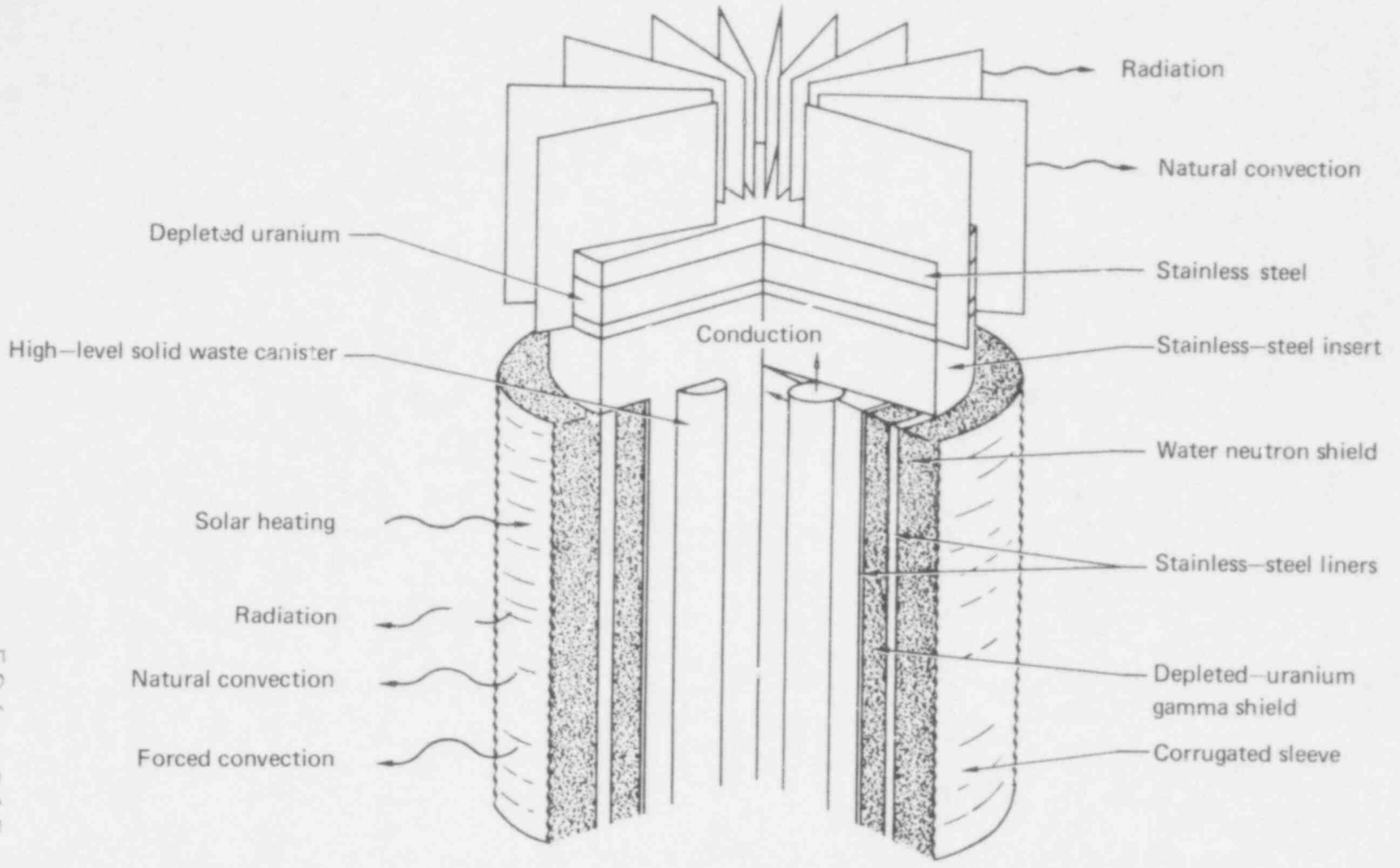

FIG. 19. Reference rail shipping cask.

- Finned ends to act as impact limiters and to augment heat transfer to the ambient air.
- A stainless-steel Grayloc seal ring to prevent the release of the contents (Grayloc is a trademark of the Gray Tool Co., Houston, Texas).
- Mechanical cooling (by fans) during transportation.

Truck Shipping Cask

The only major modification to the Nuclear Fuel Services NFS-4 (NAC-1) cask was to reduce the cavity length to coincide with present SHLW canister designs. The reference cask was rated for a maximum internal decay-heat load of 12.4 kW. Other important characteristics of the reference design (Fig. 20) are:

- A cavity 34.3 cm (13.5 in.) in diameter and 3 m (10 ft) long containing one SHLW canister 30.5 cm (12 in.) in diameter.
- Lead gamma-ray shielding 16.89 cm (6.65 in.) thick.
- Steel end caps 20.3 cm (8 in.) thick, with attached 30.5 cm (12 in.) balsa-wood impact limiters and an asbestos sheet.

Accident Scenarios

The modified designs were confirmed by ensuring that they conformed to the Code of Federal Regulations for the shipment of radioactive material, i.e., the type-B packaging criteria of 10 CFR 71 and 49 CFR 173.398. We then analyzed the responses of the casks to a series of accidents considerably more severe than those specified in the regulations. Although these accidents are highly unlikely, we included them to determine the expected risk and releases from all possible transportation events and to establish the thresholds for the release functions. All the accidents examined are listed in Table 10.

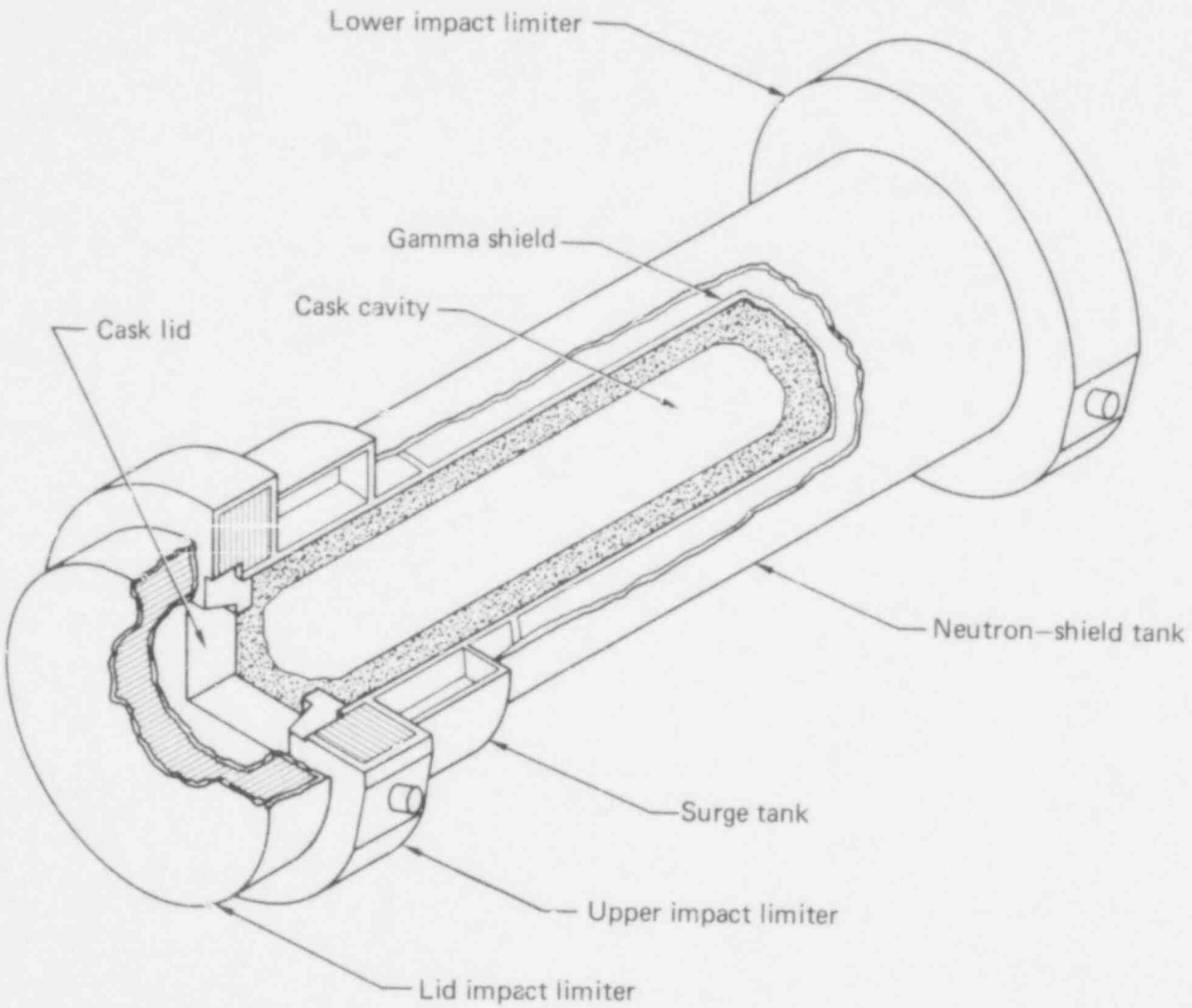

FIG. 20. Reference truck shipping cask.

TABLE 10. Accident conditions investigated for shipping casks.

Accident conditions	Rail	Truck
Normal steady-state characteristics for all reference waste forms at 10 y	x	x
Nonfire accidents (10-y-old glass and calcine)		
(a) Loss of neutron-shielding water owing to a faulty valve or puncture of the corrugated sleeve	x	
(b) Loss of mechanical cooling	x	
(c) Both (a) and (b), simultaneously	x	
Fires (10 y-old glass only)		
(a) Moderate-temperature fire such as the 1475°F, 30-min fire, type B	x	
(b) 3-h cool-down after type B fire	x	
(3) Severe high-temperature fires in excess of 1890°F that may cause waste-canister damage:		
1890°F	1-h fire	
2100°F	18-h fire	8-h fire
2400°F	12-h fire	6-h fire
2700°F	6-h fire	4-h fire
Impact accidents (all drops simulated impact with an unyielding surface)		
(a) Flat-bottom end drop from: equivalent height for 30-mph impact (30 ft)	x	
equivalent height for 60-mph impact (120 ft)	x	
equivalent height or 80-mph impact (214 ft)	x	
(b) Corner drop with center of gravity above the corner	x	

CASK FAILURE MECHANISMS

Fire

The high heat capacity of the SHLW transport casks makes it unlikely that a fire of relatively low heat output could supply enough energy to cause gross melting of the cask material. The casks most vulnerable to melting are probably those incorporating lead shielding, since the melting point of lead is 600°K (621°F), compared with 1405°K (2070°F) for uranium, 1673°K (2550°F) for stainless steel, and 1809°K (2797°F) for iron. (The formation of eutectics of steel and uranium, although important, is still not a concern below the melting point of lead.) Even with a lead-shielded cask, gross melting of the steel shell of the cask is unlikely.

A more likely serious consequence of a fire is that certain key components, which might be more sensitive to temperature, would fail. Depending on the cask design, these parts may include the seal, the pressure-relief system, the fill and drain valves, or other components. To determine the threshold for cask breaching due to fire, we identified these components for the cask design in question, estimated the conditions (temperature and length of exposure) under which they would fail, and performed heat transfer calculations to see if and when these conditions might occur in various fire scenarios.

The most likely thermal failure processes are creep, differential thermal expansion, oxidation (including combustion), corrosion, and melting. Of these mechanisms, creep, oxidation, and corrosion are Arrhenian processes, where a threshold temperature for failure is not so easily defined as it is, for example, for melting. Nonetheless, to make it easier to determine release thresholds, we have extended the concept of a failure temperature to Arrhenian processes. This is the temperature at which the component of interest will fail if held there for a time that is characteristic of the scenario being studied. Fortunately, the exponential nature of Arrhenian failure mechanisms makes the failure temperature relatively insensitive to the time chosen. This can be understood as follows. The "progress toward failure" can be characterized as the product of the rate of the process and the time. A given

component will fail when this product reaches a critical value. The rate has an Arrhenian temperature dependence:

$$R = R_o \exp(-E/kT) \quad ,$$

where R_o is a constant, E is the activation energy for the process, k is Boltzmann's constant, and T is the absolute temperature. Failure depends on an expression that includes both time and temperature ($R_o t e^{-E/kT}$), where t is the time. For a given value of this expression, the temperature is relatively insensitive to large uncertainties in time; hence the failure temperature concept is valid even when the time is not well defined.

The most accurate way to determine failure temperatures is to make thermal tests on duplicates of the actual components of interest. Second best is to use test data for components that are made of the same materials and that are similar in size and design. (For example, Machine Design (1964) gives sustained temperature limits for gasket materials.) In the absence of data, we can only make estimates from a general knowledge of processes in similar materials. The size of the breach produced in a fire accident can likewise be estimated from the design of the cask and from the way materials behave at high temperatures.

In using heat transfer calculations to simulate fires, the simplest approach is to assume that the fire completely surrounds the cask, presenting it with a uniform ambient temperature and conditions for effective emissivity. This situation is more severe than likely in an actual fire accident, hence our assessments of risk are conservative.

We have assumed the following sequence for fire accidents:

1. The fire surrounds the cask and burns continuously at a constant flame temperature.
2. The neutron-shielding water surrounding the cask is either lost by boiling off through a pressure-relief valve or lost through a puncture.
3. The cask and canister temperatures increase. The temperatures at the ends of the rail cask rise more rapidly than the middle because of the

higher surface-to-mass ratio there. For the truck cask the ends are insulated by balsa wood and asbestos, so the middle heats up more rapidly.

4. The canister(s), reach the failure temperature and fail by processes that depend on the waste form.
5. Depending on the waste form, ^{134}Cs, ^{137}Cs, and ^{106}Ru escape from the canister(s). Since the cask is hotter than the canister(s), it no longer presents an effective barrier to volatiles or to particulates.
6. The SHLW remains at a high temperature for about 4 h in the rail cask, 2 h in the truck cask. Nuclides continue to escape by volatilization and particulate dispersion.
7. The cask cools and volatilization stops. Particulate dispersion continues unless the waste has melted into a monolithic mass.

Specific assumptions for the analysis of the truck cask are (1) the rapid disappearance of the balsa-wood impact limiters, and (2) the very rapid loss of the neutron-shielding water, plus disintegration of the outer neutron-shield tank wall. Specific assumptions for the analysis of the rail cask are (1) the integrity of the corrugated sleeve in fires below 1350°K (2000°F) and (2) loss of the corrugated sleeve in fires above 1350°K (2000°F).

Impact

Three main approaches to predicting cask behavior during an impact accident have been used in the past: full-scale drop tests, scale-model drop tests, and numerical simulations and calculations. Full-scale testing, although the most direct approach, has been limited because shipping casks are expensive. Model studies are cheaper, but the scaling must be carefully verified. Numerical simulations of the transient dynamic responses of materials, involving plastic deformation and complex geometries, can be very costly in computer time. Besides, they too require verification of the models used.

With any of these approaches, we must select the orientation of the cask at impact, the rigidity of the impact surface, and the velocity of impact. The most common procedure in the past has been to attempt to meet the requirements of the Type-B package standards (10 CFR 71), which are "a free drop through a

distance of 30 ft onto a flat, essentially unyielding, horizontal surface, striking the surface in a position for which maximum damage is expected."

The corner drop is postulated to be the most severe of the many possible accidental drops. A corner drop is defined as a drop in which the center of gravity is directly above the corner that strikes the unyielding surface. In terms of radioactive release, a corner drop on the end of the container containing the bolted closure is the worst case. Such a drop produces a bending moment that can cause the bolts to fail.

Impact energy is absorbed by lateral steel fins in the rail cask and by balsa wood in the truck cask. However, any type of energy-absorbing system is limited by its maximum deflection. Because the regulations require survival in a 30-ft (9-m) drop, the energy-absorbing systems are usually designed to survive nothing worse. Increasing the drop height beyond 30 ft (9 m) will make the cask itself absorb the excess energy, thus increasing the potential for damage.

The canisters may act as a secondary barrier against the release of radioactive material, but this analysis has assumed that any accident that could cause the closure lid to fail would produce enough acceleration to release radioactive material from the canisters. Once the closure lid is removed, there is nothing to stop the canisters from coming out of the shipping container, and motion of the container after the drop is likely to make the canisters fail.

In an actual impact accident where a cask-carrying vehicle strikes a large object, the front of the vehicle would likely strike the object first. The object would then yield, the extent depending on the size of the object and the materials it is made of. Furthermore, the vehicle structure itself would deform plastically. It would absorb some of the kinetic energy of the cask, the amount depending on the strength of the tiedowns. In a rail accident further energy would be dissipated in derailment and disturbance of the rail bed. In severe accidents the cask itself might then strike the object, perhaps being cushioned by part of the vehicle structure trapped between the cask and the object. Because of these several mechanisms,

the velocity of the cask at impact would be less than the initial vehicle velocity. However, the axis of the cask at impact would most likely remain nearly parallel to the axis of the vehicle before impact; the cask is not likely to rotate significantly between the time of vehicle impact and the time of cask impact, because of the cask's large moment of inertia. In contrast, the angle between the vehicle and the object will have a range of values for different accidents.

In the face of these complexities, we have made several conservative approximations. First, we have chosen to model the impact accidents in two ways: one is to use the modified HONDO code for axial (end-on) impacts, and the other is to use the analysis given by General Electric (1973) for corner impacts, both on unyielding surfaces. Details of the impact analysis for the rail shipping cask are given in Appendix B. The corner-impact calculations were used to derive the release functions, since it is a better approximation of actual impacts. As a result, our approximation is conservative, since we chose the angle for which maximum damage is expected.

Our second approximation was to partially account for the rigidity of real objects by using only the accident probabilities for "extremely rigid" objects (Clarke et al., 1976). We believe this approach conservative, since even objects such as trains and bridges are not completely rigid.

Finally, we took the velocity (V_c) at impact to be given by $V_c^2(\text{mph}) = V_o^2(\text{mph}) - 3000$, where V_o is the vehicle velocity at impact. This equation assumes that a constant amount of cask kinetic energy is used in deforming the vehicle structure, independently of impact velocity. The constant value of 3000 was derived from a fit made to the two data points available from recent truck impact tests at Sandia-Albuquerque (reported in a private communication by H. R. Yoshimura, 1977). The cask impact velocity was 27 mph for the 60-mph collision and 62 mph for the 84-mph collision. We have used the same equation for the rail impact accidents. Obviously, the factor to which we have assigned the value 3000 depends on the vehicle and the tiedowns used. Tiedown standards are currently under discussion (proposed American National Standards Institute standard N14.2 for trucks, draft ERDA standard RDT F8-12 for trains). In view of the many uncertainties, we have

chosen to base our model on the available data from the Sandia tests, recognizing that improvements in this area may be needed later.

Puncture

Our analysis of puncture accidents showed that they presented no significant risk. We base this conclusion on the finding that the probability of an accident severe enough to rupture the shipping cask is negligible (see Fig. 21). Even if the general characteristics of the cask are modified or if more severe accidents are determined to be credible, the analysis of puncture accidents will remain secondary to that of impact accidents for the following two reasons:

- The SHLW characteristics that are critical in impact accidents include those critical in puncture accidents.
- The impact accident is considered to be a greater threat to the shipping cask than the puncture accident because the cask has a steel shell and thick walls. In uranium-shielded casks, the high density of uranium adds to the protection from penetration. It is unlikely that

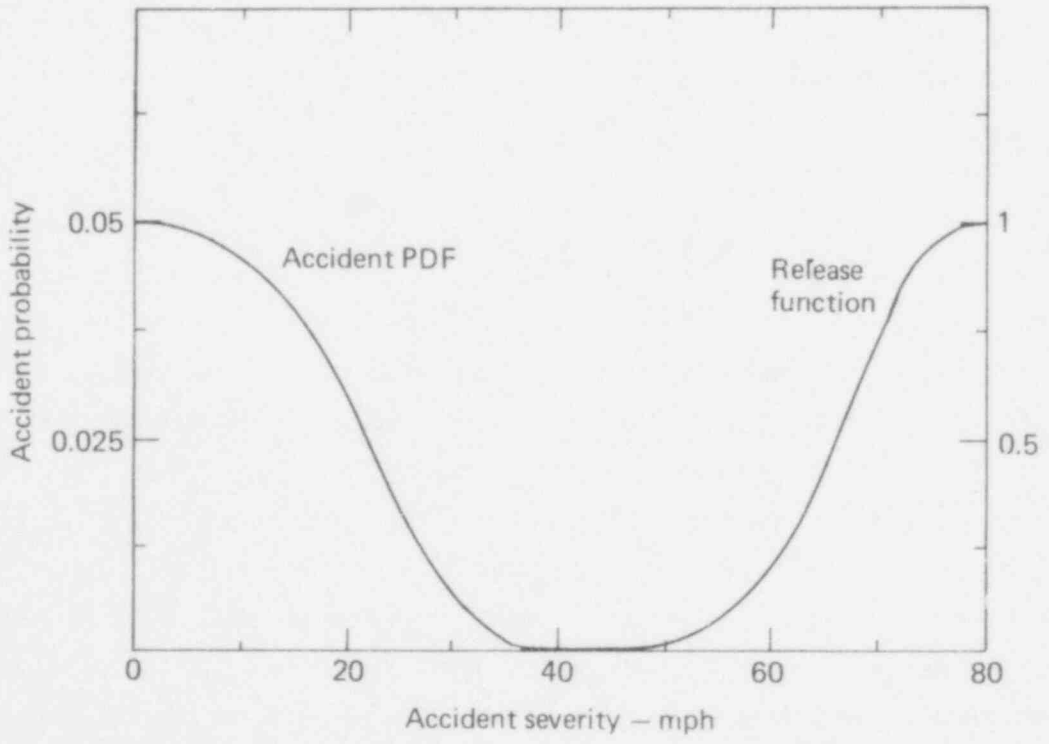

FIG. 21. Probability distribution function for accidents and release function for puncture accidents.

526 094

a penetrating object with enough energy to breach the cask will be present in an accident. Puncture of the thin water jacket, though more likely, merely makes heat dissipation more difficult, thus raising the internal temperatures. This event is less severe than the fire accidents we have analyzed.

Rupture by Thermal Shock

It is conceivable that an overheated shipping cask could be rapidly immersed in water. This might happen, for example, in a fire accident as a result of attempts to extinguish the fire. This raises the possibility that the cask might rupture because of the thermal shock. We have not analyzed this possibility in detail since it was beyond the scope of the effort; however, the outer shells of the casks are generally constructed of austenitic stainless steels, which we believe to be strong and ductile enough to withstand such thermal shock. Furthermore, the outer skin of the water jacket would make rapid cooling of the surface of the main body of the cask less likely, as would formation of a water-vapor layer at the surface of the hot cask. Besides, release of the SHLW could occur only if the canisters as well as the cask were breached, an event that seems unlikely during a plausible scenario.

Internal Pressure Buildup

Shipping casks usually have a pressure-relief valve that keeps the internal pressure below the design limit for the cask. In addition, it appears that casks without water inside the main body will not contain any materials that could generate significant pressures unless the temperatures exceed those that would produce failure by another mode first. Therefore, bursting of a cask containing SHLW does not appear to be a significant threat.

Defective Sealing

It is assumed that a standardized procedure of supervisory checks and tests for leak-tightness would be adopted for processing SHLW shipping casks. It is nonetheless conceivable that, as result of human error, a cask might not be

properly sealed. We have not analyzed the probability of such an occurence. We should note, however, that even if this should occur, there would be no release of SHLW unless some other event breached the canisters.

Explosive Attack

Explosive attack was not considered in this study.

Combinations of Failure Mechanisms

This study does not consider combinations of breaching mechanisms.

CANISTER FAILURE MECHANISMS

The canister failure mechanisms and the rates at which they take place depend on the materials involved. The following discussion pertains to the calcine and glass waste forms in canisters made of 304L stainless steel.

Overheating

Canisters could be overheated by (1) internally generated radioactive decay heat, (2) externally applied heat during a fire, or (3) adjacent canisters, as in an interim storage loss-of-coolant accident. Several temperature-dependent mechanisms come into play at high temperatures. Canister failure could result from a single mechanism or a combination of them.

Corrosion by Heated Waste. Stainless steels are protected from corrosion by an oxide layer that forms and adheres at the surface. For rapid general corrosion to take place, this layer must be removed. This is likely to occur only when the waste is molten. Then the oxide can dissolve readily in the melt and its concentration can be lowered at the interface by convection in the waste.

The gross melting point of spray calcine and fluidized-bed calcine is near 1670^{o}K. Since the melting point of the stainless steel is about the same, general corrosion by these calcines will probably not be a significant

concern. Intergranular corrosion of steel by calcines has not been thoroughly studied; however, Maiya and Busch (1973) have reported on the corrosion of 304L stainless steels by cesium oxide. They found kinetics that were linear with time, with a penetration rate given by

$$k(cm/s) = (2.90 \pm 1.78) \times 10^{-3} \exp(-9500/T) \quad ,$$

where T is the temperature in degrees Kelvin. At this rate it would require temperatures well above the melting point of the steel to penetrate a few millimeters in a few hours. Therefore, we do not regard intergranular corrosion as a significant mechanism for these calcines in 304L canisters.

Slate and Maness (1977) have reported general corrosion data for borosilicate-glass waste in 304L canisters. A fit to these data produced the equation

$$k(mm/h) = 9.38 \times 10^{17} \exp(-61,800/T) \quad ,$$

where T is expressed in degrees Kelvin. Applying this equation to a canister thickness of 9.5 mm, we find that a temperature of 1570°K is required to produce failure by this mechanism in 1 h, 1492°K in 10 h, 1413°K in 100 h.

Supercalcine multibarrier canisters are assumed to fail at 1270° ± 200°K, since nickel from the stainless steel dissolves in the molten lead. However, the alumina coatings on the pellets are taken to fail by cracking only at 1570° ± 100°K, according to J. Rusin at BNWL (private communication, 1977).

External Oxidation in Air. The rate of oxidation of 304L stainless steel in air is taken to be

$$k(mm/h) = (5.25 \times 10^{9}) \exp(-34,111/T) \quad ,$$

where T is the temperature in degrees Kelvin. This equation is a fit to the curve given by Angerman and Rankin (1977), which in turn is based on data from Miller et al. (1944). This equation is roughly compatible with the rate of 35 mm/y at 1348°K, reported by Slate and Maness (1977).

Applying this equation to a 9.5-mm-thick canister containing spray or fluidized-bed calcine, we find that the temperature needed to cause failure in 1 h would be above the melting point of the steel. Failure in 10 h would require a temperature of 1600°K. Hence, failure would occur in about 10 h at temperatures slightly below the melting point of stainless steel.

In the case of borosilicate glass, oxidation would penetrate about 2 mm under the conditions that would cause failure due to corrosion by the glass. Thus it appears that oxidation could contribute to a failure, but would not be the dominant process.

No data are available on the rate of the nickel-lead corrosion mechanism that occurs in supercalcine multibarrier canisters. However, at a temperature of 1600°K, oxidation and internal corrosion would be competing processes.

Creep. At about 770°K, creep begins to be measurable in 304L stainless steel for stresses below the room-temperature yield stress. At 1270°K, 304L can support stresses of a few kpsi (a few tenths MPa) for a few hours. Between 1470° and 1570°K, the strength of the steel becomes quite low (Hickey, 1973).

For canisters containing spray calcine or fluidized-bed calcine, the stresses in the canister wall result primarily from gravity and internal pressure buildup. Both are expected to be low for the reference canister and waste. (Pressure buildup will be discussed later.) It therefore appears that creep would not cause a rupture until temperatures near the melting point of stainless steel were reached.

For canisters containing borosilicate glass, the canister wall is highly stressed at lower temperatures because of differential thermal contraction following waste solidification. When the wall is heated to temperatures where creep becomes important, however, this stress is relieved by differential thermal expansion and by softening of the glass. Stresses due to gravity and internal pressure are again expected to be low.

These observations suggest that creep will not be the dominant failure mode for glass-containing canisters and that it will come into play only near the melting point of stainless steel for calcine-containing canisters. We have not performed a detailed creep analysis for various canister orientations, but such a study would probably not alter these conclusions.

Melting. For 304L stainless steel, melting begins at about 1670^{0}K. If the canister were heated continuously and it were able to survive the other processes discussed above, it would fail by melting at this temperature.

Impact

The probability that a full canister will breach on impact, as well as the character and size of the breach, depends on the velocity at impact, the rigidity of the impact surface, the design of the canister, the canister material and waste material (including their thermal and mechanical histories), the temperature of the canister, and the geometry of impact. The only experimental data available are those of Smith and Ross (1975). In their work, all the flat-bottomed 304L stainless-steel canisters withstood drops from a height of 9.15 m (30 ft). About half were breached during impacts at 45 mph (equivalent to a drop from more than 20 m or 66 ft). The reference canister design has a rounded bottom and is expected to be even less vulnerable to impact.

Fractures in 304L stainless steel are expected to be ductile at plausible temperatures and strain rates. Thus we expect that the breach will normally be only a small crack--say, 10^{-3} times the canister area (Smith and Ross, 1975)--for impact velocities below 45 mph.

Puncture

A bare canister would more likely be breached if dropped onto a relatively sharp object than onto a flat surface. It is difficult to assess the likelihood of such an event without detailed knowledge of the facilities

and equipment to be used. It seems possible, however, to limit the height at which a canister might be handled or to design the facility so that no sharp objects are present

Defective Sealing

Any breach due to an undetected leak or a construction defect would be small, say 10^{-4} times the canister area. Such an event has not been analyzed in this study.

Corrosion by Water

Corrosion of the canister by storage-pool water was not analyzed in detail because it will not by itself lead to exposure of the public. Occupational exposure has not been considered in this study.

Rupture by Thermal Shock

Rupture by thermal shock due to rapid quenching of the canister seems unlikely. In fact, rapid quenching may be a part of the waste-processing procedure. If the canister survives quenching during processing, it will probably survive it later. Steels generally become ductile as the temperature increases, and at high temperatures are not prone to fracture.

Internal Pressure Buildup

There are several processes that might cause a canister to burst: helium buildup, due either to alpha decay of actinides or to (n, alpha) reactions of boron; radiolysis and thermal decomposition of waste; transmutations to gaseous species; or volatilization of any water accidentally added to the filled, baked-out canister before it is closed. Bursting could also result from an increase in the pressure of confined gases if they are heated. For the waste forms we have considered, all of which are heated to at least $1170^{\circ}K$ during processing, thermal decomposition is not a problem below temperatures at which the canister would fail by corrosion or melting (Gray, 1976). Nor is radiolysis significant for any of the forms considered. Only

if organic, nitrated, or hydrated materials were proposed as waste materials could radiolysis and thermal decomposition be serious. The only gaseous transmutation product appears to be iodine (from tellurium decay), and the quantity is too small to be important. Likewise, helium buildup is not important (Mendel, 1974). Finally, pressure increases in confined gases (assuming the perfect gas law) are insignificant for plausible temperature changes.

We thus conclude that pressure buildup is insignificant for the waste forms we have considered unless water were accidentally added to the canister before it is sealed. In this case, the canister could rupture at a temperature above the boiling point of water--373^{o}K (212^{o}F). The exact value would depend on the material and design details of the canister.

Pullout of Lifting Device

The top of a canister must be fitted with lifting tabs for handling (see Fig. 11). It is conceivable that the failure of a poorly designed lifting tab might breach the canister and cause a release of radionuclides. We have assumed that the reference canister is designed to avoid this possibility.

External Pressurization

When submerged in a body of water, a canister experiences increased external pressure. For canisters of reasonable thickness submerged at moderate depths, the stresses are too low to be significant.

Combinations of Failure Mechanisms

Combined effects have not been considered, except for the case of pressurization resulting from overheating, as discussed above.

RADIONUCLIDES RELEASE MECHANISMS

Dissolution

The process of dissolution includes both leaching, which involves selective diffusion of radionuclides from inside the waste matrix, and corrosion or etching of the solid waste by a solvent, in this case water. The mechanisms for both are complex and not well understood. Important variables are the chemical properties of the solid matrix, the chemical properties of the solvent, and the temperature at the interface between them. The flow velocity of the solvent and the state of the solid also influence the rate of dissolution. For a system with fixed chemical composition, temperature, and flow velocity, the data for a single radionuclide can usually be fit with an expression of the type

$$L = At^{1/2} \exp(-H_1/RT) + B \exp(-H_2/RT) + C \quad ,$$

where L is the dissolution rate in grams per square metre-second; t is the time in seconds after the solvent contacts the solid; A, B, and C are constants; H_1 is the activation enthalpy associated with leaching in joules per mole; H_2 is the activation enthalpy associated with corrosion in joules per mole; R is the gas constant (8.314 J/mole-^{o}K), and T is the temperature at the interface in degrees Kelvin.

The rate at which the radionuclide is released to the solvent is then given by the following equation, which assumes that the concentration of solutes in the solvent is constant:

$$S = L(t)A_L C_r \quad ,$$

where S is the rate of release in curies per cubic metre-second, L(t) is the dissolution rate at time t in grams per square metre-second, A_L is the effective area of exposed solid in square metres per cubic metre, and C_r is the concentration of radioactivity in the solid for the given nuclide, in curies per gram.

526 102

Unfortunately, there are not enough data to define uniquely all the parameters in the equation for L for all the waste forms and all the nuclides of interest. In addition, the flow properties of the solvent and the effective area A_L are not well defined under all relevant conditions. For the effective area, which depends on the condition of the waste, the canister, and the leaching medium, we have made appropriate approximations for the following three scenarios.

Canister Failure in Geological Storage. Although somewhat out of context in a discussion of transportation accidents, canister failure in geological storage will be discussed here since dissolution is the dominant release mechanism. The behavior of the canister during geological storage will depend on a complex interplay of chemical, thermal, and radiolytic processes, thus we have made the conservative assumption that the canister fails immediately after the repository is backfilled and sealed. In this case, A_L for the spray calcine is equal to about 10^6 m^2/m^3. For glass, A_L is equal to $20(r + h)/rh$, where r and h are the radius and length, in metres, of the waste block. This is simply ten times the outer surface area of the glass block (per unit volume), the factor of ten accounting for fractures.

Overheating and Contact with Water. Dissolution of the waste must be considered where the canister has been exposed to high temperatures out of water (for example, because of internal heat generation or fires), then exposed to water (for example, during attempts to cool an overheated canister or to put out a fire). A temperature high enough to breach the canister in this situation would melt borosilicate-glass waste. This waste would then flow from the canister until its surface area was great enough to allow it to cool and solidify. The spray calcine and fluidized-bed calcine would melt at about the same temperature that caused the canister to fail, so the wastes would most likely slump into a pile. The lead matrix in the supercalcine multibarrier form would also be molten at the canister failure temperature. The waste matrix would then flow from the canister if it were breached. The Al_2O_3 coatings on the supercalcine particles would crack off, and the exposed pellets would probably slump into a pile. For the calcine waste forms, we take A_L to be 10^6 m^2/m^3, and for borosilicate glass we use $20(r + h)/rh$. The calcine value decreases substantially if the waste melts.

Impact and Contact with Water. For canister impact velocities below 18 m/s (40 mph), we use $A_L = 0$ for glass wastes, because the canister will probably not be breached (Smith and Ross, 1975). For impacts at velocities between 18 and 36 m/s (40 and 80 mph), breaching occurs as small cracks near the point for impact. (Higher velocities for a bare canister do not seem probable.) For these breached borosilicate-glass canisters, the effective area depends on the size of the crack and the increased surface area of the glass that flows from the fracture. The area of the crack is approximately 10^{-3} of the canister surface area, and the glass surface area increases approximately by a factor of 10 at an impact velocity of 19 m/s (43 mph) (Smith and Ross, 1975). We thus use $A_L = 0.2(r + h)/rh$ for still water and $A_L = 2(r + h)/rh$ for flowing water.

Breaching is more probable at lower impact velocities for calcine canisters, so for spray calcine we take $A_L = 10^3\ m^2/m^3$ for still water and $A_L = 10^4\ m^2/m^3$ for flowing water.

Volatilization

Volatilization is simply the evaporation of chemical species from the waste at elevated temperatures. For this to occur, the nuclide of interest must first diffuse to the surface, then acquire enough energy to break its bonds with the body of the waste. A particular nuclide may evaporate as the element or as one of its oxides, depending on the partial pressures of oxygen and water in the surrounding gas phase, normally air.

The rate of release depends strongly on the temperature and the condition of the canister. If the canister is not breached, obviously no release will occur. The events most likely to cause the canister to breach, which we have described above, can be divided into two groups: those opening only a small crack in the canister, and those exposing a large fraction of the surface area of the waste.

The mechanism of volatilization through a crack depends on whether the combined vapor pressures of the species in the canister exceed atmospheric pressure. If the total vapor pressure is below atmospheric pressure, the only

way the radionuclides can escape is by gaseous diffusion through the crack, and a state approaching thermodynamic equilibrium will exist inside the can. (Strictly speaking, calcines and glasses are amorphous, nonequilibrium materials, thus the concept of equilibrium vapor pressure cannot be rigorously applied.) If the total is above atmospheric pressure, the gases will undergo viscous flow driven by the pressure difference. This will still be a near-equilibrium condition, but at a higher pressure. Calculation of the release by these mechanisms and of the temperature at which the total vapor pressure exceeds atmospheric pressure requires a knowledge of the vapor pressures as a function of temperature for the chemical species present.

In the case where a large fraction of the waste surface is exposed and where ambient air movement is rapid, the vaporization mechanism is closer to free evaporation of material from the surface, without back condensation. The process then appears to be limited by diffusion within the solid in the case of the spray calcine, fluidized-bed calcine, and multibarrier waste forms, and by a surface release mechanism for the borosilicate glass, which is molten at the temperatures of interest (Gray, 1976).

Since complete information is lacking, the best current approach is to make an empirical fit to existing data and to apply this fit to both of the above cases. We use this approach in the sections devoted to particular scenarios.

Airborne Particulate Dispersion

Radionuclides can also disperse as part of particulate matter spread by air currents. The respirable fraction of these particulates (less than 10 μm in diameter) is particularly important. As in the other processes, canister breaching is a prerequisite for particulate dispersion.

Particulate dispersion from borosilicate glass will be quite small unless an impact fractures the glass. In this case, since a high concentration of stress is needed to break glass into fine particles, we expect the fines to be localized in the canister near the point of impact. For release to occur, the canister must rupture at a spot adjacent to this region containing the fines.

Since stress concentration is responsible for both rupturing the canister and breaking the glass, both events are likely to occur simultaneously, and release is probable. The driving force for dispersion would then have to come from the mechanical energy of the impact or the motion of ambient air. It is hard to estimate these effects in the absence of a detailed canister design and a more complete understanding of the phenomena involved. Under the circumstances, we have chosen a model based on the data of Smith and Ross (1975).

Particulate dispersion may occur with spray calcine because its particles are small. This mechanism is a less serious problem with fluidized-bed calcine because its particles are larger, and with supercalcine multibarrier waste because breaching the canister would not expose the solidified waste pellets. If the multibarrier waste pellets were then exposed by high temperatures, the pellets would tend to stick together, thus making particulate dispersion unlikely.

Melting and Liquid Flow

The calcines (spray, fluidized-bed, and supercalcine) melt at about 1670^{o}K, a temperature difficult to maintain in a plausible accident scenario. In any case, volatilization would probably predominate at this temperature.

The glass softens at 820^{o}K and flows well at about 1170^{o}K. If it melted in an accident, it could spread on the floor or ground until its larger surface area allowed it to cool and solidify. The amount of spreading, however, would be minimal, thus melting appears to be an unimportant release mechanism.

RAILROAD EVENTS

In evaluating the risk associated with railroad transport, we considered accidents involving impact and fires in detail. Both air and water pathways were modeled to calculate expected values of risk, and a new method was developed for evaluating the release function.

To evaluate the risk from impact-induced radionuclide releases, we may follow the impact branch of the event tree in Fig. 22. As we have already described, it produced a bending moment that may cause the closure bolts to fail. An impact that causes cask failure would almost certainly rupture the canisters, subsequently releasing radioactivity. Using this observation as the basis of computed radioactivity release functions, and using available accident statistics, the expected value of risk can be calculated. The water path contribution was computed using a conditional probability of 10^{-2} that the waste enters a waterway.

In fire-induced releases, the canister is the critical component: breaching of the cask occurs because of early seal failure in a fire. Canister failures then occur because of corrosion of the wall by the melted glass or, in the case of calcine, by oxidation and creep of the wall. Since these mechanisms are Arrhenian processes, we have established discrete canister failure temperatures using the kind of analysis described under Cask Failure Mechanisms above. We have then treated heat transfer through the cask as a time-dependent process and thus defined a failure locus on a plot of fire temperature vs failure time. This failure locus describes the combinations of fire temperature and duration that will cause canister failure. The temperatures above which the canisters eventually fail are $1470^{o} \pm 50^{o}K$ for glass, $1570^{o} \pm 50^{o}K$ for calcine, and $1570^{o} \pm 100^{o}K$ for multibarrier.

The thermal analysis for the rail shipping cask is described below; the impact analysis is described in Appendix B. Release function and risk calculation details appear in Appendixes C and D, respectively.

Thermal Analysis

The HEATING5 computer code was the chief computational tool for performing the thermal analysis of the rail shipping cask. This code is described in detail by Turner et al. (1972). Basically, it is a generalized heat-conduction code designed to solve steady-state or transient heat-conduction problems using one-, two-, or three-dimensional Cartesian or cylindrical coordinates or

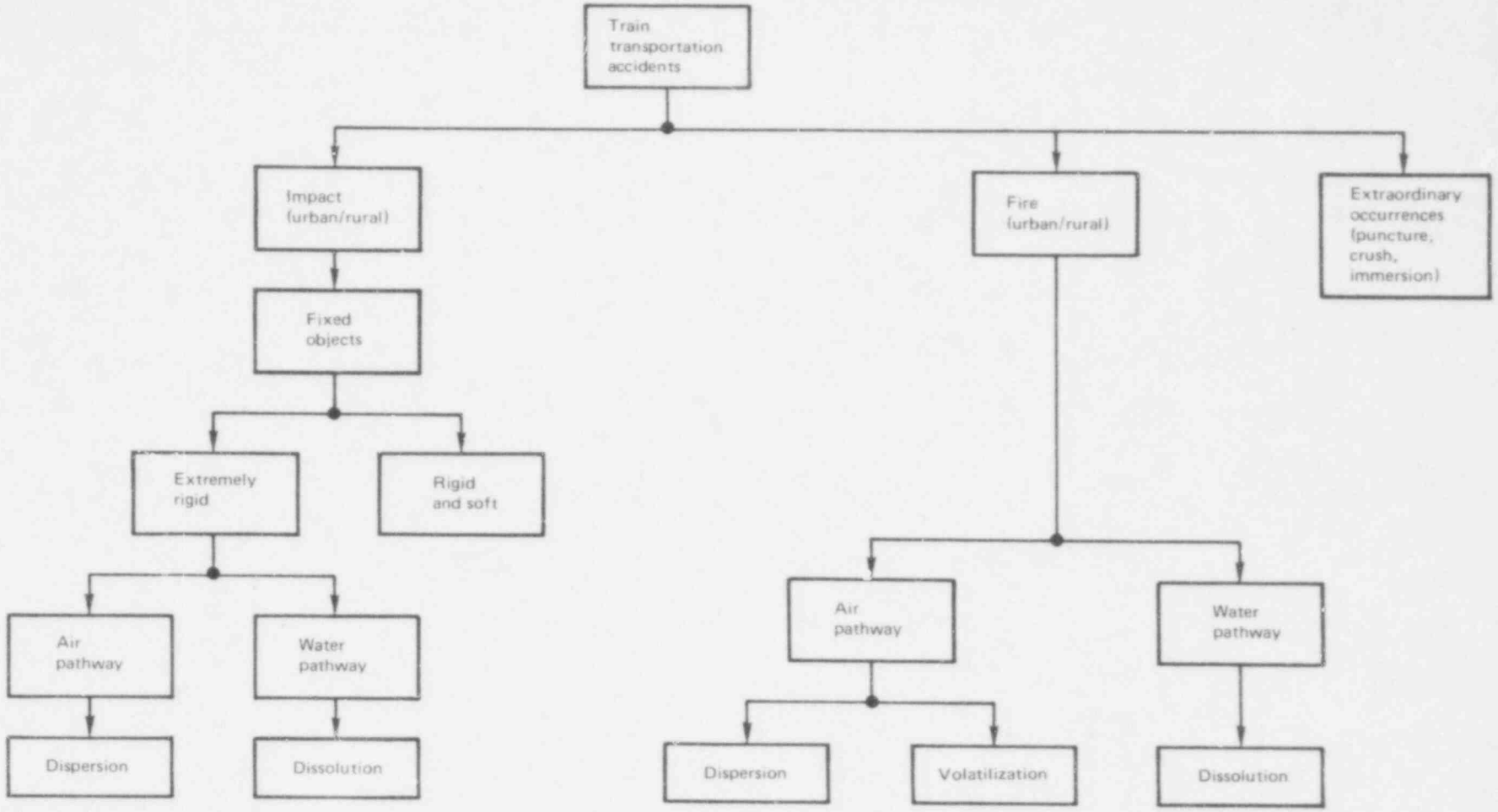

FIG. 22. Event tree for train transportation accidents.

one-dimensional spherical coordinates. Its flexibility can be emphasized by outlining its features:

- Thermal conductivity, density, and specific heat data may be spatially and temperature dependent.
- Thermal conductivity may be anisotropic.
- Materials may undergo a change of phase.
- Heat-generation rates may depend on time, temperature, and position.
- Boundary conditions, at surface-to-surface and surface-to-boundary interfaces, may be fixed temperatures or may depend on prescribed heat fluxes, forced convection, natural convection, and radiation.
- Boundary conditions may be time and temperature dependent.
- As many as 100 regions, 50 materials, and 50 boundary conditions may be specified.

The reference waste form for the analysis described below was 10-y-old borosilicate-glass solidified waste rated at 3.5 kW output. Except for the temperature distribution in the waste itself, the results apply to spray calcine, fluidized-bed calcine, and supercalcine multibarrier wastes as well, each rated at 3.5 kW output. We examined wastes with higher output only as part of preliminary studies intended mainly to test the adequacy of various cask and canister concepts for normal operation. The final designs, however, dictate the use of 10-y-old waste material.

Model Geometry. As can be seen in Fig. 19, the rail shipping cask has a complex, three-dimensional configuration. It was necessary to simplify the geometrical description of the cask and canister so that the thermal analyses could be done in a minimum of computer time. We decided that the most convenient way to proceed was to encode the cask geometry in two separate ways:

- An R-Z representation, which treats the cask as if it were radially symmetric, and which is used to examine temperature distributions axially and radially from a side view (Fig. 23).
- An R-θ representation, which treats the cask as if it were infinitely long, thereby ignoring end effects, and which is used to examine the radial and angular temperature variations from a top view (Fig. 24).

526 109

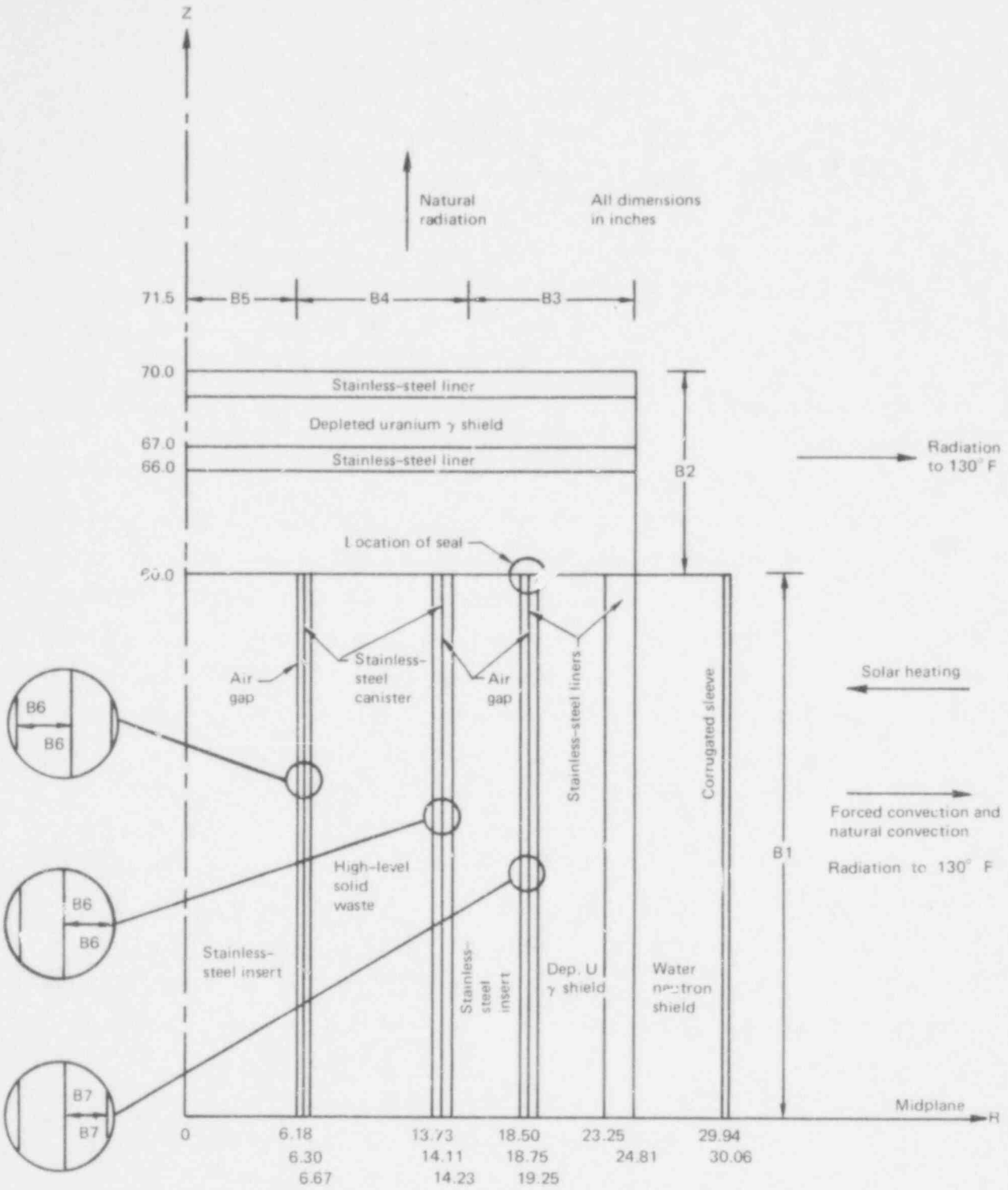

FIG. 23. Cross-sectional side view of modified GE IF-300 rail shipping cask as modeled for R-Z thermal analyses.

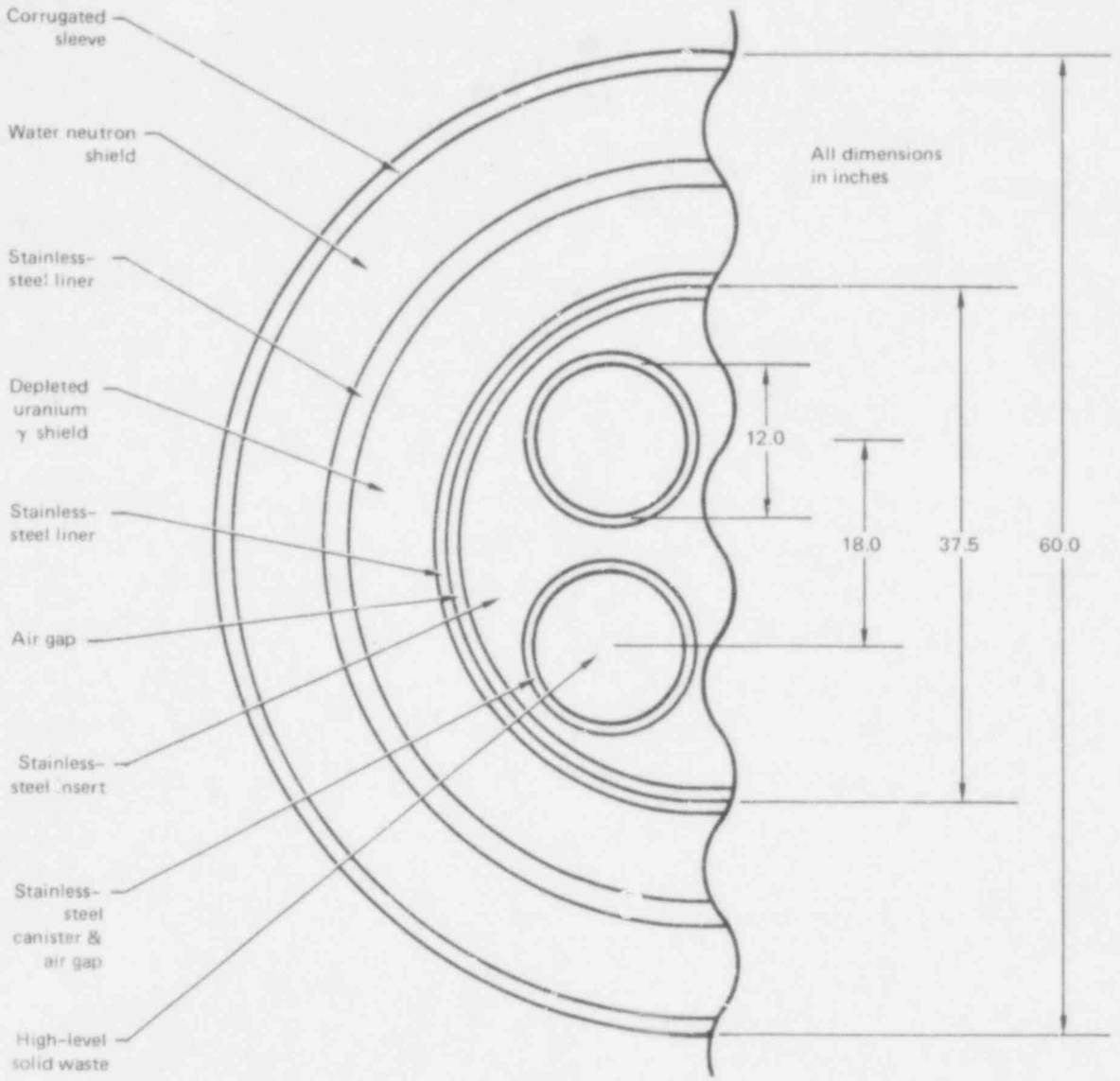

FIG. 24. Cross-sectional end view of modified GE IF-300 rail shipping cask.

We believe that the R-Z geometry gives a good picture of cask temperature profiles, although it does not provide a detailed picture of the distributions around the individual canisters. The R-θ geometry yields a better description of the canister temperatures, especially away from the cask ends and near the midplane. A combination of the two representations gives a complete thermal picture.

Since the HFATING5 code is restriced to regions defined by boundaries that are parallel to coordinate axes, it was necessary to make some approximations to the radially unsymmetric geometry of the cask. For the R-Z analysis, regions must be bounded by lines of constant radius (circles centered on the cask centering) and lines parallel to the central axis. The waste canisters themselves do not obey this restriction; they are cylinders, but are <u>not</u> centered on the central axis of the cask.

The solution was to convert the canister region into "equivalent" cylinders that could be handled by the code. Thus, the waste and the stainless-steel insert that surrounds the waste canisters (see Fig. 24) were mapped into three new regions: (1) a stainless-steel inner cylinder, (2) an annulus of waste material surrounded by thin annuli representing canisters and air gaps, and (3) an annulus of stainless-steel. Requirements for the dimensions of the waste annulus were as follows:

- The volume has to equal the total volume of the four waste canisters.
- The first moment of the mass distribution had to equal that of the actual waste cylinders.

These constraints made it possible to calculate the inner and outer radii of the waste region. These results appear in Fig. 23.

To use R-θ coordinates, the waste canisters in Fig. 24 must be described in terms of lines of constant radius (circles centered about the axis) and radial boundaries emanating from the axis. Thus the waste canisters were mapped into equivalent wedges, whose inner radius, outer radius, and wedge angle had to be determined. We obtained these unknowns from the following sufficient conditions:

526 112

- The wedge areas must be equal to the waste cylinder areas.
- The maximum distance between wedge boundary and the waste cylinder boundary must be as small as possible.

Figure 25 illustrates the R-θ geometry encoded into HEATING5, showing the smallest repeated unit (45^{o}). This symmetry cell includes half of one of the four waste canisters.

Boundary Conditions. The several boundary conditions specified in HEATING5 are indicated in Fig. 23 as B1, B2, etc. Each will be discussed below.

B1. Heat transfer mechanisms at the side of the cask include radiation and forced convection to the ambient air at $327^{o}K$ ($130^{o}F$) from a corrugated sleeve. We assumed a time-invariant solar flux of 1 Btu/h-in.^{2} Convection occurs over an increased area owing to the corrugations. The radiation view factor includes provisions for radiation to cask support structures as well as to ambient air. In scenarios in which there is accidental loss of mechanical cooling, the transfer coefficient for forced convection was replaced by a natural convection coefficient.

B2 through B5. There are four boundary conditions for the finned area of the cask since heat transfer coefficients for radiation and natural convection must accurately account for the geometry of the fins (see Fig. 19). Thus the boundaries B2 through B5 represent the following fin dimensions: B2 (6-in. fins), B3 (6-in. + 9-1/2-in. fins), B4 (9-1/2-in. fins), and B5 (no fins). Solar heating and forced convection are not heat transfer mechanisms at these boundaries.

B6 and B7. Internal boundary conditions allow for radiation and conduction across the air gaps. Emissivity of the canister was assumed to be 0.6, and that of the insert 0.3. During an accident involving loss of neutron-shielding water, radiation was also allowed across the neutron shield annulus, with conditions B7 applied to the surface-to-surface interface.

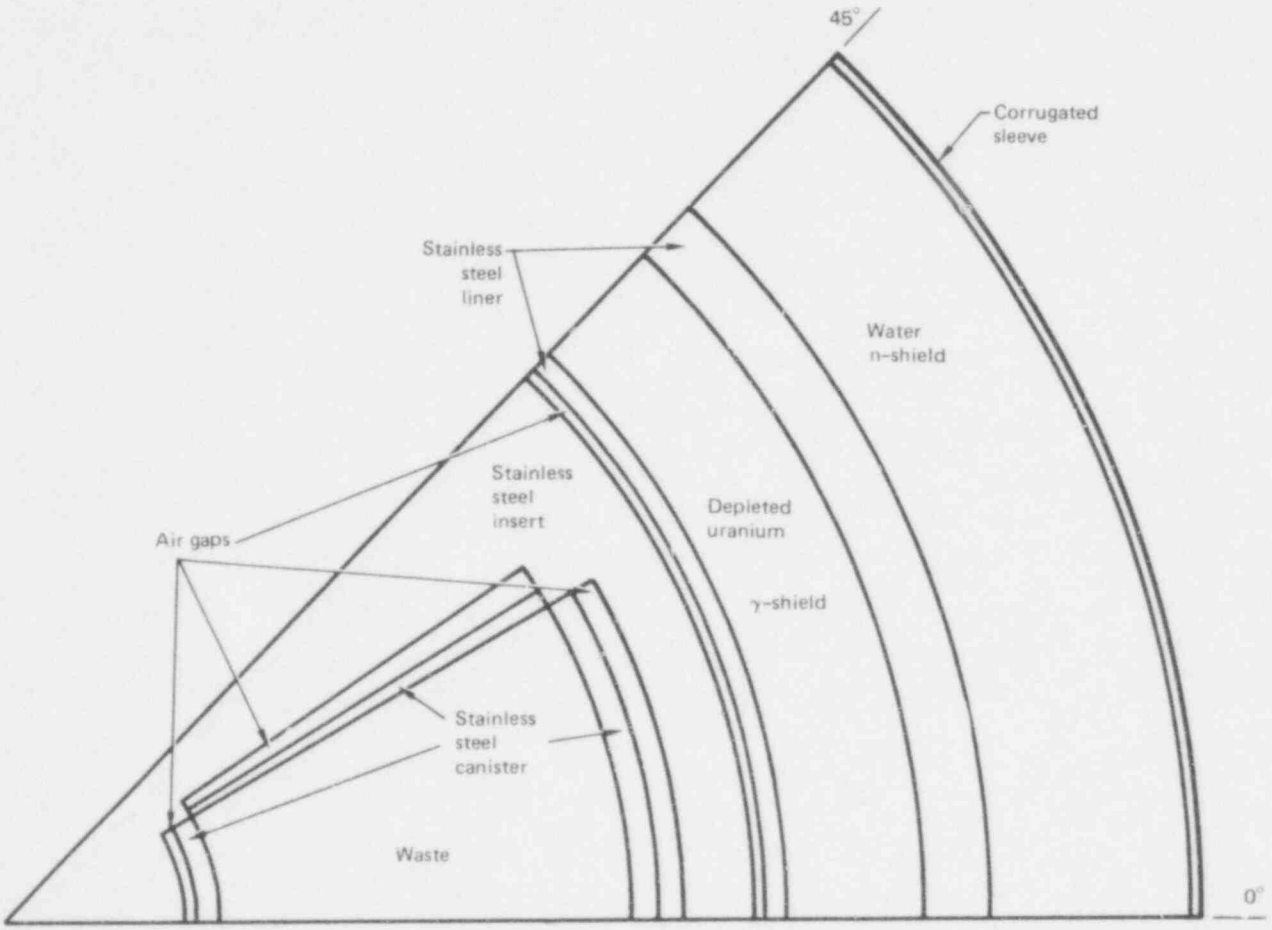

FIG. 25. Cross-sectional end view of modified GE IF-300 rail shipping cask as modeled for R-θ thermal analysis.

526 114

During fires the external boundary conditions change. The only important heat transfer mechanism is radiation from the flame at the flame temperature--1000^{o} to 1600^{o}K (1400^{o} to 2400^{o}F)--with an effective emissivity taken to be 0.8. Forced and natural convection and solar heating are insignificant. In the case of moderate-temperature fires--below 1350^{o}K (2000^{o}F)--the corrugated outer sleeve was presumed to remain intact except for loss of the water. The fire heats the sleeve, and heat is transferred across the air filling the annulus formerly occupied by the water. In severe fires--above 1350^{o}K we assumed that the sleeve would be destroyed, thus placing the external boundary at the outer gamma-shield liner.

Material Properties. The thermal properties of the shipping-cask materials are given in Table 11.

Results. Table 12 summarizes the results of the HEATING5 computer runs for the normal steady state, for nonfire accidents, and for a Type-B 1075^{o}K (1475^{o}F), 30-min fire. The table also includes results for a 3-h cooldown period following the Type-B fire, and for the postfire steady state. This last condition is equivalent to a steady state in which both shielding water and mechanical cooling have been lost. No potential damage modes are apparent for any of the conditions given in Table 12.

Figures 26 through 28 give temperature profiles for cask regions that are most likely to form release pathways for radioactive materials under severe fire conditions. In the R-Z geometry these regions can be described as follows: canister surface, axial endpoint (R = 13.73 in., Z = 60 in.); canister surface, axial midpoint (R = 13.73 in., Z = 0 in.); and seal (R = 18.75 in., Z = 60 in.). For each of the cases examined, critical temperatures are exceeded first at the canister endpoint. Table 13 summarizes the failure times for the various fires and waste forms.

TABLE 11. Thermal properties of rail-shipping-cask materials.

Property	Stainless steel (types 317, 403)	Air (narrow gap)	Air (wide annulus)	Water (with convection)	Depleted uranium	Glass HLSW	Calcine HLSW
Density ($lb/in.^3$)	0.285	$0^{\circ}F$: 5.00E-5 $500^{\circ}F$: 2.39E-5 $1000^{\circ}F$: 1.57E-5 $1400^{\circ}F$: 1.17E-5	$0^{\circ}F$: 5.00E-5 $500^{\circ}F$: 2.39E-5 $1000^{\circ}F$: 1.57E-5 $1500^{\circ}F$: 1.17E-5	0.361	0.683	0.126	0.0722
Specific heat ($Btu/lb-^{\circ}F$)	0.12	0.237	0.237	1.00	0.028	0.179	0.155
Thermal conductivity ($Btu/h-in.-^{\circ}F$	$100^{\circ}F$: 0.63 $300^{\circ}F$: 0.71 $500^{\circ}F$: 0.79 $800^{\circ}F$: 0.90 $1200^{\circ}F$: 1.05	$0^{\circ}F$: 1.09 $500^{\circ}F$: 2.05 $1000^{\circ}F$: 2.81 $1500^{\circ}F$: 3.45	0.0142	$150^{\circ}F$: 1.23 $200^{\circ}F$: 1.44 $250^{\circ}F$: 1.60 $300^{\circ}F$: 1.74 $400^{\circ}F$: 1.95	$100^{\circ}F$: 1.19 $300^{\circ}F$: 1.33 $500^{\circ}F$: 1.49 $800^{\circ}F$: 1.63 $1200^{\circ}F$: 1.83	$77^{\circ}F$: 0.0406 $1112^{\circ}F$: 0.0675 $1346^{\circ}F$: 0.1200	$32^{\circ}F$: 8.05 $1652^{\circ}F$: 18.8

TABLE 12. Summary of rail-cask temperatures (in ^{o}F), as computed by HEATING5 code, for nonfire accidents and type-B fire. Waste was taken to be 10 y old.

Location	Normal steady state	Loss of shielding water	Loss of mechanical cooling	1475°F, 30-min fire transient	3-h cooldown transient	Postfire steady state
Calcine } Waste	1340	1510	1380	1340	1340	1520
Glass }	708	883	751	708	709	904
Canister surface, axial midpoint	619	803	661	619	623	824
Cavity surface	447	571	495	448	464	590
Corrugated sleeve	172	165	257	1196	203	224
Seal	199	271	243	286	334	281
Cask top at axis	218	256	240	664	328	261

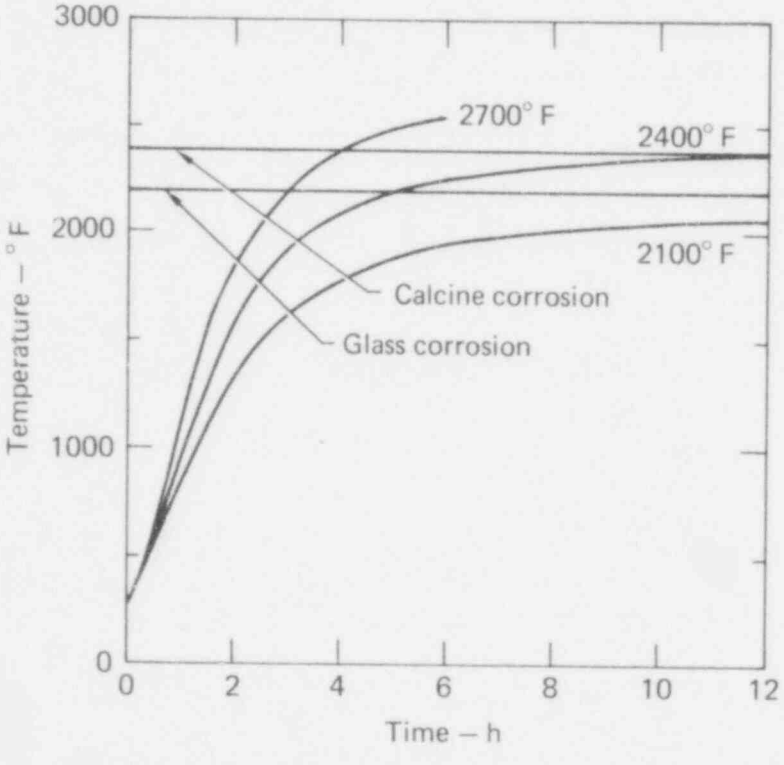

FIG. 26. Canister-endpoint temperature profiles for rail casks subjected to severe fires. The failure temperatures for glass and calcine waste are indicated by the horizontal lines; the three curves represent fires at the indicated temperatures.

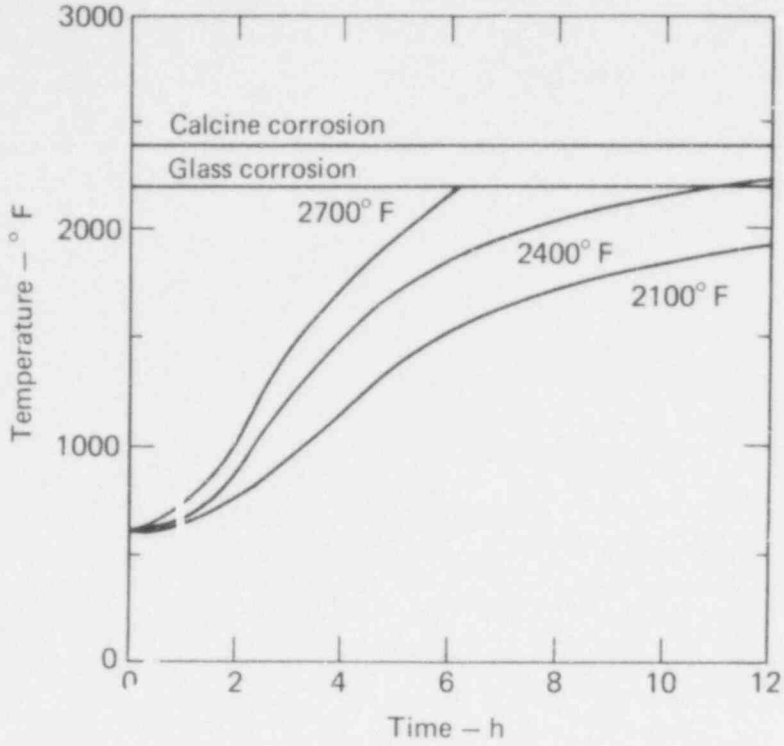

FIG. 27. Canister-midpoint temperature profiles for rail casks subjected to severe fires; other details as in Fig. 26.

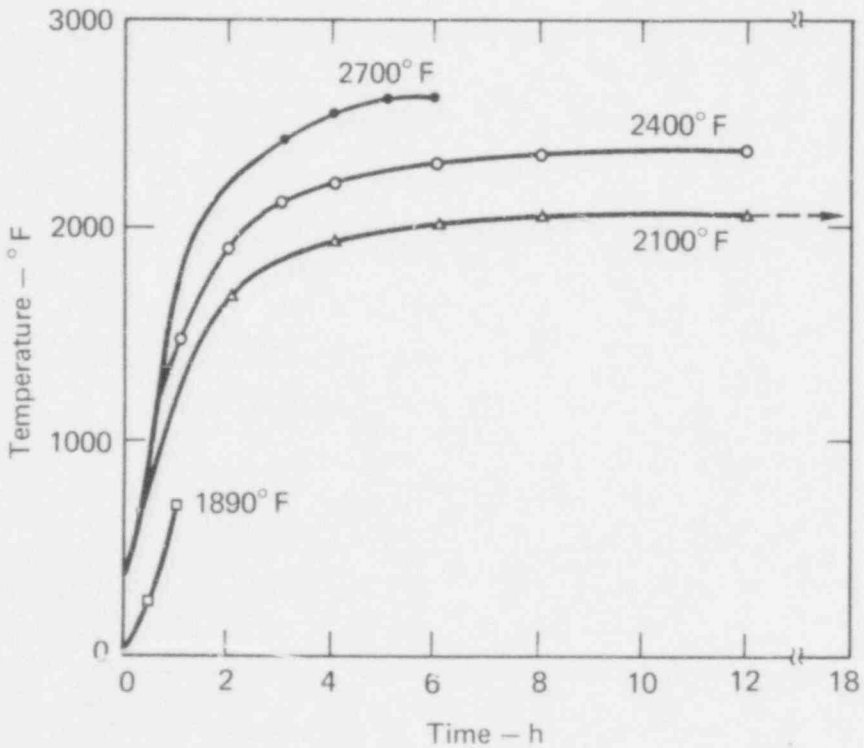

FIG. 28. Cask-seal temperature profiles for rail casks subjected to severe fires. The seal is assumed to fail at 800°K (1000°F); the four curves represent fires at the indicated temperatures.

TABLE 13. Canister failure times for rail cask in fires, assuming the lower limits for T_{fail}.

Fire Temperature		Spray calcine	Fluidized-bed calcine	Borosilicate glass	Supercalcine multibarrier
^{o}K	^{o}F				
1300	1900	No failure	No failure	No failure	No failure
1420	2100	No failure	No failure	No failure	No failure
1590	2400	6.9 h	6.9 h	4.1 h	5.2 h
1760	2700	3.5 h	3.5 h	2.8 h	3.1 h

Figure 28 shows the GrayLoc seal temperatures as a function of time for each of the three severe fire conditions, plus the 1-h, 1300^{o}K (1900^{o}F) fire. Assuming an 800^{o}K (1000^{o}F) failure point for this seal, failure occurs between 0.5 and 0.7 h under the severe conditions. The seal does not fail within 1 h during the 1300^{o}K (1900^{o}F) fire; a rough extrapolation would yield a failure time in the vicinity of 1.25 to 1.5 h at that temperature.

A least-squares fit to the canister failure locus, which is a plot of fire temperature, T_{fire}, vs failure time, t, was also performed (Fig. 29). Using the functional form, $t = a + b \ln (T_{fire} - T_{fail})$, where a and b are constants, the best fits for several failure temperatures are shown in Table 14. In these equations, t is expressed in hours, temperature in degrees Fahrenheit.

CONCLUSIONS

The failure temperature, T_{fail}, is the fire temperature above which the waste canister will eventually fail. For spray and fluidized-bed calcines, canister failure by oxidation, creep, and corrosion mechanisms occurs at fire temperatures above 1570^{o} $\pm$ 50^{o}K (2370^{o} $\pm$ 90^{o}F). For glass waste, corrosion failure takes place at fire temperatures above 1470^{o} $\pm$ 50^{o}K (2190^{o} $\pm$ 90^{o}F). The supercalcine multibarrier waste form fails because of internal corrosion and cracking of the Al_2O_3 coatings when exposed to fire temperatures above 1570^{o} $\pm$ 100^{o}K (2370^{o} $\pm$ 180^{o}F).

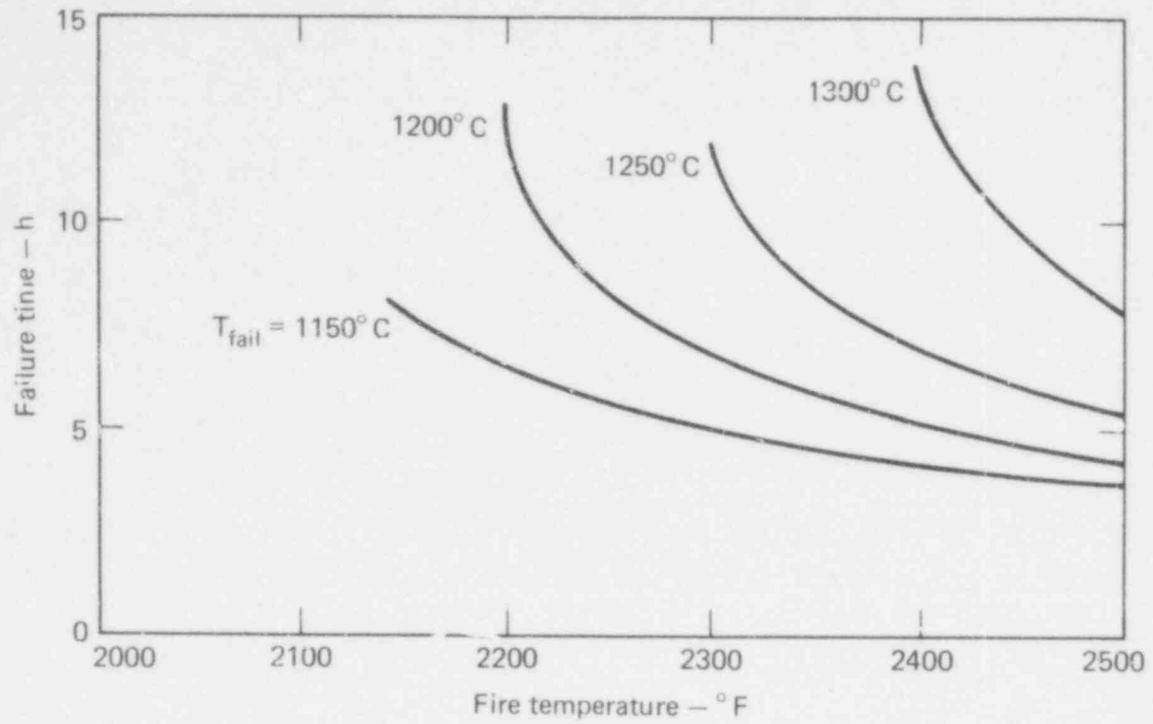

FIG. 29. Failure loci for rail accidents for several failure temperatures.

TABLE 14. Summary of least-squares fits to canister failure loci for several failure temperatures (T_{fail}).

T_{fail}, °K	T_{fail}, °F	a	b
1420	2100	15.52	-1.996
1470	2190	17.74	-2.352
1520	2280	19.82	-2.704
1570	2370	27.12	-3.982

The reference rail-cask design is adequate for normal steady-state operation (with mechanical cooling), for the following reasons:

- The calcine centerline temperature does not exceed the calcine bakeout temperature.
- The maximum canister temperature is well below that required for rapid corrosion.
- The temperatures of the stainless-steel outer tank wall are moderate, approximately 350°K (170°F).

Failure of the GrayLoc seal takes place rapidly under severe fire temperatures, but it does not fail in a 1075°K (1475°F), 30-min fire.

TRUCK EVENTS

We considered only truck accidents involving fire. Both air and water pathways were modeled, and volatilization releases were modeled using experimental laboratory data. Figure 30 is an event tree that summarizes truck accident scenarios, including those not considered. The conditional probability of impact with a train locomotive was taken to be 3.1×10^{-3}, and the probability for the waste entering a waterway was again taken to be 10^{-2}. We again assumed the corner drop to be the most severe impact case.

Volatilization release fractions for Cs, Te, and Ru are sensitive to the postaccident geometry assumed for the waste. We chose the likely case that the waste matrix lies horizontally with its upper surface exposed. On the basis of laboratory experiments, we also assumed that Cs loss from glass is surface controlled, whereas Cs loss from calcine is diffusion controlled. In both cases we fit the data to an Arrhenius-type equation. Similarly, a release function for the Ru from calcine can be developed. The remaining volatile radionuclides were found to be baked out during reprocessing.

The thermal analysis for the truck shipping cask is described below. Release function and risk calculation details are given in Appendixes C and D, respectively.

Thermal Analysis

The thermal analysis for the truck shipping cask paralleled that for the rail cask.

Model Geometry. Figure 31 is a cross-sectional side view of the NFS-4 cask, showing the dimensions (in inches) used for the R-Z thermal analysis. Boundary condition numbers are also shown. The waste is enclosed by a 3/8-in. stainless-steel canister, with a 3/8-in. air gap between the canister and the 5/16-in. stainless-steel inner shell. A lead gamma-ray shield, 6-5/8 in.

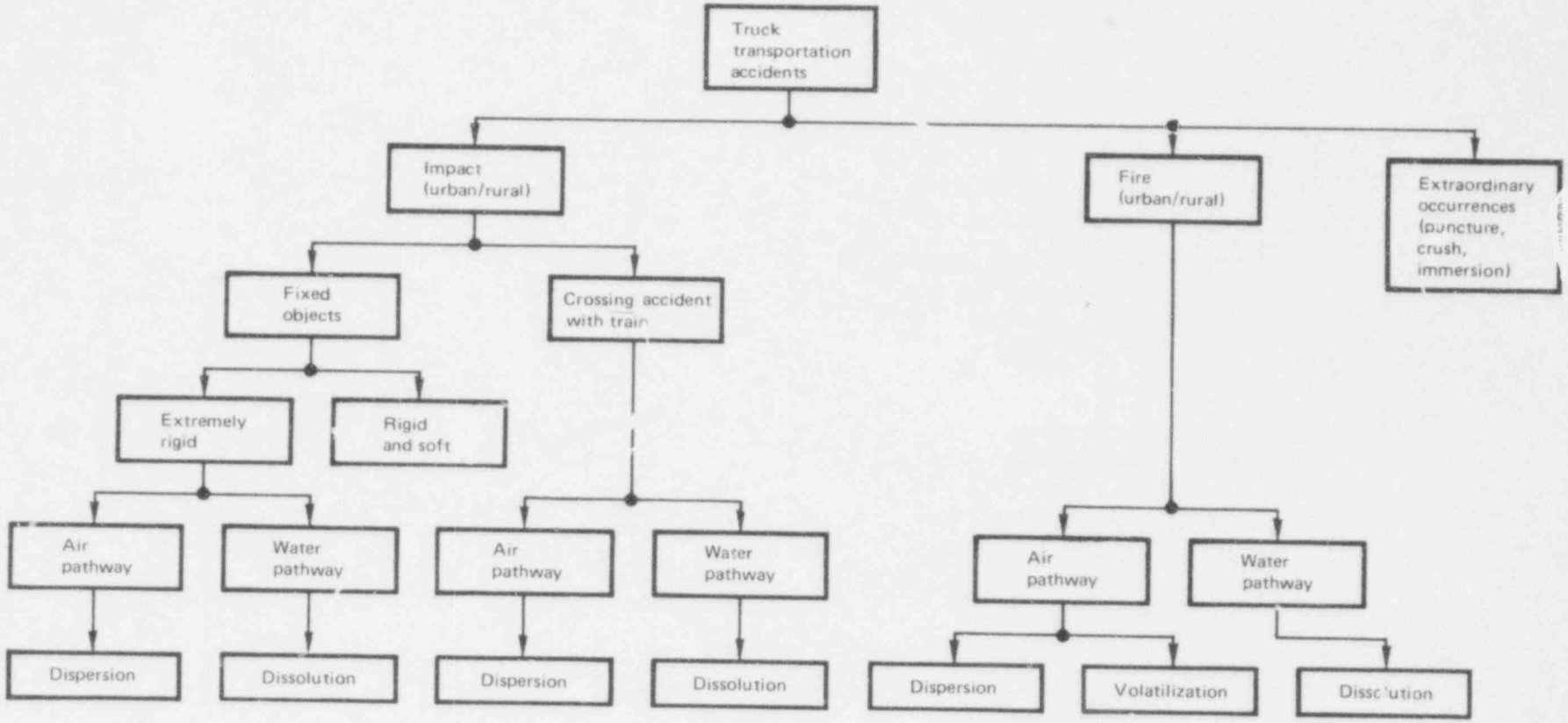

FIG. 30. Event tree for truck transportation accidents.

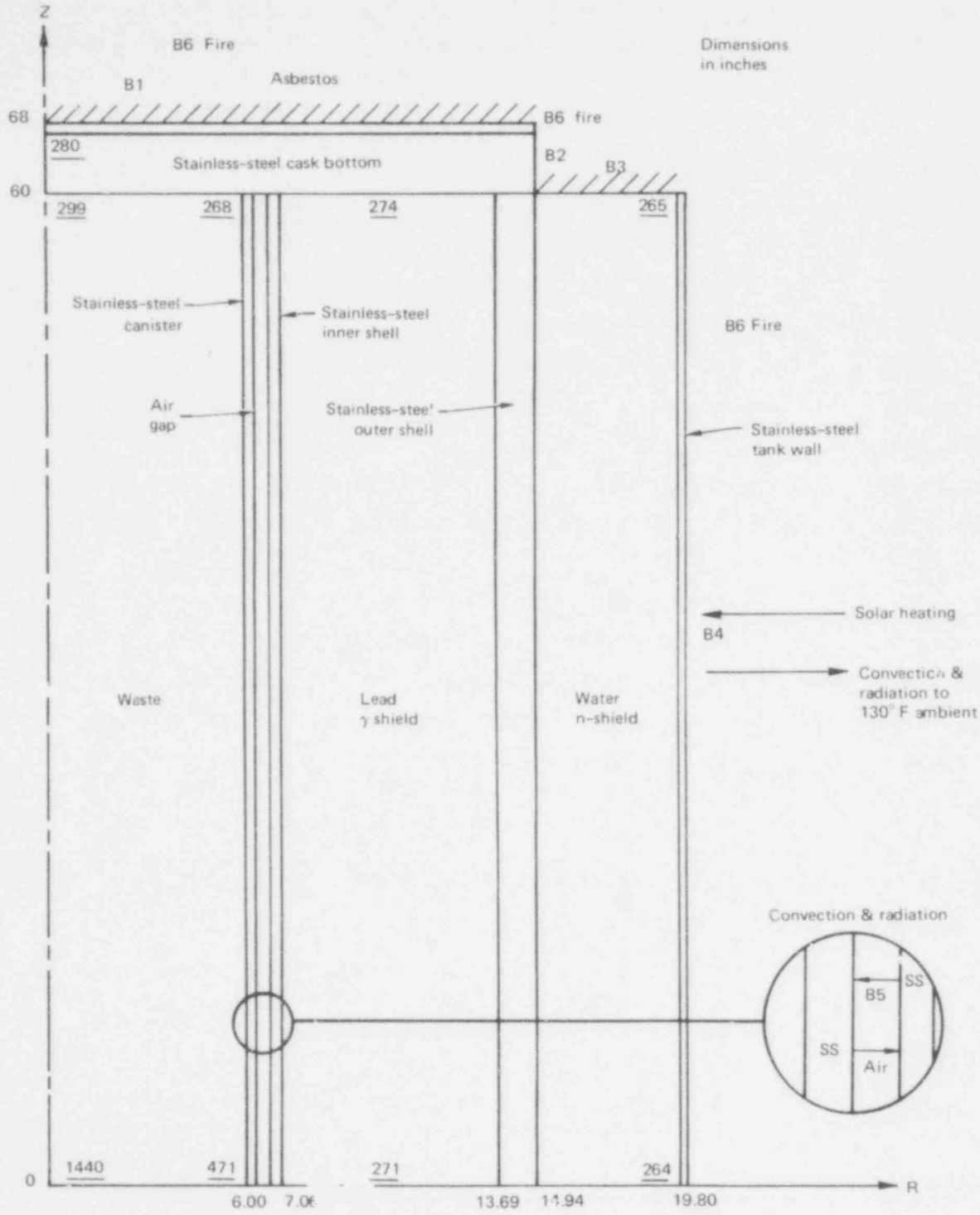

FIG. 31. Cross-sectional side view of modified NFS-4 truck shipping cask as modeled for R-Z thermal analyses. The underlined numbers are the normal steady-state temperatures in ^{o}F.

526 123

thick, is enclosed by two stainless-steel shields, the outer one being 1-1/4 in. thick. The last two regions include the 4-1/2-in. water neutron shield and a 0.165-in. tank wall.

The cask end consists of 8 in. of stainless-steel covered with a 1/8-in. asbestos layer. The balsa impact limiter is not included, as explained below.

Boundary Conditions. During normal steady-state operation, heat travels radially and is removed at the cask wall by radiation and natural convection to the ambient air at 327°K (130°F)--boundary condition B4. We have also assumed a uniform solar flux of 1 Btu/h-in.^{2} The cask end enclosed by balsa wood, which is a very poor conductor, is described by boundary conditions B1, B2, and B3. The internal boundary condition B5 allows for radiation and conduction across the air gap between the canister and the inner shell.

During fires we assumed that all external boundaries are subject to flame temperatures between 1420°K (2100°F) and 1750°K (2700°F), with a flame emissivity of 0.8. We also assumed that the cask wall will lose its mechanical integrity. Hence, during a fire the entire neutron-shield region disappears and the stainless-steel outer wall becomes the outer boundary (boundary condition B6).

Thermal Properties. The thermal properties of the truck-shipping-cask materials are shown in Table 15.

TABLE 15. Thermal properties of truck-shipping-cask materials.

Property	Spray calcine HLSW	Lead (solid)	Lead (liquid)	Asbestos
Density (lb/in.^{3})	0.045	0.40	0.38	0.0208
Specific heat (Btu/lb-°F)	150°F: 0.147 968°F: 0.160	0.0325	0.0380	0.025
Thermal conductivity (Btu/h-in.-°F)	32°F: 4.38 1652°F: 10.2	1.55	0.78	32°F: 7.25 212°F: 9.25 392°F: 10.0 752°F: 10.8

526 124

Results. Normal steady-state temperatures appear as underlined numbers in the cask diagram, Fig. 31.

Figures 32 through 34 are temperature profiles for three critical locations within the cask/canister system during severe fires: canister surface, axial midpoint (Z = 0 in., R = 6.00 in.); canister surface, axial endpoint (Z = 60 in., R = 6.00 in.); and waste centerline (Z = 0 in., R = 0 in.). The normal steady-state temperature distribution served as the initial condition for each of the three fire scenarios. The results are virtually the same for all four waste forms.

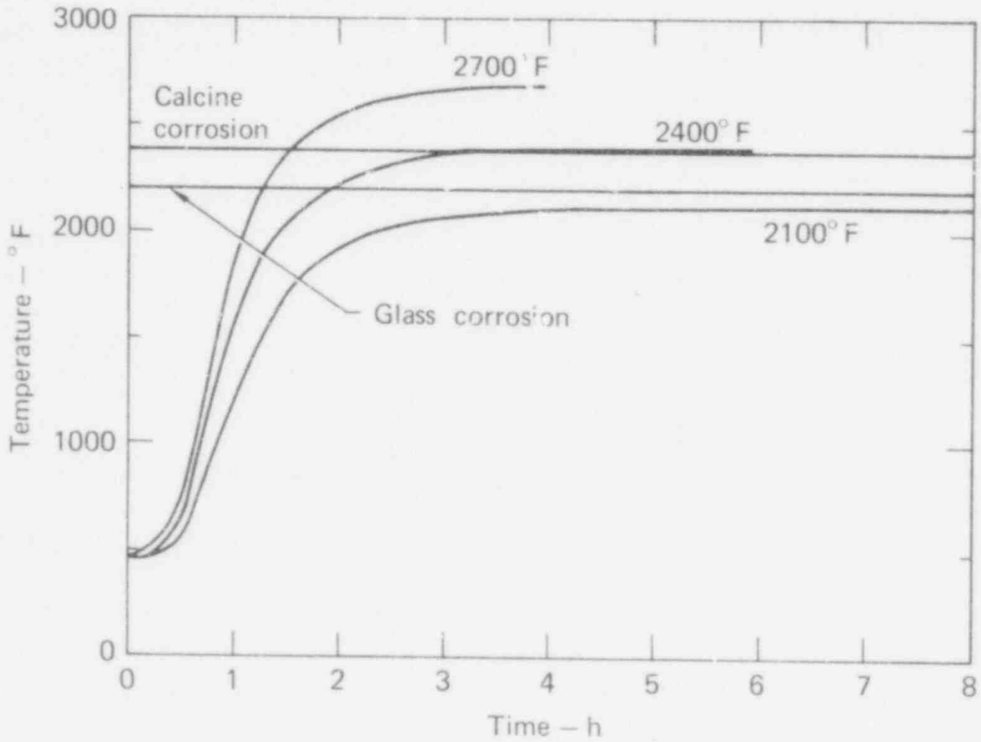

FIG. 32. Canister midpoint temperature profiles for truck casks subjected to severe fires. The failure temperatures for glass and calcine waste are indicated by the horizontal lines; the three curves represent fires at the indicated temperatures.

526 125

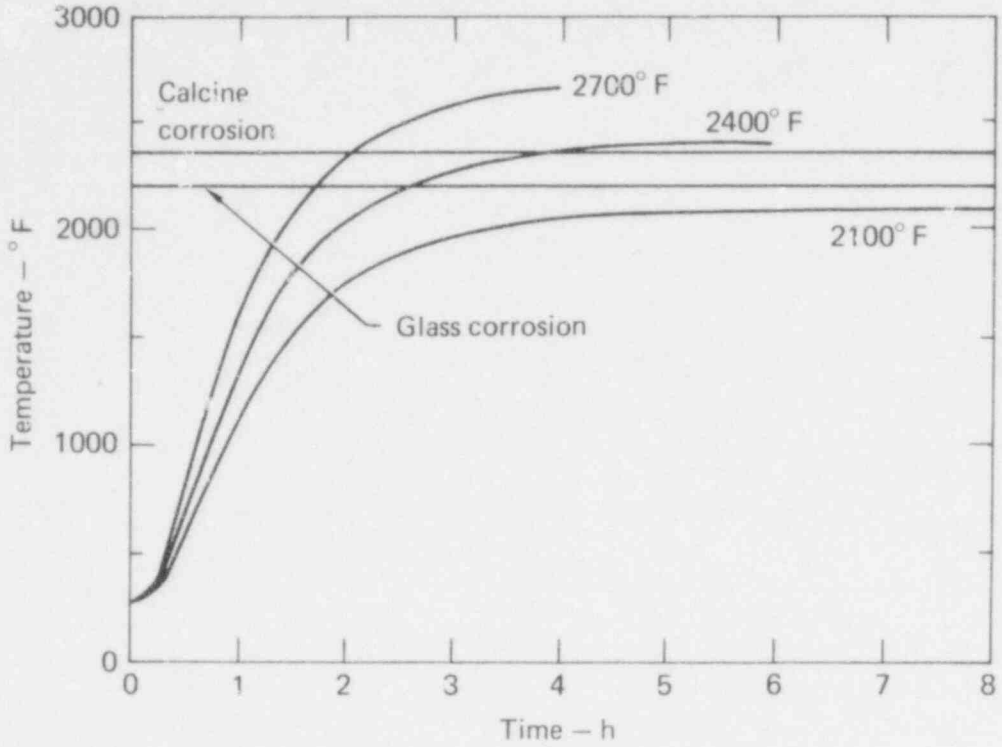

FIG. 33. Canister endpoint temperature profiles for truck casks subjected to severe fires. Other details as in Fig. 32.

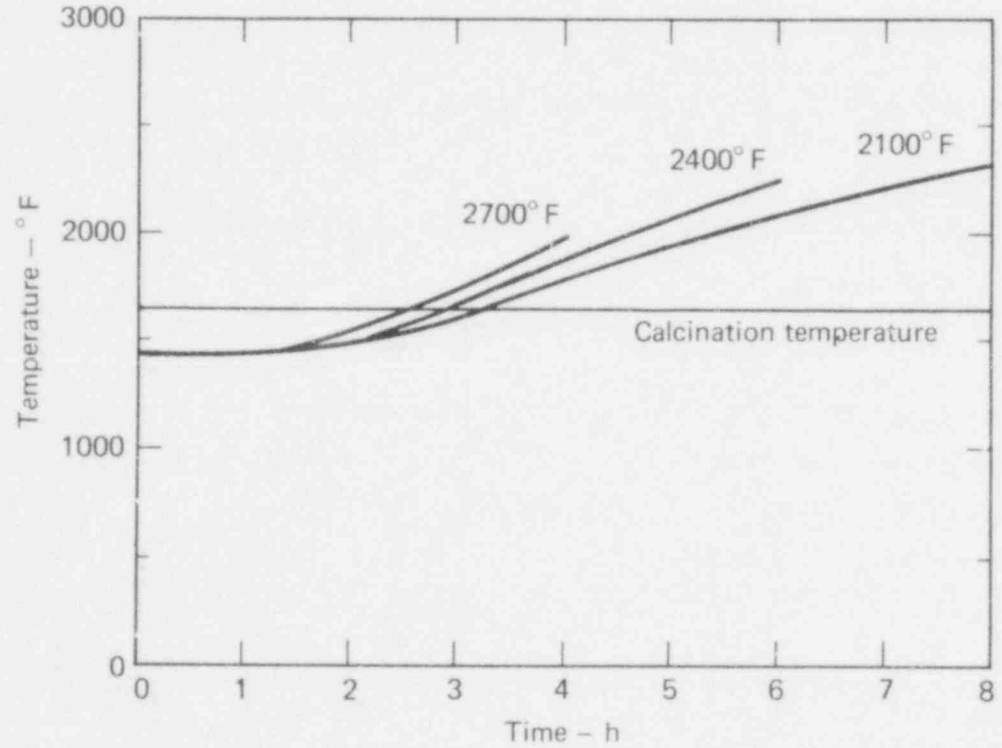

FIG. 34. Waste centerline temperature profiles for truck casks subjected to severe fires. The horizontal line indicates the bake-out temperature for the calcine wastes--the highest temperature to which they were exposed during reprocessing. The three curves represent fires at the indicated temperatures.

526 126

Unlike the rail canisters, truck canisters fail first at their midpoints. Table 16 summarizes the failure times for the various fires and waste forms.

TABLE 16. Canister failure times for truck cask in fires.

Fire Temperature		Spray calcine	Fluidized-bed calcine	Borosilicate glass	Supercalcine multibarrier
^{o}K	^{o}F				
1300	1900	No failure	No failure	No failure	No failure
1420	2100	No failure	No failure	4.8 hr	No failure
1590	2400	2.2 h	2.2 h	1.7 h	1.9 h
1760	2700	1.4 h	1.4 h	1.2 h	1.3 h

Figure 34 depicts the waste centerline temperatures as a function of time for the calcine and glass wastes. The calcine bakeout temperature is exceeded at times ranging from 2.6 to 3.2 h.

A least-squares fit to the canister failure loci (Fig. 35) was also made using an equation of the following form: $t = a + b \ln (T_{fire} - T_{fail})$, where a and b are constants. The best fits, for several values of T_{fail}, are summarized in Table 17. In these equations, t is expressed in hours, temperature in degrees Fahrenheit.

TABLE 17. Summary of least-squares fits to canister failure loci.

T_{fail}, ^{o}K	T_{fail}, ^{o}F	a	b
1411[a]	2086[a]	7.32	-0.966
1470	2192	5.207	-0.627
1520	2282	5.094	-0.609
1570	2372	4.903	-0.577

[a]Special failure criterion applies for truck only.

526 127

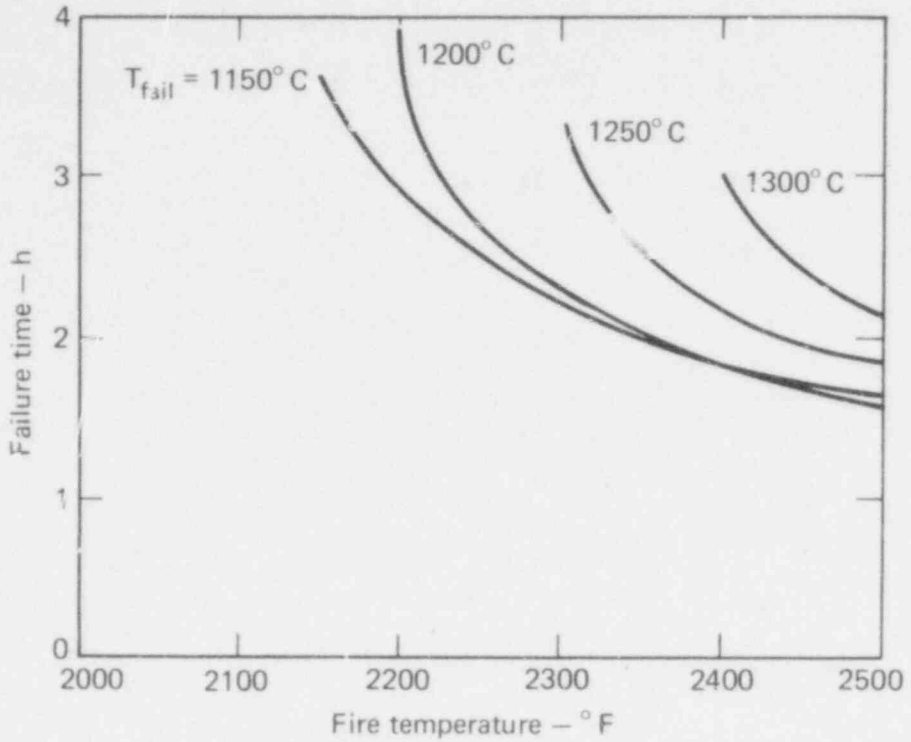

FIG. 35. Failure loci for truck accidents for several failure temperatures.

Failure of the shipping-cask TFE O-ring seal would take place quickly, within a few minutes of a severe fire. We would expect the same result for fire temperatures down to the hydrocarbon minimum, $1033^{o}K$ ($1400^{o}F$).

Conclusions. For the calcine wastes, canister failure by oxidation, creep, and corrosion occurs with fire temperatures above $1570^{o} \pm 50^{o}K$ ($2370^{o} \pm 90^{o}F$). Corrosion failure of the canister can take place with glass waste at fire temperatures over $1470^{o} \pm 50^{o}K$ ($2190^{o} \pm 90^{o}F$). The multibarrier waste form will fail from internal corrosion and from cracking of the Al_2O_3 coatings when exposed to fire temperatures above $1570^{o} \pm 100^{o}K$ ($2370^{o} \pm 180^{o}F$).

The reference truck cask design is adequate for normal steady-state operation, with no mechanical cooling needed, because:

- The calcine centerline temperature does not exceed the calcine bakeout temperature.
- The maximum canister temperature is well below that required for rapid corrosion.
- The lead shielding remains in the solid state.
- The temperatures of the stainless-steel outer wall are moderate, about $405^{o}K$ ($270^{o}F$).

SECTION 4

HANDLING AT THE REPOSITORY

We have analyzed the possible risks of accidents during handling operations at the repository by using the event tree shown in Fig. 36. The most significant dangers are handling accidents in which the canister is accidentally dropped and airplane crashes into the surface facility.

As we described in the discussion of interim storage, we have found that the conditional probability of canister rupture after a crane drop is zero. Nonetheless, in the calculatons reviewed below, we conservatively assumed that each crane drop released 100% of the volatiles in the canister. The right-hand side of the event tree considers the releases due to the impact of an aircraft while the transportation cask is at the repository site. We have found that the total risk from these two scenarios is relatively unimportant compared to that from interim storage and transportation.

ASSUMPTIONS

We made the following assumptions in analyzing this portion of the waste management sequence:

- The head of the repository shaft is contained within a sealed building. Under normal conditions any contamination escaping into the air in the building is prevented from entering the atmosphere by a filtration system. Parameters describing this filtration system are identical to those for the interim storage filtration system.
- Transportation vehicles enter the sealed storage area for unloading. The canisters are not removed from their transportation casks until they are inside the building and the air seal is reestablished.
- The only time the canisters are bare is during transfer between casks and while they are being lowered into the repository.
- Bare canisters can dissipate all generated heat into the air; therefore, the only danger to canister integrity while being actively handled is impact when accidently dropped.

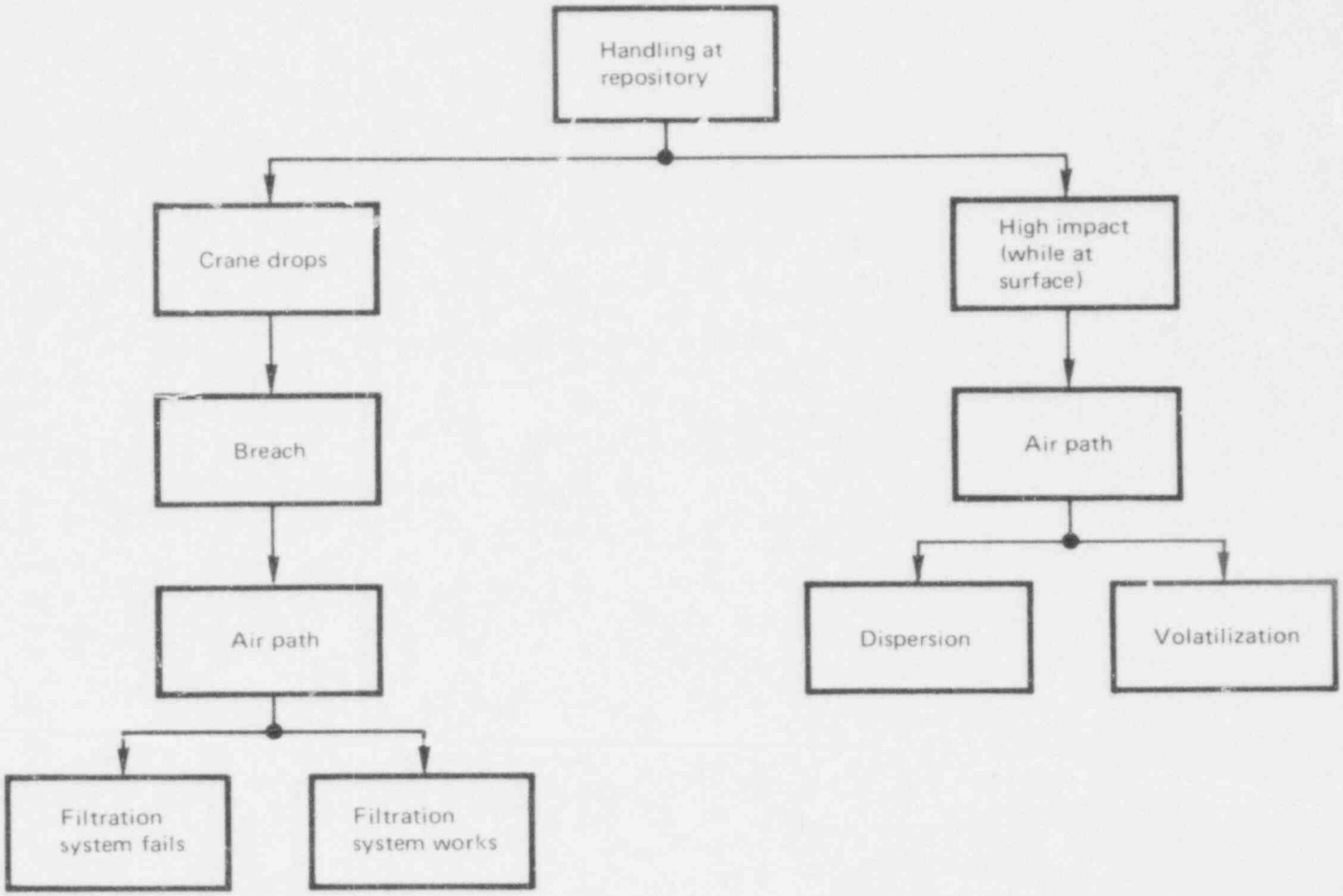

FIG. 36. Event tree for handling accidents at the repository.

- The nominal time the canister is outside the casks is 10 min per canister, which includes movement between transportation cask and transfer cask, and between transfer cask and final storage.
- The probability of a crane drop is the same as during handling at the interim storage facility: 3×10^{-6} per h of operation.
- The main danger to the canisters while waiting in the casks at the surface of the repository is impact from an aircraft. The casks protect against other dangers such as earthquake and tornado. The probability of meteor impact is insignificant.
- The transportation cask containing the waste canisters remains on the surface at the repository for a nominal period of 1 wk before the canisters are removed and stored.
- The water path for released wastes is insignificant since precautions can be taken to avoid a direct path into surface water bodies serving large populations.

MAXIMUM EXPECTED RELEASES

The maximum expected release for each path in the event tree of Fig. 36 has been calculated by making the extreme assumption that the release fractions are unity and that the canister will always be breached when dropped or struck by an aircraft.

Crane Drop

Using the crane-drop probability (3×10^{-6}/h) and the bare-canister handling time (10 min) from Table 18, the probability of a canister drop per MWe-y is

$$\left(3 \times 10^{-6} \frac{\text{accidents}}{\text{h}}\right)\left(\frac{1\ \text{h}}{6\ \text{can}}\right)\left(\frac{1\ \text{can}}{100\ \text{MWe-y}}\right) = \left(\frac{5 \times 10^{-9}\ \text{accidents}}{\text{MWe-y}}\right) .$$

This accident probability is the same as that computed for a crane stall during interim storage. The probability and effect of filter failure are also the same, thus the results from that section apply. The maximum expected release (in Ci/MWe-y) due to drops caused by crane failures is therefore 10^{-16} times the activity of volatiles in a MWe-y of waste.

TABLE 18. Conditional probabilities and release fractions for surface accidents at the repository.

	Value	Dimension	Inclusion of human factors
Handling			
Rate of crane drop	3×10^{-6}	events/h	yes
Time of operation per canister	1.67×10^{-1}	h/canister	yes
Conditional probability of canister rupture	1.0	---	no
Calcine release function for ruptured canister (worst case)	1.0	---	n/a
Glass release function for ruptured canister (worst case)	1.0	---	n/a
Fraction of released volatiles reaching filter	10^{-2}	---	n/a
Fraction of released airborne dispersable particles reaching filter	0.0	---	n/a
Rate of filter failure	1.9×10^{-8}	failures/wk	no
Time for cleanup after release	1.0	wk	yes
Transmission ratio for failed filter	1.0	---	yes
Transmission ratio for functioning filter	1.0×10^{-9}	---	no
Surface storage			
Rate of aircraft crashes	1.27×10^{-10}	events/y-mi^2	yes
Effective cask cross section	3.22×10^{-5}	mi/cask	n/a
Mean cask surface-storage time	2×10^{-2}	y	yes
Calcine release function	1.0		no
Glass release function	1.0		no

Impact By Aircraft

The maximum expected release from an aircraft accident is computed from the accident density of 1.27×10^{-10} crashes/y-mi^2 and an effective rail-cask cross section of 3.22×10^{-5} mi^2 per cask (100 yd^2 per cask). The calculation was made as follows:

$$\left(1.27 \times 10^{-10} \frac{\text{crashes}}{\text{y-mi}^2}\right)\left(3.22 \times 10^{-5} \frac{\text{mi}^2}{\text{cask}}\right) = 4.09 \times 10^{-15} \frac{\text{crashes}}{\text{cask-y}} .$$

Since each cask is on the surface for one week, there will be

$$\left(4.09 \times 10^{-15} \frac{\text{crashes}}{\text{cask-y}}\right)\left(\frac{1}{52} \text{ y}\right) = 7.09 \times 10^{-17} \frac{\text{crashes}}{\text{cask-y}} .$$

The maximum expected release (in Ci/MWe-y) is, therefore, 7.09×10^{-17} times the activity (in Ci) in a MWe-y of waste. This again follows from the conservative assumptions that release fractions are unity.

SECTION 5

REPOSITORY POSTPLACEMENT PERIOD

REPOSITORY SITE MODEL

Many stable rock formations within the conterminous United States are being investigated to determine their suitability as nuclear waste repository sites. Bedded rock formations that might be satisfactory include argillaceous formations, volcanic rocks, and bedded rock salt deposits. Generally, it is expected that suitable sites will be in regions of low earthquake activity, that the formation will contain as few joints, fractures, and faults as possible, and that the host rock will have low porosity and permeability.

We have chosen to describe the reference repository as located in a rock formation of six layers, with variable properties for each layer. The repository layer lies between adjoining barriers, or aquitard layers, which in turn are adjoined by aquifers. The lower aquifer provides the driving force for water intrusion into the repository; the upper aquifer allows transport of radioactivity away from the repository into a surface water system. This type of groundwater intrusion is the greatest threat to containment since it provides a mechanism to transport radioactivity into the biosphere.

A parametric sensitivity analysis for our repository model is given in Berman et al. (1978). A second report (Heckman et al., 1979) provides a full description of our analysis of the repository postemplacement period.

Description

Figure 37 illustrates the physical model we have chosen. We chose a simple model to retain the generic character of the study, though a more detailed model might be designed if more specific data were available (for instance, for a thoroughly explored site). The variable dimensions and

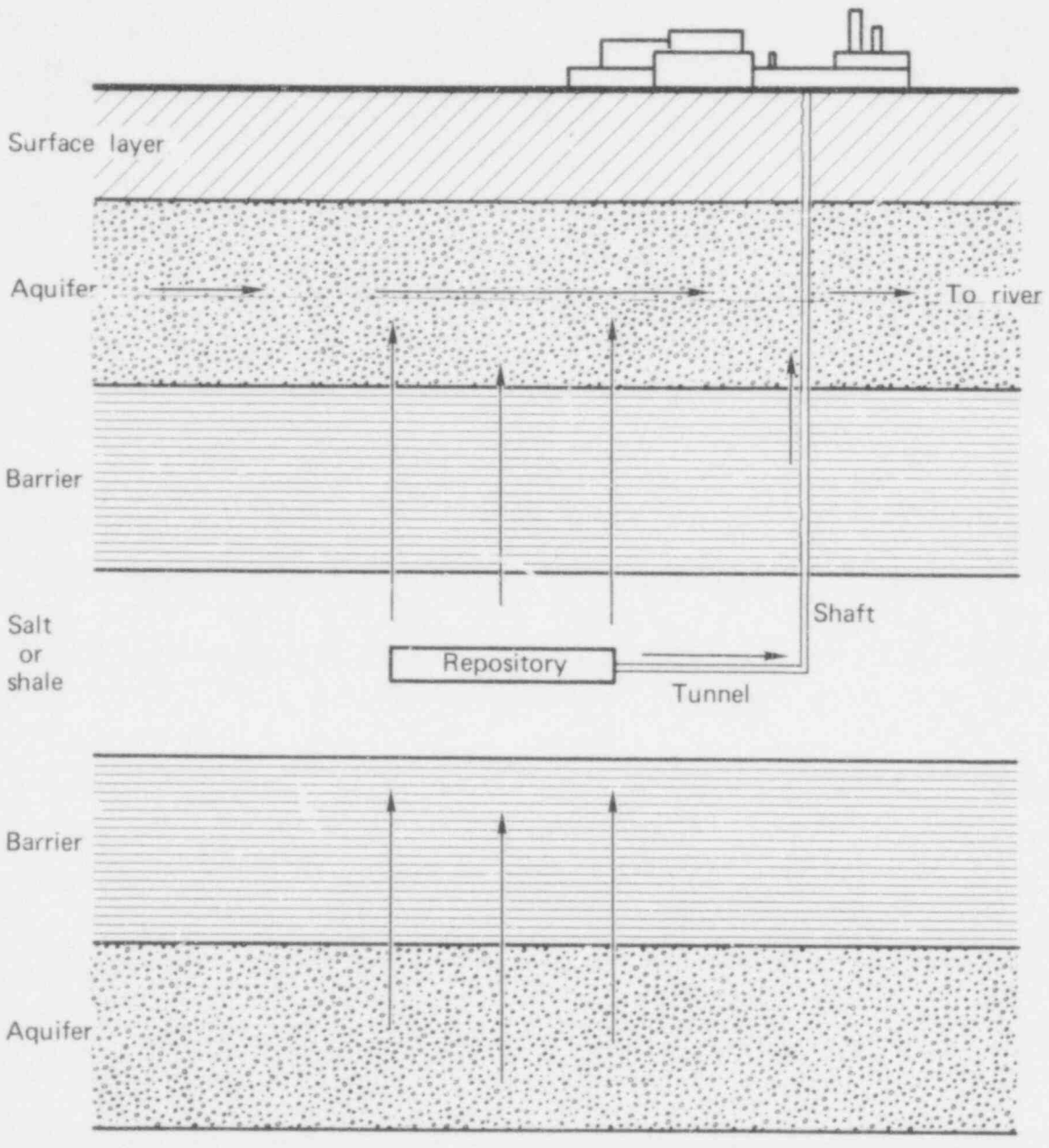

FIG. 37. Physical model for SALW repository.

526 135

variable hydrological parameters that define the repository site are listed in Table 19. These parameters and dimensions can be varied to simulate different media types and different geometric configurations. Taken together they determine flow-path configurations, path lengths, and the properties that influence flow rates and waste-product concentrations. In our studies so far, we have selected parameter values that simulate layered sedimentary environments, with the repository in either shale or salt, and with water flow through interstices or fractures. The range of values that we have used for several hydraulic parameters (as well as our preferred values) are compared with published values in Tables 20 and 21.

By varying these parameters we were able to "experiment" with the repository. By calculating radiological releases and doses and by considering a number of release mechanisms, we have come to a better understanding of the waste-containment and waste-transport processes. We have also been able to identify some of the important factors in these processes and to indicate their relative importance.

Additional variations in the reference model have been made by specifying additional flow paths by their location, dimensions, and hydraulic properties (e.g., porosity, permeability, and pressures). These added flow paths allowed us to simulate faults and breccia pipes, as well as such features as failed seals and backfill in the tunnels and shafts at the repository.

Geometry. A fracture zone with a specified permeability was assumed to be formed around all tunnels and shafts because of excavation work. Areas and lengths of the zones were calculated from the dimensions of a reference repository described by Office of Waste Isolation report #Y/OWI/SUB-76/16506 (Parsons, Brinckerhoff, Quade, and Douglas, Inc., 1976).

Vertical flow in the repository area was assumed through a horizontal area of 5×10^6 m^2, the area of a conceptual DOE repository in bedded salt. Horizontal flow in the upper aquifer takes place through an area computed by multiplying the thickness of the aquifer by 2000 m, which is the long dimension of the repository.

TABLE 19. Variable physical parameters used to describe waste repository site.

Hydraulic factors
Porosities
Permeabilities
Cross section of pathway
Length of pathway
Artesian head
Pressure head
Pressure gradient (horizontal)
Dispersion coefficient
Chemical factors
Retardation factor (K_f) of I and Tc
Retardation factor (K_f) of other fission products
Retardation factor (K_f) of actinides
Rate of waste dissolution
Geometric factors
Layer thickness
Distance to surface water
Tunnel length

TABLE 20. Parameter values for repository site model.

Region	Permeability, cm/s	Effective porosity	Cross section, m^2
Shale repository (vertical)	10^{-9}	0.05	5×10^6
Shale barrier layer (vertical)	10^{-7}	0.05	5×10^6
Fracture zone around shaft, tunnels	10^{-5}	0.02	Tunnel: 3×10^4 Shaft: 1900
Aquifers	10^{-4}	0.10	

TABLE 21. Comparison between values chosen for model parameters and published values.

Parameter	Model values[a]	Published values	
Permeabilities, cm/s			
Shale[c]	10^{-10} (10^{-9}) 10^{-4}	3.5×10^{-11} - 2×10^{-4}	(Note d)
Sandstone[c]	10^{-6} (10^{-4}) 10^{-2}	10^{-7} - 1.1×10^{-2}	(Note d)
Salt[c]	10^{-10} (10^{-9}) 10^{-5}	6.5×10^{-9} - 3.5×10^{-6}	(Note d)
Porosities			
Shale[c]	0.01 (0.05) 0.10[b]	0.07 - 0.45	(Note d)
Sandstone[c]	0.02 (0.10) 0.20[b]	0.0 - 0.51	(Note d)
Salt[c]	0.004 (0.01)0.07[b]	<0.01	(Note d)
Dispersion constant, m	10 (50) 100	11.6 - 38.1	(Note c)
Retardation factor			
I and Tc	1 (1) 1	1	(Note c)
Other fission products	1 (10^2) 10^3	1 - 10^4	(Note c)
Actinides	10^2 (10^4) 10^5	10 - 10^5	(Note c)

[a]Minimum value (preferred value) maximum value.

[b]Effective porosity (a fraction of total porosity).

[c]Heckman et al. (1979).

[d]Ekren et al. (1974).

526 138

Base case thicknesses and other dimensions in our study are similar to those of the conceptual DOE bedded-salt repository. Different stratigraphy (or erosion, or uplift and erosion) was simulated by changing thicknesses. Different geography or extreme erosion of the aquifer bed was simulated by changing the path length in the aquifer. Changes in number and location of boreholes, and changes in faults and other features, such as breccia pipes in soluble rocks, were modeled by changing both geometric and hydrologic parameters.

Chemistry. Chemical factors as applied to the physical model are handled by varying the values of retardation factors, initial inventories, and solution rates. These can be varied independently of the variables that specify the geometry and the hydrology. Our model thus allows us to analyze a variety of waste materials and waste forms.

Hydrology. The flow regime is specified by assigning values to the properties of the rocks and the hydraulic system, in addition to geometric parameters, such as pathway lengths and areas. The important properties of the rock are effective porosity and permeability. A preferred value and a generic range were assigned to both.

In our model hydraulic properties of the system include pressures and pressure gradients. We varied the excess artesian head in the lower aquifer and the horizontal pressure gradient. By affecting flow velocities in the system, these properties influence retention time and hydrodynamic dispersion. Dispersion itself is difficult to measure.

Other Variables Manmade features, such as the backfill and seals of boreholes and shafts, may have properties that vary in time; permeability and porosity in particular may increase as the seals deteriorate. The hydraulic properties of natural features such as faults, fracture zones, and breccia pipes also vary with time. Breccia pipes will form after the more soluble rocks dissolve, thus forming a cavity of some minimum critical size. Pipes may for a time provide a new permeable flow path.

Variations in climate may also affect the hydrologic regime by changing water-table levels, pressures, and pressure gradients. These can be modeled by changing the values of the appropriate parameters.

Seismic events severe enough to affect the integrity of the repository are so rare in stable geologic environments that we have deferred their consideration.

Uncertainties. Data-induced uncertainties may follow from lack of precision in measurement, which may be important in the study of actual sites. Uncertainties may also follow from a small data base or an imperfect understanding of a system, conditions that could exist in a generic model study such as ours. Since the processes of hydrodynamic dispersion and radionuclide retardation are not well known, their study needs a larger base of field measurements.

Few data exist on the hydraulic behavior of faults over long periods of time; therefore, it has to be extrapolated theoretically for our purposes. The same is true of other natural features, such as breccia pipes, and for seismic events. Manmade seals, tunnels, and shafts are better understood. Experience can be extrapolated and some technology assumed. Geometric and hydrologic parameters can also be measured precisely.

Assumptions

Our model simulates release. Waste in deep geologic repositories would never escape if it were totally insoluble, if the rocks were completely dry or impermeable, or if there were no pressure differentials.

Since these conditions cannot be permanently guaranteed in the real world, we assume some waste dissolution and transport into the hydrologic environment. Other release routes (gaseous, aerosol, etc.) might be possible, but the probabilities are so low we have deferred analysis of them.

Effects of geologic features or events and their probability or rate of occurrence need be analyzed only until we can show the point at which the

effect becomes negligible or the probability of occurrence becomes so low that it is practically impossible. This allows us to truncate our analyses at that point and keep our task manageable.

In our model: (1) dissolution and waste release begin when the repository is saturated and the hydrologic regime reestablished, (2) hydraulic continuity (flow pathways with inherent permeability, however small) exists between the repository and the biosphere, and (3) a pressure gradient causes flow toward the biosphere. We assume an artesian head in a water-bearing stratum below the repository that is sufficient to cause flow upward to a permeable stratum connected to the biosphere. We assume a reasonably stable geologic and tectonic environment similar to that of large areas of the United States.

Predicting the Future

Most of our analyses have been deterministic, i.e., they analyze the effect of a specific state. To calculate an expected value we must then multiply the deterministic consequence of a certain state by the probability of that state's occurring.

In a physical system whose properties and processes are well known, predictions of future behavior can be made with confidence. The simpler the ongoing processes and the slower the rate of change, the greater the confidence in the predictions. Geologic processes are extremely slow in human terms, and well documented over the past 10^6 to 10^7 y, thus we can predict with confidence how geologic parameters will change in the near future. In stable areas we can predict that the changes will be small. With further documentation we can estimate the possible range of variation and truncate our analyses.

Flexibility

By varying the geometry and characteristics of the flow paths we can simulate the effects of fractures around the repository, faults, breccia pipes, boreholes, and shorter aquifer paths to the biosphere. Likewise we can investigate the effects of flowing or pumped wells, changes in regional

water-flow characteristics, erosion or deposition that decreases or increases path length to the biosphere, and so on. Such unlikely factors as a meteor strike, severe fault displacement at the site, or a drill hole or mine shaft placed directly into the repository can also be simulated, but our first priority has been to study more probable natural events.

To study releases with severe consequences we have evaluated models that include several simultaneous low-probability conditions or events.

SITE HYDROLOGY

Groundwater flow into the repository from nearby aquifers provides the mechanism for the migration of radionuclides. Migration is thus a function of groundwater flow rates and the lengths of aquifers that lead to surface water systems. Hydraulic dispersion and sorption retardation reduce the risk by lowering radionuclide concentrations and by allowing more time for radioactive decay. Therefore, selection of aquifers with favorable dispersion characteristics as well as high sorption retardation factors is highly desirable.

Groundwater flow rates at the repository site are governed by local hydraulic gradients, which in turn are controlled by regional rainfall, surface water recharge rates, and regional topography. Site porosity and permeability characteristics govern flow patterns within the repository. For our modeling studies of the reference repository site, we chose the values shown in Table 22 for the hydrologic parameters.

Expected radiological risk was calculated for the average individual (in rem/MWe-y) and extended to reflect population risks (in man-rem/MWe-y). Details appear in Berman et al. (1978).

TABLE 22. Reference parameter values for hydrologic calculations.

Parameter	Value
Groundwater sorption retardation factors	
Radioiodine, technetium	1
Other fission products	10^2
Actinides and daughters (fresh water)	10^4
Dispersion constant	50 m
Excess hydraulic head in lower aquifer	60 m
Nuclear waste dissolution time	10^4 y
Barrier layer thickness	2×10^2 m
Repository layer thickness	2×10^2 m
Distance to aquifer discharge	1.6×10^4 m
Aquifer hydraulic gradient	5×10^{-3}
Length of tunnel	1.64×10^3 m

Flow Paths

We simulated two- and three-dimensional flow of groundwater with a network of pathway segments, in each of which the pressures, flow velocities, and volumes can be found by a one-dimensional analytical calculation. We specified a vertical gradient throughout, forcing the flow of water upward. In the permeable aquifer beds, we also specified a horizontal pressure gradient that forces flow in the aquifers toward the biosphere (a river in simulations so far). Within the aquitards and aquicludes (the much less permeable repository and barrier beds), we specified only a vertical gradient.

We examined the flow system in each case and specified a set of pathways to describe it. All pathway segments so far have been straight and either vertical or horizontal, connecting at right angles at all intersections. Areas, lengths, and hydrologic parameter values were specified in each segment of the flow path. Flow rates were calculated by Darcy's law, and the results used in later stages of the calculation.

Sensitivity of Dose to Waste Dissolution Time

The release of radioactive waste from an underground repository could result in doses to humans. The sensitivity of such doses to the dissolution characteristics of the waste may be studied by analyzing functional dependencies in a continuous model. The dissolution time of the waste has no significant effect on doses if

$$\lambda_\ell^{-1} \ll T_D = \sqrt{4\alpha z}\,\frac{K_j}{v} \quad ,$$

where λ_ℓ^{-1} is the dissolution time, T_D is the dispersion time of the waste, α is the dispersion constant, z is the path length, v is the velocity of water in the aquifer, and K_j is the sorption retardation factor for the dominant nuclide. Details of this analysis are given in Appendix E.

SITE CLIMATOLOGY

An evaluation of climatic stability and of the range of climatic extremes is necessary before long-term estimates of site suitability can be made. Climatic variations can influence hydrologic factors such as groundwater recharge rates and can affect surrounding demography. To predict these future variations, we must turn to what we know of climatic variation over the past 10^3 to 10^6 y.

Indirect evidence shows that our climate has varied on nearly all time scales, but patterns of temperature and precipitation appear to be correlated with

variations in the earth's orbit. This provides the basis of prediction of future climatic change. Projections based on Hays et al. (1976) and Vernekar (1972) are currently being made for the present configuration of the earth's orbital variation. To add confidence to these projections, past orbital variations are being correleated with ^{18}O concentrations from ice cores. These ^{18}O concentrations reflect global ice volume and provide a basic stratigraphy for the past million years.

Table 23 shows the various climatic regimes chosen as typical of the likely range for a glacial-interglacial period in the future. Based mainly on Lamb (unreferenced material), they refer to the correlation between the earth's orbital elements and global temperature/ice volume from Hays et al. (1976).

Once the future large-scale regimes are established, future synoptic scale features are provided in two ways. One is based on past climatic reconstructions using proxy data such as pollen records, tree rings, ice cores, and plant and animal remains. We have used Lamb's reconstruction of the 1000-500-mb atmospheric thickness for a preliminary estimate of moist and dry regions of the United States.

The other approach uses the output from large three-dimensional general circulation models with boundary conditions similar to those of the last glacial maximum (18,000 y ago). This will give in more detail the features of the synoptic scale variations over the United States under a much different climatic regime.

TABLE 23. Climate regimes chosen as typical for future projections.

Type	Time of representative climate regime	Characteristic	Orbital feature
1	20,000 - 17,000	Full glacial	Minimum eccentricity
2	7000 - 6000 B.C.	"Boreal" early warm	Few thousand years before peak in precession
3	4000 B.C.	"Atlantic" moist, postglacial-warm	Maximum in precession
4	2000 B.C.	"Sub-Boreal" dry, postglacial-warm	Maximum in precession
5	500 B.C., A.D. 1500 - 1700	"Sub-Atlantic" or "Little Ice Age"	Past maximum in precession
6	Present	-----	-----

Model Input

Climatology studies can be used to predict (1) regional precipitation patterns at a given time in the future, and (2) the extremes of future precipitation and temperature patterns. Since these patterns affect groundwater recharge (hence influence aquifer heads and local flow pathways), this climatological information can be used to adjust the regional hydrological model and to assess the effect of climate on waste transport.

A second purpose of the climatic studies is to provide estimates of future sea levels and cryospheric changes that will effect hydrologic and demographic patterns. This information, too, must be included in any complete hydrologic model.

Predicting Climate

Although the mechanisms are still being debated, more than half of the variance in past temperature data can be explained in terms of orbital parameters. The relevant orbital elements can be calculated by a simple model, which then can be used to predict future global temperature and ice volume.

Shorter-term variations in climate are harder to predict. Over periods of about 10^3 y, orbital parameters may still be controlling the natural climate fluctuations; however, with the increased anthropogenic release of CO_2 into the atmosphere, some researchers (Broecker, 1975) expect the earth to enter a "super interglacial" similar to the postglacial optimum that occurred about 6×10^3 y ago. The postglacial optimum was characterized by global temperatures 2^{o} - 2.5^{o}K warmer than the present with generally wetter deserts and drier mid-latitudes.

Global temperature ranges supplied by our predictive model give no indication of regional precipitation variations. From changes in mean temperature we can deduce only generally wetter or drier conditions. To predict more specific patterns, we must rely on climatic reconstructions of periods in the past that will then correspond to analogous periods in the future.

Regional temperature and precipitation patterns of the full glacial climate regime have been obtained from three-dimensional general circulation models that have used Ice Age boundary conditions (Gates, 1976). Although the model output is limited by its grid structure, basic patterns of regional precipitation emerge. They are consistent with the current estimates of actual precipitation during that period.

The remaining climatic regimes from Table 23 will be reconstructed and the regional variations in precipitation estimated using data from Bernabo and Webb (1977) and Fritts (1977). The methods mainly involve eigenvector analysis and pollen data, and tree rings, respectively. At this writing, the data are still in preparation. Application of the climate data to the hydrologic model will require calculation of infiltration volume as a residual of precipitation, evapotranspiration, and runoff.

WATER INTRUSION

Water intrusion is the most plausible mechanism for breaching the repository and transporting radionuclides into the biosphere. Seismic events can be important factors in increasing the rate of such water intrusion by increasing the permeability both in existing faults and in induced fracture zones around manmade boreholes and shafts. They may also produce new faults with associated fracture zones. The deterioration of seals around manmade openings in the repository host rock (such as boreholes and emplacement shafts) also increases the rate of water intrusion. Following water intrusion, any factor that increases aquifer flow rates, or decreases path lengths, sorption retardation factors, or dispersion coefficients will increase the rate or extent of nuclide dispersion.

Water intrusion along preferential flow channels can lead to void formation by dissolution. These dissolution zones can lead to underground subsidence and the formation of breccia pipes. Backfill subsidence can lead to similar phenomena. Sites with strata subject to dissolution should therefore be avoided. Figure 38 shows the potential flow paths of a typical repository.

Multiple Barrier Concept

Results of the analyses so far show that effective isolation of nuclear waste in a deep geologic repository can best be described in terms of interacting hydrologic, geometric, and chemical barriers. For each barrier important factors that can be identified, measured, and possibly controlled will ultimately define the suitability of the site (Table 24). The main objective will be to minimize the environmental effects on a repository by optimizing the barrier system.

Of the three types of barriers, the simplest to define is the geometric barrier, i.e., the physical isolation of the waste as defined by the thickness of the rock layers, the area of the fracture zone due to construction, and the distance groundwater must flow from the repository before reaching the biosphere.

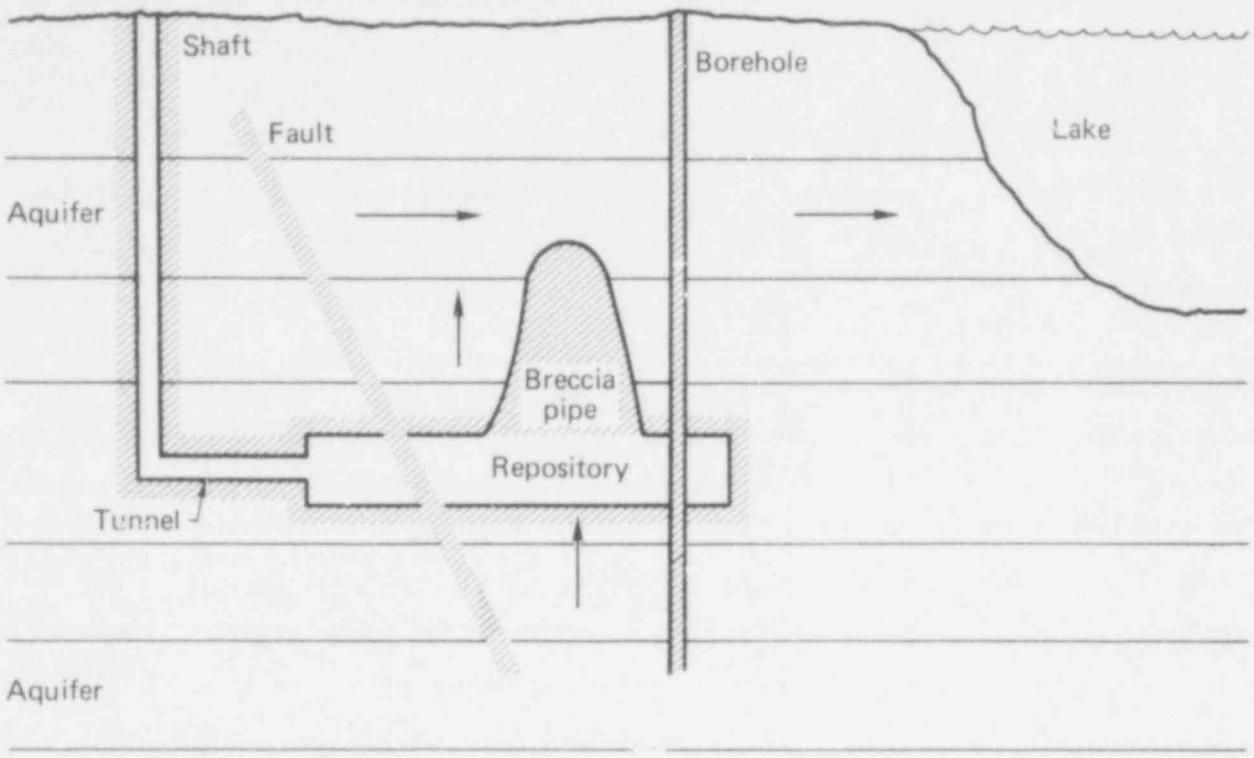

FIG. 38. Motion of groundwater at nuclear waste repository. Arrows depict the motion of groundwater and the crosshatched areas represent permeable zones.

TABLE 24. Factors influencing natural barriers to waste transport.

Hydrology	
Rock properties	System properties
Porosities	Pressures and gradients
Permeabilities (both natural and induced)	Dispersion
	Aquifer length
Chemistry	Geometry
Radionuclide retardation factors	Thicknesses of layers
Waste dissolution rates	Areas of fracture zones
	Tunnel length
	Aquifer length

526 149

Of greater complexity is the hydrologic barrier, which is defined by the parameters describing the waste dilution factors (dispersion) and groundwater flow rates (porosity, permeability, heads, gradients, and so on). In general, the hydrologic and geometric barriers isolate the waste by determining both the time required for resaturation of the repository after water begins to enter and the time required for groundwater to flow from the repository to the biosphere.

Least understood is the geochemical barrier, identified as a series of waste/water/rock interactions involving sorption (ion exchange), membrane filtration, hydrolysis, precipitation, and complexation. The geochemical barrier inhibits (retards) migration of the radionuclides and limits groundwater concentrations of relatively insoluble radionuclides. Also involved in the geochemical barrier is the leach resistance of the waste, which lengthens the time necessary for dissolution.

For our purposes the way the barriers interact depends on whether the consequence being measured is short-term (such as concentration or individual dose) or integrated over time (such as integrated population dose or total amount of radioactivity released).

When dose is integrated over time, the sensitivity analysis reveals the "plateaus and cliffs" structure in Fig. 39. This phenomenon is essentially the result of the nature of radioactive decay. Each nuclide can be thought of as escaping either before it has decayed significantly, or after it has become only an insignificant factor in the total risk. The time interval during which the decay of any individual nuclide significantly affects the overall hazard of the waste is quite short on a logarithmic time scale running from hundreds to millions of years. The exponential decay for ^{239}Pu is illustrated in Fig. 40.

Whether a particular nuclide is released into the biosphere can be determined by comparing its total travel or delay time in the system with the time required for it to decay to an insignificant level. The total delay time is the sum of all the delays in the system; however, one or a few delay times

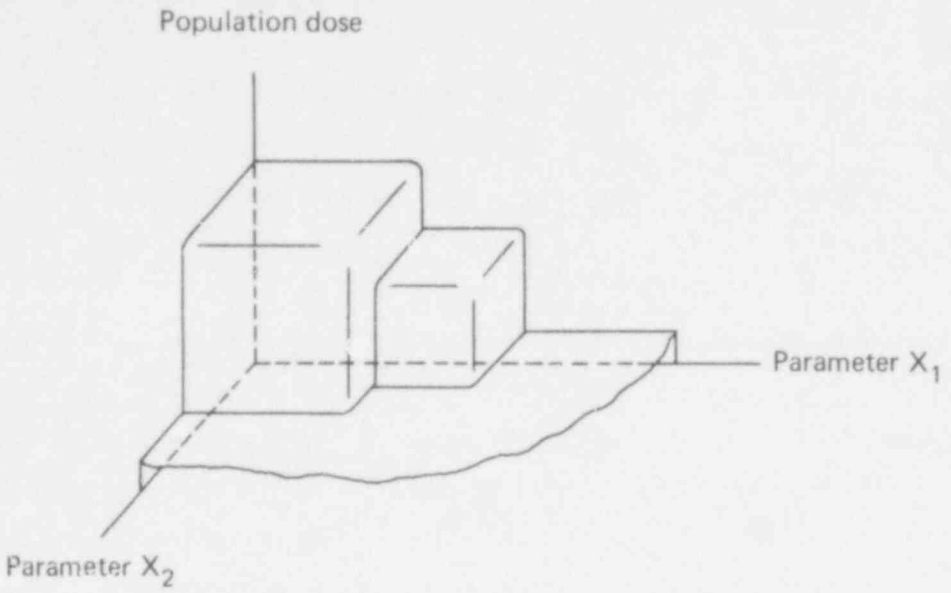

FIG. 39. Conceptual illustration of the general form of a plot of integrated population dose as a function of two of the parameters describing a repository.

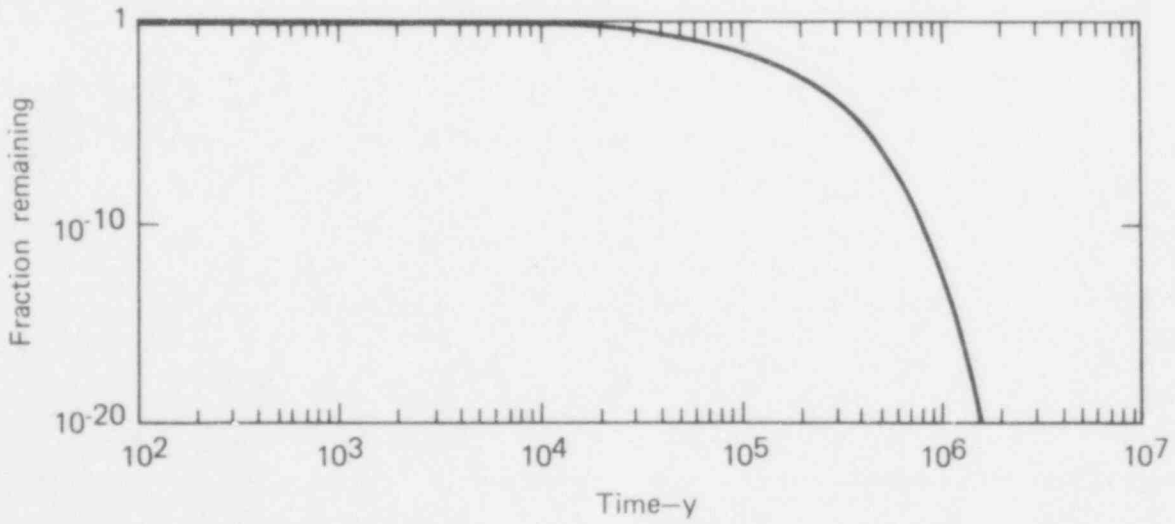

FIG. 40. Decay of ^{239}Pu on a logarithmic time scale.

will usually be orders of magnitude larger than the others, hence the barriers causing them are the critical ones in reducing radionuclide release.

Because of geochemical factors (as measured by the retardation factors), nuclides move through the ground at different velocities. Thus the delay times vary, and different barriers may be limiting for different nuclides in the same system.

For short-term consequences, dispersion over time (or dilution) joins radioactive decay as a controlling factor. Concentration or individual dose is inversely proportional to the duration of the waste pulse reaching the environment. The square of the width of this pulse is roughly the sum of the squares of the pulse widths from the different barriers. This strongly weights the final result toward the largest single contribution. Thus, unless two barriers are of nearly equal effectiveness, the pulse width is governed by the most effective barrier alone and will be nearly equal to the largest component pulse width.

Groundwater Flow Velocities

The transport model approximates the groundwater flow pattern around a repository by a network of one-dimensional flow paths or stream tubes. Each point in the network at which stream tubes branch, or at which any of the variables changes value, is defined as a node (Fig. 41). By varying permeabilities and porosities, we can describe flow as either interstitial or through fractures. An example of fracture flow through an unflawed repository is flow through the fracture zone associated with the construction of the repository, shaft, and tunnel.

The groundwater flow velocities appearing in the transport equation are the interstitial velocities (or true velocities). They were calculated for individual stream tubes in the hydrologic model by using the following equations, which are derived from Darcy's law for flow through porous media:

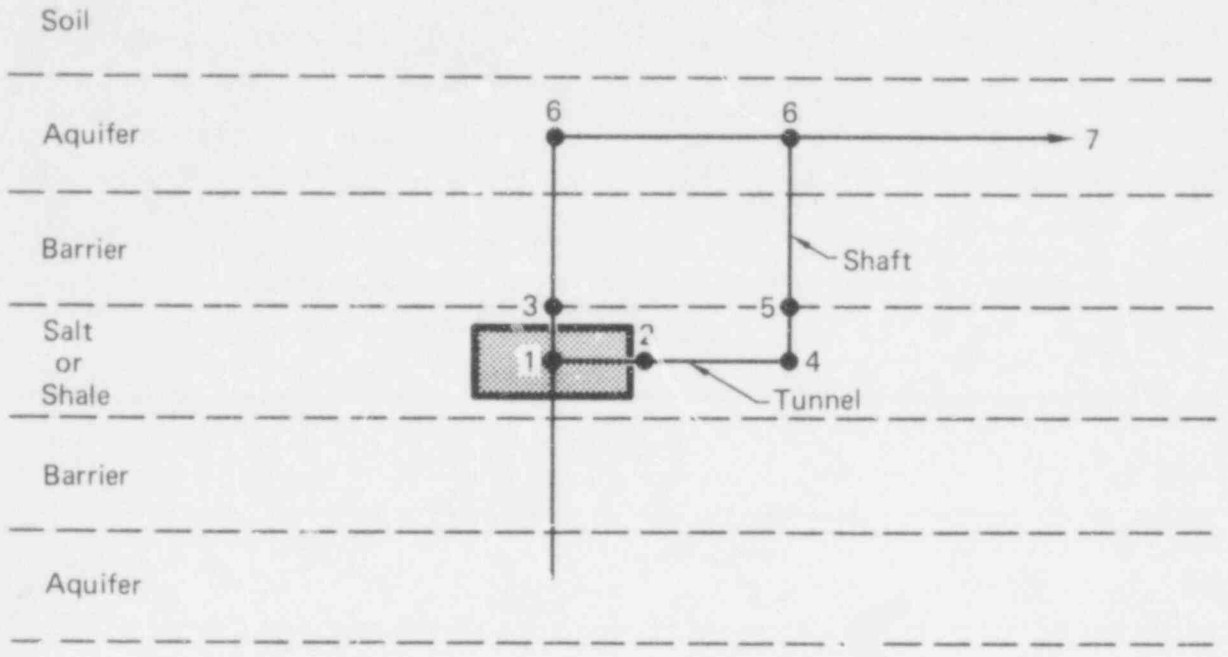

FIG. 41. Node distribution for interstitial and fracture flow pathways in the transport model for an unflawed repository. The pathway 1→3→6→7 represents interstitial flow; the pathway 1→2→4→5→6 (through the emplacement tunnel and shaft) represents fracture flow.

$$V = \frac{V_m}{\epsilon} \quad ,$$

and

$$V_m = -K \frac{\Delta H}{L} \quad ,$$

where

V = interstitial velocity
V_m = bulk velocity
ϵ = porosity
ΔH = head difference between two nodes
L = stream tube length
K = permeability.

526 153

Tables 25 and 26 list flow velocities and travel times for reference repositories in unflawed shale and salt. Velocities are given between each node for both interstitial and fracture flow pathways. With the exception of flow in the lower section of the shaft (nodes 4-5), velocities are much the same in both repositories, assuming reference values for the input parameters.

TABLE 25. Groundwater flow velocities and travel times for the model of Fig. 41.

		Shale repository		Salt repository	
Nodes	Flow Type	Velocity, m/y	Time, y	Velocity, m/y	Time, y
1-2	Fracture	5.35E-1	2.3E3	6.2E-1	1.9E3
2-4	Fracture	9.3	47	10.4	42
4-5	Fracture	1.9E3	0.05	33	3.0
5-6	Fracture	3.7E3	0.05	4.1E2	4.9E-3
1-3	Interstitial	1.8E-3	5.5E4	9.3E-3	1E4
3-6	Interstitial	1.8E-3	1.1E5	1.9E-3	1E5
6-7	Interstitial	1.6	1.0E4	1.6	1E4

TABLE 26. Total travel time (in years) from the repository to nodes 6 and 7, for several retardation factors.

		Shale		Salt	
K_j	Flow path	To aquifer (node 6)	To river (node 7)	To aquifer (node 6)	To River (node 7)
1	Tunnel/shaft[a]	2.3E3	1.2E4	6.8E3	1.7E4
1	Interstitial[b]	1.7E5	1.8E5	1.1E5	1.2E5
10^2	Tunnel/shaft	2.3E5	1.2E6	6 8E5	1.7E6
10^2	Interstitial	1.7E7	1.8E7	1.1E7	1.2E7
10^4	Tunnel/shaft	2.3E7	1.2E8	6.8E7	1.7E8
10^4	Interstitial	1.7E9	1.8E9	1.1E9	1.2E9

[a]From nodes 1, 2, 4, 5, 6.

[b]From nodes 1, 3, 6.

Total travel time from the repository to the aquifer is 2.3×10^3 y for fracture flow along the tunnel/shaft and 1.6×10^5 y for interstitial flow with no retardation ($K_f = 1$). Hence waste will reach the aquifer first as a result of fracture flow. Another 10^4 y is needed for flow from the aquifer directly above the repository to the river. Table 25 shows that the greatest hydrologic barrier to fracture flow is within the repository between nodes 1 and 2. The time for waste to travel the 1200 m from node 1 to 2 is about 2.3×10^3 y with no sorption or dispersion. This value depends on the assumption that the waste is a point source at node 1. In the suggested repository design, the waste may be distributed over most of the 5 km^2 of the repository. This could put waste within 50 m or so of the tunnel, rather than 1200 m. Travel time for 50 m is about 100 y with no retardation; when $K_f = 10^2$, $t = 10^4$ y; and when $K_f = 10^4$, $t = 10^6$ y.

In the shale repository, decreasing the effective length of the repository from 1200 m to 50 m for part of the waste has a significant effect only on the ^{129}I and ^{99}Tc concentrations and on their contributions to dose calculations. Strontium-90 and ^{137}Cs, with retardation factors of 10^2, will be retained within the repository for 10^5 y. In the salt repository, where we assume no retardation between the repository and the aquifer, we expect changes in all radionuclide concentrations and doses. Even then, the resultant change in values may not be significant. The amount of waste that flows from the salt repository through the tunnel/shaft is only about 0.5% of the total inventory. In the shale repository, about 4% of the waste is diverted through the tunnel/shaft.

With such small amounts of waste flowing through the fracture pathway, the error due to the point source assumption is probably small, but future computer simulations will correct this problem by adding nodes between nodes 1 and 2 to simulate the distribution of the waste throughout the repository.

Extent of the Hazard

Figure 42 shows the potential hazard of high-level waste from the reprocessing of light water reactor fuel, as a function of time. Potential hazard in this figure is given as the whole-body population dose (per MWe-y of waste), which is defined as the total dose to the population that would be incurred if one

MWe-y of soluble waste were to be dumped directly into the river. Curves for critical organs and for individual doses have a similar form.

Potential hazard is calculated here from the biosphere transport and dose model. The main difference between this hazard and the toxicity index calculated by the ORIGEN code (Bell, 1973) is that our model accounts for radionuclide transport in the ecosystem and bioaccumulation in the food chain.

The shapes of these curves do not depend on the half-life of ^{239}Pu. There are, rather, two time periods during which the total potential hazard from the waste declines significantly:

- The period from 30 to 400 y, during which ^{90}Sr and ^{137}Cs decay.
- The period from 5×10^5 to 2×10^6 or 3×10^6 y, during which ^{226}Ra (produced by the decay of ^{242}Cm and ^{238}Pu) decays. The time constant governing this process is the quarter-million year half-life of ^{234}U. After 3×10^6 y, the remaining ^{226}Ra in the waste is that produced by decay of the original inventory of ^{238}U.

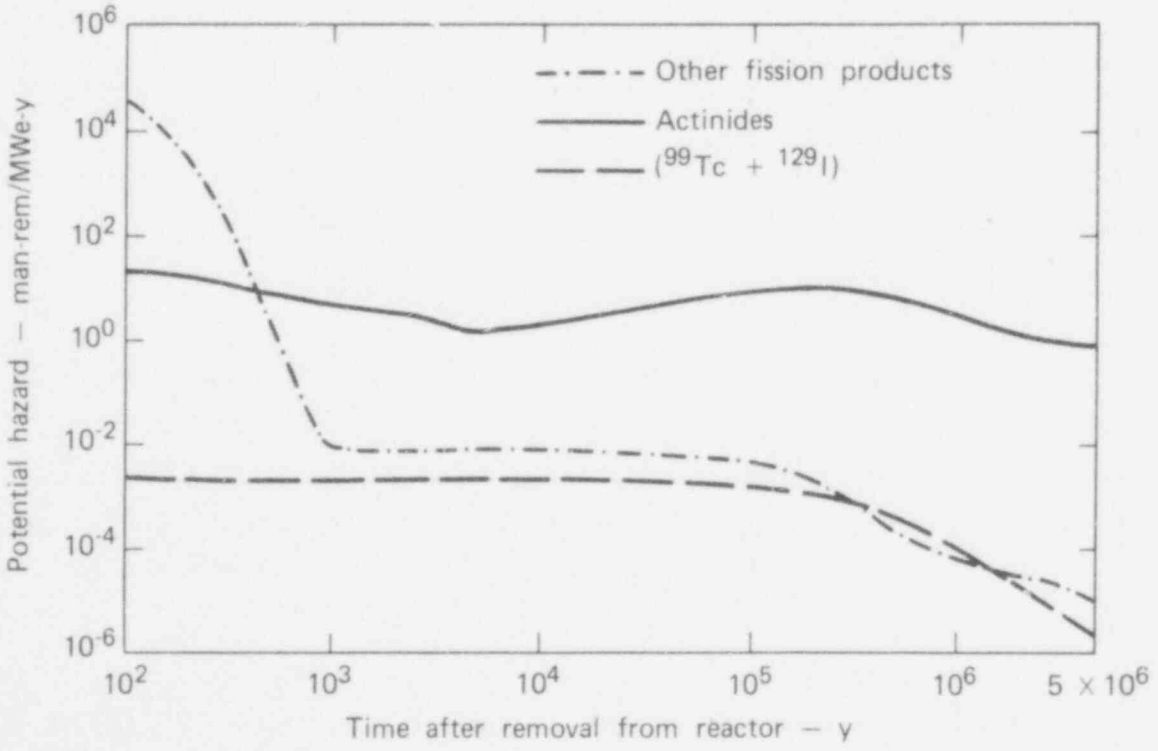

FIG. 42. Potential hazard of HLW from reprocessed LWR fuel, measured as whole-body population dose.

Given these time dependences, we can divide the future of the repository after decommissioning into three distinct periods. This division comes directly from the categorization of nuclides and the time dependence of their hazard as illustrated in Fig. 42, and does not depend on the description of the repository site. The three periods are:

- An initial period lasting not more than 400 y. During this interval the consequences of a direct release of radioactivity to the biosphere could be quite severe.
- An intermediate period lasting at least 5×10^5 y, but not more than 3×10^6 y. The consequences of release during this period would be considerably smaller than during the earlier interval.
- A final period beginning not more than 3×10^6 y after reactor shutdown. During this period the hazard of the waste will be primarily a result of natural ^{238}U and its decay products. The repository will contain little more than the equivalent of ore mined near the surface and buried in a deep, stable formation.

Individual Dose. The potential hazard of high-level waste released to the biosphere is determined by accounting for all pathways that might lead to man. This hazard is reflected in the calculation of the dose to an individual. Doses were calculated for releases into a river system at some distance from the waste repository. In all of the cases we studied the maximum dose was far below background. The data are given in Section 6.

The peak individual dose to the critical organs varied over three orders of magnitude for the salt repository and two orders of magnitude for the shale repository, depending on the values assigned to model parameters. Because different parameters were changed by differing amounts (e.g., K_f varied by two orders of magnitude, whereas dispersion varied only by a factor of five), it is difficult to suggest which of the parameters is most important.

However, we can list those parameters whose variation produced the greatest effect on the individual dose to critical organs. For example, in the unflawed shale repository with interstitial flow, variation of the following parameters caused increases of at least 200% above reference levels:

- Actinide and fission product retardation factors
- Shale permeability of shaft/tunnel
- Fracture zone permeability of shaft.tunnel
- Thickness of repository layer
- Thickness of barrier layer
- Dissolution rate of waste.

With the exception of the dissolution rate of the waste, all of these parameters are related to the travel time between the repository and the biosphere, either affecting flow velocities for the waste or changing the path length.

In the salt repository the situation is similar except that the salt permeability replaces the fracture zone permeability in the list above.

Population Dose. One can expect the dose to an individual to be far below background for any repository that isolates ^{90}Sr and ^{137}Cs for at least 400 y and allows wastes to reach the biosphere only through a sizable surface water system. For such a repository, integrated population dose rather than individual dose may be a more appropriate measure of risk.

To measure the total effect, the population dose is integrated over the lifetime of the repository, and doses are assumed to be of equal concern, regardless of when they occur. The total integrated dose is thus limited by the repository inventory, radionuclide decay, existence of paths to the biosphere, the fraction of water from liquid pathways used for irrigation and drinking water, and the quantity of aquatic food harvested from the liquid pathways.

Integrated population dose is relatively insensitive to changes in the reference repository parameters. In nearly all cases studied, the critical organ dose was between 0.16 and 0.51 man-rem/MWe-y to the gastrointestinal tract and lower large intestine (GI-LLI). The few cases where the dose

exceeded these values by significant amounts involved actinides reaching the river within about 3×10^6 y. For the actinides to affect the dose in this way, the permeability of the rock and the head gradient all alor the flow pathway must be high enough or the effective porosity low enough to overcome ion exchange processes that retard actinide migration.

The following conclusions can be drawn regarding population dose:

- Population dose showed the least variation of the three measures of risk (individual dose and concentration are the other two) in the sensitivity studies.
- Population dose varied according to whether actinides were released, which in turn depended most strongly on sorption retardation factors.
- Once waste reaches the river, the population dose depends on the yearly usage rates of the water system and is independent of the river flow rate for a fixed fractional usage rate.

Concentration. Concentrations were calculated for radionuclides in the aquifer water just above the repository cavity. We assumed a line source in the aquifer with a length equal to the width of the repository. Studies so far indicate that peak concentrations in the aquifer at this location often approach or exceed the maximum permissible concentrations in water. This would be important if the water in the aquifer is potable and if wells are drilled in the vicinity of the repository.

As with individual doses concentrations are sensitive to parameters having a major effect on travel time from the repository to the aquifer. This is because concentrations are primarily a function of the time over which radioactive decay and dispersion can occur.

The concentrations in the aquifer fall off at large distances from the repository because of dispersion. For a steady flux of waste into the aquifer, the peak concentration in the direction of water flow far from the repository is inversely proportional to the square root of the distance from the repository, even if radioactive decay is not significant. The peak concentrations at large distances perpendicular to the direction of flow fall

off exponentially. Therefore, the hazard due to possible high concentrations of waste in the aquifer depends on where the water becomes accessible to man.

Because of the greater retardation of the actinides, only the fission products are released into the aquifer from the unflawed shale repository within the first 3×10^6 y (as long as flow is assumed to be through pores and the fracture-zone of the tunnel/shaft and not through fractures in undisturbed rock). However, relatively high concentrations of both the actinides and the long-lived fission products were calculated in the aquifer for the unflawed salt repository (Table 27). The difference in concentrations between the two repositories was largely a result of the assumption that no geochemical retardation occurs in the repository and barrier layers of the salt repository.

TABLE 27. Peak aquifer concentrations[a] compared with maximum permissible concentrations (MPC_w) established in 10 CFR 20 (U.S. Code of Federal Regulations, 1976). The source was taken to be 6×10^6 MWe-y of waste.

Nuclide	Concentration (Ci/m^3)		
	MPC_w	Salt repository	Shale repository
^{99}Tc	3×10^{-4}	1.6×10^{-4}	1.2×10^{-4}
^{126}Sn	2×10^{-5}	4.2×10^{-6}	7.8×10^{-8}
^{226}Ra	3×10^{-8}	3.4×10^{-7}	b

[a]From calculations described in Section 6.

[b]Peak occurred after 3×10^6 y and was not calculated.

From concentration studies so far, we have concluded the following:

- Aquifer concentrations are most sensitive to changes in the model parameters.
- Any decrease in concentrations caused by increasing aquifer flow rates will generally increase individual and population doses from a nearby surface water body.
- Peak aquifer concentrations are very sensitive to barrier failures such as faults, boreholes, fracture zones, and breccia pipes.

526 160

Fracture Flow Versus Interstitial Flow. The foregoing discussion covered cases in which we assumed interstitial flow in undisturbed rock. In cases with fracture flow rather than interstitial flow in the shale layers, reference values were consistently higher and occurred much earlier (Table 28), mainly because of the higher flow velocities in the fractured rock. Peak concentrations obtained in the sensitivity analysis (Section 6) show the actinides reaching the aquifer in less than 3×10^6 y. Concentrations of ^{126}Sn increase by three orders of magnitude.

TABLE 28. Comparison of doses and concentrations for interstitial flow and fracture flow.[a] The time at which the pulse peak appears is given in parentheses below the individual dose and the concentration.

Flow Type	Whole-body population dose, man-rem/MWe-y	Whole-body individual dose, rem/MWe-y	Tc concentration, Ci/m^3
Shale Repository			
Interstitial	1.3×10^{-3}	6.19×10^{-14} (1.44×10^4 y)	2.02×10^{-11} (4×10^3 y)
Fracture	2.77×10^{-3}	1.86×10^{-12} (1.17×10^4 y)	6.84×10^{-10} (2.3×10^2 y)
Salt Repository			
Interstitial	1.63×10^{-3}	8.15×10^{-14} (1.49×10^5 y)	2.58×10^{-11} (1.09×10^5 y)
Fracture	2.56×10^{-3}	5.84×10^{-13} (2.56×10^4 y)	1.86×10^{-10} (1.69×10^4 y)

[a]From Section 6.

526 161

UNCERTAINTY ANALYSIS

Predictions of repository performance are subject to scientific uncertainties, both in the description of the site and in the predictive model. These uncertainties must be accounted for in the presentation of our results.

Terminology

Each numerical result of the repository analysis includes a best estimate (preferred value) and a range of uncertainty in the estimate. This uncertainty is due to both the inaccuracy and the imprecision of the scientific estimate.

The uncertainties in the performance predictions arise from imprecise data, inaccurate data, and invalid modeling. Imprecise data lead directly to a corresponding range of uncertainty in the site performance predictions. This range is obtained by propagating the uncertainties in the data through the model to the predictions using a Monte Carlo technique.

Inaccurate data, when used in a valid predictive model, lead to inaccurate predictions. This is worrisome only when the precision of the data is relatively good. Otherwise, the inaccuracies in the prediction are hidden by uncertainties due to imprecise data.

Invalid modeling, i.e., incomplete, insufficiently detailed, or erroneous numerical modeling, is the most serious of our three concerns. Incomplete modeling is the result of a failure to consider all important processes in a predictive model. It is especially easy to describe physical processes too simplistically, ignoring important synergistic effects. Insufficiently detailed models arise when critical small-scale phenomena are not adequately accounted for by the scale chosen for the model. Erroneous numerical modeling is a less subtle problem, but care must be taken to avoid careless errors.

Analog Error Analysis

Scientific analysis of uncertainty gives us scientific confidence in our predictions. Careful analysis also indicates whether accuracy and precision

can be improved, and where the most improvement can be expected. To provide a perspective on scientific error analysis, we will outline an example.
We define $H(X)$ as the probability distribution function (PDF) for a prediction, obtained for the set of site descriptors $(X) = (X_1, X_2, \ldots X_n)$. Each subscripted X represents a preferred value and a distribution about the preferred value for one of the site descriptors. H represents the predictive model. The prediction for a reference case is a one-to-one mapping of X_0 to $H(X_0)$, where the reference case is defined by a set of descriptor values, $(X_0) = (X_{1,0}, X_{2,0}, \ldots X_{n,0})$. For the sake of this discussion, we assume that there is a set of mean descriptors $(\overline{X})$ such that $H(\overline{X}) = \overline{H}$, the mean of the prediction PDF.

The precision of $H(X)$ is found by considering the spread of values from the individual j mappings, H_j, where

$$H_j = H(X_j) = H(X_{1,j}, X_{2,j} \ldots X_{n,j}) \quad .$$

In the limit of an infinite number of measurements ($N \to \infty$), the variance of H, which is the square of the standard deviation, σ_H, is

$$\sigma_H^2 = \frac{1}{N} \sum_{j=1}^{N} (\Delta H_j)^2 \quad ,$$

where $\Delta H_j = H_j - \bar{H}$, the predicted deviation of H_j from the mean prediction $\bar{H}$.

The deviations in the predictions can be expressed in terms of the descriptor deviations by use of a generalized n-dimensional Taylor's expansion about X,

$$\Delta H_k = \sum_{i=1}^{n} \frac{\partial H(\overline{X})}{\partial X_i} \Delta X_{i,k} + \frac{1}{2!} \sum_{i=1}^{n} \frac{\partial^2 H(\overline{X})}{\partial X_i^2} \Delta X_{i,k}^2$$

$$+ \sum_{\substack{i,j=1 \\ i \neq j}}^{n} \frac{\partial^2 H(\overline{X})}{\partial X_i \partial X_j} \Delta X_{i,k} \, \Delta X_{j,k} + \text{higher order terms},$$

where $\Delta X_{i,k} = X_{i,k} - \bar{X}_i$, and $\frac{\partial H(\bar{X})}{\partial X_i}$ is the partial derivative evaluated at $\bar{X}$.

If the deviations, $\Delta X_{i,k}$, are small enough, the higher order terms can be neglected. To a good approximation, the first-order Taylor's expansion, which is linear in the deviations, would be adequate for most uncertainties in the model. Under these conditions, a sensitivity study would require only n+1 computations. This is not the case for the site descriptors, for which more extensive calculations are necessary. As the $\Delta X_{i,k}$ become large, terms like

$$\frac{\partial^2 H(\bar{X})}{\partial X_i \partial X_j}$$

become important, and correlations between the parameters must be considered. In fact, many of the parameters, such as porosity and permeability, are known to be correlated. The only way to determine the precision of the predictions is a Monte Carlo-type investigation on a full-blown numerical model.

If we use the expression for the covariance of X_1 and X_2,

$$\sigma_{X_1 X_2} = \frac{1}{N} \sum_{j=1}^{N} \left[(X_{1,j} - \bar{X})(X_{2,j} - \bar{X}) \right] \quad ,$$

we get the familiar statistical form of the standard deviation of H in terms of the standard deviations and covariances of the site descriptors,

$$\sigma_H = \sqrt{\sum_{i=1}^{n} \sigma_{X_i}^2 \left(\frac{\partial H(\bar{X})}{\partial X_i} \right)^2 + 2 \sum_{i \neq j=1}^{n} \sigma_{X_i X_j} \frac{\partial H(\bar{X})}{\partial X_i} \frac{\partial H(\bar{X})}{\partial X_j}} + \text{higher order terms},$$

where σ_H and the partial derivatives are the analytical analogs of the unknowns we are looking for in our numerical sensitivity and Monte Carlo studies. Obviously, our other two concerns must be to understand the σ_X's

526 164

and to assure the validity of H. Knowing the partial derivatives and the σ_X's, we can determine the dominate terms in the expression for σ_H. This then allows us to formulate a strategy for reducing σ_H.

We have assumed to this point that our s te 'escription contains an adequate number of variable parameters, but this need not be the case. As examples, (1) the salinity of the water might be necessary in the model, (2) the permeability may have to be made nonisotropic to be realistic, or (3) the sedimentary rock may need a much more detailed description of its microstructure. Such changes can alter the sensitivities of the descriptors and lead to a change in the direction of the data base development.

In summary, improvements in the accuracy and precision of our predictions will occur when: (1) H(X) is accurately specified, (2) the σ_X's are reduced or better understood, (3) more realistic descriptive parameters are determined, and (4) the model, H, is validated.

This list of four aims implies three closely coupled efforts for developing the data base. They are:

- Developing physically realistic descriptors and evaluating their uncertainties. Initially the descriptors are generic idealizations.
- Developing a predictive model that is rigorously valid. Initially only the physical processes considered most important are included.
- Evaluating the descriptor sensitivity, the precision of the predictions, and the magnitude of the predictions. This effort suggests where resources might be best allocated.

Appendix L of Heckman et al. (1979) includes (1) a discussion of the uncertainties associated with the development of the site descriptors, (2) a description of the uncertainties in the predictive model, and, (3) a discussion of the Monte Carlo method used to establish the precision of the predictions.

SECTION 6

OVERVIEW AND SENSITIVITY ANALYSIS

SYSTEMS-ANALYSIS APPROACH

We believe the systems-analysis approach we have adopted for our study to be unique in several respects. First, it deals with the entire waste management system, not just isolated portions. Our model analyzes the solidified waste from the time it leaves the reprocessing plant until the nuclides have decayed to an insignificant level. So that we can analyze the many facets of the system, we have assembled an interdisciplinary team of specialists, including system analysts, chemical engineers, geologists, hydrologists, mining engineers, nuclear engineers, physicists, radiochemists, mechanical engineers, meteorologists, climatologists, applied mathematicians, solid-state chemists, metallurgists, electrical engineers, and decision analysts.

A second feature of our approach is a multicycle methodology. In the initial cycle extensive lists of parameters are lumped together before being used in the model. In subsequent cycles the most important parameters are identified, and additional effort is devoted to them. The project is considered complete when the residual uncertainties reach desired levels.

Finally, our approach includes both general and specific scenarios and sites. In our generic studies we can isolate the dominant parameters or factors, whereas specific analyses allow us to evaluate individual events or sites. By incorporating both random and predictable events into these studies, we can analyze probabilistic, as well as deterministic, scenarios of future events.

RADIOLOGICAL RISK ANALYSIS FOR THE WASTE MANAGEMENT SYSTEM

To minimize radiological risk from the operation of waste management system, performance objectives must be established for volatilization, particulate dispersion, and dissolution characteristics of solidified high-level waste. Our studies indicate that transportation and interim storage are the most critical operations in the management system, hence they are likely to require the greatest scrutiny as objectives are established.

A summary of the expected values of risk for both preemplacement and postemplacement activities, normalized to man-rem/MWe-y, is given in Table 29. We have calculated the risk associated with each waste management operation as a function of waste type, then integrated the risk values over 10^6 y. After 10^6 y the risk is relatively insignificant in all cases studied. We have considered radiation doses due to external irradiation as well as internal uptake of radionuclides through food, water, and air pathways. The table shows only the whole-body dose from all sources, not critical-organ doses from radionuclide deposition on the ground.

Table 29 shows that the preemplacement risks are much greater than the postemplacement risks. However, the absolute values given in the table are very sensitive to modeling assumptions, and variations of several orders of magnitude are possible. We have assumed the initial DOE-OWI repository/waste-canister criteria, i.e., a maximum thermal output of 3.5 kW per waste canister and 12-in. o.d. canisters. We have also assumed that the waste is stored for 10 y before being placed in the repository. To meet these requirements, the calcine waste forms could not be solidified until 5 y after reactor shutdown, even with dilution. The glass waste form could be solidified after 1 y. No risk assessment was made of storage before solidification. As a reference design, we chose a spacing based on a previous study, and a sequence of operations where waste canisters of a similar age are grouped together to minimize handling. These last assumptions yielded high estimates of risk when we studied the scenario of a pool drainage (see Table 29), but a change in spacing and a different handling mode would reduce

526 167

TABLE 29. Expected radiological risk (whole-body dose in man-rem/MWe-y) for different operations of the waste management system for four waste forms.

Operation	Spray calcine			Fluidized-bed calcine		
	Volatilization	Air dispersion	Dissolution	Volatilization	Air dispersion	Dissolution
Reprocessing plant						
Handling						
• Filter works	0.0	0.0	---	0.0	0.0	---
• Filter fails	0.0	0.0	---	0.0	0.0	---
Interim storage						
• Filter works	0.0	0.0	---	0.0	0.0	---
• Filter fails	0.0	0.0	---	0.0	0.0	---
Pool drains	0.0	0.0	---	0.0	0.0	---
Transportation						
Truck	3.0E-5	1.7E-0	5.4E-2	3.0E-5	3.4E-1	2.2E-2
Train	1.1E-7	3.4E-2	7.4E-3	1.1E-7	6.7E-3	2.9E-3
Repository						
Handling						
• Filter works	0.0	0.0	---	0.0	0.0	---
• Filter fails	0.0	0.0	---	0.0	0.0	---
Surface storage	1.6E-13	2.1E-13	---	1.6E-13	2.1E-13	---
Postemplacement	---	---	4.9E-7	---	---	4.9E-7
Subtotals						
Truck	3.0E-5	1.7E-0	5.4E-2	3.0E-5	3.4E-1	2.2E-2
Train	1.1E-7	3.4E-2	7.4E-3	1.1E-7	6.7E-3	2.9E-3
Totals						
Truck		1.7E-0			3.6E-1	
Train		4.1E-2			9.6E-1	

TABLE 29. (cont'd).

Operation	Borosilicate glass			Supercaline multibarrier		
	Volatization	Air dispersion	Dissolution	Volatilization	Air dispersion	Dissolution
Reprocessing plant						
Handling						
• Filter works	0.0	0.0	---	0.0	0.0	---
• Filter fails	0.0	0.0	---	0.0	0.0	---
Interim storage						
• Filter works	5.2E-13	0.0	---	8.8E-13	0.0	---
• Filter fails	9.9E-12	0.0	---	1.7E-11	0.0	---
Pool drains	9.9E-1	0.0	---	1.3E-0	0.0	---
Transportation						
Truck	7.7E-3	8.5E-4	1.6E-5	6.7E-6	8.8E-6	1.6E-7
Train	4.9E-3	1.7E-5	2.9E-6	2.6E-8	1.7E-7	2.9E-8
Repository						
Handl[illegible]						
• Fi[illegible]	0.0	0.0	---	0.0	0.0	---
• [illegible]	0.0	0.0	---	0.0	0.0	---
Surface [illegible]	1.6E-13	2.1E-13	---	1.6E-13	2.1E-13	---
P[illegible]	---	---	4.9E-7	---	---	4.9E-7
Subtota[illegible]						
Truck	1.0E-0	8.5E-4	1.6E-5	1.3E-0	8.8E-6	6.5E-7
Train	9.9E-1	1.7E-5	3.4E-6	1.3E-0	1.7E-7	5.2E-7
Totals						
Truck		1.0E-0			1.3E-0	
Train		9.9E-1			1.3E-0	

the expected risk. Finally, the calculated risk values are based on the conservative assumption that water enters the repository immediately after it is sealed.

The most critical segment in the waste management system appears to be the transportation system. The fine particle size associated with calcine leads to risks from particulate dispersion, and the solubility of calcine leads to higher risks from dissolution than expected for glass. On the other hand, a fire severe enough to melt the glass can cause rapid corrosion of the canister wall, which in turn produces risks from volatile radionuclides that are higher in the glass form than in calcine.

SENSITIVITY ANALYSIS FOR PREEMPLACEMENT ACCIDENTS

Previous calculations of expected dose for preemplacement accidents have depended on nominal data for accident probabilities, release functions, and thermal-failure temperature and age thresholds. Uncertainties exist in these nominal data, and they can be affected by engineering choices. The effect of these uncertainties on expected dose must be explored. Accordingly, we have concentrated on the two types of accidents shown in previous analyses to be major contributors to total expected preemplacement dose to man. These are (1) interim-storage-pool drainage accidents caused by severe earthquakes, and (2) impact and fire accidents involving truck and train shipment of SHLW. We looked at four forms of SHLW (spray calcine, fluidized-bed calcine, borosilicate glass, and multibarrier) and considered only those parameters that have a nonlinear effect on dose.

Interim-Storage-Pool Drainage Accidents

Figure 43 is an event tree showing the factors that contribute to pool rupture and the release of nuclides in an interim-storage-pool drainage accident (see also Section 2). The expected dose to man is a product of, and is linearly dependent on, (1) the probability of a severe earthquake; (2) the probability

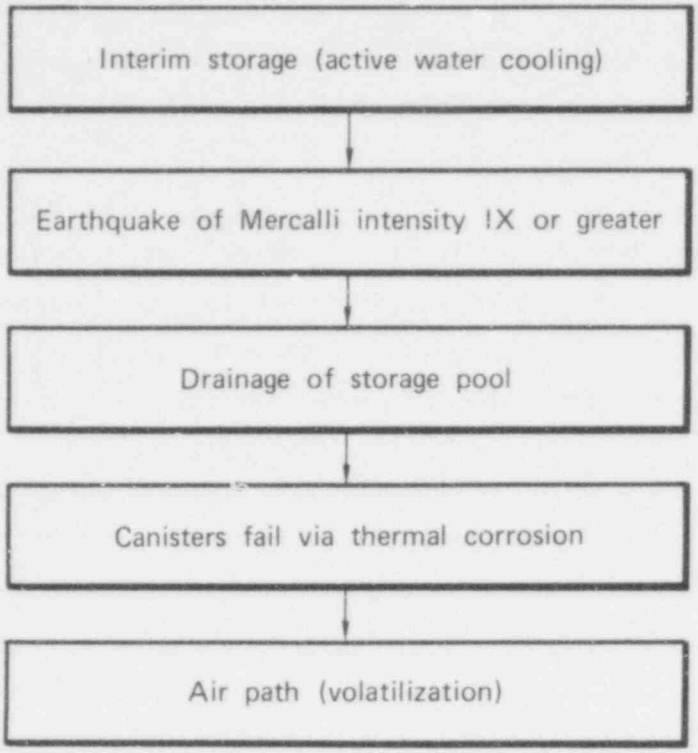

FIG. 43. Event tree for interim-storage-pool drainage accident.

of pool rupture and drainage, given a severe earthquake; and (3) the expected activity of radionuclides released as a result of canister failure, given that the pool drains. However, the expected activity of released radionuclides is a nonlinear function of the failure threshold age for a given SHLW form, i.e., the age beyond which canister failure due to thermal corrosion cannot occur. This point is discussed in more detail below. The failure threshold age, in turn, depends on two design parameters: (1) the canister spacing in the storage pool, which affects canister-to-canister heat transfer; and (2) the arrangement of canisters (by age of waste) in the pool. This second parameter can range from complete segregation of the SHLW by age to a uniform intermixing of all ages.

Once the failure threshold age has been established for a given spacing and age configuration (see Section 2), it can be used to compute the probability of canister failure, the expected activity released, and the expected dose to man, given a drainage accident. The following equation was used for expected release:

$$E[Q_r] = P_1 P_2 P_F RF \int_{t_0}^{t_F} Q_r(t)dt \quad ,$$

where

$E[Q_r]$ = expected activity of volatile radionuclide r released to the atmosphere, in Ci/MWe-y. $E[Q_r]$ is computed separately for each volatile radionuclide in each waste form.

P_1 = probability per year of a severe earthquake (y^{-1}).

P_2 = probability of pool rupture and drainage, given a severe earthquake (dimensionless).

P_F = probability of failure of all canisters holding waste younger than the failure threshold age, given pool drainage (dimensionless).

RF = fraction of volatiles released from canisters, given failure (dimensionless).

t_0 = age of waste when placed in interim storage pool (y).

t_F = failure threshold age (y).

$Q_r(t)$ = inventory of volatile radionuclide r after t y (Ci/MWe-y).

Figure 44 depicts the relationship among emplacement age, failure threshold age, and the expected release. If the age of the waste at emplacement is greater than the failure threshold age T_F, the probability of release and the expected activity are both zero, since the solid form can never fail in storage. When $t_0 < t_F$, the probability of release is proportional to $t_F - t_0$, and the expected value of the released activity of radionuclide r is proportional to the crosshatched area in the figure.

The assumptions in this analysis are:

- The inventory for each radionuclide r is approximated by a function of time with linear segments, as shown in Fig. 44.
- The total number of canisters in the pool remains constant.
- The demography is that downwind of the Barnwell, S.C., fuel-reprocessing plant.

526 172

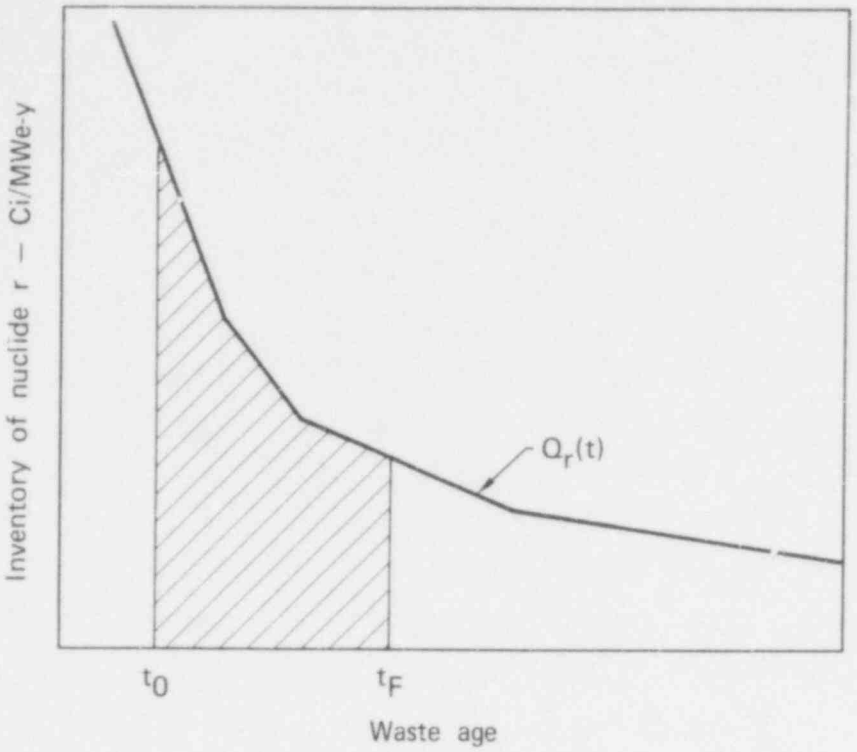

FIG. 44. Inventory of an arbitrary nuclide r as a function of waste age. The activity released during a pool drainage accident is proportional to the crosshatched area between t_0 (the emplacement time) and t_F (the failure threshold age).

- Wind speed is 5 m/s (Pasquill D-stability).
- The expected dose to man is the whole-body dose integrated over a distance of 10^6 m downwind from the storage pool.

Figure 45 displays expected dose values for worst-case, nominal-case, and best-case scenarios for glass and multibarrier waste forms. Spray calcine and fluidized-bed calcine do not fail under any conditions because for them $t_F < t_0$. The three scenarios can be described as follows:

- Worst case. All waste ages are uniformly mixed; the intercanister spacing is 1.5 ft; t_F = 10 y or more.
- Nominal case. Waste is segregated into 1-y groups; the intercanister spacing is 1.5 ft; t_F = 3 y.
- Best case. All waste ages are uniformly mixed; the intercanister spacing is 2 to 3 ft; $t_F \leq 1$ y.

526 173

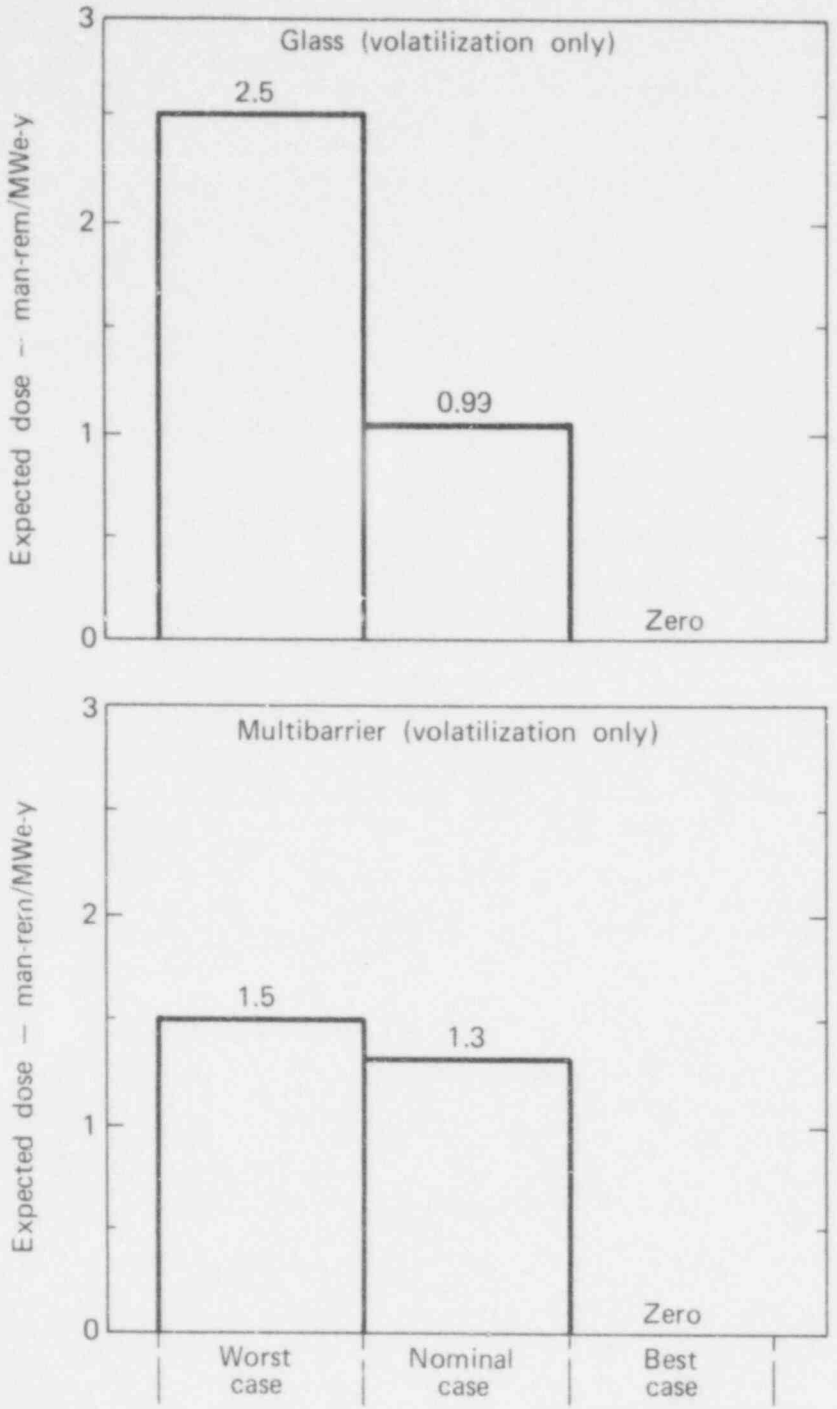

FIG. 45. Expected doses in three scenarios of a pool drainage accident for two waste forms. The uncertainty in the expected values for the best cases is large because of factors neglected in the thermal model and because of uncertainties in the corrosion failure temperature of each solid form.

From this sensitivity study and from values of t_F derived from thermal analyses, the following conclusions may be drawn:

- The worst-case multibarrier dose of 1.5 man-rem/MWe-y, is a major component of the total expected preemplacement dose.
- Through a judicious choice of age aggregation and canister spacing, the expected dose from glass and multibarrier SHLW in pool drainage accidents can probably be reduced to insignificantly small values. This conclusion must be advanced tentatively because of factors neglected in the simple thermal analysis of the waste and because of uncertainties in the failure temperatures.

Transportation Accidents

The nonlinear factors in the expected dose calculations for transportation accidents are (1) the probability density functions (PDFs), (2) the release functions (RFs), and (3) failure criteria and failure loci (for fire accidents). Each of these factors was varied to evaluate its influence on expected dose. These variations are illustrated graphically in Fig. 46 and can be described as follows:

- The tails of PDF curves were varied so that they accounted for a 95% confidence range. This was done only for those PDFs for which identifiable data points (instead of smooth curves) were available, and thus includes PDFs for truck fire durations and train impact velocities.
- Two alternative fire temperature PDFs were considered.
- Upper and lower credible bounds on release functions were established. These are used for all dispersion, volatilization, and dissolution releases that are functions of impact velocity or fire temperature.
- Upper and lower bounds were estimated for the canister-failure threshold temperature for each SHLW form, and each means of transportation. Each of these temperatures is associated with a failure locus, as shown in Fig. 46(d).

Our approach was to compute best-case, nominal-case, and worst-case expected doses for each of the two fire temperature distributions by simultaneously

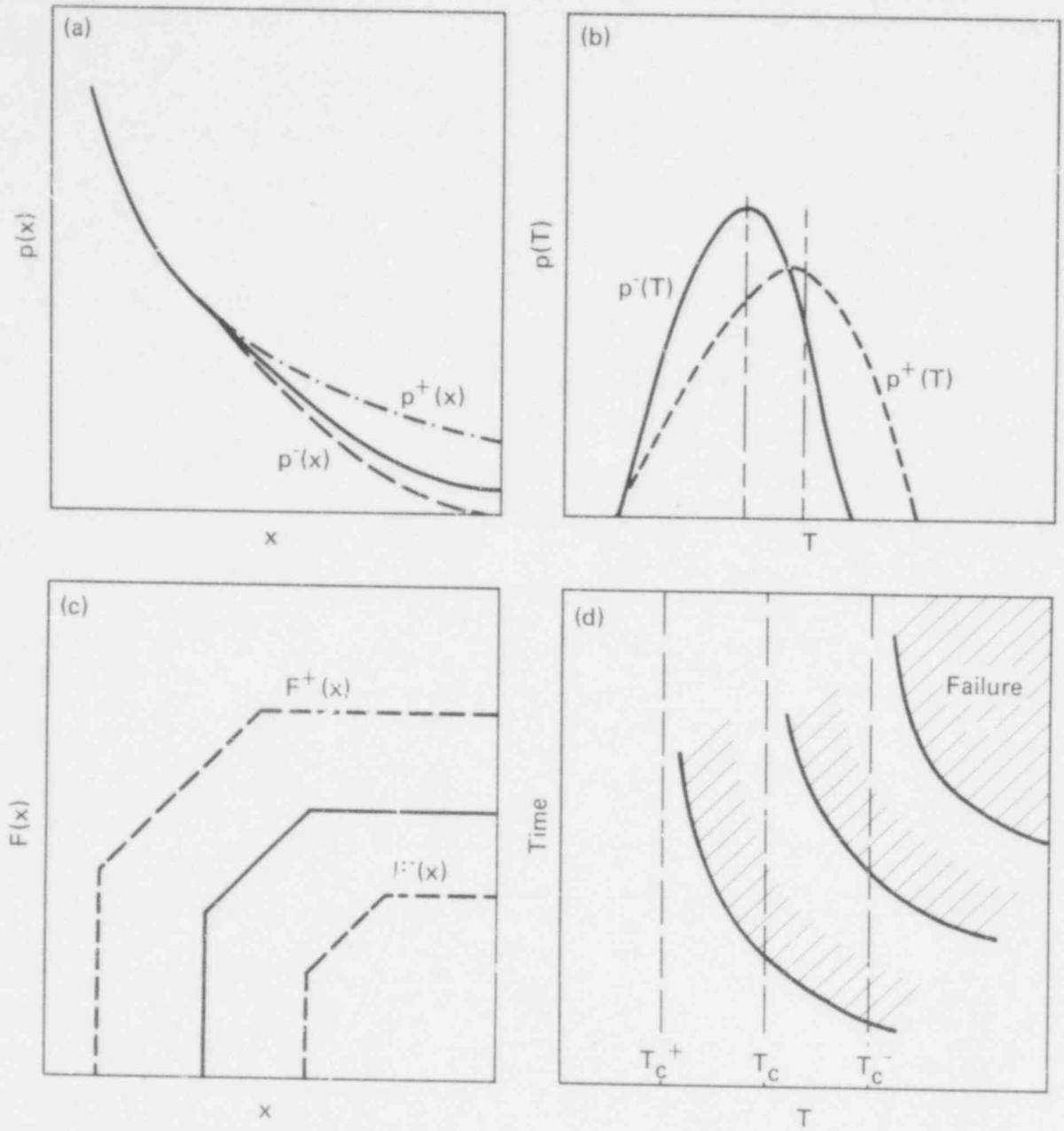

FIG. 46. Graphical representation of variations in parameters that served as basis of transportation sensitivity analysis: (a) $p^+(x)$ and $p^-(x)$ encompass 95% confidence range for tail of PDF, p(x); (b) $p^+(T)$ and $p^-(T)$ represent two fire temperature PDFs; (c) $F^+(x)$ and $F^-(x)$ represent the credible bounds of release function F(x); and (d) T_c^+ and T_c^-, with associated failure loci, represent the estimated bounds of the failure temperature T_c. 526 176

setting the remaining variable factors to their best-case, nominal-case, and worst-case values. Tables 30 through 33 present the results for each of the four waste forms.

In computing expected doses to man, we made the following assumptions:

- All SHLW shipped by truck or train is 10 y old.
- The expected dose to man is the whole-body dose integrated over a distance of 10^6 m downwind of the accident, which occurs at the center of a city (urban accidents) or at a location having a low and uniform population density (rural accidents).
- The probability of impact or fire in a given accident is equal in the rural and urban areas.
- The urban demography is that of the Dallas/Ft. Worth area.
- Wind speed is 5 m/s (Pasquill D-stability).

TABLE 30. Results of sensitivity analysis for spray calcine. Results are shown as expected doses in man-rem/MWe-y. T_c^- and T_c^+ are the low and high fire-temperature PDFs.

	Truck accients						Train accidents					
	Worst case		Nominal case		Best case		Worst case		Nominal case		Best case	
Type of accident	T_c^-	T_c^+	T_c^-	T_c^+	T_c^-	T_c^+	T_c^-	T_c^+	T_c^-	T_c^+	T_c^-	T_c^+
Dispersion												
Impact	1.8E1	1.8E1	1.7E0	1.7E0	1.4E-3	1.4E-3	4.6E-1	4.6E-1	3.4E-2	3.4E-2	3.2E-6	3.2E-6
Crossing	1.6E-1	1.6E-1	2.8E-2	2.8E-2	9.2E-5	9.2E-5	-	-	-	-	-	-
Fire	0.0	1.2E-2	0.0	2.6E-5	0.0	0.0	0.0	1.4E-3	0.0	9.7E-8	0.0	0.0
Total	1.8E1	1.8E1	1.7E0	1.7E0	1.5E-3	1.5E-3	4.6E-1	4.6E-1	3.4E-2	3.4E-2	3.2E-6	3.2E-6
Volatilization												
Impact	0.0	0.0	0.0	0.0	0.0	0.0	0.0	0.0	0.0	0.0	0.0	0.0
Crossing	0.0	0.0	0.0	0.0	0.0	0.0	-	-	-	-	-	-
Fire	0.0	1.2E-2	0.0	3.0E-5	0.0	0.0	0.0	1.5E-3	0.0	1.1E-7	0.0	0.0
Total	0.0	1.2E-2	0.0	3.0E-5	0.0	0.0	0.0	1.5E-3	0.0	1.1E-7	0.0	0.0
Dissolution												
Impact	4.0E-1	4.0E-1	5.4E-2	5.4E-2	3.4E-4	3.4E-4	7.6E-2	7.6E-2	7.4E-3	7.4E-3	6.2E-6	6.2E-6
Crossing	3.2E-3	3.2E-3	6.6E-4	6.6E-4	2.2E-5	2.2E-5	-	-	-	-	-	-
Fire	0.0	2.2E-4	0.0	2.4E-6	0.0	0.0	0.0	2.6E-5	0.0	8.8E-9	0.0	0.0
Total	4.0E-1	4.0E-1	5.4E-2	5.4E-2	3.6E-4	3.6E-4	7.6E-2	7.6E-2	7.4E-3	7.4E-3	6.2E-6	6.2E-6
Total												
Impact	1.8E1	1.8E1	1.7E0	1.7E0	1.7E-3	1.7E-3	5.3E-1	5.3E-1	4.1E-2	4.1E-2	9.4E-6	9.4E-6
Crossing	1.6E-1	1.6E-1	9.4E-2	9.4E-2	1.1E-4	1.1E-4	-	-	-	-	-	-
Fire	0.0	2.5E-2	0.0	5.8E-5	0.0	0.0	0.0	2.9E-3	0.0	2.2E-7	0.0	0.0
Total	1.8E1	1.9E1	1.7E0	1.7E0	1.9E-3	1.9E-3	5.3E-1	5.4E-1	4.1E-2	4.1E-2	9.4E-6	9.4E-6

TABLE 31. Results of sensitivity analysis for glass. Results are shown as expected doses in man-rem/MWe-y. T_c^- and T_c^+ are the low and high fire-temperature PDFs.

Type of accident	Truck accidents						Train accidents					
	Worst case		Nominal case		Best case		Worst case		Nominal case		Best case	
	T_c^-	T_c^+	T_c^-	T_c^+	T_c^-	T_c^+	T_c^-	T_c^+	T_c^-	T_c^+	T_c^-	T_c^+
Dispersion												
Impact	7.6E-2	7.6E-2	8.3E-4	8.3E-4	7.2E-6	7.2E-6	2.3E-3	2.3E-3	1.7E-5	1.7E-5	1.6E-8	1.6E-8
Crossing	3.0E-4	3.0E-4	1.5E-5	1.5E-5	9.8E-7	9.8E-7	-	-	-	-	-	-
Fire	0.0	0.0	0.0	0.0	0.0	0.0	0.0	0.0	0.0	0.0	0.0	0.0
Total	7.7E-2	7.7E-2	8.5E-4	8.5E-4	8.2E-6	8.2E-6	2.3E-3	2.3E-3	1.7E-5	1.7E-5	1.6E-8	1.6E-8
Volatilization												
Impact	0.0	0.0	0.0	0.0	0.0	0.0	0.0	0.0	0.0	0.0	0.0	0.0
Crossing	0.0	0.0	0.0	0.0	0.0	0.0	-	-	-	-	-	-
Fire	7.7E-3	2.4E-1	3.4E-6	7.7E-3	0.0	1.7E-14	3.3E-3	1.5E-1	6.5E-8	4.9E-3	0.0	6.8E-7
Total	7.7E-3	2.4E-1	3.4E-6	7.7E-3	0.0	1.7E-14	3.3E-3	1.5E-1	6.5E-8	4.9E-3	0.0	6.8E-7
Dissolution												
Impact	1.7E-3	1.7E-3	1.5E-5	1.5E-5	1.8E-7	1.8E-7	4.8E-4	4.8E-4	2.9E-6	2.9E-6	3.2E-9	3.2E-9
Crossing	1.7E-6	1.7E-6	3.8E-7	3.8E-7	3.0E-8	3.0E-8	-	-	-	-	-	-
Fire	1.2E-7	1.6E-6	3.8E-11	4.4E-8	0.0	5.4E-20	5.0E-8	9.6E-7	7.2E-13	2.4E-8	0.0	2.6E-12
Total	1.7E-3	1.7E-3	1.6E-5	1.6E-5	2.1E-7	2.1E-7	4.8E-4	4.8E-4	2.9E-6	2.9E-6	3.2E-9	3.2E-9
Total												
Impact	7.8E-2	7.8E-2	8.5E-4	8.5E-4	7.4E-6	7.4E-6	2.8E-3	2.8E-2	2.0E-5	2.0E-5	1.9E-8	1.9E-8
Crossing	3.0E-4	3.0E-4	1.5E-5	1.5E-5	1.0E-6	1.0E-6	-	-	-	-	-	-
Fire	7.7E-3	2.4E-1	3.4E-6	7.7E-3	0.0	1.7E-14	3.3E-3	1.5E-1	6.5E-8	4.9E-3	0.0	6.8E-7
Total	8.6E-2	3.2E-1	8.6E-4	8.6E-3	8.4E-6	8.4E-6	6.1E-3	1.5E-1	2.0E-5	4.9E-3	1.9E-8	7.0E-7

TABLE 32. Results of sensitivity analysis for fluidized-bed calcine. Results are shown as expected doses in man-rem/MWe-y. T_c^- and T_c^+ are low and high fire-temperature PDFs.

Type of accident	Truck accidents						Train accidents					
	Worst case		Nominal case		Best case		Worst case		Nominal case		Best case	
	T_c^-	T_c^+	T_c^-	T_c^+	T_c^-	T_c^+	T_c^-	T_c^+	T_c^-	T_c^+	T_c^-	T_c^+
Dispersion												
Impact	5.5E-1	5.5E-1	3.3E-1	3.3E-1	1.3E-3	1.3E-3	1.9E-1	1.9E-1	6.7E-3	6.7E-3	3.0E-6	3.0E-6
Crossing	7.1E-2	7.1E-2	5.5E-3	5.5E-3	9.0E-5	9.0E-5	-	-	-	-	-	-
Fire	0.0	1.1E-2	0.0	2.6E-5	0.0	0.0	0.0	1.3E-3	0.0	9.7E-8	0.0	0.0
Total	6.2E-1	6.3E-1	3.4E-1	3.4E-1	1.4E-3	1.4E-3	1.9E-1	1.9E-1	6.7E-3	6.7E-3	3.0E-6	3.0E-6
Volatilization												
Impact	0.0	0.0	0.0	0.0	0.0	0.0	0.0	0.0	0.0	0.0	0.0	0.0
Crossing	0.0	0.0	0.0	0.0	0.0	0.0	-	-	-	-	-	-
Fire	0.0	1.2E-2	0.0	3.0E-5	0.0	0.0	0.0	1.5E-3	0.0	1.1E-7	0.0	0.0
Total	0.0	1.2E-2	0.0	3.0E-5	0.0	0.0	0.0	1.5E-3	0.0	1.1E-7	0.0	0.0
Dissolution												
Impact	4.0E-1	4.0E-1	2.2E-2	2.2E-2	1.5E-4	1.4E-4	7.6E-2	7.6E-2	2.9E-3	2.9E-3	2.5E-6	2.5E-6
Crossing	3.2E-3	3.2E-3	2.6E-4	2.6E-4	8.8E-8	8.8E-6	-	-	-	-	-	-
Fire	0.0	2.2E-4	0.0	2.4E-6	0.0	0.0	0.0	2.6E-5	0.0	8.8E-9	0.0	0.0
Total	4.0E-1	4.0E-1	2.2E-2	2.2E-2	1.5E-4	1.5E-4	7.6E-2	7.6E-2	2.9E-3	2.9E-3	2.5E-6	2.5E-6
Total												
Impact	9.5E-1	9.5E-1	3.5E-1	3.5E-1	1.4E-3	1.4E-3	2.7E-1	2.7E-1	9.7E-3	9.7E-3	5.5E-6	5.5E-6
Crossing	7.4E-2	7.4E-2	5.8E-3	5.8E-3	9.9E-5	9.9E-5	-	-	-	-	-	-
Fire	0.0	2.3E-2	0.0	5.8E-5	0.0	0.0	0.0	2.8E-3	0.0	2.1E-7	0.0	0.0
Total	1.0E0	1.0E0	3.6E-1	3.6E-1	1.5E-3	1.5E-3	2.7E-1	2.7E-1	9.7E-3	9.7E-3	5.5E-6	5.5E-6

TABLE 33. Results of sensitivity analysis for multibarrier. Results are shown as expected doses in man-rem/MWe-y. T_c^- and T_c^+ are the low and high fire-temperature PDFs.

	Truck accidents						Train accidents					
	Worst case		Nominal case		Best case		Worst case		Nominal case		Best case	
Type of accident	T_c^-	T_c^+	T_c^-	T_c^+	T_c^-	T_c^+	T_c^-	T_c^+	T_c^-	T_c^+	T_c^-	T_c^+
Dispersion												
Impact	7.7E-4	7.7E-4	8.3E-6	8.3E-6	5.8E-8	5.8E-8	2.4E-5	2.4E-5	1.7E-7	1.7E-7	1.3E-10	1.3E-10
Crossing	6.0E-6	6.0E-6	1.5E-7	1.5E-7	9.0E-9	9.0E-9	-	-	-	-	-	-
Fire	1.5E-6	5.1E-3	0.0	2.6E-7	0.0	0.0	4.0E-8	1.3E-3	0.0	9.7E-10	0.0	0.0
Total	7.7E-4	5.9E-3	8.5E-6	8.8E-6	6.7E-8	6.7E-8	2.4E-5	1.3E-3	1.7E-7	1.7E-7	1.3E-10	1.3E-10
Volatilization												
Impact	0.0	0.0	0.0	0.0	0.0	0.0	0.0	0.0	0.0	0.0	0.0	0.0
Crossing	0.0	0.0	0.0	0.0	0.0	0.0	-	-	-	-	-	-
Fire	8.4E-7	6.6E-3	0.0	6.7E-6	0.0	0.0	2.2E-8	1.9E-3	0.0	2.6E-8	0.0	0.0
Total	8.4E-7	6.6E-3	0.0	6.7E-6	0.0	0.0	2.2E-8	1.9E-3	0.0	2.6E-8	0.0	0.0
Dissolution												
Impact	1.7E-5	1.7E-5	1.6E-7	1.6E-7	1.8E-9	1.8E-9	4.8E-6	4.8E-6	2.9E-8	2.9E-8	3.2E-11	3.2E-11
Crossing	2.0E-7	2.0E-7	3.8E-9	3.8E-9	3.0E-10	3.0E-10	-	-	-	-	-	-
Fire	2.8E-11	9.0E-8	0.0	4.8E-11	0.0	0.0	7.2E-13	2.4E-8	0.0	1.7E-13	0.0	0.0
Total	1.7E-5	1.7E-5	1.6E-7	1.6E-7	2.1E-9	2.1E-9	4.8E-6	4.8E-6	2.9E-8	2.9E-8	3.2E-11	3.2E-11
Total												
Impact	7.9E-4	7.9E-4	8.4E-6	8.4E-6	6.0E-8	6.0E-8	2.8E-5	2.8E-5	2.0E-7	2.0E-7	1.6E-10	1.6E-10
Crossing	6.2E-6	6.2E-6	1.5E-7	1.5E-7	9.3E-9	9.3E-9	-	-	-	-	-	-
Fire	2.4E-6	1.2E-2	0.0	7.0E-6	0.0	0.0	6.2E-8	3.3E-3	0.0	2.7E-8	0.0	0.0
Total	7.9E-4	1.2E-2	8.7E-6	1.6E-5	6.9E-8	6.9E-8	2.8E-5	3.3E-3	2.0E-7	2.3E-7	1.6E-10	1.6E-10

COMPARATIVE HAZARDS

Hazards associated with the deep burial of SHLW have been compared to the hazards of toxic elements in naturally occurring ore deposits (Tonnessen and Cohen, 1977). The basis of the comparison was the effect on drinking water. Calculations for wastes from both fast breeder reactors (FBR) and light water reactors (LWR) show that nuclear-waste toxicity decreases to levels below those of several naturally occurring elements within 10^2 to 10^3 y (see Fig. 47). The several components of the total hazard from the waste from a pressurized-water reactor are shown in Fig. 48.

The comparison summarized in Fig. 47 is not an attempt to demonstrate the validity or acceptability of any type of waste disposal. It merely puts into perspective the hazards that can be expected from SHLW, and it may increase awareness of the hazards the public routinely accepts.

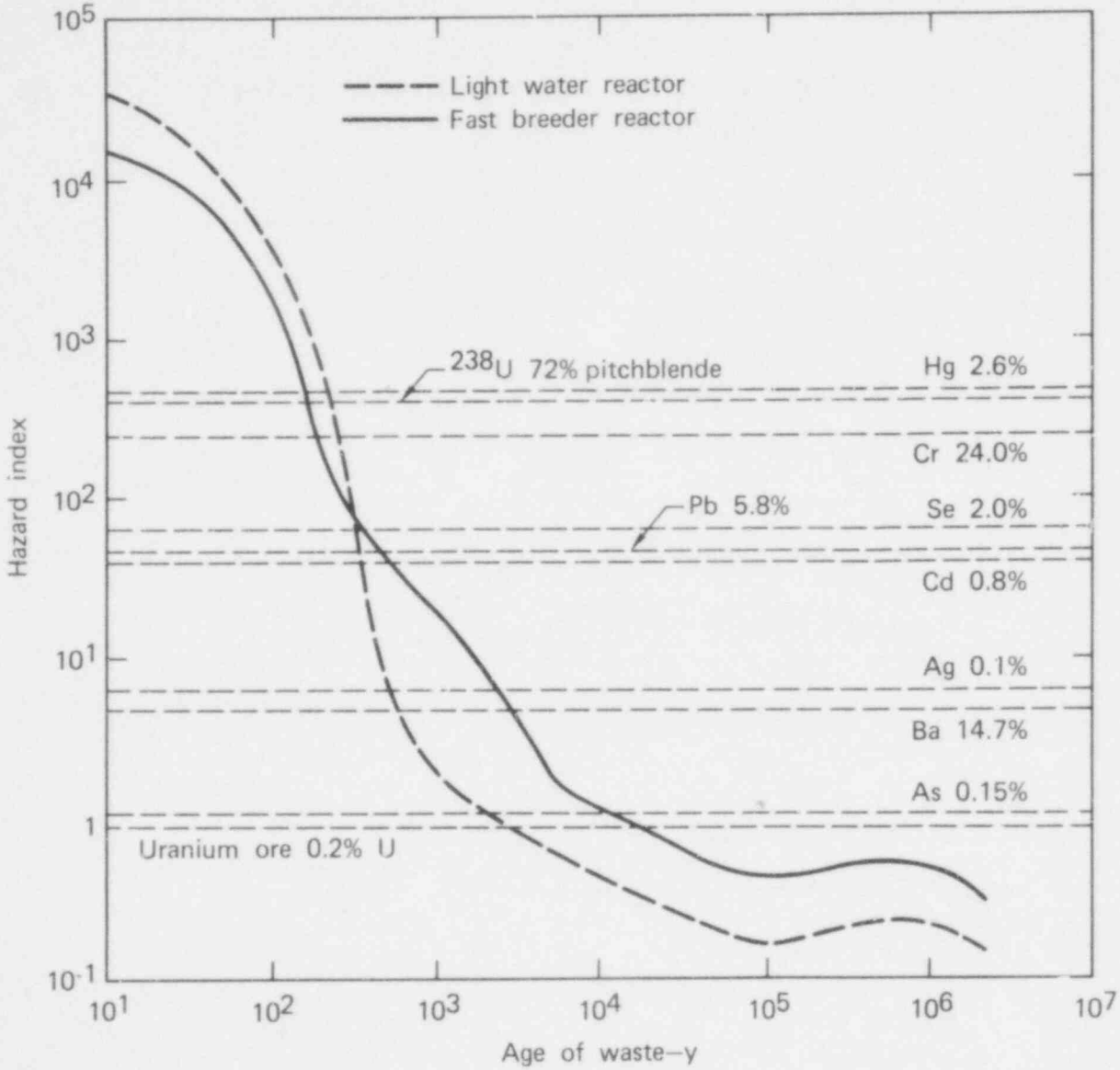

FIG. 47. Hazards from buried waste from light water reactor and fast breeder reactor, compared with hazards from average ores of toxic elements.

526 183

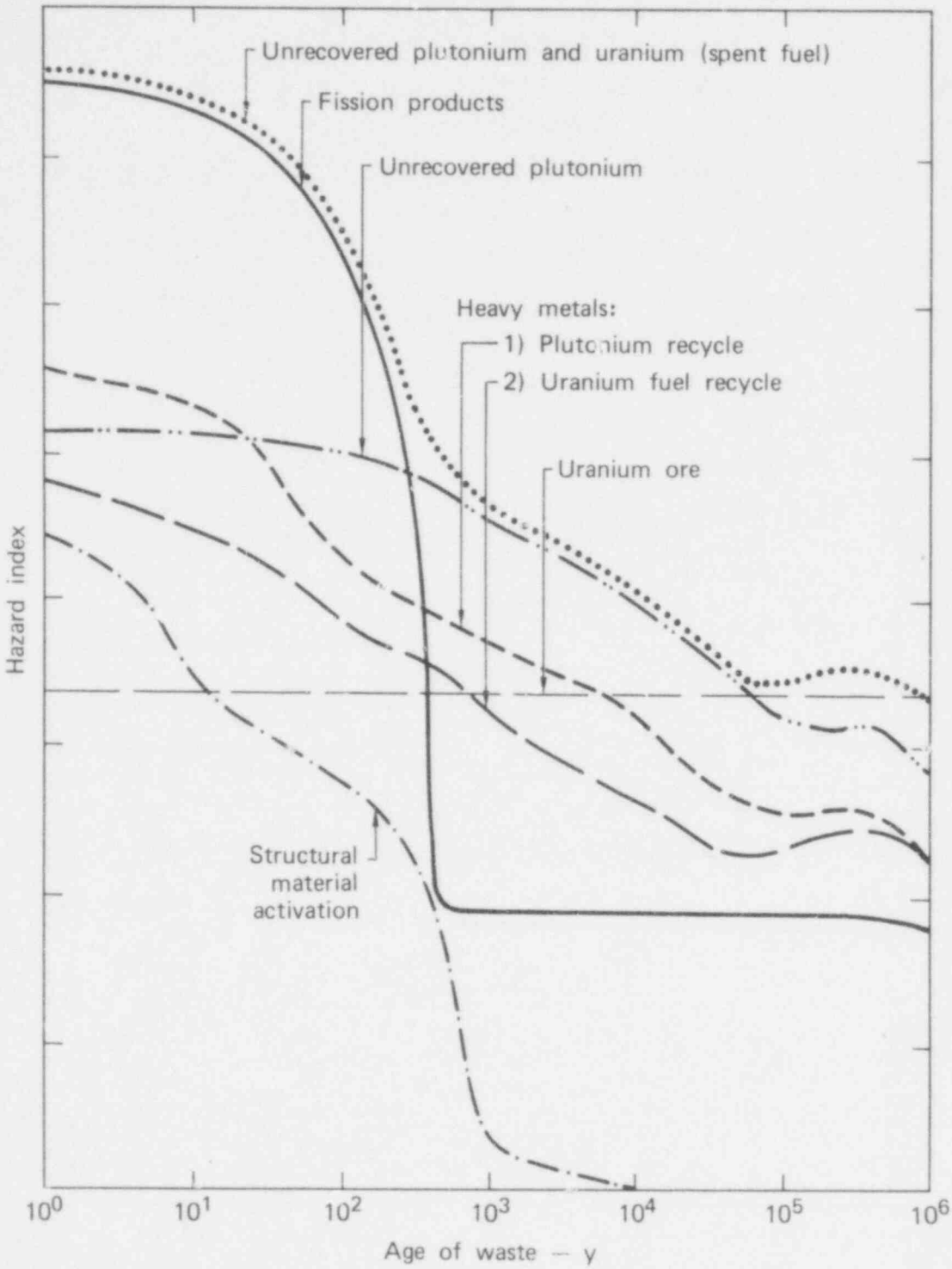

FIG. 48. Components of total hazard from waste from 1000-MWe pressurized-water reactor. Waste is taken to arise from 1 t of fuel at 3.4×10^4 MW_{TH}-d.

SENSITIVITY ANALYSIS FOR POSTEMPLACEMENT PERIOD

This section summarizes the method and gives the results of the sensitivity analysis for our SHLW repository model. By changing parameter values in the model, we simulated the results of release through a number of pathways and the breaching of barriers in four repository types:

- Sandstone-shale sedimentary sequence; repository in the shale layer with interstitial flow in the shales.
- Same as type 1 with fracture flow in the shales.
- Sandstone-shale-salt sequence; repository in the salt layer, with interstitial flow in the shales.
- Sandstone-shale-salt sequence; repository in the salt layer, with fracture flow in the shales.

The results from 85 separate computer runs are given in Tables 34 through 45; the parameter values used in the calculations are listed in Tables 46 through 59.

TABLE 34. Shale repository sensitivity analysis (interstitial flow).

VARIED PARAMETER	BASELINE VALUE	NEW VALUE	INTEGRATED POPULATION DOSE (MAN-REM/MWe-YR)			PEAK INDIVIDUAL DOSE (REM/MWe-YR)				
			WHOLE BODY DOSE	CRITICAL ORGAN DOSE	CRITICAL ORGAN	WHOLE BODY DOSE	TIME	CRITICAL ORGAN DOSE	TIME	CRITICAL ORGAN
BASELINE	–	–	1.30 E -3	1.60 E -1	GI-LLI	6.19 E -14	1.44 E 4	7.49 E -12	1.44 E 4	GI-LLI
ACTINIDE & FISSION PRODUCT SORPTION FACTORS		(1)	8.98 E -2	3.56 E -1	GI-LLI	2.78 E -12	1.24 E 6	2.31 E -11	1.44 E 4	GI-LLI
DISPERSION	50	10	1.63 E -2	1.88 E -1	GI-LLI	1.07 E -13	1.74 E 5	1.30 E -11	1.74 E 5	GI-LLI
LOW POROSITY EVERYWHERE		(2)	2.36 E -3	2.89 E -1	GI-LLI	2.94 E -13	4.52 E 4	3.56 E -11	4.52 E 4	GI-LLI
LOW POROSITY IN AQUIFER	0.1	0.02	1.35 E -3	1.65 E -1	GI-LLI	6.55 E -14	5.99 E 3	7.93 E -12	5.99 E 3	GI-LLI
POROSITY IN SHALE	0.05	0.01	2.23 E -3	2.74 E -1	GI-LLI	2.94 E -13	5.85 E 4	3.56 E -11	5.85 E 4	GI-LLI
LOW POROSITY IN SHAFT & TUNNEL FRACTURE ZONE		(3)	1.30 E -3	1.60 E -1	GI-LLI	6.55 E -14	1.17 E 4	7.91 E -12	1.17 E 4	GI-LLI
FAST SATURATION	100	20	1.30 E -3	1.60 E -1	GI-LLI	6.19 E -14	1.44 E 4	7.49 E -12	1.44 E 4	GI-LLI
MIN. AREA FRACTURE ZONE IN TUNNEL		(4)	1.29 E -3	1.59 E -1	GI-LLI	5.8 E -14	1.17 E 4	7.01 E -12	1.17 E 4	GI-LLI
MAX. AREA FRACTURE ZONE IN SHAFT AND TUNNEL		(5)	1.72 E -3	2.47 E -1	GI-LLI	7.48 E -13	1.17 E 4	9.05 E -11	1.17 E 4	GI-LLI
SHALE PERMEABILITY		(6)	2.73 E -3	4.14 E -1	GI-LLI	1.59 E -12	1.52 E 4	1.93 E -10	1.52 E 4	GI-LLI
ARTESIAN HEAD	60	150	1.93 E -3	2.37 E -1	GI-LLI	1.42 E -13	8.86 E 4	1.71 E -11	8.86 E 4	GI-LLI
AQUIFER PERMEABILITY	10^{-4}	10^{-2}	1.39 E -3	1.67 E -1	GI-LLI	6.57 E -14	3.96 E 3	7.95 E -12	3.96 E 3	GI-LLI
FRACTURE ZONE PERMEABILITY		(7)	1.60 E -3	2.23 E -1	GI-LLI	5.62 E -13	1.17 E 4	6.81 E -11	1.17 E 4	GI-LLI
HEAD GRADIENT IN AQUIFER	0.005	0.05	1.37 E -3	1.66 E -1	GI-LLI	6.64 E -14	4.87 E 3	8.04 E -12	4.87 E 3	GI-LLI
THICKNESS OF DEPOSITORY LAYER	200	20	2.44 E -3	3.12 E -1	GI-LLI	5.35 E -13	3.31 E 4	6.48 E -11	3.31 E 4	GI-LLI
THICKNESS OF BARRIER LAYER	200	20	1.76 E -3	2.26 E -1	GI-LLI	2.43 E -13	1.24 E 4	2.94 E -11	1.24 E 4	GI-LLI
LENGTH OF TUNNEL (INCREASE)	400	6000	1.30 E -3	1.60 E -1	GI-LLI	6.22 E -14	1.52 E 4	7.52 E -12	1.52 E 4	GI-LLI
LENGTH OF TUNNEL	440	200	1.30 E -3	1.60 E -1	GI-LLI	6.19 E -14	1.45 E 4	7.49 E -12	1.45 E 4	GI-LLI
DISSOLUTION RATE OF WASTE	10^{-4}	0.1	1.34 E -3	1.65 E -1	GI-LLI	2.95 E -13	1.23 E 4	3.57 E -11	1.23 E 4	GI-LLI
FISSION PRODUCT SORPTION FACTORS	10^{2}	*	3.39 E -3	3.09 E -1	GI-LLI	6.52 E -13	1.12 E 4	2.30 E -11	1.12 E 4	GI-LLI
ACTINIDE SORPTION FACTORS	10^{4}	10^{2}	8.78 E -2	8.78 E -2	WHOLE BODY	2.78 E -12	1.24 E 6	3.91 E -11	1.24 E 6	BONE
AQUIFER LENGTH	1.6 E 2	1.6 E 3	1.37 E -3	1.66 E -1	GI-LLI	6.52 E -14	5.13 E 3	7.89 E -12	5.13 E 3	GI-LLI

TABLE 34. Shale repository sensitivity analysis (interstitial flow) (continued).

VARIED PARAMETER	PEAK AQUIFER CONCENTRATION (Ci/M^3-MWe-YR)							
	^{99}Tc CONCENTRATION	TIME	^{126}Sn CONCENTRATION	TIME	^{226}Ra CONCENTRATION	TIME	^{235}Pu CONCENTRATION	TIME
BASELINE	2.02 E -11	3.96 E 3	1.31 E -14	2.14 E 5	–	–	–	–
ACTINIDE & FISSION PRODUCT SORPTION FACTORS	2.02 E -11	3.96 E 3	7.50 E -13	3.75 E 3	2.23 E -15	2.25 E 5	1.26 E -14	1.65 E 5
DISPERSION	3.44 E -11	1.65 E 5	2.60 E -14	2.37 E 5	–	–	–	–
LOW POROSITY EVERYWHERE	9.13 E -11	4.29 E 4	3.07 E -13	2.83 E 4	2.07 E -17	1.79 E 6	8.25 E -18	2.20 E 6
LOW POROSITY IN AQUIFER	2.02 E -11	3.95 E 3	1.30 E -14	2.14 E 5	–	–	–	–
POROSITY IN SHALE	9.13 E -11	4.29 E 4	1.30 E -14	2.14 E 5	–	–	–	–
LOW POROSITY IN SHAFT & TUNNEL FRACTURE ZONE	2.37 E -11	5.82 E 2	3.07 E -13	2.83 E 4	2.07 E -17	1.79 E 6	2.44 E -21	2.20 E 6
FAST SATURATION	2.02 E -11	3.88 E 3	1.31 E -14	2.14 E 5	–	–	–	–
MINIMUM AREA FRACTURE ZONE IN TUNNEL	2.15 E -11	2.18 E 2	5.67 E -13	7.37 E 3	8.22 E -18	4.65 E 5	4.81 E -16	3.78 E 5
MAXIMUM AREA FRACTURE ZONE IN SHAFT AND TUNNEL	2.69 E -10	9.28 E 2	2.18 E -12	4.52 E 4	–	–	–	–
SHALE PERMEABILITY	5.04 E -10	4.62 E 3	3.45 E -13	1.41 E 5	–	–	–	–
ARTESIAN HEAD	4.45 E -11	7.99 E 4	7.4 E -14	9.33 E 4	–	–	–	–
AQUIFER PERMEABILITY	2.02 E -13	3.98 E 3	1.30 E -16	2.14 E 5	–	–	–	–
FRACTURE ZONE PERMEABILITY	2.04 E -10	5.82 E 2	2.64 E -12	2.83 E 4	1.73 E -16	1.79 E 6	6.88 E -18	1.98 E 6
HEAD GRADIENT IN AQUIFER	2.02 E -12	3.96 E 3	1.30 E -15	2.14 E 5	–	–	–	–
THICKNESS OF DEPOSITORY LAYER	1.74 E -10	2.43 E 4	1.71 E -15	2.25 E 5	–	–	–	–
THICKNESS OF BARRIER LAYER	8.58 E -11	1.20 E 3	4.91 E -13	6.16 E 4	–	–	–	–
LENGTH OF TUNNEL (INCREASE)	2.05 E -11	4.87 E 3	1.08 E -14	2.77 E 5	–	–	–	–
LENGTH OF TUNNEL	2.02 E -11	3.96 E 3	1.32 E -14	2.14 E 5	–	–	–	–
DISSOLUTION RATE OF WASTE	1.48 E -10	2.24 E 3	1.40 E -14	1.82 E 5	–	–	–	–
FISSION PRODUCT SORPTION FACTORS	2.02 E -11	3.96 E 3	7.50 E -13	3.78 E 3	–	–	–	–
ACTINIDE SORPTION FACTORS	2.02 E -11	3.96 E 3	1.30 E -14	2.14 E 5	2.23 E -15	2.25 E 5	1.26 E -14	1.65 E 5
AQUIFER LENGTH	2.02 E -11	3.96 E 3	1.30 E -14	2.14 E 5	–	–	–	–

TABLE 35 Shale repository sensitivity analysis (multiple parameter, interstitial flow).

VARIED PARAMETER	INTEGRATED POPULATION DOSE (MAN-REM/MWe-YR)			PEAK INDIVIDUAL DOSE (REM/MWe-YR)				
	WHOLE BODY DOSE	CRITICAL ORGAN DOSE	CRITICAL ORGAN	WHOLE BODY DOSE	TIME	CRITICAL ORGAN DOSE	TIME	CRITICAL ORGAN
BASELINE	1.30 E -3	1.68 E -1	GI-LLI	6.19 E -14	1.44 E 4	7.49 E -12	1.44 E 4	GI-LLI
PERMEABILITY OF FRACTURE ZONE AND AQUIFER (1)	1.07 E -1	3.4 E -1	GI-LLI	2.17 E -12	3.87 E 4	6.54 E -11	3.87 E 4	GI-LLI
PERMEABILITY OF FRACTURE ZONE & AQUIFER AND ACTINIDE SORPTION FACTOR (2)	1.75	1.75	WHOLE BODY	4.49 E -10	4.07 E 4	4.49 E -10	4.07 E 4	WHOLE BODY
SHALE AND AQUIFER PERMEABILITY (3)	4.66 E -3	4.79 E -1	GI-LLI	1.64 E -12	2.59 E 2	1.99 E -10	2.59 E 2	GI-LLI
PERMEABILITY EVERYWHERE (4)	6.55 E -3	4.79 E -1	GI-LLI	1.64 E -12	4.87 E 3	1.98 E -10	4.87 E 3	GI-LLI
SHAFT FRACTURE ZONE AND AQUIFER PERMEABILITY AND TUNNEL FRACTURE ZONE POROSITY (5)	6.80 E -1	6.80 E -1	WHOLE BODY	2.12 E -11	1.24 E 6	1.40 E -10	1.45 E 4	GI-LLI
REDUCED SHALE PERMEABILITY AND INCREASED AQUIFER PERMEABILITY (6)	2.47 E -3	3.60 E -1	GI-LLI	1.27 E -12	8.6 E 3	1.53 E -10	8.6 E 3	GI-LLI

VARIED PARAMETER	PEAK AQUIFER CONCENTRATION (Ci/M^3 MWe-YR)							
	^{99}Tc CONCENTRATION	TIME	^{126}Sn CONCENTRATION	TIME	^{226}Ra CONCENTRATION	TIME	^{239}Pu CONCENTRATION	TIME
BASELINE	2.02 E -11	4.00 E 3	1.31 E -14	2.14 E 5	-	-	-	-
PERMEABILITY OF FRACTURE ZONE AND AQUIFER	2.04 E -12	5.82 E 2	2.64 E -14	2.83 E 4	1.73 E -18	1.79 E 6	2.21 E -22	1.98 E 6
PERMEABILITY OF FRACTURE ZONE AND AQUIFER AND ACTINIDE SORPTION FACTOR	2.04 E -12	5.82 E 2	2.64 E -14	2.83 E 4	5.42 E -16	3.14 E 4	1.26 E -13	2.69 E 4
SHALE AND AQUIFER PERMEABILITY	5.04 E -12	4.62 E 3	3.45 E -15	1.41 E 5	-	-	-	-
PERMEABILITY EVERYWHERE	5.02 E -12	4.87 E 3	3.29 E -15	1.41 E 5	3.44 E -20	1.61 E 6	3.04 E -24	1.98 E 6
SHAFT FRACTURE ZONE AND AQUIFER PERMEABILITY AND TUNNEL FRACTURE ZONE POROSITY	1.97 E -12	5.25 E 2	5.85 E -14	4.17 E 3	1.58 E -16	2.50 E 5	5.13 E -16	1.83 E 5
REDUCED SHALE PERMEABILITY AND INCREASED AQUIFER PERMEABILITY	3.90 E -12	8.61 E 3	2.72 E -16	4.19 E 5	-	-	-	-

TABLE 36. Salt repository sensitivity analysis (interstitial flow).

VARIED PARAMETER	BASELINE VALUE	NEW VALUE	INTEGRATED POPULATION DOSE (MAN-REM/MWe-YR)			PEAK INDIVIDUAL DOSE (REM/MWe-YR)				
			WHOLE BODY DOSE	CRITICAL ORGAN DOSE	CRITICAL ORGAN	WHOLE BODY	TIME	CRITICAL ORGAN DOSE	TIME	CRITICAL ORGAN
BASELINE	–	–	1.63 E -3	2.88 E -1	GI-LLI	8.15 E -14	1.49 E 5	9.86 E -12	1.49 E 5	GI-LLI
ACTINIDE & FISSION PRODUCT SORPTION FACTOR		(1)	2.81	2.61	WHOLE BODY	7.48 E -11	1.12 E 6	7.48 E -11	1.12 E 6	WHOLE BODY
DISPERSION	50	10	1.83 E -3	3.14 E -1	GI-LLI	1.70 E -13	1.27 E 5	2.05 E -11	1.27 E 5	GI-LLI
LOW POROSITY EVERYWHERE		(2)	4.19 E -3	4.38 E -1	GI-LLI	4.05 E -13	3.67 E 4	4.90 E -11	3.67 E 4	GI-LLI
LOW POROSITY IN ROCK		(3)	2.37 E -3	3.83 E -1	GI-LLI	3.87 E -13	4.58 E 4	4.68 E -11	4.52 E 4	GI-LLI
LOW POROSITY IN SHAFT & TUNNEL FRACTURE ZONE		(4)	1.63 E -3	2.81 E -1	GI-LLI	8.15 E -14	1.49 E 5	9.86 E -12	1.49 E 5	GI-LLI
MINIMUM AREA FRACTURE ZONE IN TUNNEL		(5)	1.63 E -3	2.81 E -1	GI-LLI	8.21 E -14	1.15 E 5	9.93 E -12	1.15 E 5	GI-LLI
MAXIMUM AREA FRACTURE ZONE IN SHAFT AND TUNNEL		(6)	1.64 E -3	2.87 E -1	GI-LLI	8.08 E -14	1.15 E 5	9.77 E -12	1.15 E 5	GI-LLI
SALT PERMEABILITY	10^{-9}	10^{-5}	2.75 E -3	4.29 E -1	GI-LLI	1.46 E -12	1.60 E 4	1.77 E -10	1.60 E 4	GI-LLI
ROCK PERMEABILITY MODERATELY PERMEABLE SALT		(7)	2.76 E -3	4.31 E -1	GI-LLI	1.68 E -12	1.37 E 4	2.03 E -10	1.37 E 4	GI-LLI
ROCK PERMEABILITY EXTREMELY PERMEABLE SALT		(8)	2.77 E -3	4.32 E -1	GI-LLI	1.86 E -12	1.17 E 4	2.27 E -10	1.17 E 4	GI-LLI
ARTESIAN HEAD	80	150	2.17 E -3	3.57 E -1	GI-LLI	2.29 E -13	5.85 E 4	2.78 E -11	5.85 E 4	GI-LLI
AQUIFER PERMEABILITY	10^{-4}	10^{-2}	2.81	2.81	WHOLE BODY	7.48 E -11	1.12 E 6	7.48 E -11	1.12 E 6	WHOLE BODY
FRACTURE ZONE PERMEABILITY		(9)	1.58 E -3	2.90 E -1	GI-LLI	7.88 E -14	1.17 E 4	9.55 E -12	1.17 E 4	GI-LLI
THICKNESS OF DEPOSITORY LAYER	200	20	2.56 E -3	4.06 E -1	GI-LLI	6.53 E -13	2.99 E 4	7.90 E -11	2.99 E 4	GI-LLI
THICKNESS OF BARRIER LAYER	200	20	2.13 E -3	3.52 E -1	GI-LLI	1.97 E -13	4.79 E 4	2.38 E -11	4.76 E 4	GI-LLI
LENGTH OF TUNNEL (INCREASE)	440	6040	1.63 E -3	2.86 E -1	GI-LLI	8.20 E -14	1.15 E 5	9.92 E -12	1.15 E 5	GI-LLI
LENGTH OF TUNNEL	440	200	1.64 E -3	2.87 E -1	GI-LLI	8.12 E -14	1.15 E 5	9.83 E -12	1.16 E 5	GI-LLI
DISSOLUTION RATE OF WASTE	10^{-4}	0.1	1.68 E -3	2.93 E -1	GI-LLI	8.57 E -14	1.09 E 5	1.04 E -11	1.09 E 5	GI-LLI
FISSION PRODUCT SORPTION FACTORS	10^{2}	1	4.46 E -3	3.57 E -1	GI-LLI	6.72 E -13	1.09 E 5	3.51 E -11	1.21 E 5	GI-LLI
ACTINIDE SORPTION FACTORS	10^{4}	10^{2}	2.81	2.61	WHOLE BODY	7.48 E -11	1.12 E 6	7.48 E -11	1.12 E 6	WHOLE BODY
AQUIFER LENGTH	1.6 E 4	1.6 E 3	3.28 E -3	3.42 E -1	GI-LLI	2.97 E -13	2.14 E 5	2.36 E -11	2.14 E 5	GI-LLI

TABLE 36. Salt repository sensitivity analysis (interstitial flow) (continued).

VARIED PARAMETER	PEAK AQUIFER CONCENTRATION (Ci/M^3-MW-YR)							
	^{99}Tc CONCENTRATION	TIME	^{126}Sn CONCENTRATION	TIME	^{226}Ra CONCENTRATION	TIME	^{239}Pu CONCENTRATION	TIME
BASELINE	2.58 E -11	1.09 E 5	7.04 E -13	1.04 E 5	5.67 E -14	1.15 E 5	1.64 E -12	8.41 E 4
ACTINIDE & FISSION PRODUCT SORPTION FACTOR	2.58 E -11	1.09 E 5	7.04 E -13	1.04 E 5	5.67 E -14	1.15 E 5	1.64 E -12	8.41 E 4
DISPERSION	5.40 E -11	1.21 E 5	1.42 E -12	1.15 E 5	1.22 E -13	1.21 E 5	2.62 E -12	1.15 E 5
LOW POROSITY EVERYWHERE	1.26 E -10	3.49 E 4	4.19 E -12	3.31 E 4	1.20 E -13	4.52 E 4	1.94 E -11	3.14 E 4
LOW POROSITY IN ROCK	1.26 E -10	3.49 E 4	4.19 E -12	3.31 E 4	1.20 E -12	4.52 E 4	1.94 E -11	3.14 E 4
LOW POROSITY IN SHAFT & TUNNEL FRACTURE ZONE	2.58 E -11	1.09 E 5	7.04 E -13	1.04 E 5	5.67 E -14	1.15 E 5	1.64 E -12	8.41 E 4
MINIMUM AREA FRACTURE ZONE IN TUNNEL	2.60 E -11	1.09 E 5	7.09 E -13	1.04 E 5	5.70 E -14	1.15 E 5	1.64 E -12	7.99 E 4
MAXIMUM AREA FRACTURE ZONE IN SHAFT AND TUNNEL	2.56 E -11	1.09 E 5	6.97 E -13	1.04 E 5	5.62 E -14	1.15 E 5	1.62 E -12	8.41 E 4
SALT PERMEABILITY	4.57 E -10	5.69 E 3	1.66 E -11	5.69 E 3	7.51 E -14	1.24 E 4	1.13 E -10	7.37 E 3
ROCK PERMEABILITY MODERATELY PERMEABLE SALT	5.33 E -10	3.57 E 3	2.00 E -11	3.39 E 3	6.21 E -14	1.06 E 4	1.13 E -10	4.87 E 3
ROCK PERMEABILITY EXTREMELY PERMEABLE SALT	7.10 E -10	2.68 E 2	2.74 E -11	2.68 E 2	5.17 E -14	1.17 E 4	1.07 E -10	1.73 E 3
ARTESIAN HEAD	6.89 E -11	5.28 E 4	2.26 E -12	5.01 E 4	9.69 E -14	6.17 E 4	8.51 E -12	4.07 E 4
AQUIFER PERMEABILITY	2.58 E -13	1.09 E 5	7.04 E -15	1.04 E 5	5.67 E -16	1.15 E 5	1.64 E -14	8.41 E 4
FRACTURE ZONE PERMEABILITY	2.87 E -11	5.25 E 2	1.11 E -12	5.25 E 2	5.34 E -14	1.21 E 5	4.49 E -12	4.17 E 3
THICKNESS OF DEPOSITORY LAYER	2.12 E -10	1.97 E 4	7.23 E -12	1.97 E 4	1.11 E -13	2.69 E 4	4.48 E -11	1.52 E 4
THICKNESS OF BARRIER LAYER	6.39 E -11	3.31 E 4	2.14 E -12	3.31 E 4	8.87 E -14	5.01 E 4	1.02 E -11	2.83 E 4
LENGTH OF TUNNEL (INCREASE)	2.60 E -11	1.09 E 5	7.08 E -13	1.04 E 5	5.69 E -14	1.15 E 5	1.65 E -12	7.99 E 4
LENGTH OF TUNNEL	2.57 E -11	1.09 E 5	7.01 E -13	1.04 E 5	5.65 E -14	1.15 E 5	1.63 E -12	8.42 E 4
DISSOLUTION RATE OF WASTE	2.70 E -11	9.83 E 4	8.42 E -13	1.92 E 3	5.77 E -14	1.09 E 5	3.87 E -12	2.02 E 3
FISSION PRODUCT SORPTION FACTORS	2.58 E -11	1.09 E 5	7.04 E -13	1.04 E 5	5.66 E -14	1.15 E 5	1.64 E -12	8.41 E 4
ACTINIDE SORPTION FACTORS	2.58 E -11	1.09 E 5	7.04 E -13	1.04 E 5	5.67 E -14	1.15 E 5	1.64 E -12	8.41 E 4
AQUIFER LENGTH	2.58 E -11	1.09 E 5	7.04 E -13	1.04 E 5	5.67 E -14	1.15 E 5	1.64 E -12	8.41 E 4

TABLE 37. Salt repository sensitivity analysis (multiple parameter, interstitial flow).

VARIED PARAMETER	INTEGRATED POPULATION DOSE (MAN-REM/MWe-YR)			PEAK INDIVIDUAL DOSE (REM/MWe-YR)				
	WHOLE BODY DOSE	CRITICAL ORGAN DOSE	CRITICAL ORGAN	WHOLE BODY DOSE	TIME	CRITICAL ORGAN DOSE	TIME	CRITICAL ORGAN
BASELINE	1.63 E -3	2.86 E -1	GI-LLI	8.15 E -14	1.15 E 5	9.86 E -12	1.15 E 5	GI-LLI
PERMEABILITY OF ROCK AND AQUIFER (1)	3.17	3.17	WHOLE BODY	1.22 E -10	9.61 E 5	1.56 E -9	1.01 E 6	BONE
PERMEABILITY OF SHAFT & AQUIFER POROSITY OF TUNNEL (2)	2.61	2.61	WHOLE BODY	7.45 E -11	1.12 E 6	7.45 E -11	1.12 E 6	WHOLE BODY
PERMEABILITY OF SHAFT TUNNEL & AQUIFER (3)	2.63	2.63	WHOLE BODY	7.24 E -11	1.12 E 6	7.24 E -11	1.12 E 6	WHOLE BODY
HIGH PERMEABILITY EVERYWHERE (4)	3.17	3.17	WHOLE BODY	1.22 E -10	9.61 E 5	1.56 E -9	1.01 E 6	BONE

VARIED PARAMETER	PEAK AQUIFER CONCENTRATION (Ci/M^3-MWe-YR)							
	^{99}Tc CONCENTRATION	TIME	^{126}Sn CONCENTRATION	TIME	^{226}Ra CONCENTRATION	TIME	^{239}Pu CONCENTRATION	TIME
BASELINE	2.58 E -11	1.05 E -11	7.04 E -13	1.04 E 5	5.67 E -14	1.15 E 5	1.64 E -12	8.41 E 4
PERMEABILITY OF ROCK & AQUIFER	7.10 E -12	2.68 E 2	2.74 E -13	2.68 E 2	5.17 E -16	1.17 E 4	1.07 E -12	1.73 E 3
PERMEABILITY OF SHAFT & AQUIFER POROSITY OF TUNNEL	2.57 E -13	1.09 E 5	7.00 E -15	1.04 E 5	5.64 E -16	1.15 E 5	1.63 E -14	8.41 E 4
PERMEABILITY OF SHAFT TUNNEL & AQUIFER	2.87 E -13	5.25 E 2	1.11 E -14	5.25 E 2	5.34 E -16	1.21 E 4	4.50 E -14	4.17 E 3
HIGH PERMEABILITY EVERYWHERE	7.10 E -12	2.68 E 2	2.74 E -13	2.67 E 2	5.17 E -16	1.17 E 4	1.07 E -12	1.73 E 3

TABLE 38. Shale repository sensitivity analysis (fracture flow).

VARIED PARAMETER	BASELINE VALUE	NEW VALUE	INTEGRATED POPULATION DOSE (MAN-REM/MWe-YR)			PEAK INDIVIDUAL DOSE (REM/MWe-YR)				
			WHOLE BODY DOSE	CRITICAL ORGAN DOSE	CRITICAL ORGAN	WHOLE BODY DOSE	TIME	CRITICAL ORGAN DOSE	TIME	CRITICAL ORGAN
BASELINE	–	–	2.77 E -3	4.32 E -1	GI-LLI	1.86 E -12	1.17 E 4	2.26 E -10	1.17 E 4	GI-LLI
AQUIFER LENGTH	1.6 E 4	1.6 E 3	6.76 E -3	5.15 E -1	GI-LLI	2.08 E -12	1.92 E 3	2.53 E -10	1.92 E 3	GI-LLI
DISPERSION DOWN	50	10	2.77 E -3	4.33 E -1	GI-LLI	2.03 E -12	1.12 E 4	2.45 E -10	1.12 E 4	GI-LLI
ACTINIDE SORPTION	10^4	10^2	3.14	3.14	WHOLE BODY	1.19 E -10	9.61 E 5	1.57 E -9	1.01 E 6	BONE
AQUIFER LENGTH HEAD GRADIENT, SIMULTANEOUSLY		(1)	2.32	2.32	WHOLE BODY	2.66 E -11	1.24 E 6	3.63 E -10	1.69 E 4	GI-LLI
PERMEABILITY & ACTINIDE SORPTION SIMULTANEOUSLY		(2)	3.53	3.53	WHOLE BODY	1.47 E -9	1.60 E 4	1.47 E -9	1.60 E 4	WHOLE BODY
DISPERSION UP	50	100	2.77 E -3	4.31 E -1	GI-LLI	1.74 E -12	1.24 E 4	2.11 E -10	1.24 E 4	GI-LLI
ACTINIDE SORPTION, LEACH RATE + AQUIFER PERMEABILITY		(3)	2.49	2.49	WHOLE BODY	4.88 E -9	1.24 E 4	5.16 E -8	2.29 E 2	GI-LLI

VARIED PARAMETER	PEAK AQUIFER CONCENTRATION (Ci/M^3-MWe-YR)							
	^{99}Tc CONCENTRATION	TIME	^{126}Sn CONCENTRATION	TIME	^{226}Ra CONCENTRATION	TIME	^{239}Pu CONCENTRATION	TIME
BASELINE	6.84 E -10	2.29 E 2	1.65 E -11	5.69 E 3	2.92 E -14	1.93 E 5	4.14 E -13	1.27 E 5
AQUIFER LENGTH	6.84 E -10	2.29 E 2	1.65 E -11	5.69 E 3	2.92 E -14	1.93 E 5	4.14 E -13	1.27 E 5
DISPERSION DOWN	6.84 E -10	2.29 E 2	1.65 E -11	5.69 E 3	2.92 E -14	1.93 E 5	4.14 E -13	1.27 E 5
ACTINIDE SORPTION	6.84 E -10	2.29 E 2	1.65 E -11	5.69 E 3	7.36 E -14	1.17 E 4	1.12 E -10	7.37 E 3
AQUIFER LENGTH HEAD GRADIENT, SIMULTANEOUSLY	6.84 E -11	2.29 E 2	1.65 E -12	5.69 E 3	2.92 E -15	1.93 E 5	4.14 E -14	1.27 E 5
PERMEABILITY & ACTINIDE SORPTION SIMULTANEOUSLY	6.84 E -12	2.29 E 2	1.65 E -13	5.69 E 3	7.36 E -16	1.17 E 4	1.12 E -12	7.37 E 3
DISPERSION UP	6.84 E -10	2.29 E 2	1.65 E -11	5.69 E 3	2.92 E -14	1.93 E 5	4.14 E -13	1.27 E 5
ACTINIDE SORPTION, LEACH RATE + AQUIFER PERMEABILITY	1.46 E -9	1.23 E 2	7.33 E -13	2.02 E 3	5.70 E -16	3.57 E 3	3.29 E -12	2.13 E 3

TABLE 39. Salt repository sensitivity analysis (fracture flow).

VARIED PARAMETER	BASELINE VALUE	NEW VALUE	INTEGRATED POPULATION DOSE (MAN-REM/MWe-YR)			PEAK INDIVIDUAL DOSE (REM/MWe-YR)				
			WHOLE BODY DOSE	CRITICAL ORGAN DOSE	CRITICAL ORGAN	WHOLE BODY DOSE	TIME	CRITICAL ORGAN DOSE	TIME	CRITICAL ORGAN
BASELINE	–	–	2.56 E -3	4.06 E -1	GI-LLI	5.84 E -13	2.56 E 4	7.07 E -11	2.56 E 4	GI-LLI
SALT PERMEABILITY	10^{-9}	10^{-5}	2.77 E -3	4.32 E -1	GI-LLI	1.88 E -12	1.17 E 4	2.27 E -10	1.17 E 4	GI-LLI
DISPERSION	50	10	2.64 E -3	4.18 E -1	GI-LLI	1.00 E -12	2.56 E 4	1.12 E -10	2.56 E 4	GI-LLI

VARIED PARAMETER	PEAK AQUIFER CONCENTRATION (CI/M^3-MWe-YR)							
	^{99}Tc CONCENTRATION	TIME	^{126}Sn CONCENTRATION	TIME	^{226}Ra CONCENTRATION	TIME	^{239}Pu CONCENTRATION	TIME
BASELINE	1.86 E -10	1.69 E 4	6.5 E -12	1.60 E 4	8.98 E -14	2.69 E 4	4.97 E -11	1.17 E 4
SALT PERMEABILITY	6.62 E -10	3.13 E 2	2.64 E -11	2.13 E 2	5.17 E -14	1.17 E 4	1.12 E -10	1.73 E 3
DISPERSION	3.15 E -10	1.60 E 4	1.11 E -11	1.52 E 4	1.27 E -13	1.97 E 4	7.66 E -11	1.37 E 4

TABLE 40. Shale repository sensitivity analysis (deteriorated backfill, interstitial flow).

VARIED PARAMETER	INTEGRATED POPULATION DOSE (MAN-REM/MWe-YR)			PEAK INDIVIDUAL DOSE (REM/MWe-YR)				
	WHOLE BODY DOSE	CRITICAL ORGAN DOSE	CRITICAL ORGAN	WHOLE BODY DOSE	TIME	CRITICAL ORGAN DOSE	TIME	CRITICAL ORGAN
BASELINE	1.60 E -3	2.23 E -1	GI-LLI	5.70 E -13	1.18 E 4	6.90 E -11	1.18 E 4	GI-LLI
FURTHER DETERIORATED BACKFILL (1)	2.31 E -3	3.54 E -1	GI-LLI	1.39 E -12	1.18 E 4	1.69 E -10	1.18 E 4	GI-LLI
IMPERMEABLE SHAFT (2)	1.30 E -3	1.60 E -1	GI-LLI	6.78 E -14	1.45 E 4	8.20 E -12	1.45 E 4	GI-LLI
IMPERMEABLE SHAFT & HIGHLY PERMEABLE TUNNEL (3)	1.29 E -3	1.56 E -1	GI-LLI	4.22 E -14	1.74 E 5	5.11 E -12	1.74 E 5	GI-LLI

VARIED PARAMETER	PEAK AQUIFER CONCENTRATION (CI/M^3-MWe-YR)							
	^{99}Tc CONCENTRATION	TIME	^{126}Sn CONCENTRATION	TIME	^{226}Ra CONCENTRATION	TIME	^{239}Pu CONCENTRATION	TIME
BASELINE	2.20 E -10	5.25 E 2	2.64 E -12	2.89 E 4	1.58 E -16	2.32 E 6	2.09 E -20	2.32 E 6
FURTHER DETERIORATED BACKFILL	5.15 E -10	2.54 E 2	1.26 E -11	1.06 E 4	1.10 E -14	6.35 E 5	1.19 E -15	4.42 E 5
IMPERMEABLE SHAFT	2.20 E -11	3.76 E 3	1.68 E -14	1.83 E 5	–	–	–	–
IMPERMEABLE SHAFT & HIGHLY PERMEABLE TUNNEL	1.34 E -11	1.57 E 5	1.76 E -18	1.53 E 6	–	–	–	–

TABLE 41. Salt repository sensitivity analysis (deteriorated backfill, interstitial flow).

VARIED PARAMETER	INTEGRATED POPULATION DOSE (MAN-REM/MWe-YR)			PEAK INDIVIDUAL DOSE (REM/MWe-YR)				
	WHOLE BODY DOSE	CRITICAL ORGAN DOSE	CRITICAL ORGAN	WHOLE BODY DOSE	TIME	CRITICAL ORGAN DOSE	TIME	CRITICAL ORGAN
BASELINE	1.79 E -3	3.08 E -1	GI-LLI	3.74 E -13	1.75 E 4	4.53 E -11	1.18 E 4	GI-LLI
FURTHER DETERIORATED BACKFILL (1)	2.26 E -3	3.84 E -1	GI-LLI	1.33 E -12	1.24 E 4	1.61 E -10	1.24 E 4	GI-LLI
IMPERMEABLE SHAFT (2)	1.63 E -3	2.86 E -1	GI-LLI	8.28 E -14	1.15 E 5	1.00 E -11	1.15 E 5	GI-LLI
IMPERMEABLE SHAFT HIGHLY PERMEABLE TUNNEL (3)	1.63 E -3	2.86 E -1	GI-LLI	8.26 E -14	1.15 E 5	9.99 E -12	1.15 E 5	GI-LLI
PERMEABLE TUNNEL & SHAFT (4)	2.76 E -3	4.30 E -1	GI-LLI	1.84 E -12	1.18 E 4	2.23 E -10	1.18 E 4	GI-LLI

VARIED PARAMETER	PEAK AQUIFER CONCENTRATION (Ci/M^3/MWe-YR)							
	^{99}Tc CONCENTRATION	TIME	^{126}Sn CONCENTRATION	TIME	^{226}Ra CONCENTRATION	TIME	^{239}Pu CONCENTRATION	TIME
BASELINE	1.35 E -10	8.37 E 2	5.20 E -12	8.37 E 2	4.02 E -14	1.27 E 5	2.13 E -11	2.02 E 3
FURTHER DETERIORATED BACKFILL	4.63 E -10	1.48 E 3	1.79 E -11	1.48 E 3	4.09 E -14	1.52 E 5	7.89 E -11	2.02 E 3
IMPERMEABLE SHAFT	2.61 E -11	1.09 E 5	7.16 E -13	9.83 E 4	5.73 E -14	1.27 E 5	1.67 E -12	8.45 E 4
IMPERMEABLE SHAFT HIGHLY PERMEABLE TUNNEL	2.61 E -11	1.04 E 5	7.16 E -13	9.83 E 4	5.70 E -14	1.15 E 5	1.68 E -12	7.99 E 4
PERMEABLE TUNNEL & SHAFT	6.61 E -10	9.28 E 2	2.55 E -11	9.28 E 2	5.37 E -14	9.07 E 3	1.06 E -10	2.01 E 3

TABLE 42. Shale repository sensitivity analysis (boring seal dissolution, interstitial flow).

VARIED PARAMETER	BASELINE VALUE	NEW VALUE	INTEGRATED POPULATION DOSE (MAN-REM/MWe-YR)			PEAK INDIVIDUAL DOSE (REM/MWe-YR)				
			WHOLE BODY DOSE	CRITICAL ORGAN DOSE	CRITICAL ORGAN	WHOLE BODY DOSE	TIME	CRITICAL ORGAN DOSE	TIME	CRITICAL ORGAN
BASELINE	–	–	1.28 E -3	1.58 E -1	GI-LLI	6.11 E -14	1.45 E 4	7.39 E -12	1.45 E 4	GI-LLI
COMPLETE MIXING	–	–	1.29 E -3	1.58 E -1	GI-LLI	6.09 E -14	1.45 E 4	7.37 E -12	1.45 E 4	GI-LLI
MAXIMUM PERMEABILITY IN BORING	10^{-4}	10^{-2}	1.37 E -3	1.78 E -1	GI-LLI	2.44 E -13	1.30 E 4	2.96 E -11	1.30 E 4	GI-LLI

TABLE 43. Salt repository sensitivity analysis (boring seal dissolution, interstitial flow).

VARIED PARAMETER	BASELINE VALUE	NEW VALUE	INTEGRATED POPULATION DOSE (MAN-REM/MWe-YR)			PEAK INDIVIDUAL DOSE (REM/MWe-YR)				
			WHOLE BODY DOSE	CRITICAL ORGAN DOSE	CRITICAL ORGAN	WHOLE BODY DOSE	TIME	CRITICAL ORGAN DOSE	TIME	CRITICAL ORGAN
BASELINE	–	–	1.63 E -3	2.85 E -1	GI-LLI	7.99 E -14	1.21 E 5	9.67 E -12	1.21 E 5	GI-LLI
COMPLETE MIXING	–	–	1.63 E -3	2.85 E -1	GI-LLI	7.99 E -14	1.21 E 5	9.66 E -12	1.21 E 5	GI-LLI
MAXIMUM PERMEABILITY IN BORING	10^{-4}	10^{-2}	1.66 E -3	2.88 E -1	GI-LLI	1.59 E -13	1.24 E 4	1.93 E -11	1.24 E 4	GI-LLI

TABLE 44. Shale repository sensitivity analysis (faulting, interstitial flow).

VARIED PARAMETER	BASELINE VALUE	NEW VALUE	INTEGRATED POPULATION DOSE (MAN-REM/MWe-YR)			PEAK INDIVIDUAL DOSE (REM/MWe-YR)				
			WHOLE BODY DOSE	CRITICAL ORGAN DOSE	CRITICAL ORGAN	WHOLE BODY DOSE	TIME	CRITICAL ORGAN DOSE	TIME	CRITICAL ORGAN
BASELINE	–	–	1.27 E -3	1.57 E -1	GI-LLI	6.07 E -14	1.45 E 4	7.32 E -12	1.45 E 4	GI-LLI
FAULT STAYS OPEN AND A HIGHER PROBABILITY OF OCCURRENCE	5. E -7	5. E -5	1.27 E -3	1.57 E -1	GI-LLI	6.34 E -14	1.45 E 4	7.70 E -12	1.45 E 4	GI-LLI

TABLE 45. Salt repository sensitivity analysis (breccia formation, interstitial flow).

VARIED PARAMETER	BASELINE VALUE	NEW VALUE	INTEGRATED POPULATION DOSE (MAN-REM/MWe-YR)			PEAK INDIVIDUAL DOSE (REM/MWe-YR)				
			WHOLE BODY DOSE	CRITICAL ORGAN DOSE	CRITICAL ORGAN	WHOLE BODY DOSE	TIME	CRITICAL ORGAN DOSE	TIME	CRITICAL ORGAN
BASELINE	–	–	1.62 E -3	4.84 E -1	GI-LLI	8.05 E -14	1.15 E 5	9.74 E -12	1.15 E 5	GI-LLI
HIGH PROBABILITY OF BRECCIA FORMATION	5. E -7	5. E -5	1.18 E -3	1.94 E -1	GI-LLI	1.72 E -13	2.43 E 4	2.08 E -11	2.43 E 4	GI-LLI
BRECCIA PIPE INITIALLY PRESENT	–	–	2.75 E -3	4.29 E -1	GI-LLI	1.48 E -12	1.60 E 4	1.79 E -10	1.60 E 4	GI-LLI

TABLE 46. Baseline parameters for unflawed shale repository.

PATHWAY	LENGTH (m)	CROSS SECTION (m^2)	EFFECTIVE POROSITY	PERMEABILITY (cm/sec)	RETARDATION FACTOR	DISPERSION (m)
1st Segment of Tunnel Fracture Zone	1200	316	0.1	0.1	^{129}I, ^{99}Tc: 1 Other Fission Products: 10^2 Actinides: 10^4	50
2nd Segment of Tunnel Fracture Zone	440	18.96	0.1	0.1	^{129}I, ^{99}Tc: 1 Other Fission Products: 10^2 Actinides: 10^4	50
Fracture Zone Around Shaft in Depository Layer	100	10	10^{-3}	10^{-4}	^{129}I, ^{99}Tc: 1 Other Fission Products: 10^2 Actinides: 10^4	50
Fracture Zone Around Shaft in Shale Barrier Layer	200	5	10^{-3}	10^{-4}	^{129}I, ^{99}Tc: 1 Other Fission Products: 10^2 Actinides: 10^4	50
Depository Layer	100	5×10^6	0.05	10^{-9}	^{129}I, ^{99}Tc: 1 Other Fission Products: 10^2 Actinides: 10^4	50
Barrier Layer	200	5×10^6	0.05	10^{-7}	^{129}I, ^{99}Tc: 1 Other Fission Products: 10^2 Actinides: 10^4	50
Aquifer	1.6×10^4	4×10^5	0.1	10^{-4}	^{129}I, ^{99}Tc: 1 Other Fission Products: 10^2 Actinides: 10^4	50

TABLE 47. Baseline parameters for unflawed salt repository.

PATHWAY	LENGTH (m)	CROSS SECTION (m^2)	EFFECTIVE POROSITY	PERMEABILITY (cm/sec)	RETARDATION FACTOR	DISPERSION (m)
1st Segment of Tunnel Fracture Zone	1200	3300	10^{-3}	10^{-6}	1	50
2nd Segment of Tunnel Fracture Zone	440	198	10^{-3}	10^{-6}	1	50
Fracture Zone Around Shaft in Depository Layer	100	60	10^{-3}	10^{-6}	1	50
Fracture Zone Around Shaft in Shale Barrier Layer	200	5	10^{-3}	10^{-6}	1	50
Depository Layer	160	5×10^6	10^{-2}	10^{-9}	1	50
Barrier Layer	200	5×10^6	0.05	10^{-7}	1	50
Aquifer	1.6×10^4	4×10^5	0.1	10^{-4}	^{129}I, ^{99}Tc: 1 Other Fission Products: 10^2 Actinides: 10^4	50

TABLE 48. Baseline parameters for shale with fracture flow. These values were substituted for those in Table 46 to get the results in Table 38, and the values for the barrier layer were substituted in Table 47 to get the results in Table 39.

PATHWAY	LENGTH (m)	CROSS SECTION (m^2)	EFFECTIVE POROSITY	PERMEABILITY (cm/sec)	RETARDATION FACTOR	DISPERSION (m)
Depository Layer	100	5×10^6	10^{-5}	10^{-8}	SAME	50
Barrier Layer	200	5×10^6	10^{-4}	10^{-6}	SAME	50

TABLE 49. Additional baseline parameters for deteriorated backfill cases (Tables 40 and 41). Note: These values must be added to those in Tables 46 and 47.

PATHWAY	LENGTH (m)	CROSS SECTION (m^2)	EFFECTIVE POROSITY	PERMEABILITY (cm/sec)	RETARDATION FACTOR	DISPERSION (m)
1^{st} Segment of Tunnel Backfill	1200	3100	10^{-2}	10^{-4}	^{129}I, ^{99}Tc: 1 Other Fission Products: 10^2 Actinides: 10^4	50
2^{nd} Segment of Tunnel Backfill	440	150	10^{-2}	10^{-4}	SAME	50
Shaft Backfill	300	64	10^{-2}	10^{-4}	SAME	50

TABLE 50. Additional baseline parameters for cases with failed boring seals (Tables 42 and 43). Note: These values must be added to those in Tables 46 and 47.

PATHWAY	LENGTH (m)	CROSS SECTION (m^2)	EFFECTIVE POROSITY	PERMEABILITY (cm/sec)	RETARDATION FACTOR	DISPERSION (m)
Borehole Path Less Than 500 Years	300	0.1	10^{-2}	10^{-4}	^{129}I, ^{99}Tc: 1 Other Fission Products: 10^2 Actinides: 10^4	50
Borehole Path Between 500 and 1000 Years	300	0.3	10^{-2}	10^{-4}	SAME	50
Borehole Path After 1000 Years	300	0.5	10^{-2}	10^{-4}	SAME	50

TABLE 51. Baseline parameters for case with fault (Table 44).

PATHWAY	LENGTH (m)	CROSS SECTION (m^2)	EFFECTIVE POROSITY	PERMEABILITY (cm/sec)	RETARDATION FACTOR	DISPERSION (m)
Change from Table 46						
Depository Layer	100	4.9×10^6	0.05	10^{-9}	SAME	50
Barrier Layer	200	4.9×10^6	0.05	10^{-7}	SAME	50
Add:						
*Fault Open in Barrier Layer	200	10^5	10^{-3}	10^{-4}	^{129}I, ^{99}Tc: 1 Other Fission Products: 10^2 Actinides: 10^4	50
Fault Closed in Barrier Layer	200	10^5	10^{-3}	10^{-6}	SAME	50
Fault Open in Depository Layer	100	10^5	10^{-3}	10^{-5}	SAME	50
Fault Closed in Depository Layer	100	10^5	10^{-3}	[illegible]	SAME	50

*The probability of a fault is 5×10^{-7} per year

TABLE 52. Baseline parameters for case with breccia pipe (Table 45).

PATHWAY	LENGTH (m)	CROSS SECTION (m^2)	EFFECTIVE POROSITY	PERMEABILITY (cm/sec)	RETARDATION FACTOR	DISPERSION (m)
Change from Table 47						
Depository Layer	100	4.9×10^6	10^{-2}	10^{-9}	1	50
Barrier Layer	200	4.9×10^6	0.05	10^{-7}	1	50
Add:						
*Breccia Pipe	300	10^5	0.3	10^{-2}	1	50

*The probability of a breccia pipe formation is 5×10^{-7} per year.

TABLE 53. Parameters varied in Table 34.

RUN INDEX NUMBER	VARIED PARAMETER	BASELINE VALUE	NEW VALUE
(1)	Retardation Factor of Fission Products other than I and Tc	10^2	1
	Retardation Factor of Actinides	10^4	10^2
(2)	Porosity of the Tunnel Fracture Zone	10^{-1}	10^{-2}
	Porosity of the Shaft Fracture Zone	10^{-3}	10^{-4}
	Porosity of the Depository Layer	5×10^{-2}	10^{-2}
	Porosity of the Barrier Layer	5×10^{-2}	10^{-2}
	Porosity of the Aquifer	10^{-1}	2×10^{-2}
(3)	Porosity of the Tunnel Fracture Zone	10^{-1}	10^{-2}
	Porosity of the Shaft Fracture Zone	10^{-3}	10^{-4}
(4)	Cross Section of the 1st Segment of the Tunnel Fracture Zone (m^2)	316	580
	Cross Section of the 2nd Segment of the Tunnel Fracture Zone (m^2)	18.91	34.8
	Permeability of the Tunnel Fracture Zone (cm/sec)	10^{-1}	10^{-4}
(5)	Cross Section of the 1st Segment of the Tunnel Fracture Zone (m^2)	316	785
	Cross Section of the 2nd Segment of the Tunnel Fracture Zone (m^2)	18.91	47.1
	Cross Section of the 1st Segment of the Shaft Fracture Zone (m^2)	10	100
	Cross Section of the 2nd Segment of the Shaft Fracture Zone (m^2)	5	100
(6)	Permeability of the Depository Layer (cm/sec)	10^{-5}	10^{-7}
	Permeability of the Barrier Layer (cm/sec)	10^{-7}	10^{-5}
(7)	Permeability of the Tunnel Fracture Zone (cm/sec)	10^{-1}	1
	Permeability of the Shaft Fracture Zone (cm/sec)	10^{-4}	10^{-3}

TABLE 54. Parameters varied in Table 35.

RUN INDEX NUMBER	VARIED PARAMETER	BASELINE VALUE	NEW VALUE
(1)	Permeability of the Tunnel Fracture Zone (cm/sec)	10^{-1}	1
	Permeability of the Shaft Fracture Zone (cm/sec)	10^{-4}	10^{-3}
	Permeability of the Aquifer (cm/sec)	10^{-4}	10^{-2}
(2)	Permeability of the Tunnel Fracture Zone (cm/sec)	10^{-1}	1
	Permeability of the Shaft Fracture Zone (cm/sec)	10^{-4}	10^{-3}
	Permeability of the Aquifer (cm/sec)	10^{-4}	10^{-2}
	Actinide Retardation Factor	10^4	10^2
(3)	Permeability of the Aquifer (cm/sec)	10^{-4}	10^{-2}
	Permeability of the Depository Layer (cm/sec)	10^{-9}	10^{-7}
	Permeability of the Barrier Layer (cm/sec)	10^{-7}	10^{-5}
(4)	Permeability of the Tunnel Fracture Zone (cm/sec)	10^{-1}	1
	Permeability of the Shaft Fracture Zone (cm/sec)	10^{-4}	10^{-3}
	Permeability of the Aquifer (cm/sec)	10^{-4}	10^{-2}
	Permeability of the Depository Layer (cm/sec)	10^{-9}	10^{-7}
	Permeability of the Barrier Layer (cm/sec)	10^{-7}	10^{-5}
(5)	Permeability of the Shaft Fracture Zone (cm/sec)	10^{-4}	10^{-3}
	Permeability of the Aquifer (cm/sec)	10^{-4}	10^{-2}
	Porosity of the Tunnel Fracture Zone	10^{-1}	10^{-2}
(6)	Permeability of the Aquifer (cm/sec)	10^{-4}	10^{-2}
	Permeability of the Depository Layer (cm/sec)	10^{-9}	10^{-11}
	Permeability of the Barrier Layer (cm/sec)	10^{-7}	10^{-9}

526 200

TABLE 55. Parameters varied in Table 36.

RUN INDEX NUMBER	VARIED PARAMETER	BASELINE VALUE	NEW VALUE
(1)	Retardation Factor of Fission Products (Except I, Tc) in Aquifer	10^2	1
	Retardation Factor of Actinides in Aquifer	10^4	10^2
(2)	Porosity in the Tunnel and Shaft Fracture Zone	10^{-3}	10^{-4}
	Porosity in the Depository Layer	10^{-2}	4×10^{-3}
	Porosity in the Barrier Layer	5×10^{-2}	10^{-2}
(3)	Porosity in the Depository Layer	10^{-2}	4×10^{-3}
	Porosity in the Barrier Layer	5×10^{-2}	10^{-2}
(4)	Porosity in the Tunnel and Shaft Fracture Zone	10^{-3}	10^{-4}
(5)	Cross Section in the 1st Segment of the Tunnel Fracture Zone (m^2)	3.3×10^3	190
	Cross Section in the 2nd Segment of the Tunnel Fracture Zone (m^2)	198	11.4
(6)	Cross Section in the 1st Segment of the Tunnel Fracture Zone (m^2)	3.3×10^3	6.4×10^3
	Cross Section in the 2nd Segment of the Tunnel Fracture Zone (m^2)	198	384
	Cross Section in the 1st Segment of the Shaft Fracture Zone (m^2)	60	110
	Cross Section in the 2nd Segment of the Shaft Fracture Zone (m^2)	5	100
(7)	Permeability of the Depository Layer (cm/sec)	10^{-9}	10^{-7}
	Permeability of the Barrier Layer (cm/sec)	10^{-7}	10^{-5}
(8)	Permeability of the Depository Layer (cm/sec)	10^{-9}	10^{-5}
	Permeability of the Barrier Layer (cm/sec)	10^{-7}	10^{-5}
(9)	Permeability of the Shaft Fracture Zone (cm/sec)	10^{-6}	10^{-5}
	Permeability of the Tunnel Fracture Zone (cm/sec)	10^{-6}	10^{-5}

TABLE 56. Parameters varied in Table 37.

RUN INDEX NUMBER	VARIED PARAMETER	BASELINE VALUE	NEW VALUE
(1)	Permeability of the Aquifer (cm/sec)	10^{-4}	10^{-2}
	Permeability of the Depository Layer (cm/sec)	10^{-9}	10^{-5}
	Permeability of the Barrier Layer (cm/sec)	10^{-7}	10^{-5}
(2)	Permeability of the Shaft Fracture Zone (cm/sec)	10^{-6}	10^{-5}
	Porosity of the Tunnel Fracture Zone	10^{-3}	10^{-4}
	Permeability of the Aquifer (cm/sec)	10^{-4}	10^{-2}
(3)	Permeability of the Shaft Fracture Zone (cm/sec)	10^{-6}	10^{-5}
	Permeability of the Tunnel Fracture Zone (cm/sec)	10^{-6}	10^{-5}
	Permeability of the Aquifer (cm/sec)	10^{-4}	10^{-2}
(4)	Permeability of the Shaft Fracture Zone (cm/sec)	10^{-6}	10^{-5}
	Permeability of the Tunnel Fracture Zone (cm/sec)	10^{-6}	10^{-5}
	Permeability of the Depository Layer (cm/sec)	10^{-9}	10^{-5}
	Permeability of the Barrier Layer (cm/sec)	10^{-7}	10^{-5}
	Permeability of the Aquifer (cm/sec)	10^{-4}	10^{-2}

TABLE 57. Parameters varied in Table 38.

RUN INDEX NUMBER	VARIED PARAMETER	BASELINE VALUE	NEW VALUE
(1)	Aquifer Length (m)	1.6×10^{4}	1.6×10^{3}
	Head Gradient	5×10^{-3}	5×10^{-2}
(2)	Permeability of the Aquifer (cm/sec)	10^{-4}	10^{-2}
	Actinide Retardation Factor	10^{4}	10^{2}
(3)	Permeability of the Aquifer (cm/sec)	10^{-4}	10^{-2}
	Actinide Retardation Factor	10^{4}	10^{2}
	Leach Rate (yr^{-1})	10^{-4}	10^{-1}

TABLE 58. Parameters varied in Table 40.

RUN INDEX NUMBER	VARIED PARAMETER	BASELINE VALUE	NEW VALUE
(1)	Permeability of Backfill in the Tunnel (cm/sec)	10^{-4}	10^{-3}
	Permeability of Backfill in the Shaft (cm/sec)	10^{-4}	10^{-3}
	Porosity of Backfill in the Shaft and Tunnel	10^{-2}	10^{-1}
(2)	Permeability of Backfill in the Tunnel (cm/sec)	10^{-4}	10^{-3}
	Permeability of Backfill in the Shaft (cm/sec)	10^{-4}	10^{-6}
	Porosity of Backfill in the Shaft and Tunnel	10^{-2}	10^{-1}
(3)	Permeability of Backfill in the Tunnel (cm/sec)	10^{-4}	10^{-1}
	Permeability of Backfill in the Shaft (cm/sec)	10^{-4}	10^{-6}
	Porosity of Backfill in the Shaft and Tunnel	10^{-2}	10^{-1}

TABLE 59. Parameters varied in Table 41.

RUN INDEX NUMBER	VARIED PARAMETER	BASELINE VALUE	NEW VALUE
(1)	Permeability of Backfill in the Tunnel (cm/sec)	10^{-4}	10^{-3}
	Permeability of Backfill in the Shaft (cm/sec)	10^{-4}	10^{-3}
	Porosity of Backfill in the Shaft and Tunnel	10^{-2}	10^{-1}
(2)	Permeability of Backfill in the Tunnel (cm/sec)	10^{-4}	10^{-3}
	Permeability of Backfill in the Shaft (cm/sec)	10^{-4}	10^{-6}
	Porosity of Backfill in the Shaft and Tunnel	10^{-2}	10^{-1}
(3)	Permeability of Backfill in the Tunnel (cm/sec)	10^{-4}	10^{-1}
	Permeability of Backfill in the Shaft (cm/sec)	10^{-4}	10^{-6}
	Porosity of Backfill in the Shaft and Tunnel	10^{-2}	10^{-1}
(4)	Permeability of Backfill in the Tunnel (cm/sec)	10^{-4}	10^{-1}
	Permeability of Backfill in the Shaft (cm/sec)	10^{-4}	10^{-1}
	Porosity of Backfill in the Shaft and Tunnel	10^{-2}	10^{-1}

Tables 34 through 45 show how peak individual dose, population dose, and individual radionuclide concentrations are affected by changes in parameter values. For each table, baseline parameters were established and results calculated. The values of various parameters were then varied and the doses and concentrations recalculated. Where the change in parameter value is not explicitly shown, a run index number is given in parentheses and reference made to another table for new parameter values. For example, the second line of Table 34 does not give the new parameter values for actinide and fission product sorption factors. Instead, it shows a run index of (1) and refers to Table 53, which shows that the retardation factors were changed from 10^2 to 1 for the fission products and 10^4 to 10^2 for the actinides.

Computer Simulations

In the unflawed cases (Tables 34 through 39) with no faults, breccia pipes, or seal failures, we varied single parameters in 52 runs and varied two to five parameters simultaneously in 10 multiparameter runs. By observing the resulting changes in dose and concentrations, we gained an understanding of the relative importance of the parameters that define the multiple barrier repository system.

Parameters describing hydrologic properties, chemistry, and geometry (path lengths) were varied from baseline values to the credible limits in the direction that increased nuclide release. Further experiments are planned in which values are varied so as to minimize release. A fracture zone with a specified permeability was assumed to exist around all tunnels and shafts. Areas and lengths of these zones were calculated from the dimensions of a reference repository described by Office of Waste Isolation Report #Y/OWI/SUB-76/16506 (Parsons, Brinckerhoff, Quade, and Douglas, Inc., 1976).

The rest of the simulations calculated the effect of introducing failure mechanisms. In the shale repository, we simulated (1) a fault (Table 44), (2) failed borehole seals (Table 42), and (3) failed backfill and shaft seals (Table 40); and in the salt repository, (4) failed borehole seals (Table 43), (5) failed backfill and shaft seals (Table 41), and (6) formation of a solution breccia pipe (Table 45). Planned sequences of simulations were

truncated when it became clear that results would be similar to, or could be extrapolated from, other runs. Figures 49 through 52 illustrate these, as well as the unflawed, repositories.

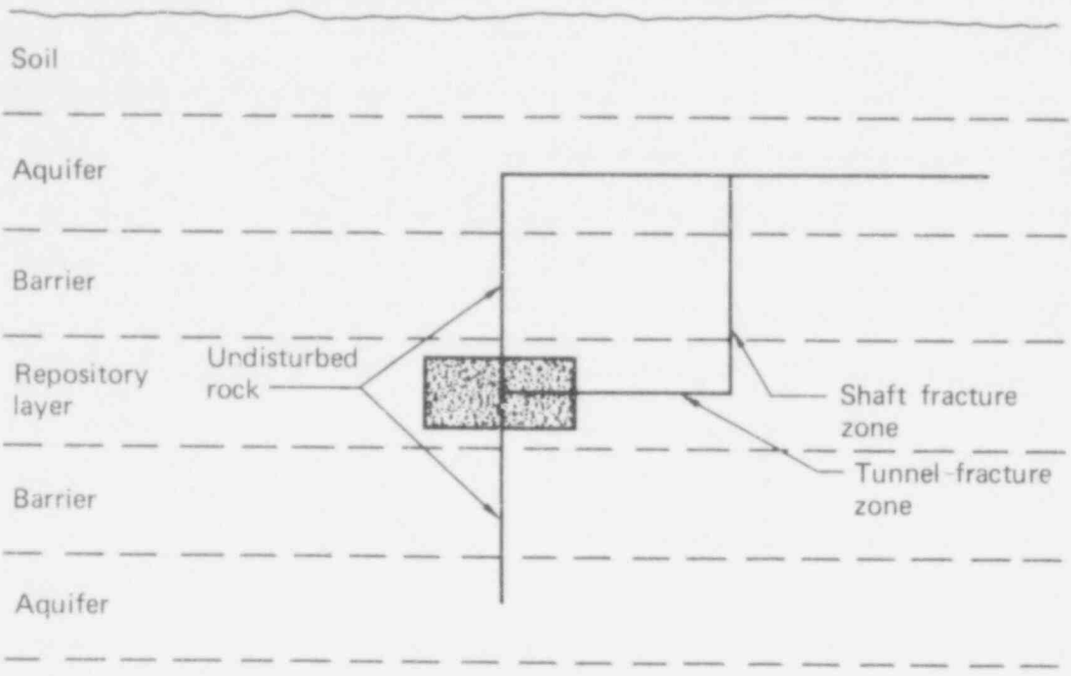

FIG. 49. Flow pathways for unflawed repository (Tables 34 through 39).

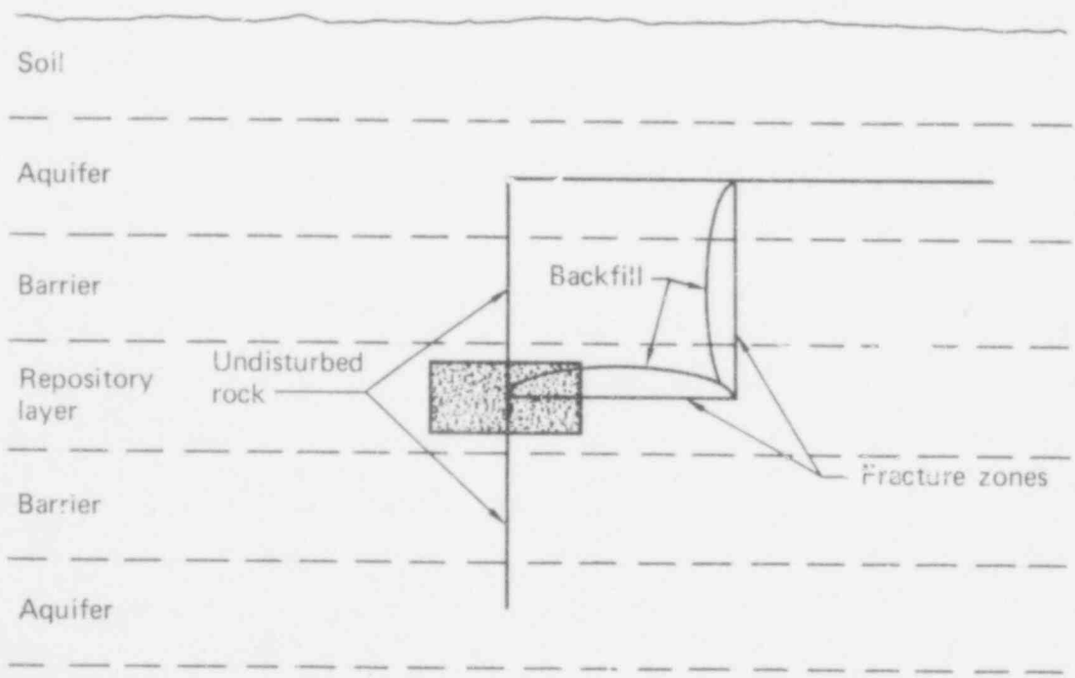

FIG. 50. Flow pathways for repository with deteriorated backfill (Tables 40 and 41).

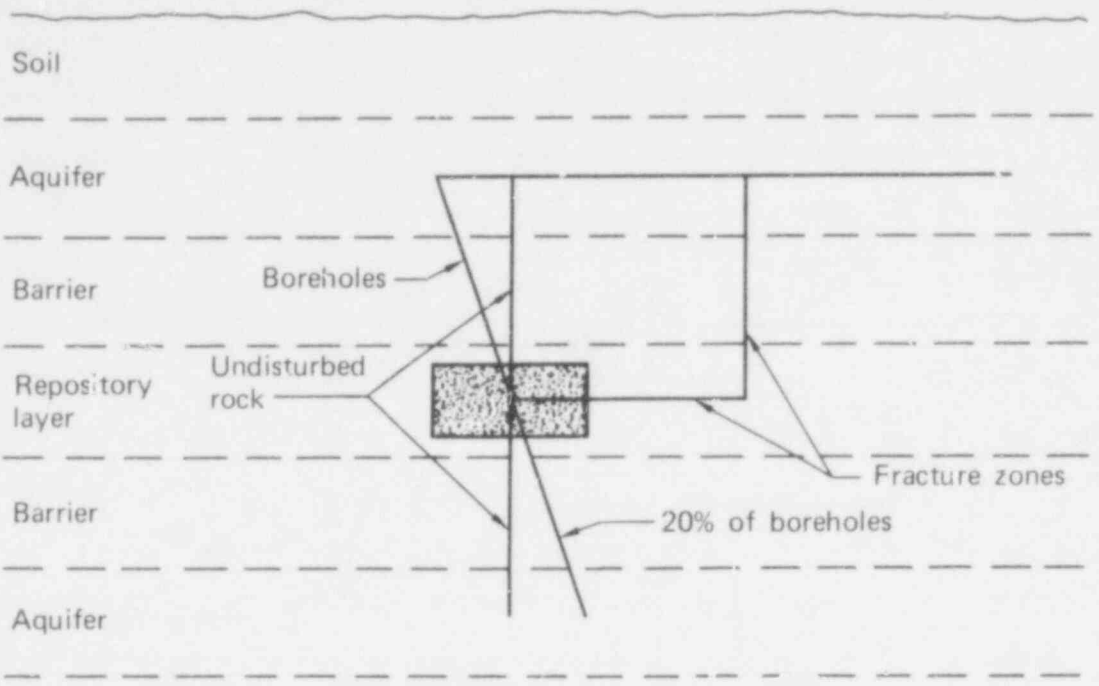

FIG. 51. Flow pathways for repository with failed boring seals (Tables 42 and 43).

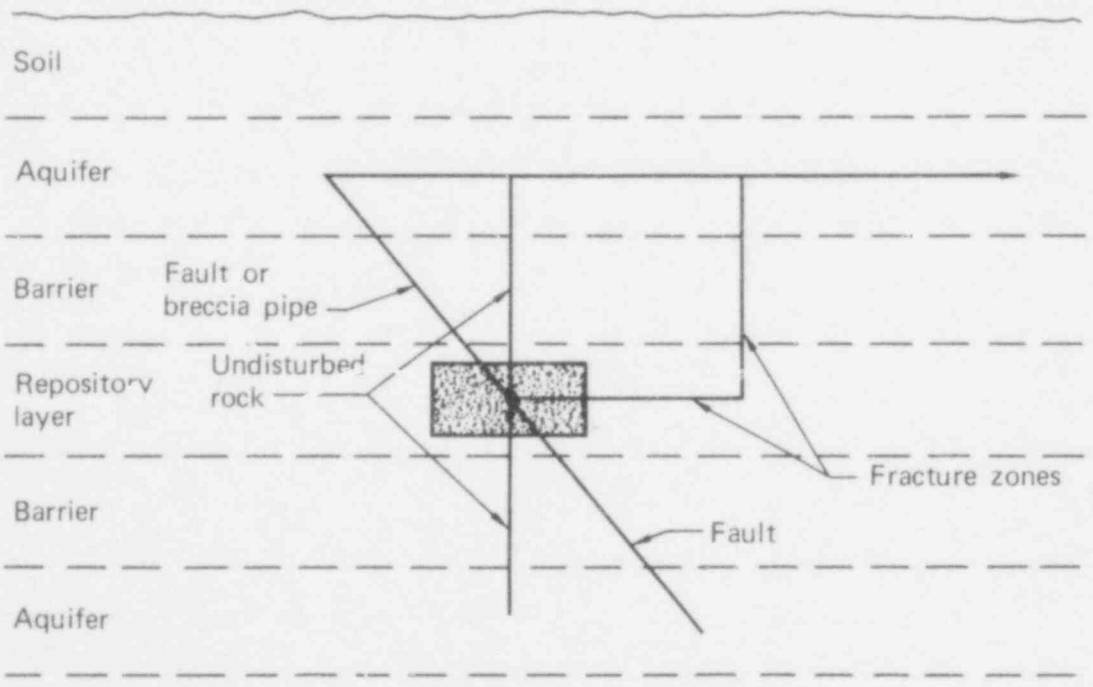

FIG. 52. Flow pathways for repository with fault (Table 44) or breccia pipe (Table 45).

Performance Measures

The consequences of release can be stated in a number of ways. The three performance measure selected in this study were:

- The dose received by an individual consuming an average diet consisting entirely of contaminated food.
- The dose to the population integrated over the 3×10^6 y following decommissioning.
- The maximum groundwater concentrations of ^{99}Tc, ^{126}Sb, ^{226}Ra, and ^{239}Pu in an aquifer immediately above the repository cavity.

The tables also include the time (in years following decommissioning) that individual dose and nuclide concentrations reach their peak.

Description of Analyses

Radionuclide concentrations were calculated assuming a line source in the aquifer with a length of 2 km. Mixing through the full height of the aquifer was assumed. Concentrations were not calculated beyond 3×10^6 y; therefore, peak concentrations are omitted from the table when the peak occurred later than 3×10^6 y. Further assumptions are discussed below.

Assumptions for Tables 34 and 35. Tables 34 and 35 describe a shale repository with flow paths to the aquifer through a fracture zone surrounding the tunnel and shaft, and through the repository layer and the overlying layer of shale. We assumed interstitial flow through the shale. Flow pathways are shown in Fig. 49.

Assumptions for Tables 36 and 37. Tables 36 and 37 describe a bedded-salt repository with flow paths to the aquifer through a fracture zone surrounding the tunnel and shaft, and through the overlying salt and shale layers. We assumed interstitial flow through the barrier layers. Flow pathways are shown in Fig. 49.

Assumptions for Tables 38. Table 38 describes a shale repository with flow paths to the aquifer through a fracture zone surrounding the tunnel and shaft, and through the overlying layer of shale. We assumed fracture flow through the shale layers. Figure 49 shows the flow pathways.

Assumptions for Table 39. Table 39 describes a bedded-salt repository with flow paths to the aquifer through a fracture zone surrounding the tunnel and shaft, and through the overlying salt and shale layers. We assumed fracture flow through the shale barrier layer and interstitial flow through the salt layer. Flow pathways are shown in Fig. 49. Baseline parameter values are as given in Table 47, except for flow through the shale barrier layer, which is described by the values given in the second row of Table 48.

Assumptions for Tables 40 and 41. Tables 40 and 41 assume the same flow paths as in the shale and salt repositories of Tables 34 and 36, respectively, with an additional flow path to the aquifer through a deteriorated backfill in the tunnel and shaft. Partial mixing between the backfill and the surrounding fracture zone was assumed. Flow pathways are shown in Fig. 50. Baseline parameter values for the deteriorated backfill are given in Table 49.

Assumptions for Tables 42 and 43. The flow paths assumed in Tables 42 and 43 are the same as in the baseline shale and salt repositories of Tables 34 and 36, respectively, with an additional flow path to the aquifer through borings on which the seals have failed. We assumed that 10% of the seals failed immediately, 30% after 5×10^2 y, and 50% after 10^3 y. Flow pathways are shown in Fig. 51. Baseline parameter values for the failed borings are given in Table 50.

Assumptions of Table 44. Table 44 describes a shale repository with the possibility that a fault will open. The probability of such an event in any given year was assumed to be 5×10^{-7} in the baseline case. We further assumed that when a fault does open it will close almost completely after a mean time of 70 y. The opening is assumed to be along an existing fault; we omitted consideration of new faults because new faulting was less probable and would result in less significant consequences that movements along an existing fault. Flow pathways are shown in Fig. 52. Baseline parameter values are as given in Table 46, with additions and changes indicated in Table 51.

Assumptions of Table 45. Table 45 describes a salt repository with the probability that a breccia pipe will form between the repository and the

aquifer. The probability of such an occurrence in a given year was assumed to be 5×10^{-7} in the baseline case. Figure 52 shows the flow pathways. Baseline parameter values are as given in Table 47, with additions and changes indicated in Table 52.

SECTION 7

REFERENCES

Angerman, C. L., and Rankin, W. N. 1977. Durability of containers for storing solidified radioactive wastes. Paper 83 presented at Corrosion/77, San Francisco.

Bell, M. T. 1973. ORIGEN--the ORNL isotope generation and depletion code. Oak Ridge National Laboratory report ORNL-4628.

Berman, L. E.; Ensminger, D. A.; Giuffre, M.S.; Koplik, C. M.; Oston, S. G.; Pollak, G. D.; and Ross, B. I. 1978. Analysis of some nuclear waste management options. The Analytical Sciences Corporation report TR-1103-1-1.

Bernabo, J. C., and Webb, T., III. 1977. Changing patterns in the Holocene pollen record of northeastern North America: a map summary. Quat. Res. 8(1):65-96.

Berreth, J.R.; Hoskins, A.P.; and Rindfleisch, J. A. 1977. Stabilization and storage of solidified high-level radioactive wastes. Nucl. Technol. 32:16.

Bishop, W. P., and Miraglia, F. J., Jr., eds. 1976. Environmental survey of the reprocessing and waste management portions of the LWR fuel cycle. U.S. Nuclear Regulatory Commission report NUREG-0116 (Supp. 1 to WASH-1248).

Blomeke, J. O.; Kee, C. W.: and Nichols, J. P. 1974. Projections of radioactive wastes to be generated by the U.S. nuclear power industry. Oak Ridge National Laboratory report ORNL-TM-3965.

Bonner, W.F.; Blair, H.T.; and Romero, L.S. 1976. Spray solidification of nuclear waste. Battelle Pacific Northwest Laboratories report BNWL-2059.

Broecker, W.S. 1975. Climate change: are we on the brink of a pronounced global warming? Science 189:460-63.

526 209

Clarke, R.K.; Foley, J. T.; Hartman, W.F.; Larson, D. W. 1976. Severities of transportation accidents. Sandia Laboratories, Albuquerque, report SLA-74-0001.

Dickey, B. R.; Wheeler, B. R.; and Buckham, J. A. 1974. High-level waste solidification: applicability of fluidized-bed calcination to commercial wastes. Nucl. Technol. 24:371.

Draper, N. R., and Smith, H. 1966. Applied regression analysis. New York: John Wiley and Sons.

Ekren, E. B.; Dinwiddie, G. A.; Mytton, J. W.; Thordarson, W.; Weir, J. E., Jr.; Hinrichs, E. N.; and Schroeder, L. J. 1974. Geologic and hydrologic considerations for various concepts of high-level radioactive waste disposal in the conterminous U.S. U.S. Geological Survey open-file report 74-158.

Freeby, W. A. 1975. Interim report: fluidized-bed calcination of simulated high-level commercial wastes. Allied Chemical Corp., Idaho Falls, Idaho, report ICP-1075.

Fritts, H. C. 1977. Tree rings and climate. New York: Academic Press.

Gates, W. L. 1976. The numerical simulation of ice-age climate with a global general circulation model. J. Atmos. Sci. 33:1844-73.

General Electric Company Nuclear Fuel Department. 1973. Design and analysis report--IF-300 shipping cask. Report NEDO-10084-1.

Gera, F. 1975. Geochemical behavior of long-lived radioactive wastes. Oak Ridge National Laboratory report ORNL-TM-4881.

Gray, W. J. 1976. Volatility of a zinc borosilicate glass containing simulated high-level radioactive waste. Battelle Pacific Northwest Laboratories report BNWL-2111.

Hays, J. D.; Imbrie, J.; and Shackleton, N. J. 1976. Variations in the earth's orbit: pacemaker of the ice ages. Science 194:1121-32.

Heckman, R. A.; Towse, D. F.; Isherwood, D.; Harvey, T.; and Holdsworth, T. 1979. High-level waste site suitability study--interim report. Lawrence Livermore Laboratory report UCRL 52633.

Hickey, C. F., Jr. 1973. Ferrous alloys. In Aerospace Structural Metals Handbook. Syracuse Univ. Press.

International Atomic Energy Agency. 1976. Proceedings, international symposium on the management of radioactive wastes from the nuclear fuel cycle. Vienna: IAEA.

Janson, G., et al. 1974. Heat transfer calculations for conceptual design of retrievable surface storage facilities for high-level radioactive wastes. Battelle Pacific Northwest Laboratories draft report BNWL-B-324

Machine Design. 1964. Seals reference issue, Vol. 36(6).

Maiya, P. S., and Busch, D. E. 1973. Met Trans. 4:663.

McCarthy, G. J. 1977. High-level waste ceramics: materials considerations, process simulation, and product characterization. Nucl Technol. 32:92.

Mendel, J. E. 1974. Commercial radioactive waste composition used in the waste fixation program. In Quarterly progress report. Battelle Pacific Northwest Laboratories report BNWL-1871.

Mendel, J. E. 1977. High-level waste glass. Nucl Technol. 32:72.

Miller, R. F.; Benz, W. G.; and Day, M. J. 1944. Trans. Amer. Soc. for Metals 32:381.

Oak Ridge National Laboratory. 1970. Siting of fuel reprocessing plants and waste management facilities. Report ORNL-4451.

526 211

Organization for Economic Cooperation and Development. 1972. Techniques for the solidification of high-level wastes. IAEA technical report, series 176.

Parsons, Brinckerhoff, Quade, and Douglas, Inc. 1976. Waste isolation facility description--bedded salt. Union Carbide Office of Waste Isolation report Y/OWI/SUB-76/16506.

Perona, J. J., and Blomeke, J. O. 1972. A parametric study of shipping casks for solid radioactive wastes. Oak Ridge National Laboratory report ORNL-TM-3651.

Perona, J. J.; Dillon, R. S.; and Blomeke, J. O. 1970. Design and safety consideration of shipping solidified high-level radioactive wastes. Oak Ridge National Laboratory report ORNL-TM-2971.

Rindfleisch, J. A. 1976. Stabilization of simulated commercial waste calcine. Idaho National Engineering Laboratory report ICP-1087.

Slate, S. C., and Maness, R. F. 1977. Corrosion experience in Nuclear waste processing at Battelle-Northwest. Paper 81 presented at Corrosion/77, San Francisco.

Smith, T. H., and Ross, W. A. 1975. Impact testing of vitreous simulated high level waste in canisters. Battelle Pacific Northwest Laboratories report BNWL-1903.

TERA Corporation. 1977. Production of solidified high-level wastes--a cost comparison of solidification processes. Berkeley, CA.

Turner, W. D.; Elrod, D. C.; and Siman-Tov, I. E. 1972. HEATING5--an IBM Heat Conduction Program. Union Carbide Nuclear Division report ORNL/CSD/TM-15.

United States Code of Federal Regulations. 1976.

United States Energy Research and Development Administration. 1976. The management and storage of commercial power reactor wastes. Report ERDA 76-162.

526 212

United States Nuclear Regulatory Commission. 1976. Calculation of annual doses to man from routine releases of reactor effluents for the purpose of NRC regulatory guide 1.109. USNRC Office of Standards Development.

Van Geel, J.; Eschrich, H.; Heimerl, H.; and Grziwa, P. 1976. Solidification of high-level liquid wastes to phosphate glass-metal matrix blocks. Paper IAEA-SM-207/83 in Proceedings, international symposium on the management of radioactive wastes from the nuclear fuel cycle. Vienna: IAEA.

Vernekar, A. D. 1972. Long-period global variations of incoming solar radiation. Meteorological Monographs. 12:34.

APPENDIX A

STORAGE-POOL EVENTS: HEAT TRANSFER EQUATIONS

After a catastrophic loss of cooling water from an interim storage pool, naturally circulating airflow is the principal path by which the stored SHLW canisters lose heat to the surroundings. The flow patterns are quite complex, with cooler air moving rapidly down the sides of the basin and air circulating more slowly back up, while being heated by the waste canisters. Figure A1 illustrates the natural convection process with air entering the bottom of the basin at an initial ambient temperature, T_o, of 322°K (120°F) and leaving the top of the canister array at temperature T_A after exchanging heat isothermally with the canisters at temperature T_c.

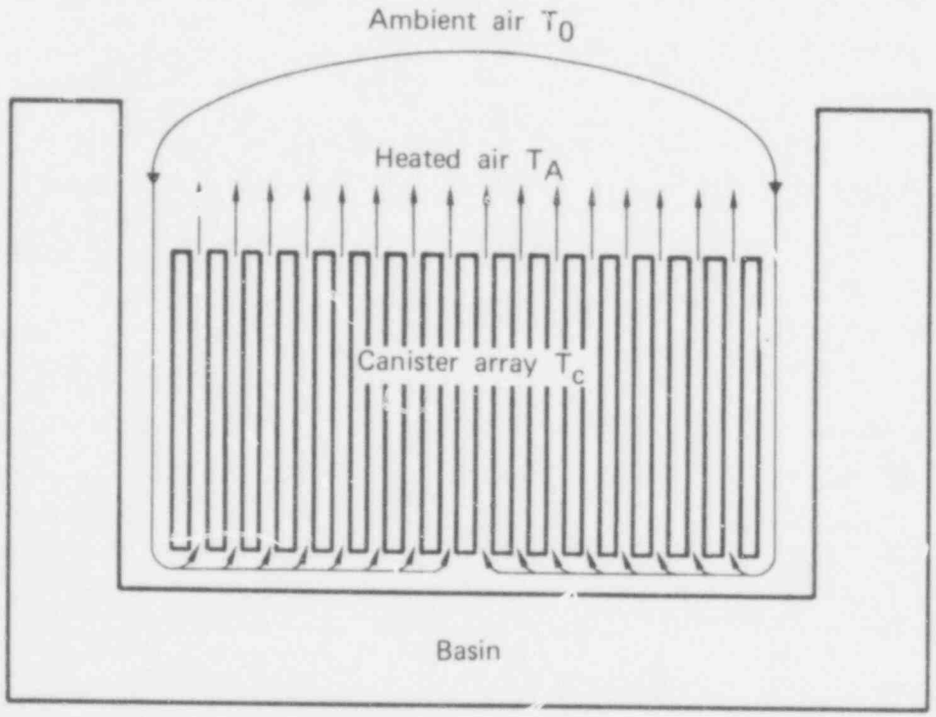

FIG. A1. Natural convection in interim storage canister array.

526 214

A heat balance for the air gives

$$q = C_A W_A A_f (T_A - T_o) = hA_c (T_c - T_A) \quad ,$$

where

q = heat exchange rate between canisters and air (Btu/h)

W_A = mass flow of air (lb/h-ft^2)

C_A = heat capacity of air (Btu/lb-^{o}F)

A_f = flow area between canisters (ft^2)

h = heat transfer coefficient between air and vertical cylinders (Btu/h-ft^2-^{o}F)

A_c = surface area of canisters (ft^2)

Solution of this equation for T_A gives $T_A = C_1 T_o + C_2 T_c$, a formulation similar to that used by Janson et al. (1974). The TASC coefficients (see Section 2), however, are temperature dependent.

Heat transfer across the gap between the heated air and the waste block in Fig. A2 (boundary condition B1) over an area πR^2 approximates the right side of the heat balance equation with a heat transfer coefficient

$$h' = hA_c/\pi R^2 \quad .$$

Heat transfer from heated air to ambient air in Fig. A2 (boundary condition B4), also over an area πR^2, approximates the left side of the equation with a heat transfer coefficient

$$h'' = \frac{C_A W_A A_f}{\pi R^2} \quad ,$$

where W_A, the natural circulation flow rate, is unknown. This quantity was estimated by equating the h determined from natural convection heat transfer

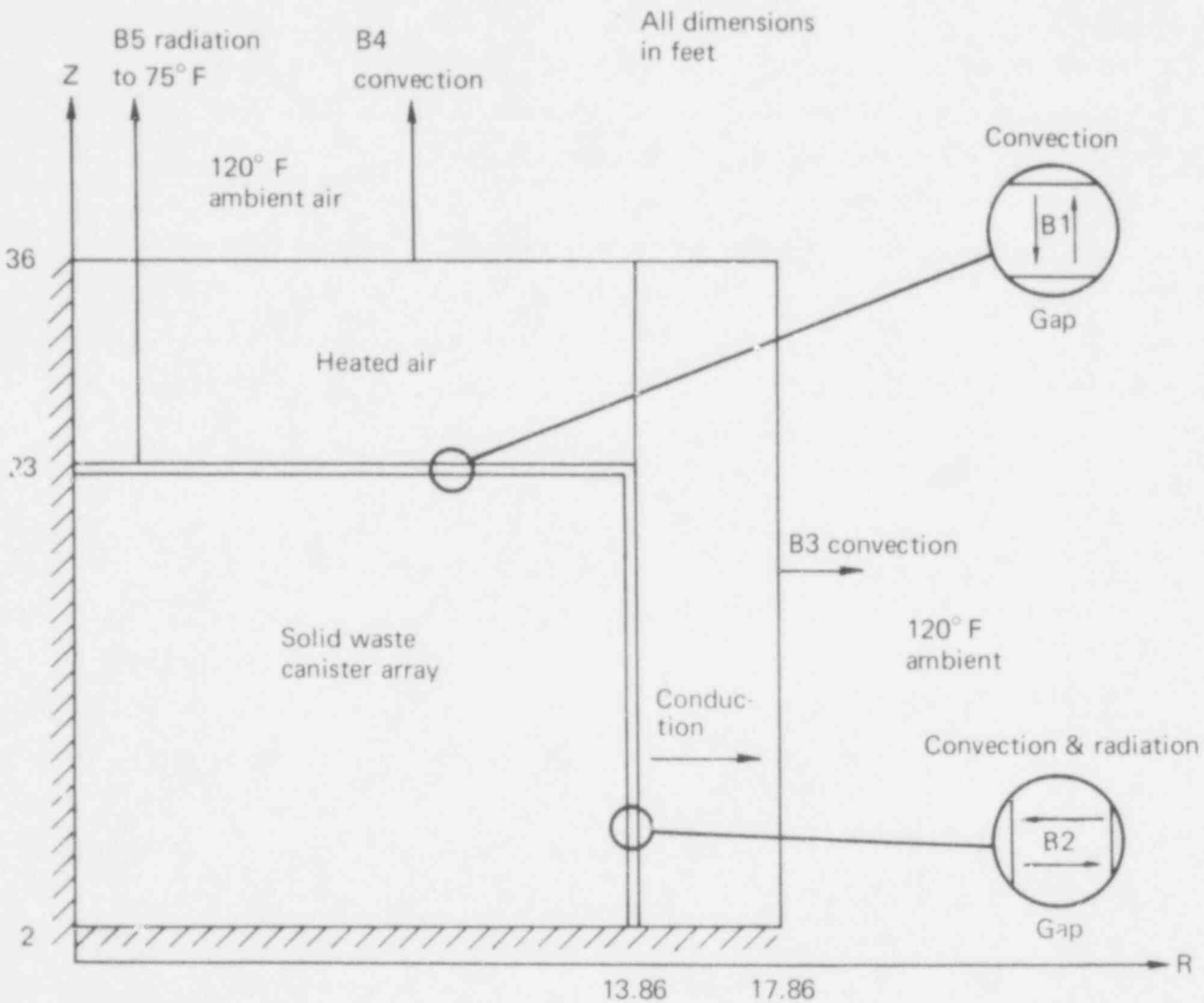

FIG. A2. Geometry for interim storage thermal model.

526 216

correlations with an h determined from forced convection (turbulent flow). The latter depends on W_A, thus a solution for the mass flow can be obtained. Both h' and h", the convective heat transfer coefficients for naturally circulating air, are temperature dependent.

Boundary condition B5 represents radiation from canister tops to space at $297^{o}K$ ($75^{o}F$). A view factor of 0.5 and an emissivity of 0.45 have been assumed.

Boundary condition B2 accounts for both radiation and convective losses from the waste block across the gap to the concrete basin wall. Heat transfer from canister tops, bottoms, and sides is included here.

Boundary condition B3 is shown as a convective heat loss from the outer side of the concrete wall to the $322^{o}K$ ($120^{o}F$) ambient air. However, the heat transfer coefficient was selected to match the thermal conduction resistance of an additional 1.2 m (4 ft) of concrete. Therefore, the concrete temperatures are those of the inner 1.2 m (4 ft) of a 2.4-m (8-ft) thick basin wall.

APPENDIX A REFERENCE

Janson, G., et al. 1974. Heat transfer calculations for conceptual design of retrievable surface storage facilities for high-level radioactive wastes. Battelle Pacific Northwest Laboratories draft report BNWL-B-314.

526 218

APPENDIX B

IMPACT ANALYSIS FOR RAIL SHIPPING CASK

The probability of radioactive release as a function of the accidental drop parameters is the subject of this appendix. Specifically, we answered the following question for a corner-drop accident: if a container is designed so that no radioactivity is released following a drop from 30 ft (10 CFR 71), at what drop height will significant release occur? End-drop accidents were also studied using HONDO V, an asymmetric finite-element code. This information is used with probability estimates on accidental drops to predict the expected amount of radioactivity released during SHLW transportation.

CORNER-DROP ANALYSIS

The container analyzed is the modified General Electric IF-300 spent-fuel cask shown in Fig. 19 of the report. The corner drop is postulated to be the worst of the many possible accidental drops. A corner drop is defined as a drop in which the center of gravity is directly above the corner that hits the unyielding surface. In terms of radioactive release, a corner drop on the end of the cask containing the bolted closure is the worst case. A bending moment results and the lid bolts tend to fail in tension.

The IF-300 cask has an energy absorbing system of lateral steel pins that limits the impact deceleration to 57 g for drop heights up to 30 ft. According to a TASC analysis* similar to that performed by G.E. to show the container would survive a 30-ft drop, impact deceleration of 92 g will produce sufficient moment to cause tensile failure of the closure lid bolts during the worst-case drop.

---

*D. A. Ensminger, The Analytic Science Corp., Reading Mass., private communication (1977).

Any kinetic energy remaining after the energy absorber has bottomed out is absorbed by the cask. The calculations below show that a 12% increase in impact velocity above that at which the cask remains intact increases the impact deceleration from 57 g to 92 g, at which level the lid bolts fail according to TASC. Because the modified container is lighter than the standard G.E. IF-300 container, it will sustain a higher impact velocity (36 mph) before the impact limiter bottoms out. Thus, a 36-mph impact velocity will release no radioactivity while a 40-mph velocity will release radioactivity caused by complete failure of the closure lid bolts. The 12% increase in impact velocity corresponds to a 25% increase in drop height.

Release is so sensitive to impact velocity because the impact surface is assumed to be rigid. Any real surface will yield when a 50-ton container hits it. Yielding will reduce the loads significantly.

A free-body diagram of the modified G.E. IF-300 container is shown in Fig. B1. The loads shown are the forces in kilopounds (kips) that result from an acceleration of 1 g (32.2 ft/sec^2). The total weight of the container is assumed to be 99.3 kip. The lid weighs 7.4 kip, and the contents weighs 25.45 kip.

According to the G.E. procedure, which assumes that the loads are twice the weight of the empty cask times the acceleration plus the weight of the contents, the "reaction force" of an unyielding surface at the point of impact is

$$2 \times (99.3 - 25.45) + 25.45 = 173.15 \text{ kip}$$

This reaction force multiplied by the acceleration (in units of g) of the container's center of gravity (CG) gives the load acting on the rigid surface at the point of impact.

The component of this force parallel to the end of the cask is 60.6 kip, and the component perpendicular to the lid is 162.2 kip. The components of the lid weight are

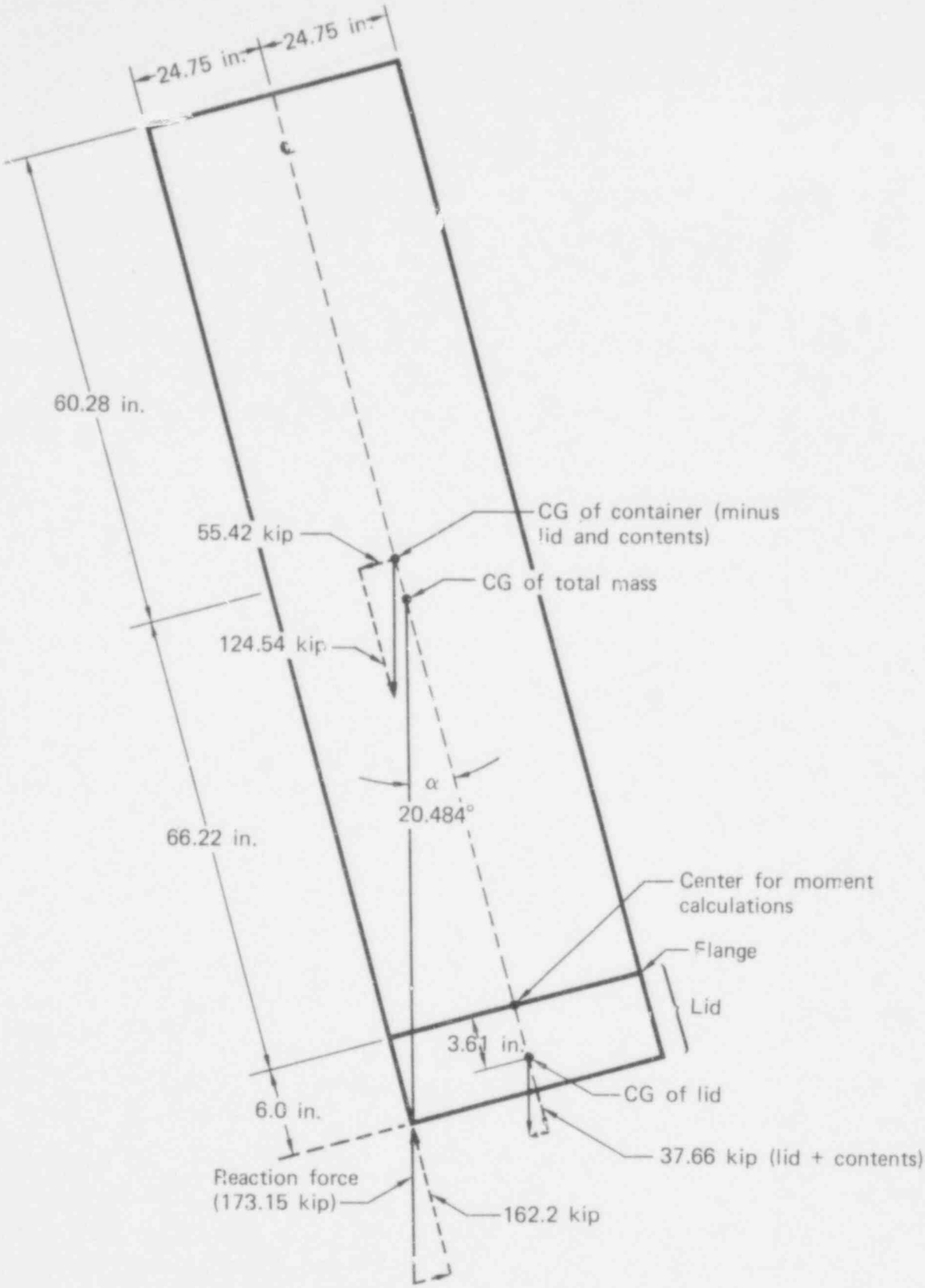

FIG. B1. Corner drop loads.

526 221

$7.4 \times 2 \cdot \sin 20.484 = 5.18$ kip parallel to the end of the container

and

$7.4 \times 2 \cdot \cos 20.484 = 13.86$ kip perpendicular to the end of the container.

This last component can be added to the component from the contents giving a total axial load of 37.66 kips. Balancing forces, the axial load on the cask minus lid and contents must be 124.54 kip and the lateral load 59.36 kip.

The moment on the cask lid calculated relative to the point shown in Fig. B1 is

$$M = 162.2 \times 24.75 - 60.6 \times 6 + 3.61 \times 5.18 = 3670\ G \text{ kip-in.}$$

and the axial load is

$$P = 124.54\ G - 639 \text{ kip} \quad ,$$

where G is the maximum impact deceleration (in units of g) during the drop, and the 639 kip represents the sum of the preload on the bolts and the internal pressure. Because impact energy ($1/2\ mv^2$) is proportional to mass, the impact energy will be less for the modified cask than the original cask by the ratio of the masses

$$\frac{99{,}300 \text{ lb}}{140{,}000 \text{ lb}} = 70.9\% \quad .$$

Following the G.E. procedures, the decelerations experienced while the impact absorber is acting will be the same for the modified cask as the original design. Maximum safe deceleration was predicted to be 57 g. After the impact absorber bottoms out, the closure lid must absorb the remaining impact energy. By assuming that the stainless steel lid is at yield, the peak acceleration can be estimated by equating the excess impact energy to the work done in deforming the lid. Because the cask is still falling on its corner the work done in deforming the lid is a function of the area of the corner that is crushed. Figure B2 shows how the corner may crush when striking a

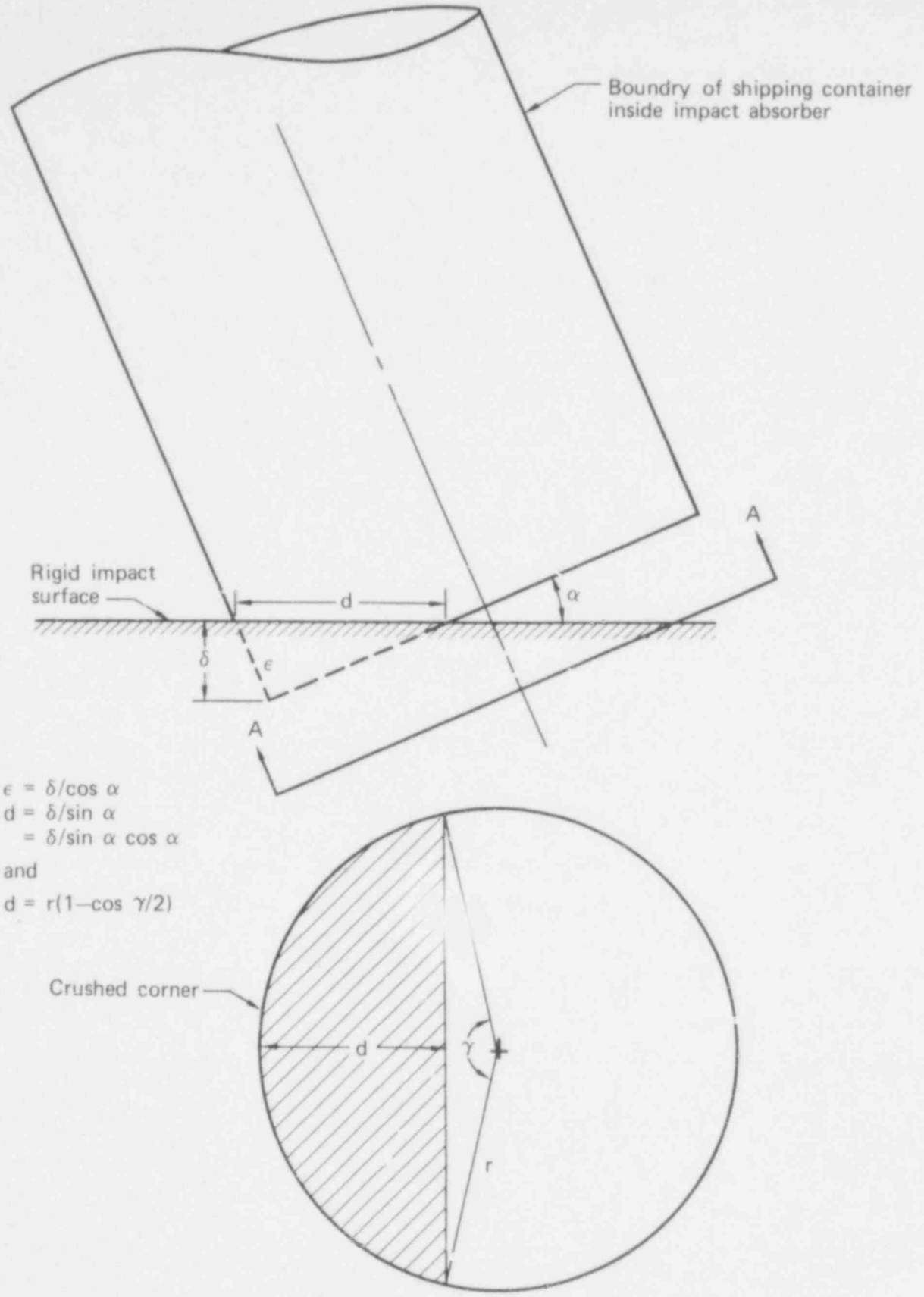

FIG. B2. Idealized corner impact geometry (ellipse approximated by a circle).

rigid surface. The failure deceleration, G, of 92 g, according to TASC, can be related to the crushed area, A, of the lid and its yield stress, σ. Conversely, given the deceleration at which the lid bolts will fail, the crushed area can be calculated

$$A = \frac{G \times wt}{\sigma} = \frac{92 \times 99.3 \text{ kip}}{40 \text{ ksi}} = 228 \text{ in.}^2$$

This can be compared to 1924 in.^{2}, the total area of the lid. The deformation, δ, can be calculated by solving the following two equations for δ and γ given A, r, and α:

$$A = r^2 \left(\frac{\pi\gamma}{360} - \cos \gamma/2 \sin \gamma/2 \right)$$

and

$$\delta = r \sin \alpha \cos \alpha \, (1 - \cos \gamma/2) \quad .$$

If A = 228 in.^{2} and r = 24.75 in., then $\gamma/2 = 49.6^0$ and δ = 2.9 in.

If one assumed a linear relationship between inpact force and deformation, the additional energy absorbed by crushing the corner of the cask can be calculated by

$$\Delta E = 1/2 \, \sigma \, A \, \delta$$

and the energy required to bottom out the impact absorber is

$$E = m \, g \, h$$

so the fractional increase in energy (above the safe impact energy) required to completely fail the closure bolts is

$$\frac{\Delta E}{E} = \frac{\sigma \, A \, \delta}{2 \, m \, g \, h} = \frac{40 \text{ ksi} \times 228 \text{ in.}^2}{2 \times 99.3 \text{ kip} \times .705} \cdot \frac{9 \text{ in.}}{12 \text{ in.}} = 25\% \quad .$$

526 224

Because the energy is a function of the velocity squared, the increase in the drop velocity is approximately 12%.

END-DROP ANALYSIS

In addition to the corner drop, several end-drop conditions were examined using the asymmetrical finite-element code HONDO V (Hallquist, 1977). The main change is allowance for relative motion (slipping or separation) at interfaces.

This analysis was done to verify the structural integrity of the reference design and see whether vertical drops up to 80-mph-equivalent would damage the cask enough to cause a release. This study was conducted for the rail cask only, since it was soon learned that the corner drop imposes the more severe loading and would be used to determine the thresholds on the release function curves. Several end-drop analysis results are noted below.

Impact at 30 mph (30-ft Drop)

- With no fins, high compressive stresses ($\sim 10^5$ psi) were calculated in the area of impact.
- A more detailed model showed that these peak stresses occur away from critical weld areas.
- Without fins, the cask would sustain considerable yielding, but probably no path would open because of the stainless steel.
- With fins, the peak stresses were low ($\sim$30 to 40 psi).

The constant fin load was just enough to keep the cask from bottoming out against the rigid surface.

Impact at 60 mph (120-ft Drop)

- With fins, high compressive stresses ($\sim 10^5$ psi) were calculated in the area of impact.
- The tensile stresses on the end away from impact were moderate ($\sim 10^4$ psi).
- The cask would sustain considerable yielding, but would probably not open.

Impact at 80 mph (214-ft Drop)

- With fins, high compressive peak stresses ($\sim 10^5$ psi) were calculated in the area of impact.
- High tensile stresses were calculated on the end away from the impact.
- It is probable that the cask would not open because of the high compressive stress on the impact end.
- The high tensile load on the other end could cause the cask to open.

APPENDIX B REFERENCES

General Electric Co. 1973. Design and analysis report IF-300 shipping container. Nuclear Fuel Dept. Report NEDO-10084-1.

Hallquist, J.; Young, R. W.; and Goudeau, G. L. 1977. HONDO V Upgrade. Lawrence Livermore Laboratory report UCID 17611.

526 227

APPENDIX C

RELEASE FUNCTIONS FOR TRANSPORTATION ACCIDENTS

To estimate the expected release of radionuclides from the spectrum of accidents that may occur during shipment of SHLW, we must quantify the likely release as a function of accident severity for the major accident types and release modes. Table C1 lists the types of accident, release modes, and SHLW forms for which release functions, F_{ijqr}, were derived. Since the casks to be used for SHLW are massive, we have limited our consideration to impact and fire accidents, believing that crush and puncture accidents will not pose significant threats. The radionuclide release modes considered are dissolution, volatilization, and particulate dispersion. Melting and liquid flow are not believed to constitute a significant mechanism for the spread of radionuclides, since the temperatures required to prevent solidification are extremely high. The effects of melting on the other mechanisms are taken into account, however.

It must be noted that the release functions presented are the result of the limited effort performed over the past year. This work has involved a review of the waste characterization efforts of ERDA contractors, as well as reports of European work. Release thresholds for impact accidents were guided by calculations performed by the Nuclear Test Engineering Division at LLL and by The Analytic Sciences Corporation (TASC). Work at TASC was the basis of the failure-locus threshold technique for fire accidents. The reference shipping casks and waste canisters were described in Section 3.

The two major difficulties in deriving release functions are the undefined nature of the accidents being modeled and the lack of data on the behavior of the waste matrices, canisters, and casks under extremes of temperature and stress. Accordingly, there is considerable uncertainty in the release functions. The dotted curves in Figs. C1 through C8 represent an attempt to show the magnitude of the uncertainties. The functions themselves should be regarded as estimates.

TABLE C1. Indexes that define release functions for SHLW. Each release function, F_{ijqr}, is described by four indexes--one for accident type (i), one for type of release (j), one for waste form (q), and one for the nuclide (r). Waste ages of 150 d, 1 y, 2 y, 5 y, and 10 y were considered.

Index (i)	Accident type
1	Handling at reprocessing plant, crane stall or drop, filtration works
2	Handling at reprocessing plant, crane stall or drop, filtration fails
3	Interim storage, loss of cooling circulation, filtration works
4	Interim storage, loss of cooling circulation, filtration fails
5	Interim storage, drainage of storage pool
6	Truck impact with extremely rigid fixed object (urban)
7	Truck impact with extremely rigid fixed object (rural)
8	Railroad crossing accident, truck impact with train (urban)
9	Railroad crossing accident, truck impact with train (rural)
10	Truck fire (urban)
11	Truck fire (rural)
12	Truck puncture (urban)
13	Truck puncture (rural)
14	Train impact with extremely rigid fixed object (urban)
15	Train impact with extremely rigid fixed object (rural)
16	Train fire (urban)
17	Train fire (rural)
18	Train puncture (urban)
19	Train puncture (rural)
20	Handling at repository prior to emplacement, crane drop, filtration works
21	Handling at repository prior to emplacement, crane drop, filtration fails
22	Storage outside repository, airplane impact with cask

TABLE C1 (continued).

Index (j)	Type of release
1	Air dispersion
2	Air volatilization
3	Water dissolution

Index (q)	Reference form of SHLW
1	Spray calcine
2	Borosilicate glass
3	Fluidized-bed calcine
4	Supercalcine multibarrier

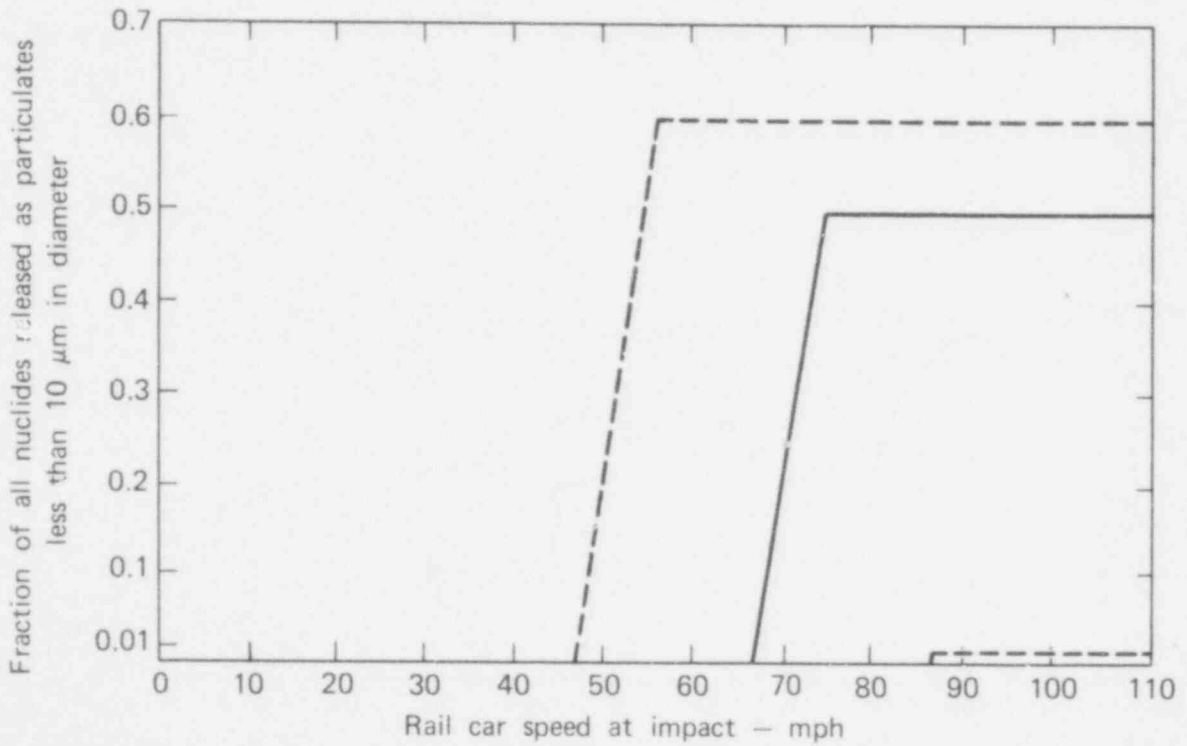

FIG. C1. Release function for particulate dispersion, train impact, spray calcine. Dashed lines define limits of uncertainty.

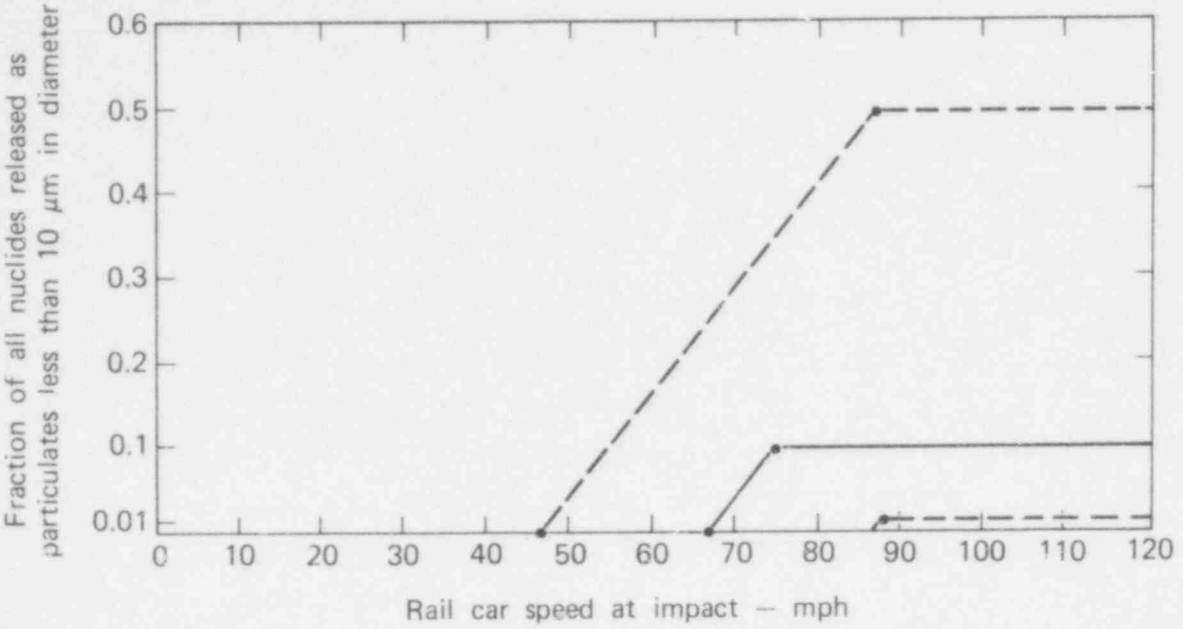

FIG. C2. Release function for particulate dispersion, train impact, fluidized-bed calcine. Dashed lines define limits of uncertainty.

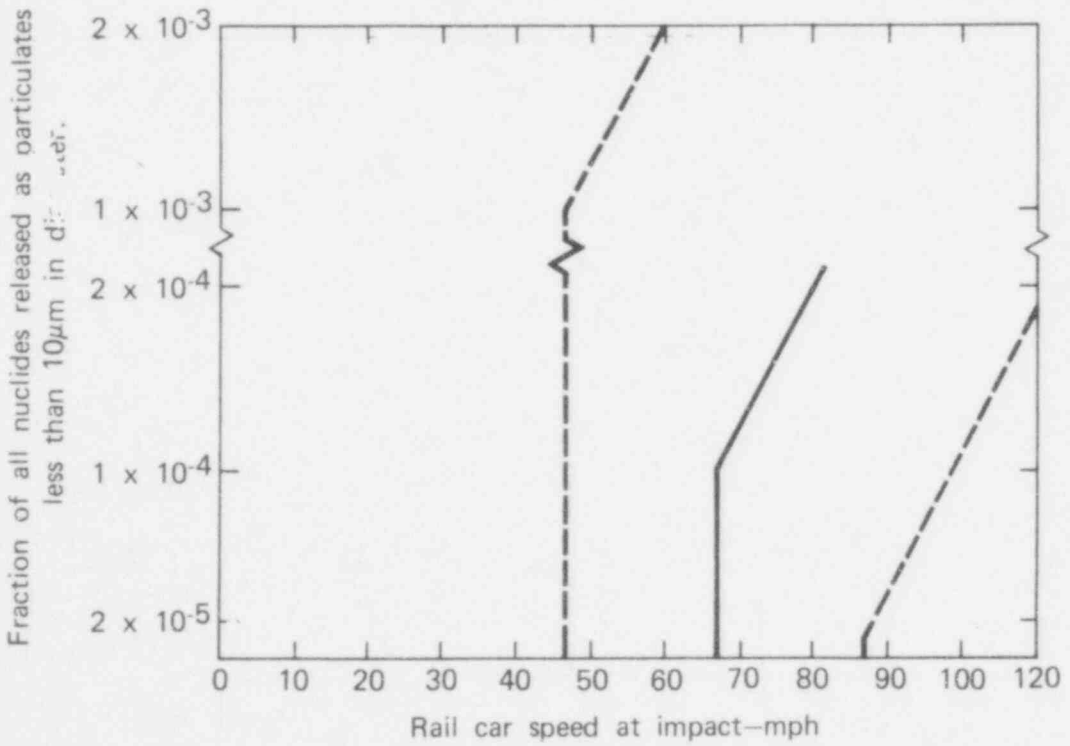

FIG. C3. Release function for particulate dispersion, train impact, glass. Dashed lines define limits of uncertainty.

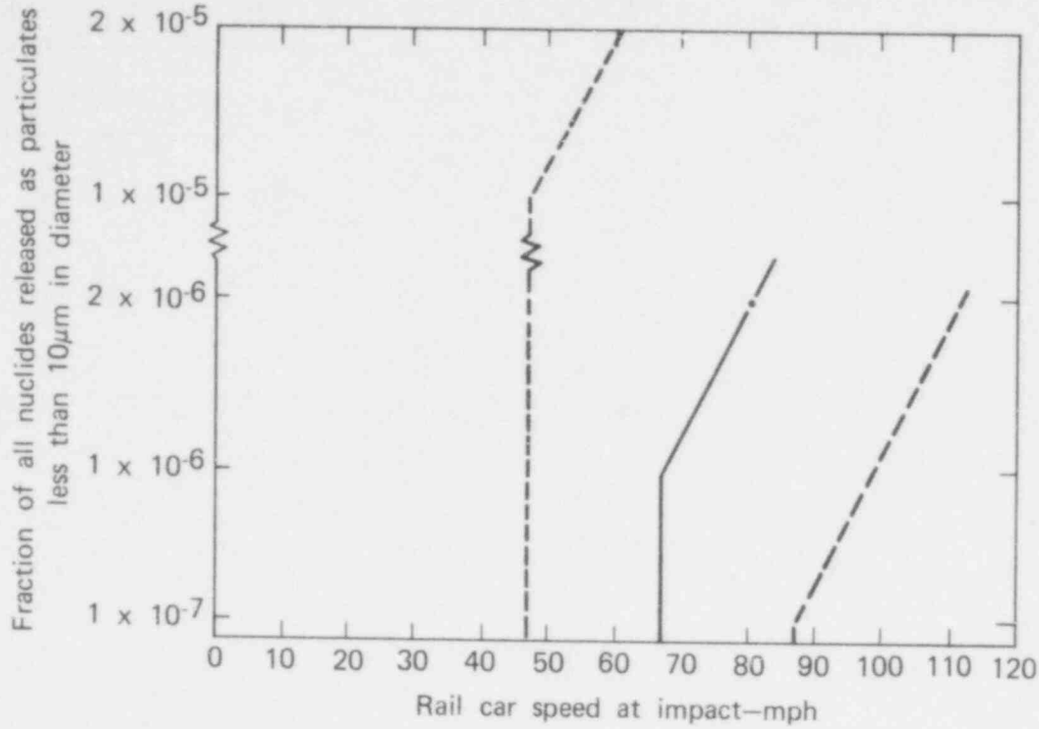

FIG. C4. Release function for particulate dispersion, train impact, multibarrier. Dashed lines define limits of uncertainty.

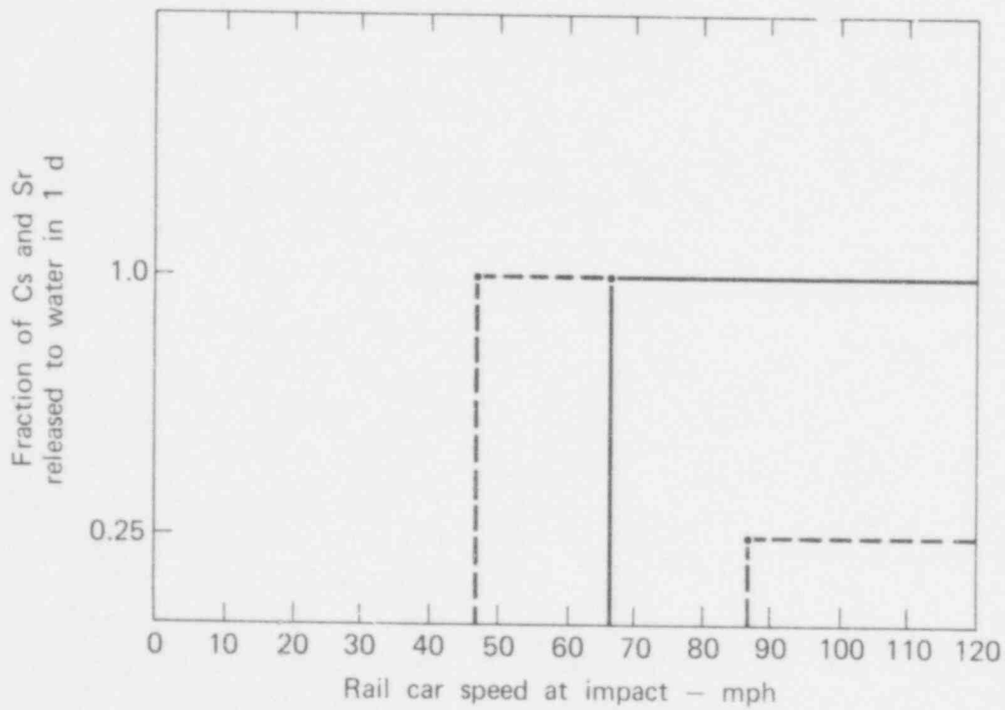

FIG. C5. Release function for dissolution, train impact, spray calcine. Dashed lines define limits of uncertainty.

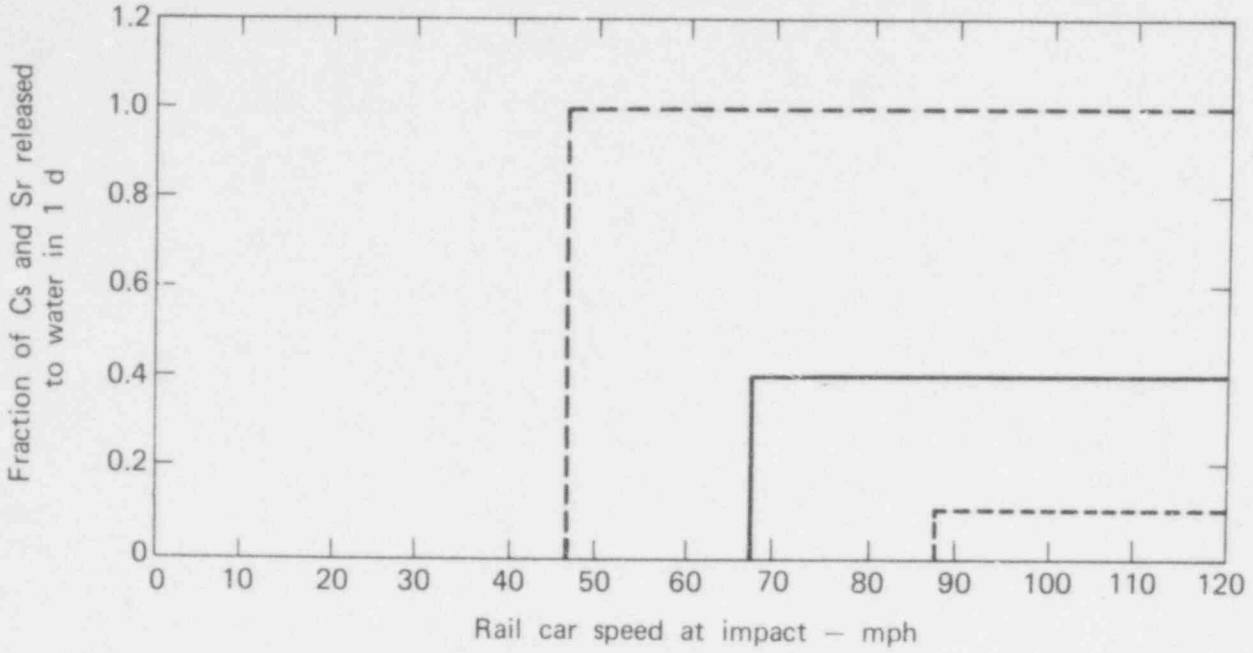

FIG. C6. Release function for dissolution, train impact, fluidized-bed calcine. Dashed lines define limits of uncertainty.

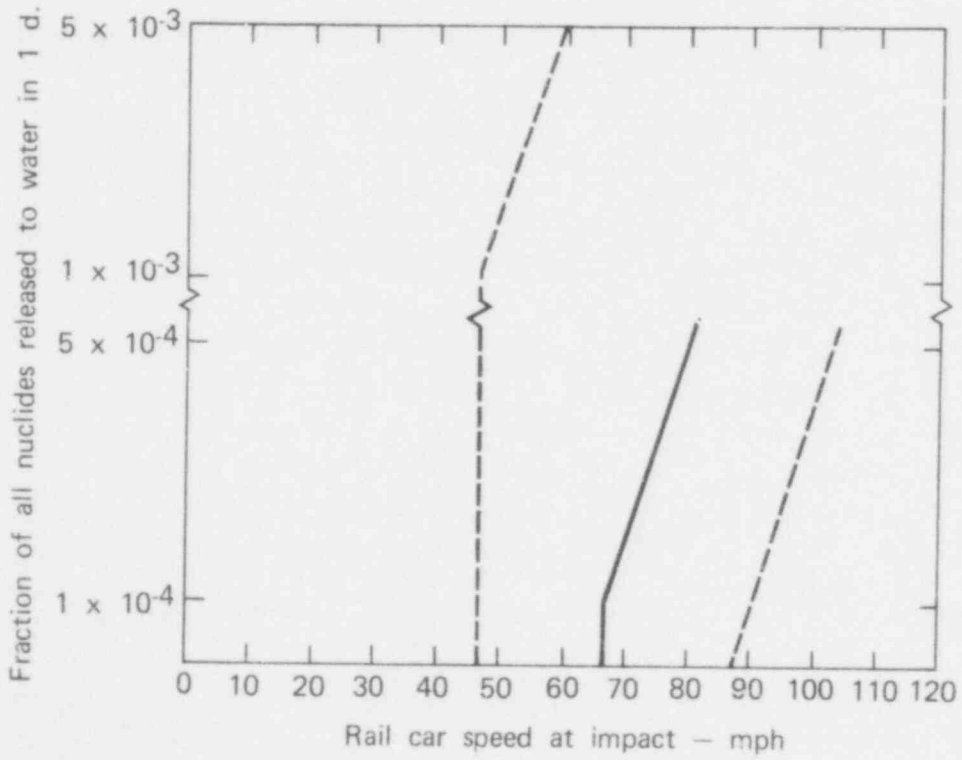

FIG. C7. Release function for dissolution, train impact, glass. Dashed lines define limits of uncertainty.

526 233

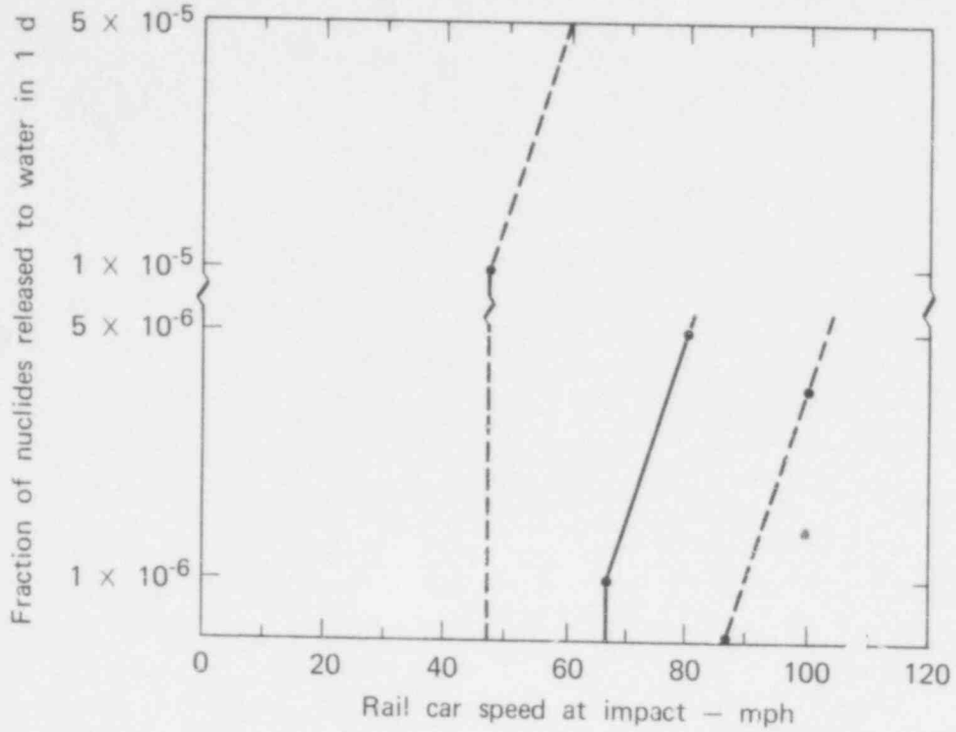

FIG. C8. Release function for dissolution train impact, multibarrier. Dashed lines define limits of uncertainty.

The functions illustrated are for rail impact accidents. Release functions for truck impacts are expected to be similar except that the thresholds must be estimated from heat transfer and impact calculations on a reference truck cask. The analytic forms used to model the functions are summarized in Tables C2 and C3 for fire and impact accidents, respectively.

The shapes chosen for the release functions are the simplest ones that describe the physics of the situation. More complicated functions cannot be supported with the data available at this time. In the following paragraphs, we give the reasoning behind each release function.

526 234

Table C2. Analytic forms used to model transportation release functions for fire accidents (Maximum credible temperature, T_f, = 1590 ^{o}K).

Function index q	j	i	Range of temperature, T, ^{o}K	Release function, $F_{ijqr}(T)$	Nuclides released	Duration of release
1,3	1	10,11	$0 \leq T \leq 1573$	0	All	
		16,17	$1573 \leq T \leq T_f$	0.01		
1,3	2	10,11	$0 \leq T \leq 1573$	0		
				$1.74 \exp(-7{,}600/T)$	Cs	4 h
		16,17	$1573 \leq T \leq T_f$	$2.36 \times 10^{6} \exp(-27{,}900/T)$	Ru	4 h
1,3	3	10,11	$0 \leq T \leq 1573$	0	Cs, Sr	1 d
		16,17	$1573 \leq T \leq T_f$	0.5		
2	1	10,11		0		
		16,17				
2	2	10,11	$0 \leq T \leq 1473$	0	Cs	4 h
		16,17	$1473 \leq T \leq T_f$	$8.13 \times 10^{6} \exp(-29{,}200/T)$		
2	3	10,11	$0 \leq T \leq 1473$	0	All	1 d
		16,17	$1473 \leq T \leq T_f$	10^{-4}		
4	1	10,11	$0 \leq T \leq 1573$	0	All	
		16,17	$1573 \leq T \leq T_f$	10^{-4}		
4	2	10,11	$0 \leq T \leq 1573$	0	Cs	4 h
		16,17	$1573 \leq T \leq T_f$	$5.89 \times 10^{6} \exp(-33{,}700/T)$		
4	3	10,11	$0 \leq T \leq 1573$	0	All	1 d
		16,17	$1573 \leq T \leq T_f$	10^{-5}		

TABLE C3. Analytic forms used to model transportation release functions for impact accidents.

Function index q	j	i	Max. credible velocity, v_f, mph	Range of impact velocity, v, mph	Release function, $F_{ijqr}(v)$	Nuclides released
1	1	7,9,15	180	$0 \leq v \leq 67$	0	All
				$67 \leq v \leq 75$	0.0625 (v-67)	
		6,8	120	$75 \leq v \leq v_f$	0.5	
1	3	7,9,15	180	$0 \leq v \leq 67$	0	Sr, Cs
		6,8	120	$61 \leq v \leq v_f$	1.0	
2	1	7,9,15	180	$0 \leq v \leq 67$	0	All
		6,8	120	$67 \leq v \leq v_f$	7.69×10^{-6} (v-67) + 10^{-4}	
2	3	7,9,15	180	$0 \leq v \leq 67$	0	All
		6,8	120	$67 \leq v \leq v_f$	3.1×10^{-5} (v-67) + 10^{-4}	
3	1	7,9,15	180	$0 \leq v \leq 67$	0	All
				$67 \leq v \leq 75$	0.0125 (v-67)	
		6,8	120	$75 \leq v \leq v_f$	0.1	
3	3	7,9,15	180	$0 \leq v \leq 67$	0	Sr, Cs
		6,8	120	$67 \leq v \leq v_f$	0.4	
4	1	7,9,15	180	$0 \leq v \leq 67$	0	All
		6,8	120	$67 \leq v \leq v_f$	7.69×10^{-8} (v-67) + 10^{-6}	
4	3	7,9,15	180	$0 \leq v \leq 67$	0	All
		6,8	120	$67 \leq v \leq v_f$	3.1×10^{-7} (v-67) + 10^{-6}	

FIRE-INDUCED RELEASES

In the case of fire-induced releases, the cask seal is breached early in the fire; consequently, breach of the canister determines the threshold for release.

Both the heat transfer through the cask and the canister failure mechanisms are time dependent. Because of the Arrhenian nature of the canister failure mechanisms, however, it is possible to establish a discrete temperature for canister failure (see Section 3). This approach allows us to separate the two parts of the analysis and to consider the time dependence of the heat transfer process by itself. We adopted a failure locus approach, in which the time to canister failure for fires of several temperatures was calculated. These points describe a failure locus on a plot of time vs fire temperature. Whenever a cask experiences a fire whose intensity and duration are above and to the right of this locus, canister failure is deemed to have occurred.

The canister failure temperature (below which failure never occurs) has been taken as $1200^{o} \pm 50^{o}C$ ($2190^{o} \pm 90^{o}F$) for the borosilicate-glass form, $1300^{o} \pm 50^{o}C$ ($2370^{o} \pm 90^{o}F$) for spray and fluidized-bed calcine, and $1300^{o} \pm 100^{o}C$ ($2370^{o} \pm 180^{o}F$) for multibarrier. Glass failure is expected from waste-on-canister corrosion, with small contributions from external oxidation and creep-rupture. The spray and fluidized-bed calcines will fail mainly because of external oxidation, with contributions from the other two mechanisms. Multibarrier failure is expected from nickel-lead corrosion and from cracking of the Al_2O_3 coatings.

Given an accident that exceeds the limits established by the failure locus, the magnitude of the release depends primarily on the release mode, the properties of the waste form, the mechanical configuration assumed for the cask, canister(s), and waste, and environmental factors at the time of the accident. Since many of these factors are not well defined, the magnitude of release is subject to uncertainties that may be as large as a few orders of magnitude in some cases. Estimating these uncertainties is difficult without a more precise knowledge of the likely range of the contributing factors.

Volatilization

Volatilization functions apply to a fire accident in which cask and canister breaching occurs and the radionuclides are driven off as gases because of the elevated temperature. The calculation of thresholds is the same as for other fire cases, but an Arrhenius-type function was used to describe the release after the threshold is reached. A 4-h release period was assumed, because it is comparable to the time constant of large casks and the duration of large fires.

The volatilization release functions are based mainly on work done at Battelle Pacific Northwest Laboratories (BNWL) (Gray, 1976) on volatilization from small samples of borosilicate glass and spray calcine as a function of temperature.

Because of the high threshold temperatures and the high temperatures at which volatilization is significant, we assumed that the cask no longer presents an effective barrier to volatilization in these scenarios. The canister was assumed to be lying on its side, and the surface of the waste was exposed on the upper side (see Fig. C9).

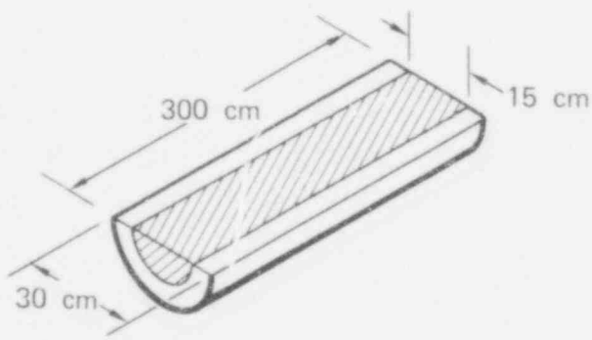

FIG. C9. Canister configuration for fire-volatilization release function.

The exposed surface was taken to be 15 × 300 cm. It was necessary to scale Gray's results for small samples to this situation. Our approach was to do this at 1200°C (2128°F), then to derive an Arrhenius expression that fits Gray's data over a range of temperatures.

Gray's 2-g glass sample had a surface area of 1.98 cm^2 and a thickness of about 34.2 mm. In 4 h, the Cs loss was about 20 mg/cm^2. He states that a sample about 1 cm thick would have twice the loss. His experiments indicate that the process is surface controlled.

The inventory of Cs in a fresh waste canister can be determined approximately by scaling up Gray's Cs inventory:

$$(360.0\ mg) \times \frac{0.2 m^3 \times 3300\ kg/m^3}{0.002\ kg} \times \frac{155\ kg/t\ of\ uranium}{207\ kg/t\ of\ uranium} = 8.77 \times 10^6\ mg \quad .$$

The fraction lost is then obtained by assuming that the surface loss rate is the same for the large and small samples:

$$\frac{2 \times 20\ mg/cm^2 \times 15\ cm \times 300\ cm}{8.77 \times 10^6\ mg} = 0.02 \quad .$$

A fit to Gray's data in dry air gives an Arrhenius factor exp (-29,200/T). Matching at 1200°C gives an expression for the release fraction:

$$RF\ (Cs\ in\ glass) = 8.13 \times 10^6 \exp(-29{,}200/T) \quad .$$

For spray calcine and fluidized-bed calcine the calculation is similar, except that the process is diffusion controlled rather than surface controlled. At 1200°C, Gray's sample lost about 18 mg/cm^2 in 4 h out of an inventory of 142 mg of Cs. The amount lost for a thick (1-cm) sample would be twice as much, but the inventory would also be twice as large. The fraction for a thick sample would be

$$\frac{2 \times 18\ mg/cm^2 \times 2\ cm^2}{2 \times 142\ mg} = 0.253 \quad .$$

526 239

For the canister, the effective thickness would be about 25 cm. Assuming a diffusion-controlled process for which a 1-cm-thick sample is a "thick" sample, the canister release fraction would be given by:

$$0.253 \times \frac{1 \text{ cm}}{25 \text{ cm}} = 0.01 \quad .$$

In the same way as before, the following equation is derived:

$$\text{RF (Cs in calcine)} = 1.74 \exp(-7600/T) \quad ,$$

Likewise, the Ru release from calcine is given by

$$\text{RF (Ru in calcine)} = 2.36 \times 10^{6} \exp(-27{,}900/T) \quad .$$

For the multibarrier waste form, the same canister failure temperature and coating failure temperature were used as in other fire cases; namely, $1000^{\circ} \pm 200^{\circ}$C and $1300^{\circ} \pm 100^{\circ}$C, respectively. Cesium was the only element considered. The release fraction is taken to be

$$\text{RF} = 5.89 \times 10^{6} \exp(-33{,}700/T) \quad .$$

The uncertainty bounds are one order of magnitude above and three below the calculated value. These results are based on unpublished data from Gray at BNWL (J. Rusin, private communication, 1977).

Particulate Dispersion

These dispersion functions apply to fire accidents that breach the cask and canister, and to the dispersion of the waste as respirable particulates (less than 10 μm in diameter). The convection resulting from the fire and any wind that is present act as the driving force for dispersion. The failure threshold was obtained as it was for the other fire cases and we assumed a step function release once the threshold is exceeded. A step function was chosen because we felt that, although a more severe fire will produce more convection, it will also tend to sinter and fuse the particulates. These two effects are likely to cancel, at least partially.

For spray calcine, the canister failure temperature was taken to be $1300^{o} \pm 50^{o}C$. All nuclides were considered, as in the impact-particulate case. The expected release fraction was taken to be 0.01, with an upper bound of 0.1 and a lower bound of 0.001. This estimate was based on the maximum fraction of respirable size (0.5), and on judgments regarding breach size, strength of convection currents, and degree of sintering due to the high temperature. Few data are available.

The function for fluidized-bed calcine was taken to be the same as that for spray calcine. The large initial average particle size would tend to give a smaller release, but the effects of the fire would probably mask any major differences.

The function for borosilicate glass was taken to be zero, because the glass would be molten at the canister failure temperature. We would not expect a significant fraction of particulates when it solidifies.

For the multibarrier waste form, the canister failure temperature was taken to be $1000^{o} \pm 200^{o}C$ and the coating failure temperature was taken to be $1300^{o} \pm 100^{o}C$. All nuclides were again considered, and the expected release fraction was taken as 10^{-4}, with an upper bound of 10^{-2} and a lower bound of 10^{-6}. These values can only be estimated, because data are lacking.

Dissolution

These dissolution functions apply to fires severe enough to breach both the cask and the canister, followed by contact with water and dissolution of the waste. The failure threshold occurs when the combination of fire temperature and time is great enough to breach the cask and canister. Once the threshold is reached, the dissolution is described by a step function, since greater fire severity is not likely to result in greater dissolution.

For spray and fluidized-bed calcine, the canister failure temperature was taken to be $1300^{o} \pm 50^{o}C$. This figure was based on the belief that the combined processes of oxidation, creep, and corrosion by the waste will bring

about failure of the canister at a somewhat lower temperature than the start of melting at 1400°C.

Only Cs and Sr were considered, because of their high solubility and hazard index. The expected fraction released after one day in contact with water was taken to be 0.5, with a upper bound of 1.0 and a lower bound of 0.01. Because we expect the heat to change the Cs and Sr into a less soluble form, the expected value is somewhat lower than for the impact-dissolution case. The uncertainly limits are intended to account for lack of data and the unspecified nature of the dissolution conditions.

The canister failure temperature for borosilicate glass was taken as 1200° ± 50°C. This estimate was derived from the corrosion data of Slate and Maness (1977). All nuclides were considered, since the glass is expected to dissolve uniformly. The expected fraction released to water in one day is 10^{-4}, with an upper bound of 10^{-3} and a lower bound of 10^{-7}. The release fraction was estimated using the dissolution data of Mendel (1977), assuming gross breaching of the canister. The uncertainty bounds account for uncertainties in breach size and dissolution conditions.

The multibarrier canister is assumed to fail at 1000° ± 200°C as a result of dissolution of nickel from the stainless steel in the molten lead. The alumina coatings on the pellets are taken to fail by cracking at 1300° ± 100°C, an estimate based on discussions with Rusin at BNWL (private communication, 1977). All nuclides were assumed to dissolve, and the expected value was taken to be 10^{-5} in one day, with upper and lower bounds of 10^{-4} and 10^{-7}. These are estimates based on the belief that the dissolution of the multibarrier form can be made lower than that of the glass, because the coatings will still afford partial protection. Few data are available fo this waste form.

Summary

Fire--volatilization — Spray calcine and fluidized-bed calcine

Arrhenius function after failure locus is exceeded.
Canister failure temperature = $1300^{o}C \pm 50^{o}C$.
Fraction of Cs released in 4 h
= 1.74 exp (-7600/T), expected
= 17.4 exp (-7600/T), maximum
= 17.4×10^{-3} exp (-7600/T), minimum
Fraction of Ru released in 4 h
= 2.36×10^{6} exp (-27,900/T), expected
= 2.36×10^{7} exp (-27,900/T), maximum
= 2.36×10^{3} exp (-27,900/T), minimum

Fire--volatilization — Borosilicate glass

Arrhenius function after failure locus is exceeded.
Canister failure temperature = $1200^{o} \pm 50^{o}C$.
Fraction of Cs released in 4 h
= 8.13×10^{6} exp (-29,200/T), expected
= 8.13×10^{7} exp (-29,200/T), maximum
= 8.13×10^{3} exp (-29,200/T), minimum

Fire--volatilization — Multibarrier

Arrhenius function after failure locus is exceeded.
Canister failure temperature = $1000^{o} \pm 200^{o}C$.
Coating failure temperature = $1300^{o} \pm 100^{o}C$.
Fraction of Cs released in 4 h
= 5.89×10^{6} exp (-33,700/T), expected
= 5.89×10^{7} exp (-33,700/T), maximum
= 5.89×10^{3} exp (-33,700/T), minimum

526 243

Fire--particulate dispersion — Spray and fluidized-bed calcine

Step function after failure locus is exceeded.
Canister failure temperature = $1300^{o} \pm 50^{o}C$.
Fraction of all nuclides released as particulates less than 10 μm in diameter is

0.01, expected
0.1, maximum
0.001, minimum

Fire--particulate dispersion — Borosilicate glass

This function was taken to be zero.

Fire--particulate dispersion — Multibarrier

Step function after failure locus is exceeded.
Canister failure temperature = $1000^{o} \pm 200^{o}C$.
Coating failure temperature = $1300^{o} \pm 100^{o}C$.
Fraction of all nuclides released as particulates less than 10 μm in diameter is

10^{-4}, expected
10^{-2}, maximum
10^{-6}, minimum

Fire--dissolution — Spray calcine

Step function after failure locus is exceeded.
Canister failure temperature = $1300^{o} \pm 50^{o}C$.
Fraction of Cs and Sr released to water in one day is

0.5, expected
1.0, maximum
0.01, minimum

526 244

Fire--dissolution — Fluidized-bed calcine

Step function after failure locus is exceeded.
Canister failure temperature = $1300^{o} \pm 50^{o}C$.
Fraction of Cs and Sr released to water in one day is
0.5, expected
1.0, maximum
0.01, minimum

Fire--dissolution — Borosilicate glass

Step function after failure locus is exceeded.
Canister failure temperature = $1200^{o} \pm 50^{o}C$.
Fraction of nuclides released to water in one day is
10^{-4}, expected
10^{-3}, maximum
10^{-7}, minimum

Fire--dissolution — Multibarrier

Step function after failure locus is exceeded.
Canister failure temperature = $1000^{o} \pm 200^{o}C$.
Coating failure temperature = $1300^{o} \pm 100^{o}C$.
Fraction of all nuclides released to water in one day is
10^{-5}, expected
10^{-4}, maximum
10^{-7}, minimum

IMPACT-INDUCED RELEASES

The thresholds for impact-induced releases were calculated from the corner-drop model and corrected for vehicle crush using the equation discussed in Section 3. There was no correction for the fact that real objects are not completely rigid.

Particulate Dispersion

These dispersion functions apply to impact accidents that release particulates of respirable size (less than 10 μm in diameter) to the air.

The threshold for spray calcine was found in the same way as for the impact-dissolution functions below. The ramp-step function shape was used to account for the fact that the mechanical energy involved in the collison acts as a driving force for the dispersion, until the respirable fraction is completely dispersed.

All nuclides were considered, since they were taken to be well mixed on the scale of the particle size, therefore equally likely to be dispersed.

The expected release fraction was taken to reach a maximum at 0.5, with an upper bound of 0.6 and a lower bound of 0.01 (Fig. C1). The expected value, taken from Bonner et al. (1976) represents the weight fraction of calcine smaller than 10 μm in diameter. The uncertainty limits are estimates, which account for uncertainties in the collision mechanism and the geometry of the breached cask and canister. Wind velocity is also a large uncertainty. The speed at which maximum dispersion occurs is also an estimate subject to considerable uncertainty.

With fluidized-bed calcine, we adopted the same threshold and function shape as for spray calcine, and we considered the same nuclides. The expected release fraction reaches a maximum value of 0.1, with an upper bound of 0.5 and a lower bound of 0.01 (Fig. C2). The lower numbers reflect the larger particle size of fluidized-bed calcine compared to spray calcine. The expected value is an estimate based on discussions with R. Schindler of Idaho

National Engineering Laboratory (INEL) (private communication, 1977), The same comments hold for the origin of the uncertainties as for spray calcine.

We used the same threshold for borosilicate glass as for the calcines and again considered all nuclides. The step-ramp function accounts for an initial fraction of respirable particulates released at canister breaching and an increase from greater fracturing as the speed increases. Estimates based on the work of Smith and Ross (1975) give values of 1×10^{-4} at the threshold and 2×10^{-4} at 80 mph (Fig. C3). Uncertainties, estimated at one order of magnitude at the threshold, result from the same factors discussed for spray calcine.

The function for the multibarrier waste form is similar to that for glass, except that the release fractions were taken to be two orders of magnitude lower to account for the protection afforded by the metal matrix. Few data are available for this waste form.

Dissolution

These dissolution functions apply to impact accidents followed by contact with water and dissolution of the waste.

The threshold for spray calcine was taken to be 67 mph with an uncertainty of ±20 mph (Fig. C5). This value was derived by calculating the velocity required to produce failure of the closure bolts during a corner drop of the reference train cask on an unyielding surface. This velocity was then adjusted to account for energy absorption by the rail car itself, using the equation $V_{train} = (V^2_{cask} + 3000)^{1/2}$, where both velocities are expressed in mph (see Section 3). The uncertainty accounts for the lack of definition of the tiedown system, the probable variation in energy absorption of rail cars and trucks, the fact that real objects will exhibit some yielding, and the fact that all collisions are not as severe as a corner impact.

The shape of the curve was taken to be a step function because the particle size distribution of the spray calcine is not expected to change significantly as a result of the impact.

Only Cs and Sr were considered, since these are the most soluble nuclides and have the largest hazard index. The fraction released was taken to be 1.0 based on discussions with W. F. Bonner and W. A. Ross of BNWL (private communication, 1977). The lower limit of uncertainty was 0.25. This figure reflects uncertainty in the dissolution conditions, including water temperature, composition, flow velocity, and size of the canister breach.

For fluidized-bed calcine, the same comments hold for the threshold, function shape, and nuclides considered. The fraction released was taken as 0.4, with an upper limit of 1.0 and a lower limit of 0.1 (see Fig. C6). These values, which reflect the larger particle size of fluidized-bed calcine are based on literature values and discussions with R. Schnindler of INEL (private communication, 1977). The wider uncertainty reflects the fact that there are few experimental data for the steam-fluidized, electrically heated bed product modeled in this study.

The threshold for the borosilicate glass is the same as for the calcines. The shape of the curve is a step-ramp function, reflecting the facts that there is a certain surface area-to-volume ratio for the glass when breaching first occurs and that this ratio increases at higher impact velocities owing to greater fracturing (Fig. C8). All nuclides were considered because the Cs and Sr are now fixed in a less soluble state than in calcines, so that the other nuclides can also make significant contributions.

The release fractions were derived by combining leaching rates derived from the data of Mendel (1977) with surface area estimates made from the data of Smith and Ross (1975). Uncertainties were estimated at one order of magnitude, reflecting both the lack of data on fracturing of glass inside a shipping cask and the uncertainty in the dissolution conditions.

The same comments hold for the multibarrier waste form as for the glass. The release fraction was taken to be two orders of magnitude lower to account for protection by the metal matrix. Few data are available for this waste form.

APPENDIX C REFERENCES

Berman, L. E.; Ensminger, D. A.; Giuffre, M. S.; Koplik, C. M.; Oston, S. G.; Pollak, G. D.; and Ross, B. I. 1978. Analysis of some nuclear waste management options. The Analytic Corporation report TR-1103-1-1.

Bonner, W. F.; Blair, H. T.; and Romero, L. S. 1976. Spray solidification of nuclear waste. Battelle Pacific Northwest Laboratories report BNWL-2059.

Gray, W. J. 1976. Volatility of a zinc borosilicate glass containing simulated high-level radioactive waste. Battelle Pacific Northwest Laboratories report BNWL-2111.

Mendel, J. E. High-level waste glass. Nucl. Technol. 32:77.

Slate, S. C., and Maness, R. F. 1977. Corrosion experience in nuclear waste processing at Battelle-Northwest. Paper 81 presented at Corrosion /77, San Francisco.

Smith, T. H., and Ross, W. A. 1975. Impact testing of vitreous simulated high-level waste in canisters. Battelle Pacific Northwest Laboratories report BNWL-1903.

APPENDIX D

RISK CALCULATIONS FOR TRANSPORTATION ACCIDENTS

The risk equation for transportation accidents is:

$$E\left[Q_{ijqr}\right] = \left[\prod_{m=1}^{M_i} P_{im}\right] RF_{ijqr} \times PP_{ij}\, Q_r(t_s) \quad ,$$

where

$$RF_{ijqr} = \int_{x=(x_0)_i}^{x=(x_f)_i} p_i(x)\, F_{ijqr}(x)\, dx \quad . \qquad \text{(D1)}$$

The indices and variables are defined as follows:

i,j,q,r = indices (see Table C1 in Appendix C).

$E\left[Q_{ijqr}\right]$ = the expected activity of radionuclide r released to the biosphere via pathway j in all transportation accidents of type i involving SHLW of form q (units are Ci/MWe-y).

m = index of conditional probability P_{im} of transportation accident i.

M_i = the number of conditional probabilities associated with transportation accident i.

P_{im} = the mth conditional probability of transportation accident i.

RF_{ijqr} = the expected fraction of the inventory of radionuclide r that is released from canister(s) and available for dispersion to the biosphere via pathway j, given a transportation accident of type i involving SHLW of form q (dimensionless).

PP_{ij} = the fraction of available radionuclides released from canister(s) in transportation accident i that enters the biosphere via pathway j (dimensionless).

$Q_r(t_s)$ = the activity of radionuclide r shipped at age t_s (units are Ci/MWe-y). For all transportation accidents, t_s = 10 y.

x = accident severity, in mph for impact accidents, in ^{o}F for fire accidents.

$(x_0)_i$ = severity threshold of transportation accident i that, when exceeded, results in the release of SHLW (units are mph or ^oF).

$(x_f)_i$ = maximum credible severity for transportation accident i, in excess of which the probability density function $p_i(x)$ is taken to be zero (units are mph or ^oF).

$p_i(x)$ = the probability density function (PDF) of accident severity x in transportation accident i (units are mph^{-1} or $^oF^{-1}$).

$F_{ijqr}(x)$ = the fraction of the inventory of radionuclide r that is released from canister(s) and available for dispersion to the biosphere via pathway j, given a transportation accident of type i and severity level x involving SHLW of form q (dimensionless).

The probability density functions (PDFs) used in the risk analyses for impact accidents (Berman et al., 1978) were obtained by graphical differentiation of the cumulative distribution functions (CDFs) of accident frequency vs severity. In cases where such quantitative data were not available, engineering judgment together with a Monte Carlo prediction scheme was used to determine the PDF (Clarke et al., 1976). The severity of an impact accident depends on the speed at which it occurs. Equation D1 was used to determine the probability of release. Certain assumptions were made to make an appropriate division of frequencies among rural and urban train accidents (see Table A.3-3 in Berman et al., 1978). Fire PDFs depend upon two variables: fire temperature and duration. Therefore, the expected release for fire accidents was determined using locus analysis.

Graphical methods were used to fit Weibull-type CDFs, of the form $F(x) = 1 - \exp\left[-(x/\alpha_1)^{\alpha_2}\right]$; $\alpha_1, \alpha_2 > 0$, to the tabulated CDF values obtained for impact severity. Weibull-type functions were chosen because they can be used to fit a wide variety of distributions and because they were used in the Sandia analysis (Clarke et al., 1976). The procedure used for obtaining estimates of α_1 and α_2 is outlined below.

526 251

The PDF was then computed as the analytic derivative with respect to x of the CDF, which has the form

$$p(x) = (\alpha_2/\alpha_1)\ \exp\left[-(x/\alpha_1)^{\alpha_2}\right]\ (x/\alpha_1)^{\alpha_2-1}\ ;\ \alpha_1,\ \alpha_2 > 0\ .$$

Table D1 summarizes the calibration results. In some cases, a compromise had to be made between the desire to fit the function to all points equally well and the desire to use only one analytic PDF function throughout the entire severity range. Where one analytic function did not fit the data well over the entire severity range, calibration was done by fitting a single function to the tail of the curve (i.e., for large severities). As discussed further below, the rationale for choosing this severity range for calibration was to provide the best PDF fit where the value of the corresponding release function curve was appreciably different from zero and to minimize the chance of errors in evaluating the area under the tail of the PDF curve.

TABLE D1. Estimated parameter values for impact accident probability distribution functions. The data were taken from Clarke et al., (1976).

Accident type	Index i[a]	α_{1i}	α_{2i}	Range of calibration, mph
Truck				
Impact on extremely rigid fixed object	6.7	46.41	3.03	40-75
Crossing accident	8.9	10.49	0.82	5-70
Train				
Impact on extremely rigid fixed object (rural)[b]	15	30.49	1.703	40-70

[a]See Table C1.

[b]We assumed that half of all accidents in each 5-mph group under 40 mph, and all accidents above 40 mph, occur in rural areas.

In addition to the substitution of new continuous PDF curves in the probability calculations, the following major changes were made to the assumptions outlined in pp. 2-16 to 2-19 of Center et al,. (1976). (Sources of these new data are stated in parentheses.)

TRAIN

(1) The overall probability of a rail car accident per mile rises to 1.5×10^{-6} (Clarke et al., 1976, Vol. IV, p. 16).

(2) Only four canisters of SHLW will be transported per rail cask.

(3) The probability of an "extremely rigid" impact accident, given that an accident has occurred, is the same for both urban and rural trains ($1/2 \times 0.051 = 0.0255$ for each). This assumption follows from the previous assumption of equal frequency of accidents in urban and rural areas (Center et al., 1976, p. 2-16).

(4) The fire duration expression for truck and rail transportation contains a nonflammable derating factor of 0.625 that accounts for the fact that trucks and trains will contain only SHLW. The fire duration PDFs are as follows:

$$f_1(t) = 0.0025t^{0.807} \exp\left(\frac{-t}{38.2}\right)^{1.807} \qquad 0 \leq t \leq 50 \text{ min} \ ,$$

$$f_1(t) \quad 0.0019 \exp\left(-\frac{t-50}{104}\right) \qquad t > 50 \text{ min} \ .$$

TRUCK

(1) Only one canister of SHLW will be transported in a truck cask.

(2) The fire duration PDFs are as follows:

$$f_2(t) = 0.032t^{0.38} \exp\left(\frac{-t}{15.3}\right)^{1.38} \quad 0 \leq t \leq 20 \text{ min} \ ,$$

$$f_2(t) = \frac{0.023}{(t-20)^{0.448}} \exp\left(-\frac{t-20}{24.3}\right)^{0.552} \quad t > 20 \text{ min} \ .$$

A parabola with zero points at 1400°F and 2400°F was used to describe the fire temperature PDF. It was based on the range of temperatures for open fires of hydrocarbon fuels and other expected combustibles. It is impossible to predict the temperature of a fire exactly because of the wide variety of combustible materials and the lack of quantitative data. Therefore, the following temperature PDF was used for both truck and train transportation, where T is in °F:

$$f_2(t) = 1.5 \times 10^{-3} - 6.0 \times 10^{-9} (T - 1900)^2 \qquad 1400 \leq T \leq 2400$$

$$f_2(t) = 0 \qquad \text{otherwise} \ .$$

We can now determine the probability that a canister will fail in a fire accident in the range beyond the temperature-time failure loci that have been described for the different solid waste forms. Given a fire, the probability density that a canister will fail at a temperature T is given by

$$p(T) = f_2(T) \int_t^{\infty} f_1(t^1) dt^1 \ . \qquad \text{(D2)}$$

The failure locus is of the form

$$t = a + b \ln (T_{fire} - T_{fail}) \ , \qquad \text{(D3)}$$

where a and b are constants. For a particular temperature, the value of t determined from Equation D3 defines the lower limit of integration in Equation D2. The probability of failure is then given by Equation D2.

The following paragraphs outline the method we adopted to evaluate α_1 and α_2 for the continuous PDFs. These computations require a knowledge of the individual data values used. Such data were available for PDFs of

- Train impact velocity at collisions with trucks during railroad crossings.
- Train impact velocity at collisions with extremely rigid fixed objects,
- Truck fire durations.

In each case, the raw data were tabulated in formats most easily transformable into cumulative distribution functions (CDFs). The resulting CDFs were then graphically or analytically differentiated to form their associated PDFs for use in the expected release fraction calculations.

Computing confidence intervals about the PDFs began by taking the general two-parameter Weibull cumulative distribution function (Clarke et al., 1976; Berman et al., 1978),

$$F(v) = 1 - \exp\left[-(v/\alpha_1)^{\alpha_2}\right] \quad ,$$

and transforming it to

$$\ln\left[-\ln\left(1-F(v)\right)\right] = \alpha_2 \ln v - \alpha_2 \ln \alpha_1 \quad . \tag{D4}$$

Letting

$$x = \ln v \tag{D5}$$

$$g(v) = \ln\left[-\ln\left(1-F(v)\right)\right] \tag{D6}$$

$$h(x) = g\left(v(x)\right) \tag{D7}$$

Equation D4 becomes

$$h(x) = \alpha_2 x - \alpha_2 \ln \alpha_1 \quad .$$

$$= A_1 x + A_2 \quad .$$

This is now an estimation problem amenable to solution by linear regression analysis after transforming each of the original data points $(v_i, F(v_i))$ to $(x_i, h(x_i))$ using Equations D5 through D7. Least-squares estimates, $\hat{A}_1$ and $\hat{A}_2$, were then obtained and transformed to the estimates $\hat{\alpha}_1$ and $\hat{\alpha}_2$:

$$\hat{\alpha}_1 = \left[-\hat{A}_2/\hat{A}_1\right]$$

$$\hat{\alpha}_2 = \hat{A}_1$$

The standard error, s, of the estimate was also calculated.

Next the 95% confidence intervals about h(x) at each independent observation, x_k, were computed (Draper and Smith, 1966):

$$h(x_k) = \hat{h}(x_k) \pm t(n - 2, 0.95)\, s \left[1 + \frac{1}{n} + \frac{\left(x_k - \sum x_i/n\right)^2}{\sum x_i^2 - \frac{1}{n}\left(\sum x_i\right)^2}\right]^{1/2} \quad .$$

where

$$\hat{h}(x_k) = \hat{\alpha}_2 x_k - \hat{\alpha}_2 \ln \hat{\alpha}_1 \quad ,$$

and

$t(n - 2, 0.95)$ = the 95 percentage point of the t-distribution having n - 2 degrees of freedom (two-sided test)

n = the number of data points used to estimate $\hat{\alpha}_1$ and $\hat{\alpha}_2$

526 256

i = index of a data point used to estimate $\hat{\alpha}_1$ and $\hat{\alpha}_2$

x_i = $\ln v_i$, the transformed value of the i^{th} data observation

k = index of an independent data point not used in the estimation of $\hat{\alpha}_1$ and $\hat{\alpha}_2$

x_k = $\ln v_k$, the transformed value of the k^{th} independent observation

Solving Equation D6 for $F(v)$ and substituting the equality $h(x) = g(v)$ yields

$$F(v) = 1 - \exp\left[-e^{h(x)}\right] .$$

This equation can then be used to map the confidence intervals about $h(x)$ at each point x_k into confidence intervals about $F(v)$ at each point v_k, as follows:

$$F^{\pm}(v_k) = 1 - \exp\left[-e^{h^{\pm}(x_k)}\right] ,$$

where the superscript $\pm$ refers to the high (+) and low (-) confidence bounds about each function. The high bound $h^{+}(x_k)$ maps into high bound $F^{+}(v_k)$, and the low bound $h^{-}(x_k)$ maps into low bound $F^{-}(v_k)$.

A simple graphical differentiation technique can be used to compute the desired PDF confidence bounds, $p^{+}(v)$ and $p^{-}(v)$, on a pointwise basis from $F^{-}(v)$ and $F^{+}(v)$, respectively:

$$p\left(\frac{v_k + v_{k+1}}{2}\right) \cong \frac{F(v_{k+1}) - F(v_k)}{v_{k+1} - v_k} \cong \left.\frac{dF}{dv}\right|_{v = \frac{v_k + v_{k+1}}{2}} .$$

Thus, confidence intervals for the PDFs can be generated over any severity range on a point-by-point basis. Straight-line segments can then be used to connect these points to form a piecewise-linear continuous function for use in release fraction calculations. It is believed that these numerical calculations are accurate to three decimal places, which is sufficient precision for use in the remaining analysis.

APPENDIX D REFERENCES

Berman, L. E.; Ensminger, D. A.; Ginffre, M. S.; Koplik, C. M.; Oston, S. G.; Pollak, G. D.; and Ross, B.I. 1978. Analysis of some nuclear waste management options. The Analytic Sciences Corporation report TR-1103-1-1.

Center, J. L.; Crawford, B. S.; Ross, B.; and Sutherland, A. A. 1976. Analysis of nuclear waste management. The Analytic Sciences Corporation report TR-772-2-1.

Clare, R. K.; Foley, J. T.; Hartman, W. F.; and Larson, D. W. 1976. Severities of transportation accidents. Sandia Laboratories, Albuquerque, report SLA-74-0001.

Draper, N. R., and Smith, H. 1966. Applied regression analysis. New York: John Wiley and Sons.

APPENDIX E

REPOSITORY RELEASE: SENSITIVITY OF DOSE TO WASTE DISSOLUTION TIME

In our model, water enters the repository at some time after the repository is sealed. (This time, whose probability density can be calculated from the geological model, is taken here as a parameter.) The water then dissolves the radionuclides in the repository. The time, λ_{ℓ}^{-1}, required for this dissolution depends on the physical and chemical form of the waste. After flowing through an aquifer, the waste then enters surface waters, passes through various ecological systems, and irradiates humans. We do not consider the effects of directly withdrawing well water from the aquifer. The analysis begins with the dose from a single radionuclide. Results of this calculation are then used to study the total dose from all nuclides.

FLOW IN AN AQUIFER

We will begin by considering the motion of a nuclide through an aquifer after it has been released from a repository, neglecting radioactive decay for the moment. The waste moves at velocity v/K_j, where v is the velocity of the water in the aquifer and K_j is the sorption retardation factor for the nuclide in question. In the aquifer hydraulic dispersion causes narrow pulses to spread. Only longitudinal spreading need be considered, since lateral spreading will not affect the time of release into surface waters. We therefore treat motion in one dimension only and describe it by a diffusion-type differential equation (Grove, 1970):

$$\frac{\partial c}{\partial t} = - \frac{v}{K_j} \frac{\partial c}{\partial x} + \frac{\alpha v}{K_j} \frac{\partial^2 c}{\partial x^2} \quad ,$$

where α is the dispersion constant; c is the nuclide concentration; t is time; and x is the dimensional coordinate of the aquifer. This equation has a well-known solution by the method of Green's function:

$$G(x,t;\xi,\tau) = \sqrt{\frac{K_j}{4\pi\alpha v(t-\tau)}} \exp\left\{-\frac{\left(x-\xi-\frac{v}{K_j}(t-\tau)\right)^2}{\frac{4\alpha v}{K_j}(t-\tau)}\right\}.$$

The Green's function, G, is the response of the aquifer to a unit impulse input at ξ, and at time τ. If the input into the aquifer is a pulse with concentration $c_{in}(\xi,\tau)$, the output from the aquifer will be

$$c_{out} = \iint G\, c_{in}\, d\xi d\tau \quad . \tag{E1}$$

For ease of calculation we assume that the input pulse, which represents the course of dissolution of waste in the repository, has the form

$$c_{in}(\xi) = Q_j \frac{\lambda_\ell K_j}{v\pi^{1/2}} \exp\left\{\frac{-\lambda_\ell^2 \xi^2 K_j^2}{v^2}\right\}, \quad (\tau = 0)$$

where Q_j is the total amount of nuclide j in the repository. This choice implies that waste begins to leave the repository before containment is breached. It will be shown, however, that the final answer is not sensitive to the pulse shape chosen.

Performing the integration in Equation E1 gives

$$c_{out}(t) = \frac{Q_j}{\sqrt{\pi\left(\frac{4\alpha v t}{K_j} + \frac{v^2}{\lambda_\ell^2 K_j^2}\right)}} \exp\left\{\frac{-\left(z-\frac{vt}{K_j}\right)^2}{\frac{v^2}{K_j^2\lambda_\ell^2} + \frac{4\alpha v t}{K_j}}\right\},$$

where z is the path length through the aquifer. The substitution $t = K_j z/v$ gives the maximum concentration (which is the maximum release rate/v)

$$c_{out}^{max} = \frac{Q_j}{\sqrt{\pi\left(4\alpha z + \frac{v^2}{\lambda_\ell^2 K_j^2}\right)}}. \tag{E2}$$

In the limit where

$$\frac{v^2}{\lambda_\ell^2 K_j^2} \ll 4\alpha z \qquad \text{(E3)}$$

the maximum release rate is independent of the dissolution time, λ_ℓ^{-1}. In the opposite limit the maximum release rate is inversely proportional to the dissolution time.

The condition of Equation E3 is equivalent to

$$\lambda_\ell^{-1} \ll T_D = \sqrt{4\alpha z}\ \frac{K_j}{v} \quad , \qquad \text{(E4)}$$

where T_D is the time over which dispersion spreads a pulse.

For the reference case without ion exchange (α = 50 m, z = 10 mi, K_j = 1, and v = 1.57 m/y), this formula gives $T_D = 10^3$ y. If ion exchange is included (K_j = 100), $T_D = 10^5$ y.

The behavior of release rates in the two limiting cases does not depend on the shape of the input pulse. Consider first the case where the condition of Equation E3 is satisfied. The input pulse is then relatively narrow. Its structure is entirely obliterated by the spreading due to hydraulic dispersion, and the shape of the output pulse depends only on how much waste is in the input pulse. This situation is represented mathematically by a Green's function that is wider than the input pulse. The input pulse can be approximated by a delta function. The output will have the same time dependence as the Green's function, with its amplitude proportional to the total amount of waste in the input pulse.

If, on the other hand, the input pulse is wide (and smooth), hydraulic dispersion has little effect and the output has about the same shape as the input. This situation corresponds to an input pulse much wider than the Green's function. The amplitude of the output is then simply equal to the amplitude of the input.

This argument shows that the behavior of a pulse of radionuclides in an aquifer is governed by the relationship between the initial width of the pulse, λ_ℓ^{-1}, and the length of time, T_D, across which hydraulic dispersion spreads the pulse. If the pulse is initially much longer than the spreading time, the output pulse has the same maximum amplitude as the input pulse. If, however, the pulse is initially much shorter than the spreading time, the maximum amplitude of the output depends on the total quantity of waste contained in the pulse and not on the rate at which waste enters the aquifer at any instant.

DOSE COEFFICIENTS

The dose to a person from each radionuclide is given by the rate at which the nuclide enters the surface environment, multiplied by a dose coefficient reflecting that person's diet and living habits. Using a model that accounts for the accumulation of radionuclides in sediment, topsoil, plants, animals, and human tissues, these coefficients have been calculated for a typical individual and for a "maximum" individual whose exposure is the largest likely to be experienced by members of the general population.

If we assume that all radionuclides have the same retardation factor, we would find that they move through an aquifer at the same speed, so the same fraction of the total remaining inventory of each nuclide would reach the surface in a given year. This assumption is conservative because it ignores spreading of the concentration pulse by variations in migration speed among different elements. It permits us to simplify calculations, because the ratio between the amounts of any two nuclides reaching the surface in any year is equal to the ratio of the total amounts of those nuclides in the waste at that time. We can then calculate a total dose coefficient by multiplying the amount of each nuclide in the waste at a given time by the coefficient giving the dose to a human per unit of nuclide reaching the surface per year, and adding together the contributions from each nuclide.

A total dose coefficient is plotted as a function of time in Fig. E1, which shows the 50-y body dose to a typical individual per MWe-y of waste reaching

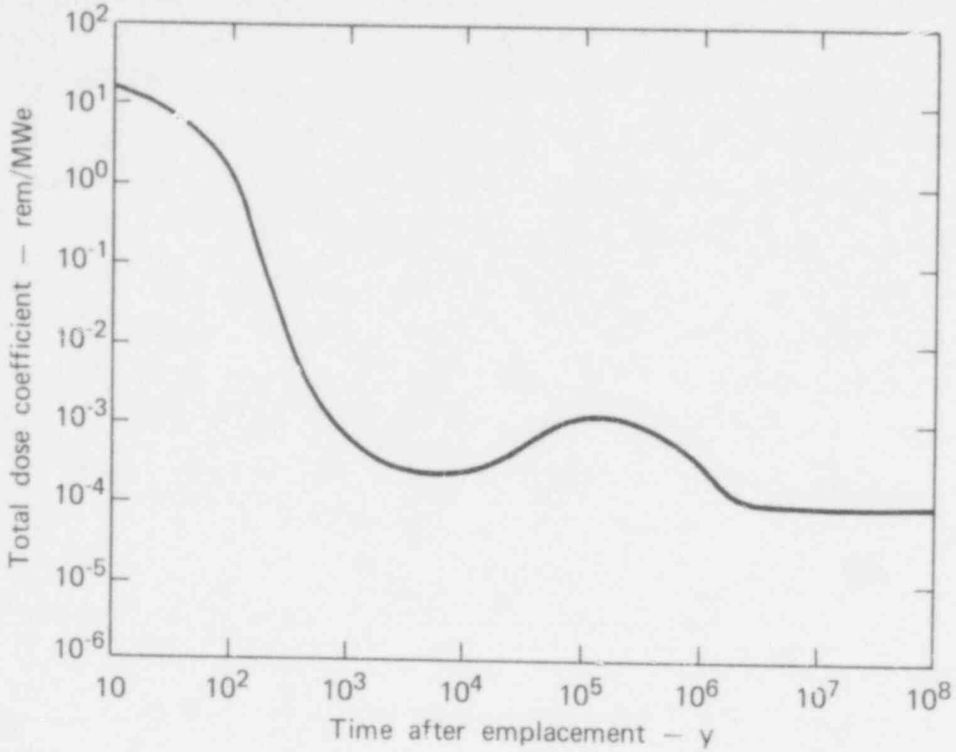

FIG. E1. Fifty-year body dose to typical individual per year per MWe-y of waste entering surface water ecosystem.

the surface per year. It is assumed that the waste enters a lake with a flushing time of 1 y. This average dose is defined as the doses received over 50 y by an adult with an average diet and life-style. This individual is assumed to drink all his water and eat all his aquatic food from the river or lake system into which radioactive material has been released. Furthermore, his diet is assumed to be composed solely of food products that have been either directly or indirectly contaminated by the river or lake water. Finally, all water-related recreation time is assumed to be spent somewhere within the river, estuary, and ocean system. These assumptions ensure that no important pathway for exposure is overlooked for each nuclide in the system.

For the first 500 y, the dominant nuclides are the fission products ^{137}Cs and ^{90}Sr. During this period the total dose coefficient declines rapidly from 27 to 1.3×10^{-3} rem/MWe. This period is of limited significance.

After 500 y, ^{241}Am and ^{243}Am are the dominant nuclides and the total dose coefficient declines slowly. At about 6000 y it reaches a minimum of 2.5 $\times 10^{-4}$ rem/MWe. It then begins to rise because ^{226}Ra accumulates. The radium is retained in foodstuffs and man far more efficiently than are its parent nuclides (^{242}Cm, ^{238}Pu, ^{234}U, and ^{230}Th). Hence, its formation greatly increases the ability of the waste to irradiate human beings. The coefficient reaches a maximum of 1.3×10^{-3}, about equal to the value at 500 y, at about 10^5 y. It then declines in secular equilibrium with ^{234}U (half-life 2.4×10^5 y) until the ^{234}U initially formed from ^{238}Pu has been eliminated and the remaining ^{234}U is in secular equilibrium with ^{238}U. At 2×10^6 y, the concentration of ^{234}U from ^{238}Pu is half that from ^{238}U. It finally reaches a constant value of 4×10^{-5} due to the 0.5% of ^{238}U that was not removed from the fuel by reprocessing. Nuclide concentrations in waste at distant times are taken from Gera (1975), Table 3.

As Fig. E1 and the above discussion show, the total dose coefficient does not vary by more than a factor of five over the entire period from 500 y to 10^6 y. Furthermore, its behavior within that period is rather complex. Variations resulting from changes in the time of final emergence during this period will therefore be small and uncertain. Thus, it is possible to apply a single constant value of dose coefficient to all events in this period.

DOSES

Almost all of the exposure to radioactivity in our model is due to ingestion of foodstuffs and water (see Table E1). The integrated population dose is therefore limited by the amount of drinking water and food that can be produced by the lake into which the waste flows. If more people want to live near the lake, they will have to import food and water from uncontaminated areas. If the climate changes and more water flows through the lake, greater dilution will compensate for increased food and water yield. Consequently, given the model's conservative assumption that the water body into which waste flows is intensively used, the integrated population dose for a given rate of waste entering the surface waters will be nearly independent of the size of the population living near the repository.

TABLE E1. Critical pathways for 50-y body dose.

Critical nuclide	Time, y	Pathway	
^{243}Am	10^3, 10^4	Exposure	61%
^{241}Am	10^3	Vegetables	26%
^{229}Th	10^6	Aquatic foods	85%
^{226}Ra	10^4, 10^5, 10^6	Animal	47%
^{137}Cs	1, 10, 10^2	Animal	45%
^{90}Sr	1, 10, 10^2	Vegetables	69%

The total dose coefficient gives the ratio between the amount of wastes entering the surface water body and the dose to an average person. If the waste emerges over a longer period of time, each person will receive a smaller dose, but more generations may be affected. Since all the relationships are linear, the integrated population dose will depend only on the total amount of waste dissolved, not on the dissolution time.

The peak dose to a maximum individual will be equal to the maximum rate at which waste enters the surface water, given by Equation E2, multiplied by the total dose coefficient for a maximum individual. In Fig. E2, the peak dose is shown as a function of dissolution time for two values of the sorption retardation factor, K_j. The figure assumes a repository containing SHLW from 10^6 MWe-y of electricity production, which is roughly the total waste generation expected by the year 2000. It should be noted that if actinides and their daughters have retardation factors much greater than 100, the curves shown in the figure will be lowered by several orders of magnitude, but the form of their dependence on dissolution time will not change.

All of these conclusions are sensitive to a number of assumptions made in our model, namely:

- Waste does not reach the surface before 500 y. This assumption is justified in the next section.

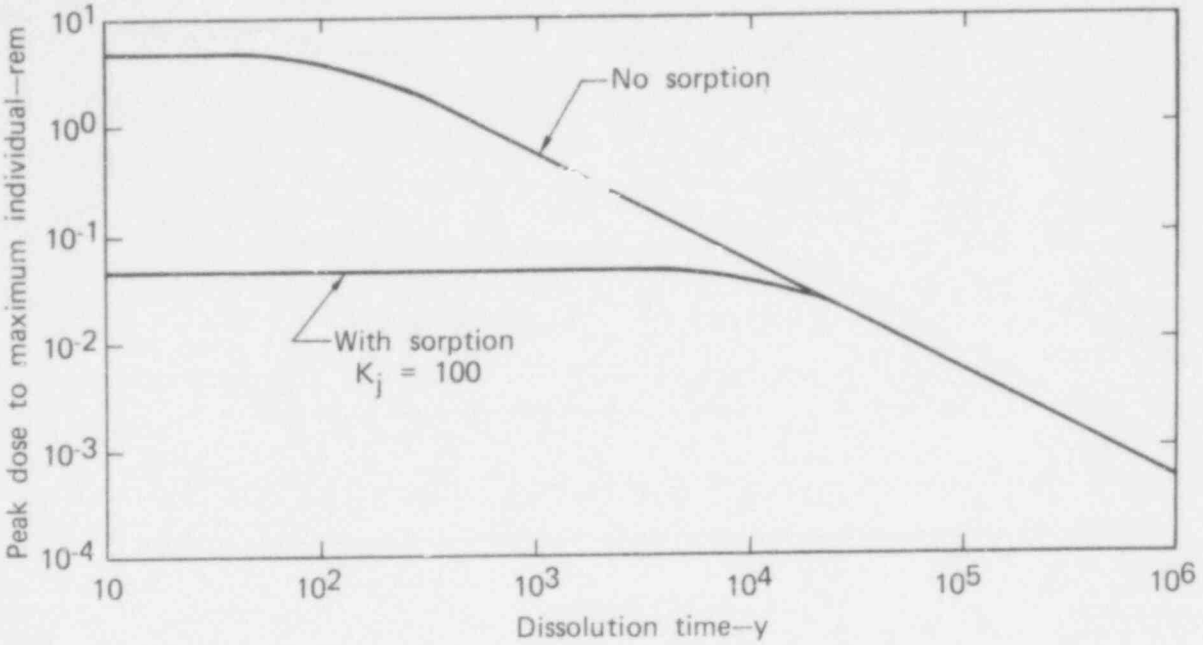

FIG. E2. Peak 50-y body dose to maximum individual from $\geq 10^6$ MWe-y repository as a function of dissolution time.

- Dissolution times are less than 10^6 y. If attainable, dissolution times in excess of 10^6 y would reduce both peak dose and integrated population dose.
- Fractures permitting water to reach a repository do not become resealed. If the fractures do reseal, only the portion of the waste that dissolved before resealing would be able to escape. Dissolution times longer than resealing times would reduce integrated population dose and, if T_D were greater than resealing time, peak dose as well.
- No wells are drilled into the contaminated aquifer. Well water could contain radionuclides from fast-dissolving wastes at high concentrations, little affected by hydraulic dispersion. On the other hand, no fish live in wells. A principal pathway for human doses would thus be eliminated and the total dose coefficients for well water would be quite different from those for surface water.

The sensitivity of dose to dissolution time is shown in Fig. E3, which shows the dose to an average individual as a function of time for different dissolution times. In these cases it has been assumed that release from the repository begins immediately after emplacement.

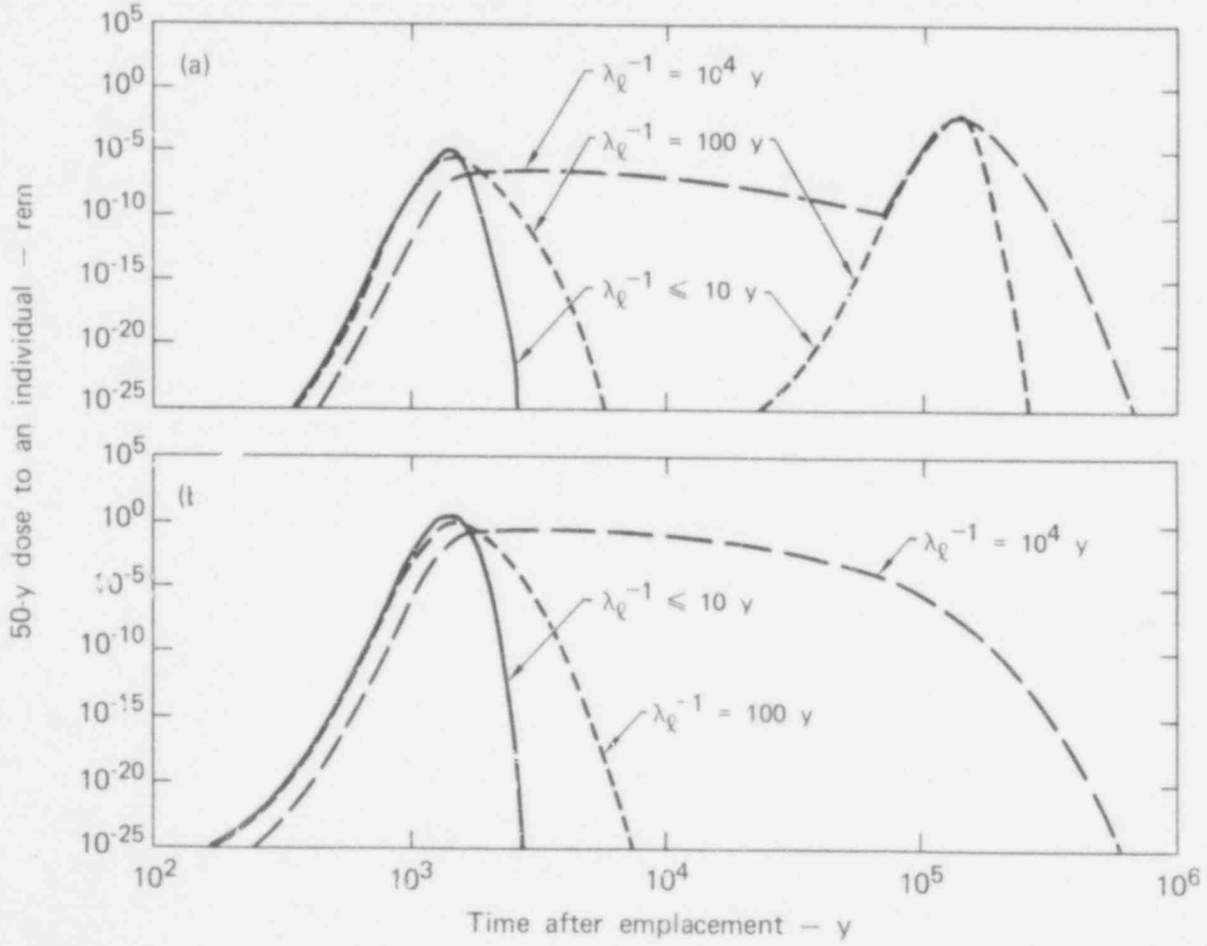

FIG. E3. Fifty-year body dose to a typical individual as a function of time after emplacement, for different dissolution times, (a) K_j is taken as 100 for all nuclides except I and Tc, (b) no sorption is assumed. Both plots assume immediate loss of containment in a 10^6 MWe-y repository.

SENSITIVITY OF DOSE TO PATH LENGTH

The path length, z, through the aquifer affects doses most directly by changing the passage time, $K_j z/v$.

Passage times of less than 500 would, in the case of immediate loss of geologic containment, allow waste to reach the surface when cesium and strontium are still dangerous. This situation could occur, however, only for very short path lengths. With the reference velocity of 1.57 m/y, passage times of less than 500 y occur only for path lengths of less than 7.8 m with sorption (K_j = 100) or 785 m without sorption.

For times between 500 y and 10^6 y, it was shown above that changes in passage time will not materially affect the total dose coefficient. Hence, changes in passage time, and therefore in path length, do not change the integrated population dose.

Peak dose to the maximum individual is described by Equation E2. The peak dose is inversely proportional to the square root of the path length when the dissolution time is less than T_D. When the dissolution time greatly exceeds T_D, path length will not affect peak dose.

CONCLUSIONS

Our findings regarding the sensitivity of human doses to dissolution time can be summarized as follows:

- If the dissolution time is much less than the dispersion time defined by Equation E4 (10^4 y in the reference case), neither integrated population dose nor peak dose will be sensitive to dissolution time.
- If dissolution time is greater than the dispersion time, but less than 10^6 y, the integrated population dose will be independent of dissolution time, but the peak dose will be inversely proportional to the dissolution time.
- If the dissolution time exceeds 10^6 y, increases in dissolution time will reduce both integrated population dose and peak dose.

Some changes in our model that might increase the sensitivity of dose to dissolution time are:

- Inclusion of mechanisms that reseal underground fractures in the geological model.
- Use of a very high groundwater velocity or a very short path length.
- Accounting for withdrawal of contaminated well water from the aquifer.

APPENDIX E REFERENCES

Gera, F. 1975. Geochemical behavior of long-lived radioactive wastes. Oak Ridge National Laboratory report ORNL-TM-4881.

Grove, D. B. 1970. A method to describe the flow of radioactive ions in groundwater. Sandia Laboratories, Albuquerque, report SC-CR-70-6139.

APPENDIX F

RADIONUCLIDE SOURCE TERMS

BIOLOGICALLY SIGNIFICANT RADIONUCLIDES IN HIGH-LEVEL WASTE

The composition of high-level wastes varies greatly as a function of time because of the different decay rates of the constituent radionuclides. Although the waste includes an abundant variety of radioactive species, only relatively few are potentially significant as biological hazards at any time.

Source Terms

A list of the major radioactive fission products and actinides that have intermediate or long half-lives is given in Table F1. Source terms are listed for these nuclides at several times after fuel irradiation. Data for this table were taken from a report from Oak Ridge National Laboratory (1 for postirradiation times up to 100 y, and from Gera (1975) for longer times.

We have assumed that the fuel has been irradiated for a 3.3×10^4 MWt-d/t of uranium at a thermal efficiency of 35.4%. We also assumed that the quantity of ^{129}I present in high-level waste will depend on solidification time (taken to be 150 d). If the waste is not solidified until 1 y after irradiation, the amount present will be about one-half that shown in Table F1.

Biologically Significant Airborne Radionuclides

Tables F2 and F3 list the most biologically significant radioactive species in terms of toxicity indexes for airborne radioactivity. The toxicity index for each nuclide represents the volume of air necessary to dilute that quantity of the nuclide formed during the production of a MWe-y of power to the maximum

TABLE F1. Source terms of biologically significant nuclides in Ci/MWe-y.

Nuclide	Time following irradiation					
	150 d	1 y	10 y	10^2 y	10^3 y	10^4 y
^{89}Sr	3.0E3	1.7E2	0.0	0.0	0.0	0.0
^{90}Sr	2.4E3	2.4E3	1.9E3	2.0E2	4.7E-8	0.0
^{90}Y	2.4E3	2.4E3	1.9E3	2.0E2	4.7E-8	0.0
^{91}Y	5.0E3	3.9E2	0.0	0.0	0.0	0.0
^{93}Zr	5.9E-2	5.9E-2	5.9E-2	5.9E-2	5.9E-2	5.9E-2
^{93m}Nb	1.2E-3	2.9E-3	2.4 E-2	5.9E-2	5.9E-2	5.9E-2
^{95}Zr	8.6E3	8.7E2	0.0	0.0	0.0	0.0
^{95}Nb	1.6E4	1.9E3	5.9E-7	0.0	0.0	0.0
^{99}	4.4E-1	4.4E-1	4.4E-1	4.4E-1	4.4E-1	4.4E-1
^{106}Ru	1.3E4	8.5E3	1.7E1	0.0	0.0	0.0
^{106}Rh	1.3E4	8.5E3	1.7E1	0.0	0.0	0.0
^{125}Sb	2.5E2	2.2E2	2.2E1	0.0	0.0	0.0
^{126}Sn	1.7E-2	1.7E-2	1.7E-2	1.7E-2	1.7E-2	1.7E-2
^{129}I	2.4E-6	2.4E-6	2.4E-6	2.4E-6	2.4E-6	2.4E-6
^{134}Cs	6.7E3	5.5E3	2.6E2	0.0	0.0	0.0
^{137}Cs	3.3E3	3.3E3	2.7E3	3.3E2	3.1E-7	0.0
^{144}Ce	2.4E4	1.4E4	4.7E0	0.0	0.0	0.0
^{147}Pm	3.1E3	2.7E3	2.5E2	1.1E-8	0.	0.0

TABLE F1 (continued).

Nuclide	Time following irradiation					
	150 d	1 y	10 y	10^2 y	10^3 y	10^4 y
^{154}Eu	2.1E2	2.1E2	1.4E2	2.9E0	0.0	0.0
^{210}Pb	0.0	0.0	0.0	2.3E-8	2.2E-6	8.8E-5
^{210}Po	0.0	0.0	0.0	2.3E-8	2.2E-6	8.8E-5
^{226}Ra	0.0	0.0	3.4E-9	3.5E-8	2.2E-6	8.8E-5
^{229}Th	0.0	0.0	1.3E-9	2.3E-8	2.2E-6	1.7E-4
^{230}Th	6.6E-7	6.6E-7	6.6E-7	1.0E-6	1.2E-5	1.1E-4
^{231}Pa	7.7E-7	7.7E-7	7.7E-7	7.7E-7	8.1E-7	1.2E-6
^{233}U	4.6E-7	4.6E-7	4.6E-7	4.6E-6	4.8E-5	4.9E-4
^{237}Np	1.1E-2	1.1E-2	1.1E-2	1.1E-2	1.2E-2	1.2E-2
^{238}Pu	1.1E0	2.5E0	3.2E0	1.6E0	3.8E-3	0.0
^{239}Pu	5.2E-2	5.2E-2	5.2E-2	5.2E-2	6.4E-2	1.3E-1
^{240}Pu	7.6E-2	8.1E-2	1.4E-1	2.7E-1	2.5E-1	9.9E-2
^{241}Pu	1.8E1	1.7E1	1.0E1	1.5E-1	9.8E-3	4.6E-3
^{241}Am	5.4E0	5.4E0	5.3E0	5.1E0	1.1E0	4.6E-3
^{243}Am	5.4E-1	5.4E-1	5.4E-1	5.4E-1	5.0E-1	2.3E-1
^{242}Cm	4.7E2	1.9E2	2.2E-1	1.5E-1	2.4E-3	0.0
^{244}Cm	7.8E1	7.6E1	5.4E1	1.7E0	0.0	0.0

TABLE F2. Inventory of biologically significant airborne nuclides, assumed released 1 y after irradiation of 32 MWe-y/t of uranium.

Nuclide	$t_{1/2}$	MPC_a, Ci/m^3	Q, Ci/MWe-y	Toxicity index, m^3/MWe-y
Fission products				
^{89}Sr	53 d	3E-10	1.7E2	6E11
^{90}Sr	28 y	3E-11	2.4E3	8E13
^{90}Y	64 h	3E-9	2.4E3	8E11
^{91}Y	59 d	1E-9	3.9E2	4E11
^{95}Zr	66 d	1E-9	8.7E2	9E11
^{95}Nb	35 d	3E-9	1.9E3	6E11
^{106}Ru	1.0 y	2E-10	8.5E3	4E13
^{106}Rh[a]	30 s	1E-9	8.5E3	9E12
^{125}Sb	2.7 y	9E-10	2.2E2	2E11
^{134}Cs	2.0 y	4E-10	5.5E3	1E13
^{137}Cs	30 y	5E-10	3.3E3	7E12
^{144}Ce	280 d	2E-10	1.4E4	7E13
^{147}Pm	2.6 y	3E-9	2.7E3	9E11
^{154}Eu	16 y	2E-10	2.1E2	1E12
Fission product totals			5.1E4	2E14
Actinides				
^{238}Pu	86 y	7E-14	2.5	4E13
^{240}Pu	6.6E3 y	7E-14	0.081	1E12
^{241}Pu	13 y	3E-12	17	6E12
^{241}Am	460 y	2E-12	5.4	3E13
^{243}Am	8E3 y	2E-13	0.54	3E12
^{242}Cm	160 d	4E-12	190	5E13
^{244}Cm	18 y	3E-13	76	2E14
Actinide Totals			2.9E2	3E14
Grand Totals			5.1E4	5E14

[a] In equilibrium with ^{106}Ru. MPC_a is an estimate.

TABLE F3. Inventory of biologically significant airborne nuclides, assumed released at 10 y after irradiation of 32 MWe-y/t of uranium.

Nuclide	$t_{1/2}$	MPC_a, Ci/m^3	Q, Ci/MWe-y	Toxicity index, m^3/MWe-y
Fission products				
^{90}Sr	28 y	3E-11	1.9E3	6E13
^{90}Y	64 h	3E-9	1.9E3	6E11
^{134}Cs	2.0 y	4E-10	2.6E2	7E11
^{137}Cs	30 y	5E-10	2.7E3	5E11
Fission product totals			6.8E3	7E13
Actinides				
^{238}Pu	86 y	7E-14	3.2	5E13
^{240}Pu	6.6E3 y	6E-14	0.14	2E12
^{241}Am	460 y	2E-13	5.5	3E13
^{243}Am	8E3 y	2E-13	0.54	3E12
^{244}Cm	18 y	3E-13	54	2E14
Actinide totals			63	3E14
Grand totals			6.9E3	4E14

526 276

permissible concentration in air (MPC_a). Table F2 gives toxicity indexes for the mixture of radionuclides that exist 1 y after fuel irradiation. The only nuclides included in the list are those with toxicity indexes no lower than two orders of magnitude below that of the most toxic nuclide (which is ^{90}Sr for the fission products and ^{244}Cm for the actinides). Table F3 contains the same information for the mixture of radionuclides that exist 10 y after fuel irradiation. Dose conversion factors have been calculated for all nuclides shown in Table F1. Note that biologically significant airborne nuclides have not been identified for postirradiation times greater than 10 y. Since proposed regulations require all high-level waste to be placed in an underground repository no more than 10 y after it has been generated, there is no credible mechanism whereby such waste can become airborne more than 10 y after fuel irradiation.

Biologically Significant Waterborne Radionuclides

Tables F4 through F10 list the most biologically significant radioactive species in terms of toxicity indexes for waterborne radioactivity. These indexes are calculated in the same way as the airborne radioactivity indexes except that appropriate MPC_w values have been taken from 10 CFR 20 (U.S. Code of Federal Regulations, 1976).

TABLE F4. Inventory of biologically significant waterborne nuclides, assumed released 1 y after irradiation of 32 MWe-y/t of uranium.

Nuclide	$t_{1/2}$	MPC_w, Ci/m^3	Q, Ci/MWe-y	Toxicity index, m^3/MWe-y
Fission products				
^{89}Sr	53 d	3E-6	1.7E2	6E7
^{90}Sr	28 y	3E-7	2.4E3	8E9
^{90}Y	64 h	2E-5	2.4E3	1E8
^{91}Y	59 d	3E-5	3.9E2	1E7
^{95}Zr	66 d	6E-5	8.7E2	1E7
^{95}Nb	35 d	1E-4	1.9E3	2E7
^{106}Ru	1.0 y	1E-5	8.5E3	9E8
^{106}Rh[a]	30 s	1E-4	8.5E3	9E7
^{134}Cs	2.0 y	9E-6	5.5E3	6E8
^{137}Cs	30 y	2E-5	3.3E3	2E8
^{144}Ce	280 d	1E-5	1.4E4	1E9
^{147}Pm	2.6 y	2E-4	2.7E3	1E7
^{154}Eu	16 y	2E-5	2.1E2	1E7
Fission product total			5.1E4	1E10
Actinides				
^{238}Pu	86 y	5E-6	2.5	5E5
^{239}Pu	2.4E4 y	5E-6	0.052	1E4
^{240}Pu	6.6E3 y	5E-6	0.081	2E4
^{241}Pu	13 y	2E-4	17.0	9E4
^{241}Am	460 y	4E-6	5.4	1E6
^{243}Am	8E3 y	4E-6	0.54	1E5
^{242}Cm	160 d	2E-5	190	9E6
^{244}Cm	18 y	7E-6	76	1E7
Actinide Totals			2.9E2	2E7
Grand Totals			5.1E4	1E10

[a]In equilibrium with ^{106}Ru, MPC_w is an estimate.

TABLE F5. Inventory of biologically significant waterborne nuclides, assumed released 10 y after irradiation of 32 MWe-y/t of uranium.

Nuclide	$t_{1/2}$	MPC_w, Ci/m^3	Q, Ci/MWe-y	Toxicity index, m^3/MWe-y
Fission products				
^{90}Sr	28 y	3E-7	1.9E3	6E9
^{90}Y	64 h	2E-5	1.9E3	9E7
^{134}Cs	2.0 y	9E-6	2.6E2	3E7
^{137}Cs	30 y	2E-5	2.7E3	1E8
Fission product totals			6.8E3	6E9
Actinides				
^{238}Pu	86 y	5E-6	3.2	6E5
^{241}Am	460 y	4E-6	5.5	1E6
^{243}Am	8E3 y	4E-6	0.54	1E5
^{244}Cm	18 y	7E-6	51	8E6
Actinide totals			63	1E7
Grand totals			6.9E3	6E9

TABLE F6. Inventory of biologically significant waterborne nuclides, assumed released 100 y after irradiation of 32 MWe-y/t of uranium.

Nuclide	$t_{1/2}$	MPC_w Ci/m^3	Q, Ci/MWe-y	Toxicity index, m^3/MWe-y
Fission products				
^{90}Sr	28 y	3E-7	2.0E2	7E8
^{90}Y	64 h	2E-5	2.0E2	1E7
^{137}Cs	30 y	2E-5	3.3E2	2E7
Fission product totals			7.3E2	7E8
Actinides				
^{238}Pu	86 y	5E-6	1.6	3E5
^{241}Am	460 y	4E-6	5.1	1E6
^{243}Am	8E3 y	4E-6	0.54	1E5
^{244}Cm	18 y	7E-6	1.7	2E5
Actinide totals			8.9	2E6
Grand totals			7.4E2	7E8

TABLE F7. Inventory of biologically significant waterborne nuclides, assumed released 10^3 y after irradiation of 32 MWe-y/t of uranium.

Nuclide	$t_{1/2}$	MPC_w, Ci/m^3	Q, Ci/MWe-y	Toxicity index, m^3/MWe-y
Fission products				
^{93}Zr	1.5E6 y	8E-4	5.9E-2	7E1
^{93m}Nb	14 y	4E-4	5.9E-2	1E2
^{99}Tc	2.1E5 y	3E-4	4.5E-1	2E3
^{126}Sn[a]	1E5 y	2E-5	1.7E-2	9E2
^{129}I	1.7E7 y	6E-8	2.4E-6	4E1
Fission product totals			5.9E-1	3E3
Actinides				
^{237}Np	2.1E6 y	3E-6	1.2E-2	4E3
^{239}Pu	2.4E4 y	5E-6	6.4E-2	1E4
^{240}Pu	6.6E3 y	5E-6	2.5E-1	5E4
^{241}Am	4.6E2 y	4E-6	1.1E0	3E5
^{243}Am	8.0E3 y	4E-6	5.0E-1	1E5
Actinide totals			1.9	5E5
Grand totals			2.5	5E5

[a] MPC_w assumed to be equal to the smallest of all other Sn isotopes. Present in secular equilibrium with ^{126}Sn are ^{126m}Sb and ^{126}Sb. If release pathway does not partition Sb and Sn, consideration should be given to these additional isotopes.

526 281

TABLE F8. Inventory of biologically significant waterborne nuclides, assumed released 10^4 y after irradiation of 32 MWe-y/t of uranium.

Nuclide	$t_{1/2}$	MPC_w, Ci/m^3	Q, Ci/MWe-y	Toxicity index, m^3/MWe-y
Fission products				
^{93}Zr	1.5E6 y	8E-4	5.9E-2	7E1
^{93m}Nb	14 y	4E-4	5.9E-2	1E2
^{99}Tc	2.1E5 y	3E-4	4.4E-1	2E3
^{126}Sn[a,b]	1E5 y	2E-5	1.6E-2	9E2
^{129}I	1.7E7 y	6E-8	2.4E-6	4E1
Fission product totals			5.7E-1	3E3
Actinides (plus other alpha-emitters)[c]				
^{210}Pb	2.0E1 y	1E-7	8.8E-5	9E2
^{210}Po	3.8E-1 y	7E-7	8.8E-5	1E2
^{226}Ra	1.6E3 y	3E-8	8.8E-5	3E3
^{237}Np	2.1E6 y	3E-6	1.2E-2	4E3
^{239}Pu	2.4E4 y	5E-6	1.7E-1	3E4
^{240}Pu	6.6E3 y	5E-6	9.9E-2	2E4
^{241}Am	4.6E2 y	4E-6	4.6E-3	6E2
^{243}Am	8.0E3 y	4E-6	2.3E-1	6E4
Actinide totals			5.2E-1	1E5
Grand totals			1.1E0	1E5

[a] MPC_w is an estimate.

[b] Existing in equilibrium with ^{126}Sn are ^{126m}Sb and ^{126}Sb.

[c] Besides ^{210}Pb, ^{210}Po, and ^{226}Ra, other isotopes of the 4n+1 and 4n+2 decay series are present in the source in secular equilibrium (almost) with 1.7×10^{-4} Ci/MWe-y of ^{229}Th and 1.0×10^{-4} Ci/MWe-y of ^{230}Th.

526 282

TABLE F9. Inventory of biologically significant waterborne nuclides, assumed released 10^5 y after irradiation of 32 MWe-y/t of uranium.

Nuclide	$t_{1/2}$	MPC_w, Ci/m^3	Q, Ci/MWe-y	Toxicity index, m^3/MWe-y
Fission products				
^{93}Zr	1.5E6 y	8E-4	5.7E-2	7E1
^{93m}Nb	1.4E1 y	4E-4	5.7E-2	1E2
^{99}Tc	2.1E5 y	3E-4	3.3E-1	1E3
^{126}Sn[a,b]	1E5 y	2E-5	9.1E-3	5E2
^{129}I	1.7E7 y	6E-8	2.4E-6	4E1
Fission production totals			4.5E-1	2E3
Actinides (plus other alpha emitters)[c]				
^{210}Pb	2.0E1 y	1E-7	7.0E-4	7E3
^{210}Pb	3.8E1 y	7E-7	7.0E-4	1E3
^{226}Ra	1.6E3 y	3E-8	7.0E-4	2E4
^{229}Th[a]	7.3E3 y	7E-6	3.7E-3	5E2
^{230}Th[c]	8.0E4 y	2E-6	6.9E-4	3E2
^{233}U	1.6E5 y	3E-5	4.0E-3	1E2
^{237}Np	2.1E6 y	3E-6	1.1E-2	4E3
^{239}Pu	2.4E4 y	5E-6	1.8E-2	4E3
Actinide totals			3.9E-2	4E4
Grand totals			4.9E-1	4E4

[a] The MPCs are estimates equal to the lowest for all other isotopes of the element.

[b] Existing in equilibrium with ^{126}Sn are ^{126m}Sb and ^{126}Sb.

[c] Besides ^{210}Pb, ^{210}Po, and ^{226}Ra, other isotopes of the 4n+1 and 4n+2 decay series are present in the source in secular equilibrium with ^{229}Th and ^{230}Th.

TABLE F10. Inventory of biologically significant waterborne nuclides, assumed released 10^6 yr after irradiation of 32 MWe-y/t of uranium.

Nuclide	$t_{1/2}$	MPC_w, Ci/m^3	Q, Ci/MWe-y	Toxicity index, m^3/MWe-y
Fission products				
^{93}Zr	1.5E6 y	8E-4	3.9E-2	5E1
^{93m}Nb	1.4E1 y	4E-4	3.9E-2	1E2
^{129}I	1.5E7 y	6E-8	2.3E-6	4E1
Fission product totals			7.8E-2	2E2
Actinides (plus other alpha-emitters)[a]				
^{210}Pb	2.0E1 y	1E-7	1.7E-4	2E3
^{210}Po	3.8E-1 y	7E-7	1.7E-4	2E2
^{226}Ra	1.6E3 y	3E-8	1.7E-4	6E3
^{229}Th[a]	7.3E3 y	7E-6	9.1E-3	1E3
^{230}Th	8.0E4 y	2E-6	1.7E-4	9E1
^{231}Pa	3.3E4 y	9E-7	1.0E-5	1E1
^{233}U	1.6E5 y	3E-5	9.0E-3	3E2
^{237}Np	2.1E6 y	3E-6	8.5E-3	3E3
Actinide totals			2.7E-2	1E4
Grand totals			1.1E-1	1E4

[a]Besides ^{210}Pb, ^{210}Po, and ^{226}Ra, other isotopes of the 4n+1, 4n+2 and 4n+3 decay series are present in the source in secular equilibrium with ^{229}Th, ^{230}Th, and ^{231}Pa. MPC is an estimate--equal to the lowest of all other isotopes of Th.

526 284

DOSE CONVERSION FACTORS

Airborne Radioactivity

Only radioactive species having relatively short half-lives ($t_{1/2} < 10^4$ y) were assumed to contribute significantly to radiation exposures from airborne nuclides. Doses to the exposed population were considered to result from three processes: (1) inhalation of radioactivity from the passing cloud, (2) exposure to the gamma radiation emitted by nuclides deposited from the cloud onto the ground, and (3) ingestion of radioactivity that has entered food chains after having been deposited on the ground (only the forage-cow-milk-person pathway was considered).

Inhalation Dose Conversion Factors. The dose delivered over a 50-y period after radioisotope intake was determined for the critical organs of a "standard man" (International Commission on Radiological Protection, 1959) for each of the nuclides of interest (Table F11). We assumed that the radioactivity was taken up over a 1 d period by inhalation. The total amount of air inhaled during this period was taken as 20 m^3 (International Commission on Radiological Protection, 1959). The dose conversion factors given in the tables were calculated with the Oak Ridge INREM code (Turner et al., 1968; Killough and McKay, 1976). This code employs the single exponential model used by the International Commission on Radiological Protection (ICRP) to calculate "maximum permissible concentrations in air and water" of radioactivity. In the latter reference, chronic exposure is assumed.

Turner et al. (1968) and Killough and McKay (1976) describe the method of calculating the critical-organ dose commitment resulting from exposure to a given amount of radioactivity ingested over a finite period of time. This calculation will therefore not be discussed further here. However, the method of converting the critical-organ dose conversion factor to the whole-body equivalent dose conversion factor warrants further discussion.

This conversion is based on the implicit equivalence of doses to various human organs as exemplified by the maximum permissible dose equivalents for

TABLE F11. Dose conversion factors for biologically significant nuclides in air: inhalation. It was assumed that the dose is delivered over a 50-y period following a brief period of inhalation.

Nuclide	Critical-organ dose conversion factor, rem-m^3/Ci-y	Critical organ	Whole-body equivalent dose conversion factor, rem-m^3/Ci-y	Whole-body dose conversion factor, rem-m^3/Ci-y
Fission products				
^{89}Sr	2.8E8	Bone	8.3E8	7.9E6
^{90}Sr	9.1E10	Bone	1.8E10	5.6E9
^{91}Y	4.2E8	Bone	1.0E9	1.1E7
^{95}Zr	1.6E9	Lung	9.3E8	2.1E7
^{95}Nb	4.6E8	Lung	2.9E8	3.8E6
^{103}Ru	4.6E8	Lung	2.8E8	6.0E5
^{106}Ru	8.6E9	Lung	4.8E9	7.9E6
^{125}Sb	1.6E9	Lung	8.9E8	1.2E7
^{127m}Te	8.7E8	Lung	5.2E8	1.4E6
^{127}Te	5.9E6	Lung	2.4E7	2.8E2
^{129m}Te	1.1E9	Lung	7.2E8	1.4E6
^{129}Te	1.8E6	Lung	9.9E5	1.1E1
^{134}Cs	8.9E7	Lung	9.4E8	6.6E8
^{137}Cs	6.9E7	Lung	6.2E8	3.9E8
^{144}Ce	3.1E9	Bone	4.8E9	1.7E8
^{147}Pm	6.1E8	Bone	3.7E8	2.3E7
^{154}Eu	5.4E9	Bone	4.0E9	4.7E8
Actinides				
^{238}Pu	2.0E13	Bone	3.8E12	5.1E11
^{240}Pu	2.3E13	Bone	4.2E12	5.7E11
^{241}Pu	4.7E11	Bone	6.1E10	9.4E9
^{241}Am	7.4E12	Bone	2.6E12	4.9E11
^{243}Am	7.4E12	Bone	2.5E12	4.8E11
^{242}Cm	1.1E11	Liver	2.0E11	7.2E9
^{244}Cm	9.2E12	Bone	1.5E12	2.6E11

occupational workers recommended by the ICRP (1959)--see Table F12. It can be seen, for instance, that a dose of 30 rem/y is permissible to the skin, in contrast to 5 rem/y to the whole body. Thus, one might infer that the risk of a dose of 1 rem to the skin is only one-sixth as great as that of a 1-rem dose to the whole body. Consequently, the whole-body equivalent of a 1-rem dose to the skin would be 0.17 rem. This procedure has been followed to calculate the whole-body equivalent dose conversion factors in Table F11.

Deposition Dose Conversion Factor: External Dose. Fifty-year integrated gamma-ray doses to the whole body have been calculated, assuming uniform deposition of the nuclides on the ground (Table F13). The calculations assume that the whole body is being exposed at a point 0.9 m (3 ft) above an infinite plane source of the radioactive species. The method of calculation and a correction for the air attenuation of the gamma radiation have been discussed in detail elsewhere (Higgins, 1963).

TABLE F12. Maximum permissible dose equivalents recommended for occupational workers by the International Commission on Radiological Protection (1959).

Organ	Maximum permissible dose equivalent, rem/y
Red bone marrow, whole body, and gonads	5
Skin, thyroid, and bone[a]	30
All other single organs	15

[a]The National Council on Radiation Protection and Measurement (1971) currently specifies a maximum permissible annual dose of 15 rem for these organs as well.

TABLE F13. Conversion factors for radioactivity released to the atmosphere and deposited on the ground: external exposure. It was assumed that the dose is delivered over a 50-y period following a single deposition of radioactivity on the ground.

Nuclide	Whole-body dose conversion factor, rem-m^2/Ci
Fission products	
^{89}Sr	3.0
^{90}Sr	--
^{91}Y	1.3E2
^{95}Zr	2.9E4
^{95}Nb	1.8E4
^{106}Ru	6.9E4
^{125}Sb	2.4E5
^{127m}Te	7.2E3
^{129m}Te	6.8E3
^{134}Cs	8.3E5
^{137}Cs	3.1E6
^{144}Ce	9.6E3
^{147}Pm	--
^{154}Eu	1.0E6
Actinides	
^{238}Pu	2.9E4
^{240}Pu	8.6E4
^{241}Pu	2.5E5
^{241}Am	5.1E5
^{243}Am	3.1E6
^{242}Cm	3.0E4
^{244}Cm	3.5E4

Only gamma energy released in the first 50 y after deposition of the nuclides is considered in the dose conversion factors shown in Table F13. For the nuclides with shorter half-lives, such as ^{89}Sr, essentially all the dose is delivered in the first year after deposition. For the very long-lived species, such as ^{243}Am, the dose rate is essentially constant over the period of interest. The gamma-ray energies used in these calculations were obtained from Lederer et al. (1967).

It should be noted that these dose conversion factors have not been corrected for weathering, which will slowly move the radioactivity into the soil, thus attenuating the gamma-ray intensity and decreasing the dose. Clearly this process will not be important for the shorter-lived nuclides, such as ^{89}Sr, but for the longer-lived nuclides (especially those having relatively low-energy gamma rays), the dose conversion factors in Table F13 could be high by a factor of two or three. However, no data exist whereby a reasonable correction for this effect can be estimated.

Deposition Dose Conversion Factor: Internal Dose. Dose conversion factors have also been calculated that give the internal dose (to a critical organ) delivered over a 50-y period following the deposition of the radioactive species. It has been assumed that the predominant pathway for the ingestion of nuclides is the forage-cow-milk-person food chain. The method used here has been discussed in detail by Ng and Thompson (1966) and more recently by Ng et al.(1976).

The dose to a given organ by means of the forage-cow-milk-person pathway is calculated as the product of the total activity ingested as milk per unit deposition and the 50-y dose per unit of activity ingested. The total activity ingested as milk (in Ci) is given by integrating the activity ingested daily (I*) over 50 y:

$$\int_0^{50\ y} I^* dt = \frac{Jr(UAF)F(0)f_m^*}{\lambda_p} ,$$

where J is the rate of milk consumption (l/d), r is the retention factor on forage, UAF is the utilized area factor (i.e., the effective area of pasture grazed daily by the cow (m^2/d), F(0) is the deposition at time zero (Ci/m^2), f_m^* is the transfer coefficient to milk (i.e., the fraction of the nuclide ingested daily by the cow that is secreted in a litre of milk d/l), and λ_p is the effective rate of removal from forage (d^{-1}).

The doses in Table F14 are those calculated by Ng et al.(1976) for the adult. Assumptions are J = 1, r = 0.5, and UAF = 45. The half-residence time for nuclide particles on forage is assumed to be 14 d, which leads to the following expression for λ_p:

$$\lambda_p = \frac{\ln 2}{T_r} + \frac{\ln 2}{14} \quad ,$$

where T_r is the half-life for radioactive decay, in days. The transfer coefficient to milk, f_m^*, and the 50-y dose to the critical organs and to the whole body per unit activity ingested, $D'_{50\ y}$, in rem/Ci, are listed in Ng et al. (1976).

Internal dose conversion factors were calculated both for the critical organ and for the whole body. Also, the whole-body equivalent dose conversion factors were calculated by the method discussed under Inhalation Dose Conversion Factors above.

Waterborne Radioactivity

Only the relatively long-lived radioactive species were assumed to contribute significantly to radiation exposures resulting from groundwater transport. However, for the sake of completeness, a few of the shorter-lived species are included in this compilation. Critical-organ doses to members of the population who drink contaminated water can be calculated with dose conversion

TABLE F14. Dose conversion factors for radioactivity released to the atmosphere and deposited on the ground: internal exposure by means of the forage-cow-milk-person pathway. It was assumed that the dose is delivered over a 50-y period following a single deposition of radioactivity on forage.

Nuclide	Critical-organ dose conversion factor, rem-m^2/Ci	Critical organ[a]	Whole-body equivalent dose conversion factor, rem-m^2/Ci	Whole-body dose conversion factor, rem-m^2/Ci
Fission products				
^{89}Sr	1.4E5	Bone	2.5E4	4.1E3
^{90}Sr	4.8E6	Bone	1.6E6	1.2E6
^{91}Y	5.6E2	G.I.[b]	2.3E2	2.7E-2
^{95}Zr	2.2E3	G.I.	9.0E2	4.9E-1
^{95}Nb	1.3E3	G.I.	5.4E2	8.7E-2
^{106}Ru	4.7E1	G.I.	1.9E1	9.3E-2
^{125}Sb	1.7E2	G.I.	1.1E3	4.0
^{127m}Te	1.8E3	G.I.	1.3E3	6.5E1
^{129m}Te	3.5E3	G.I.	2.2E3	1.1E2
^{134}Cs	3.8E5	Whole body	5.5E5	3.8E5
^{137}Cs	2.3E5	Whole body	3.7E5	2.3E5
^{144}Ce	1.4E3	G.I.	5.7E2	2.3E-1
^{147}Pm	8.0E1	G.I.	3.2E1	2.6E-2
^{154}Eu	5.0E2	G.I.	2.0E2	4.9E-1
Actinides				
^{238}Pu	3.1E1	Bone	6.0	7.6E-1
^{240}Pu	3.4E1	Bone	6.5	8.5E-1
^{241}Pu	7.1E-1	Bone	1.2E-1	1.5E-2
^{241}Am	7.4E3	Bone	2.6E3	4.8E2
^{243}Am	7.4E3	Bone	2.6E3	4.7E2
^{242}Cm	1.3E2	Bone	3.2E2	8.7
^{244}Cm	4.4E5	Bone	1.5E3	2.6E2

[a]Inferred from recommendations of the ICRP (1959).

[b]Gastrointestinal tract.

factors based on the values of the MPC_w, given in Appendix B, Table 2, of the Nuclear Regulatory Commission Standards for Protection Against Radiation (U.S. Code of Federal Regulations, 1976). These dose conversion factors (both for critical organs and the whole body), which are given in Table F15, are calculated assuming a long-term exposure (integrated over 50 y) to water containing the radionuclides listed in the first column. The appropriate values of MPC_w are also listed in Table F15 for the nuclides of interest (both for the critical organs and the whole body), as are the annual doses that would be delivered to the critical organs by exposure to the indicated concentrations of radioactivity. (These doses were inferred by using the MPC_w values of the ICRP 1959 .) The critical organs were also identified through use of these references. Once again, the whole-body equivalent dose conversion factors were determined using the approach outlined under Inhalation Dose Conversion Factors above.

TABLE F15. Dose conversion factors for biologically significant nuclides in water.

Nuclide	MPC_w,[a] Ci/m^3	Critical organ[b]	Annual dose,[b,c] rem	Critical organ dose conversion factor,[d] rem-m^3/Ci	Whole-body equivalent dose conversion factor,[d] rem-m^3/Ci	Whole-body MPC_w,[e] Ci/m^3	Whole-body dose conversion factor,[d] rem-m^3/Ci
Fission products							
^{90}Sr[f]	3E-7	Bone	3	3E8	5E7	1E-6	1E7
^{93}Zr	8E-4	G.I.[g]	1.5	9E4	3E4	6E-1	4E1
^{99}Tc	3E-4	G.I.	1.5	3E5	8E4	1E-2	3E3
^{126}Sn	2E-5	G.I.	1.5	4E6	1E6	2E-3	1E4
^{129}I	6E-8	Thyroid	0.5	4E8	4E8	8E-6	3E6
^{137}Cs[f]	2E-5	Whole body	0.5	7E5	7E5	2E-5	7E5
Actinides							
^{210}Pb[h]	1E-7	Kidney	1.5	7E8	3E8	1E-7	3E8
^{210}Pb[h]	7E-7	Spleen	1.5	1E3	4E7	8E-6	3E6
^{226}Ra[h]	3E-8	Bone	3	5E9	8E8	6E-8	4E8
^{237}Np	3E-6	Bone	3	5E7	8E6	1E-5	3E6
^{238}Pu[f]	5E-6	Bone	3	3E7	5E6	4E-5	6E5
^{239}Pu	5E-6	Bone	3	3E7	5E6	3E-5	8E5
^{240}Pu	5E-6	Bone	3	3E7	5E6	3E-5	8E5
^{241}Am	4E-6	Kidney	1.5	2E7	6E6	1E-5	3E6
^{243}Am	4E-6	Bone	3		6E6	1E-5	3E6
^{244}Cm[f]	7E-6	Bone	3	[illegible]	2E6	2E-5	7E5

[a] From NCRPM (1971)

[b] Inferred from ICRP (1959).

[c] Steady-state exposure at MPC_w.

[d] For integral dose from 50 y of exposure.

[e] For annual dose of 0.5 rem; inferred from ICRP (1959).

[f] Assuming an initial concentration equal to MPC_w and allowing for radioactive decay.

[g] Gastrointestinal tract.

[h] In equilibrium with parent ^{230}Th.

APPENDIX F REFERENCES

Gera, F. 1975. Geochemical behavior of long-lived radioactive wastes. Oak Ridge National Laboratory report ORNL-TM-4881.

Higgins, G. 1963. Calculation of radiation fields from fallout. Lawrence Livermore Laboratory report UCID-4539.

International Commission on Radiological Protection. 1959. Recommendations of the International Commission on Radiological Protection (report of committee 2 on permissible dose for internal radiation. ICRP publication 2. London: Pergamon Press.

Killough, G. G., and McKay, L. R. 1976. A methodology for calculating radiation doses from radioactivity released to the environment. Oak Ridge National Laboratory report ORNL-4992.

Lederer, C. M.; Hollander, J. M.; and Perlman, I. 1967. Table of isotopes. New York: John Wiley and Sons.

National Council on Radiation Protection and Measurement. 1971. Basic radiation protection criteria. NCRP report 39.

Ng, Y. C.; Burton, C. A.; Thompson, S. E.; Tandy, R. K.; Kretner, H. K.; and Pratt, M. W. 1966. Prediction of the maximum dosage to man from the fallout of nuclear devices, IV. Handbook for estimating the maximum internal dose from radionuclides released to the biosphere. Lawrence Livermore Laboratory report UCRL-50163, part IV.

Ng, Y. C., and Thompson, S. E. 1966. Prediction of the maximum dosage to man from the fallout of nuclear devices, II. Estimation of the maximum dose from internal emitters. Lawrence Livermore Laboratory report UCRL-50163, part II.

Oak Ridge National Laboratory. 1970. Siting of fuel reprocessing plants and waste management facilities. Report ORNL-4451.

Turner, W. D.; Kaye, S. V.; and Rohner, P. S. 1968. EXREM and INREM computer codes for estimating radiation doses to populations from construction of a sea-level canal with nuclear explosives. Oak Ridge Gaseous Diffusion Plant report K-1752.

United States Code of Fereral Regulations. 1976.

RKJ/jvb

526 295

NRC FORM 335 (7-77)

U.S. NUCLEAR REGULATORY COMMISSION

BIBLIOGRAPHIC DATA SHEET

1. REPORT NUMBER (Assigned by DDC)
NUREG/CR-0577
UCRL-52632

4. TITLE AND SUBTITLE (Add Volume No., if appropriate)
A Probabilistic Safety Analysis for Solidified High-Level Nuclear Waste Management Systems: A Status Report

2. (Leave blank)

3. RECIPIENT'S ACCESSION NO.

7. AUTHOR(S)
Richard A. Heckman, Thomas Holdsworth

5. DATE REPORT COMPLETED
MONTH: February YEAR: 1979

9. PERFORMING ORGANIZATION NAME AND MAILING ADDRESS (Include Zip Code)
Lawrence Livermore Laboratory
Livermore, California 94550

DATE REPORT ISSUED
MONTH: July YEAR: 1979

6. (Leave blank)

8. (Leave blank)

12. SPONSORING ORGANIZATION NAME AND MAILING ADDRESS (Include Zip Code)
Office of Nuclear Material Safety and Safeguards
U.S. Nuclear Regulatory Commission

10. PROJECT/TASK/WORK UNIT NO.

11. CONTRACT NO.
NRC FIN No. A0277

13. TYPE OF REPORT
Status

PERIOD COVERED (Inclusive dates)
Thru September 1977

15. SUPPLEMENTARY NOTES

14. (Leave blank)

16. ABSTRACT (200 words or less)

The Lawrence Livermore Laboratory is providing technical support to the Nuclear Regulatory Commission in the development of regulations and regulatory guidance for the management and disposal of high-level radioactive waste in geologic repositories. This report covers work completed during FY77 on those characteristics of solidified high-level waste which influence radiological risk during both the preemplacement portion of the waste management system and the postsealing period.

17. KEY WORDS AND DOCUMENT ANALYSIS

17a. DESCRIPTORS

17b. IDENTIFIERS/OPEN-ENDED TERMS

18. AVAILABILITY STATEMENT
Unlimited

19. SECURITY CLASS (This report)

21. NO. OF PAGES

20. SECURITY CLASS (This page)

22. PRICE
$

NRC FORM 335 (7-77)